Characteristics of the late Mesozoic tectonic evolution of the South China block and geodynamic implications : Multi-approach study on the Qingyang-Jiuhua, Hengshan and Fujian coastal granitic massifs

Wei Wei

ÉCOLE DOCTORALE [SCIENCES DE LA TERRE ET DE L'UNIVERS]

Institut des Sciences de la Terre d'Orléans

School of Earth Science, University of Chinese Academy of Sciences

THÈSE EN COTUTELLE INTERNATIONALE présentée par :

Wei WEI

soutenue le 27 décembre 2013

pour obtenir le grade de :

Docteur de l'université d'Orléans
et de l'Université de l'Académie des Sciences de Chine

Discipline : Sciences de la Terre et de l'Univers

Characteristics of the Late Mesozoic tectonic evolution of the South China Block and geodynamic implications

-multi-approach study on Qingyang-Jiuhua, Hengshan and Fujian coastal granitic massifs

THÈSE dirigée par :

Yan CHEN	Professeur, Université d'Orléans
Quanlin HOU	Professeur, University of Chinese Academy of Sciences

RAPPORTEURS :

Xianhua Li	Professeur, Inst. Geol. Geophys, CAS
Baochun Huang	Professeur, Université d'Pékin

JURY :

Yan CHEN	Professeur, Université d'Orléans
Quanlin HOU	Professeur, University of Chinese Academy of Sciences
Michel FAURE	Professeur, Université d'Orléans
Wei LIN	Professeur, Institute of Geology and Geophysics, CAS
Rixiang ZHU	Professeur, Institute of Geology and Geophysics, CAS
Quanren YAN	Professeur, University of Chinese Academy of Sciences

Acknowledgements

At the moment when this thesis is reaching its finalizing state, my heart is but filled with the deepest gratitude for all the people who have helped me in one way or another during my years of academic voyage toward the temporary but important harbor.

Professor Chen Yan offered me the most treasured moral and professional support a student working overseas can hope for, during my two and a half years of Ph.D research in France. He broadened my horizon with ideas and methods and cutting-edge technologies of contemporary geosciences. His profound knowledge and rigorous training helped build in me a firm foundation in magnetic fabrics and paleomagnetism. Without his guidance, I would not have been able to tackle questions in my Ph.D study with a multi-disciplinary approach involving a rich variety of methods.

My deepest gratitude also goes to Professor Hou Quanlin, my respected mentor in academic pursuit and life. Professor Hou ushered me into the present tectonic enquiries at the Chinese Academy of Sciences. During my four years of Ph.D research, I have received from him valuable professional guidance and intellectual stimulation. I was particularly grateful for his unfailing support and precious patience when my work seemed to get stagnant. His inspiration and encouragement are a valuable asset and will always urge me to go on and on, ever approaching my career goals with unshakable faith and perseverance.

Professor Michel patiently explained to me many a time ideas and concepts in a vast amount of tectonics literature and taught me skills and methods in investigating granitic structure. I benefited a great deal from his timely and insightful comments on my research manuscripts. Professor Lin Wei and Professor Wang Qingchen selflessly gave me opportunities to do filed survey and laboratory experiment, teaching me to effectively organize data for in-depth analysis every time we met.

A special word of thanks must be extended to Professor Wu Chunming, who always placed confidence in me and encouraged me in times of difficulty.

At the Universite d'Orleans, I learned from Dr. Guillaume Martele how to construct geometric shapes of granites through gravity modeling data. And Nicole Le Breton taught me methods of treating electron probe data and calculating crystallization pressures by use of an amphibole barometer. In addition, the generous help of Nicolas Charles, Michael Laumonier and Flavien Choulet constantly filled me with warmth and gratitude. Thanks to Mr and Mrs He Chenwei, Dr. Liu Qiangwei, and other friends and colleagues, their accompaniment and laughter alleviated my anxiety and loneliness in the foreign land. Space does not allow me to mention all their names in paper, but they get remembered in my heart.

I also express my heart-felt thanks to Wei Mingming, Wan Xiaoyun, Yu Liye and other fellow Ph.D candidates at the Chinese Academy of Sciences, who undertook to deal with much routine work for me at home during my absence. Special thanks also go to Chen Ke, Chu Yang, Ji Wenbin, Xue Zhenhua, Jiang Lin, Tao Huifei, Yang Xiaofa, Wang Jun, Qiu Zhen and Wan Jialing for their help and friendship on the same academic voyage.

Last but not the least, I am indebted to my parents. Their conscientious education and example have led me onto the path of academic and spiritual pursuit, bolstered with a comfortable material life. Their love, care and support have sustained me through all these years, particularly in times of difficulty and frustration.

To conclude, please allow me to present as a gift to readers of my thesis a poem my father taught me when I was a senior high school student:

Stopping By Woods On A Snowy Evening

By Robert Frost

Whose woods these are I think I know.
His house is in the village though;
He will not see me stopping here
To watch his woods fill up with snow.

My little horse must think it queer
To stop without a farmhouse near
Between the woods and frozen lake
The darkest evening of the year.

He gives his harness bells a shake
To ask if there is some mistake.
The only other sound's the sweep
Of easy wind and downy flake.

The woods are lovely, dark and deep.
But I have promises to keep,
And miles to go before I sleep,
And miles to go before I sleep.

Author

October 2013

Abstract

The vast distribution and long duration of the Late Mesozoic magmatism in the eastern part of South China presents a unique case in the world. This offers a natural laboratory to study the process of magma genesis, the magma emplacement mode, the relationship between magmatism and tectonics, the geodynamic role on the magma emplacement and lithospheric evolution. Since 50's, particularly 90's of the last century, geoscientists have made important efforts in geological cartography and carried out numerous studies with remarkable scientific achievements, building a solid background to understand the tectonic evolution of the South China Block (SCB). However, certain fundamental questions mentioned above remain unsolved and/or are in hot debate. In order to make progress in these scientific issues, we have carried out in a multi-disciplinary study in the Late Mesozoic Qingyang-Jiuhua massif, Hengshan massif and Fujian coastal zone according to their distance with respect to the paleo subduction zone of the Paleo-Pacific plate, the ages of granitic massifs and related tectonics, including field observation on the structure geology, micro-observation on thin section, U-Pb dating on monazite, AMS, paleomagnetism, gravity modeling and P condition concern the granite emplacement. In the view of deformation in these granitic massifs and their country rocks, mode and influence of regional tectonics on the emplacement, though each studied zone reveals its distinguished characteristics, they show some intrinsic and common relationships between them. With our new results and integrating previous data, in this thesis, we discuss the tectonic context of emplacement of these Late Mesozoic magmatic massifs and the geodynamic evolution of the SCB., We propose a 3-step geodynamic model: (1) during 145-130 Ma period, the Paleo-Pacific plate subducted northwestwardly, the West Philippines micro-continent, approaching to SCB, important subduction-related arc volcanism was produced in the coastal areas of Southeast China coast (Zhejiang-Fujian-Guangdong), forming a back-arc extension tectonic system in SCB; (2) during 130-110 Ma period, due to the collision between the West Philippines micro-continent and SCB, the compressional tectonic structures were developed in the Changle-Na'ao coastal zone, producing ductile deformation zones. However, the inland of the eastern part of SCB was under a NW-SE extensional tectonic regime; (3) during 105-90 Ma period, a new subduction zone was developed in the SE flank of the West Philippines micro-continent, the subducting slab reached the Changle-Nan'ao tectonic belt, with the possible break-off of slab, the asthenospheric ascent was responsible for the important emplacement of plutonic massifs and dykes. The tectonics of the eastern part of SCB was characterized by a general extensional system in this period. This tectonic pattern has been significantly disturbed by the Oligocene-Eocene opening of the South China sea,and the Miocene shortening of the SCB margin in Taiwan. Of course, this model should be

improved by more geological, geophysical and geochemical investigations.

KEY WORDS : South China Block lithospheric tectonic evolution, Late Mesozoic, Magma emplacement mechanism, Structural observation, Anisotropy of Magnetic Susceptibility, Paleomagnetism, Gravity modeling, Amphibole Al_{Total} geobarometry.

Caractéristiques de l'évolution de la partie orientale du Bloc de Chine du Sud au Mésozoïque supérieur et implications géodynamiques

-Etude pluridisciplinaire de la mise en place des massifs granitiques de Qingyang-Jiuhua, Hengshan et de la côte du Fujian et des structures tectoniques associées

La vaste distribution geographique et la longue durée du magmatisme au Mésozoïque supérieur (Jurassique et Cretace) en Chine du Sud présente le cas unique dans le monde. Ceci présente un laboratoire naturel tres favorable a l'étude des processus de magmatogenese, et des modes de mise place des plutons granitiques. Il permet egalement d'aborder l'analyse des relations magmatisme-tectonique et les contextes géodynamiques de la la mise en place de magma dans leur cadre lithosphérique. Depuis les années 50, et surtout les années 90, des scientifiques ont mis un effort important sur la cartographie géologique, mené des études petrologiques et geochronologiques et ainsi obtenu une base solide pour la compréhension de l'évolution tectonique du Bloc de Chine du Sud (SCB). Cependant, des questions fondamentales restent encore sans réponses ou vivement débatues. Dans le but de progresser sur ces sujets fondamentaux, nous avons mené des études pluridisciplinaires sur les massifs d'age Mésozoïque supérieur de Qingyang-Jiuhua (Province d'Anhui), Hengshan (Province de Hunan) et certains plutons affleurant dans la zone côtière du Fujian. Le choix des massifs est fonde sur leur distance variable par rapport à la paleozone de subduction, les ages comparables de ces massifs et les deformations associées. Les méthodes d'étude comprennent l'observation de terrain, l'analyse microscopique de lames minces, la datation par U-Pb de monazite, l'ASM, le paléomagnétisme, la modélisation gravimétrique et la barométrie a partir de Al-total dans l'amphibole magmatique. Bien que chaque massif presente des caractéristiques distinctes, ils partagent des points communs du point de vue de leur orientation preferentielle, de la déformation de leurs encaissants et de l'influence de la tectonique régionale sur leur mise en place,. D'après nos nouveaux résultats et en intégrant les données précédentes, nous discutons dans cette thèse les contextes tectoniques de mise en place de ces massifs granitiques et l'évolution géodynamique de SCB, et proposons un scénario géodynamique en 3 étapes. (1) Pendant la periode 145-130 Ma, la subduction vers le NW de la plaque Paléo-Pacifique sous le contient asiatique fait rapprocher le micro-continent de l'Ouest-Philippines avec le continent de Chine du Sud, produisant l'important magmatisme d'arc et formant un regime tectonique en extension en SCB ? dans l'arrière-arc; (2) Pendant la periode 130-110 Ma, dûe à la collision entre le micro-continent de l'Ouest Philippines et SCB, une structure compressive vers le NW a été développée dans la zone

de Changle-Nan'ao, produisant des déformations ductiles. Cependant, l'intérieur de la partie orientale du SCB était encore en régime tectonique extensif de direction NW-SE; (3) Pendant la periode 105-90Ma, une nouvelle zone de subduction a été développée au SE du micro-continent de l'Ouest Philippines, le panneau subductant atteint la zone de Changle-Nan'ao, avec probablement des morceaux de panneau cassé, provocant l'ascension de l'asthénosphère, responsable de la mise en place d'importants massifs granitiques et de filons. La tectonique de SCB pendant cette période est caractérisée par un système tectonique d'extension générale. Ce dispositif a ete significativement perturbe par l'ouverture oligo-miocene de la mer de Chine du Sud et par la compression miocene de la marge a Taiwan. Ce modèle géodynamique reste à être amélioré par de futures investigations géologiques, géophysiques et géochimiques.

Mots clés: Bloc de Chine du Sud, zone tectonique de Changle-Nan'ao, Cretace Mésozoïque supérieur, extension lithosphérique, mise en place passive de magma granitique, massif de Qingyang-Jiuhua, massif de Hengshan, etude pluridisciplinaire, analyse multi-échelle, micro-continent Ouest Philippines, magmatisme insulaire-arc, extension d'arrière-arc, Anisotropie de la Susceptibilité magnétique (AMS), paléomagnétisme, modélisation gravimétrique, barométrie d'Al-total dans l'amphibole.

摘 要

中国华南地块晚中生代的岩浆活动分布之广、规模之大且持续时间之长是世界上绝无仅有的。这为研究岩浆形成机制、岩体侵位方式、岩浆活动与大地构造可能的关系、岩体侵位的地球动力学背景以及岩石圈演化过程提供了一个天然试验场。至从上世纪五十年代，特别是九十年代以来，众多地质科学工作者进行了大量的填图工作和科学研究，硕果累累，为不断地加深理解华南地块构造演化奠定了坚实的基础。然而，以上所提出的一些问题尚未得到解决或正处于争论之中。为了对这些基础科学问题的研究取得新的进展，通过本论文我们根据与古太平洋俯冲带距离、花岗岩岩体以及构造活动年龄，对皖南青阳－九华、湖南衡山以及福建沿海三个地区晚古生代岩浆岩岩体和相关构造带进行了包括野外考察采样、室内薄片观察、年龄测定、磁组构及古地磁测量、重力模拟、独居石电子探针测年以及角闪石总铝压力计计算等多学科的研究。从岩体和围岩的变形强度和形式、岩体侵位方式以及区域构造影响等方面来看，每个地区均有与其它岩体不同的各自特征，同时具有一脉相承的共性。根据我们所获的最新数据以及前人成果，本论文对华南东部晚中生代岩浆岩岩体侵位的构造背景以及相应的地球动力学演化进行了讨论，并提出了一个三阶段的地球动力学模型：(1) 在 145-130Ma 期间，古太平洋向 NW 的俯冲并使其驮负的菲律宾微陆块向华南地块靠近，在浙江-福建-广东沿海地区诱发了大量的陆弧火山活动并发育了与俯冲相关的火山岩和侵入岩，在弧后形成伸展体制；(2) 在 130Ma-110Ma 期间，由于菲律宾微陆块与华南地块相碰撞，并将 NW 向的挤压构造体制引入东南沿海，发育了长乐-南澳挤压构造带，发育韧性变形；但华南东部的内陆地区依然处于 NW-SE 向的伸展体制控制下；此时，在菲律宾微陆块的 SE 侧开始发育新的俯冲带，而老的俯冲板片则发生断离并导致软流圈物质开始影响华南岩石圈板块，这是因为已俯冲的板片因惯性而继续俯冲，而菲律宾微陆块因碰撞而不能随之俯冲，这就造成了断离的产生；(3) 在 105Ma-90Ma 期间，上一阶段新发育的俯冲板片俯冲至长乐-南澳构造带之下，加之可能的先前俯冲板片的断离作用，使软流圈大规模上涌，造成大量岩体和岩墙侵位，此阶段整个华南地块处于伸展体制控制之下。当然，这个模式尚需更多的地质、地球物理以及地球化学方面的数据加以完善。

关键词：华南地块岩石圈构造演化，晚中生代，岩浆侵位机制，构造观察，磁组构，古地磁、重力模拟，角闪石总铝压力计

Content

Part I

Part II

Chapter 1 Introduction

The South China Block in the Late Mesozoic is characterized by the formation of many graben basins or semi-graben basins, the emplacement of plutons, as well as the formation of a number of ore deposits. A variety of models have been proposed with regard to the tectonic regime and the geodynamic background associated with these geological phenomena, but there is no consensus so far. In this study, the emplacement mechanism of plutons and their related tectonic environment have been chosen as the starting point. In practical, one or more plutons in three regions of South China are selected for multi-disciplinary systematic investigations in the expectation of exploring the emplacement of plutons and their tectonic regimes. In combination of the previous researches on basins and pluton geochemistry, the paper proposes a geodynamic model compatible with multi-disciplinary data.

This chapter provides a brief introduction to the thesis. It begins with the Late Mesozoic tectonic background of the eastern area of the South China block, and then generalizes previous findings and their geodynamic models in different disciplines as well as the focus of their debate. After that, we propose several core scientific issues and introduce the research methods, work load, major findings and their significance. At the end of this chapter, there is a structure of the thesis.

1 Research Background

1.1 Geological Phenomena of the Late Mesozoic Tectonic Events in the South China Block

1.1.1 Normal Faults and Graben- and half-Graben Basins

The most conspicuous geological event in the Late Mesozoic was the massive emplacement of granites and the formation of many faulted basins. (Li, 2000; Sun and Zhou, 2002; Zhou et al., 2006; Shu et al., 2009b). Statistics show that the outcrop of Late Mesozoic granites covered an

area of 127300 km^2, basins an area of 143100 km^2 and the adjacent Late Mesozoic granites were often coupled with the basins of the same time in the form of normal fault (Zhou et al., 2006; Shu et al., 2009b).

The faulted basin first appeared in NanLing area. During the Middle Jurassic period， in the NanLing area, it developed a series of faulted basins filled with continental margin clastic rocks and bimodal volcanites, which are representative of an intracontinental extensional regime. (Zhou et al., 2006; Shu et al., 2009b).

In the Early Cretaceous, the extensional faulted basin was mainly distributed in southern Anhui, Hubei, Hunan and Guangxi. For example, the Guangde faulted basin in Southern Anhui takes up an area of 6000 km^2，infilling the Lower Cretaceous, Upper Cretaceous and the Tertiary, with a total thickness of more than 9000m (AHBGMR, 1987). During these periods, there were substantial emplacements of plutons， such as the Qingyang pluton, the Langqiao pluton, the Jingde pluton, etc.(Wu et al., 2012) The Zhajiang basin in Hunan, however, began to open due to the displacement of the Xiushui-Yongzhou normal fault formed in 136Ma. The oldest deposition are the Late Cretaceous Dongjing formations, unconformably overlying the underlying strata of the Jurassic and older periods. (HNBGMR, 1987; Li et al., 2013a). The adjacent Liling-Youxian basin and the Chaling basin began to open at the same time (HNBGMR, 1987).

In the Late Cretaceous the newly-formed faulted basins were distributed mainly over Zhejiang, Jiangxi and Guangdong areas, indicating a migration tendency towards the southeast coast during the Early and Late Cretaceous. Many faulted basins formed in Early Cretaceous were still growing with continual deposition. (Shu et al., 2009b) For example, most faulted basins in Zhejiang run in the NE-SW direction. Composed of Jurassic fluvial-lacustrine sediments and volcanites, they are mostly semi-graben basins, under the control of the large faults of the Jiangshan-Shaoxing Fault, the Lishui-Yuyao Fault and the Wenzhou-Zhenhai Fault. In addition to the Late Cretaceous fluvial-lacustrine sediments, the basins also developed the basalt-andesite-rhyolite combination，featured by the Jinhua-Quzhou basin (ZJBGMR, 1989).

In Jiangxi, most basins, typically semi-graben basins, were formed in the Late Cretaceous, with piedmont pluvial face at the bottom and fluvial and lacustrine facies on the top. Basalt or andesitic basalt often erupted on the side of the basins near the fault (JXBGMR, 1984). Jitai basin is representative of the Late Cretaceous faulted basins in Jiangxi (Deng et al., 2003; Shu et

al., 2004).

Nanxiong basin features the Late Cretaceous faulted basins in Guangdong. Covering an area of 1800km^2 , it stretches along the northern Guangdong and southern Jiangxi in the ENE-WSW direction. Its major fault is on the north boundary of the basin, running through the Zhuguang Mountain， while its southern part outcrops the unconformity of the basin and the underlying strata (Shu et al., 2004).

1.1.2 Bimodal Volcanites

The earliest Late Mesozoic bimodal volcanites in South China were erupted in the east-west rift basins located in the eastern Nanling (Chen et al., 1999; Xie et al., 2005; Zhou et al., 2006; Shu et al., 2009b). Several researchers, who have conducted detailed geochemical studies on the bimodal volcanites there of this time, suggest that they are representatives of the intra-continental extensional environment (Xu, 1992; Chen et al., 1999; Fan and Chen, 2000). During the Cretaceous period, bimodal volcanites were widely distributed in Fujian, Jiangxi, Zhejiang areas (Gilder et al., 1991a; Goodell et al., 1991; Qiu et al., 1999; Yu et al., 2006b). The bimodal volcanites in Jiangxi and Zhejiang were concentrated particularly in the Late Cretaceous faulted basins developed on the basement of the Neoproterozoic suture zone. The combination of these faulted basins and bimodal volcanites is known as the “Ganhang rift” (Gilder et al., 1991a; Goodell et al., 1991). In addition, it is noteworthy that most of the Cretaceous volcanites, including the bimodal volcanites of this time, were formed on the eastern side of Ganjiang fault. (Shu et al., 2009b).

1.1.3 Mafic Dyke Swarms

During the Late Mesozoic period, large dyke emplacements occurred in South China, spanning from the Late Jurassic to Late Cretaceous (Xie et al., 2006), forming the dyke swarms on the Southeast coast, covering the north of Zhejiang, running through Fujian, and finally extending to the south by Guangdong and Hainan (Dong et al., 2010; Dong et al., 2006; Tang et al., 2010).

1.1.4 Granite Emplacements and their Geochemical Features

After the magmatic quiescence in 200Ma-190Ma, large magma emplacements began in the South China. In the transitional period of the Jurassic and the Cretaceous, the magmatic quiescence returned to the South China, and the granite emplacements weakened in the later stage of Early-Cretaceous (Li et al., 2010b). In terms of age-spatial distribution, the Jurassic granites were located in inland areas, while the Cretaceous granites were found in the southeast coastal areas, indicating an emplacement tendency of coastal ward migration. As to their geochemical composition, these granites are mostly A-type granites and I-type granites (Li, 2000). Some regions, such as the Lower Yangtze River Area, show a wide distribution of adakitic granites (Sun et al., 2007; Ling et al., 2009). In the trace element tectonic diagrams, these granites fall mostly in the intra-plate and back-arc areas, featuring an extensional environment (Li, 2000). Many granites and their adjacent basins were coupled to a normal fault and granite emplacement and the opening of basin occurred at approximately the same time. in some cases, the elevation of the granite was higher than it neighboring basin. In the process of some basins' formation, sediment detritus were partly supplied from their neighboring granite so the granite and basin formed a "basin and ridge" couple (Shu et al., 2009b). Some researchers, therefore, argue that the tectonic environment in South China is equivalent to the Basin and Range Province in West America (Li, 2000; Shu et al., 2009b).

1.2 Late Mesozoic Tectonic Geodynamic Models in the South China

Extensive research has been carried out on the Late Mesozoic tectonic regime in South China, making it one of the most active research areas in the geological research. Generally speaking, in terms of extensional structure, the Late Mesozoic geodynamic models can be included in five hypotheses: hypothesis of deepening of subduction angle and back-arc extension retreat, hypothesis of flat subduction and subduction slab roll back, hypothesis of Mid-Ocean Ridge subduction, hypothesis of Plateau collapse, and hypothesis of strike-slip and pull-apart caused by the northward subduction of Kula plat.

1.2.1 Hypothesis of Deepening of Subduction Angle and Back-arc Extension Retreat

Mesozoic intrusive granites indicate statistical patterns in terms of spatial distribution.

Jurassic granites were found in the northwest inland of South China Block, while Cretaceous granites were on the southeast coast, this suggests that the magma emplacement through the Late Mesozoic has a coastal ward migration tendency (Zhou and Li, 2000). In order to explain the temporal-spatial distribution of granites, Zhou and Li（2000）proposed a hypothesis that in the Late Mesozoic paleo-Pacific plate subducted beneath the South China Block with low angle at first， and since then as the subduction angle increased, volcanic arcs retreated toward the southeast coastal area (Zhou and Li, 2000). However, more elaborate temporal-spatial data of plutons, demonstrate that the temporal-spatial distribution of Late Mesozoic pluton emplacement was more complex than the migration towards southeast coast (Li et al., 2007; Li and Li, 2007). In addition, Jurassic volcanites and intrusive rocks do not show any arc affinity (Chen et al., 2008; Li et al., 2003b; Zhu et al., 2010d).

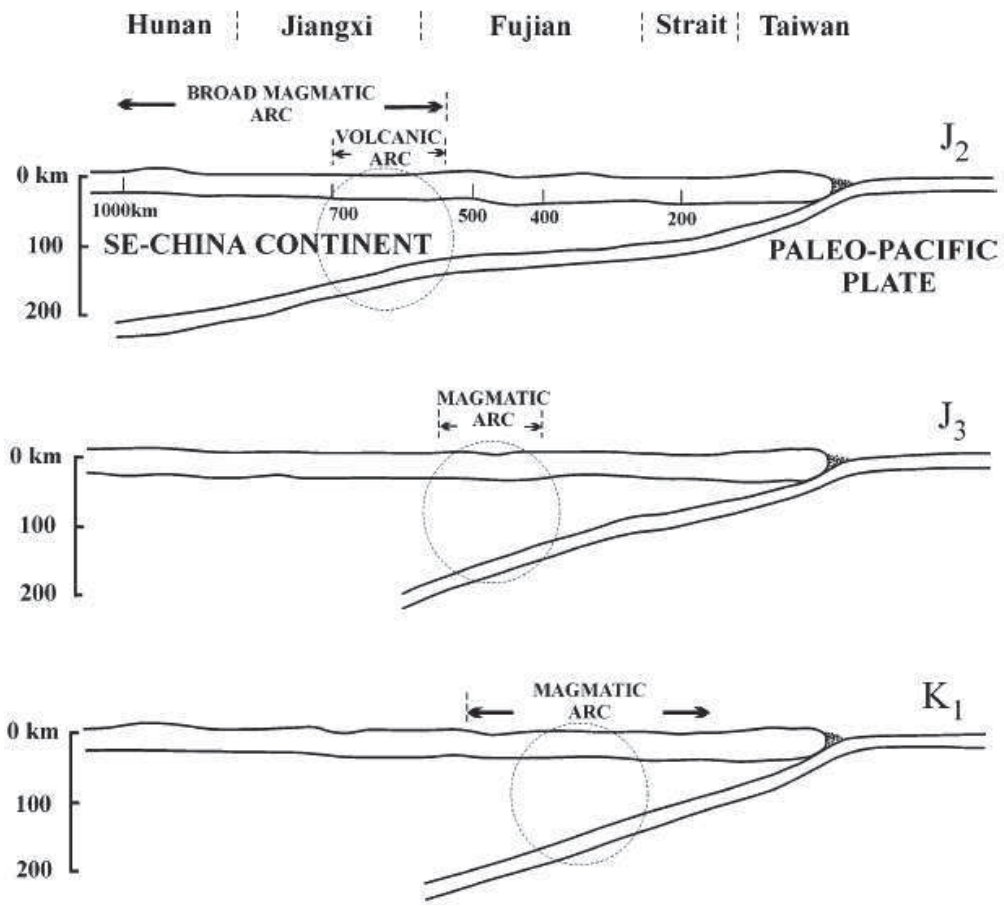

Figure 1 1: Hypothesis of deepening of subduction angle and back-arc extension retreat After (Zhou and Li, 2000)

1.2.2 Hypothesis of Flat Subduction and Subduction Slab Roll Back

After generalizing the deformation and metamorphism from the late Permian to Cretaceous as well as the age of pluton emplacements in South China, Li and Li (2007) finds that the deformation and metamorphism migrated from southeast coast to northwest inland China, leaving a South China fold belt as wide as 1300km (Li and Li, 2007). In 190Ma, the pluton emplacement began in the middle of the South China fold belt. Intrusive plutons of this time were mostly highly fractionated I-type granites, A-type granites, and other plutons which were representatives of intra-continental extension. Between 190 Ma and 150 Ma, the migration of pluton emplacement could be divided into two systems: one system was that granite emplacement migrate from the front and central areas of the South China Fold Belt towards their middle ground; the other was the migration towards southeast coast from the middle area of the fold belt (Li and Li, 2007). After 150 Ma, all the granite emplacements in the South China migrated to the southeast coast (Li and Li, 2007; Zhou and Li, 2000).

According to such elaborate age-spatial structure of plutons, Li and Li（2007）proposes the possibility of flat subduction of Late Mesozoic paleo-Pacific plate beneath the South China and subduction slab roll back. The hypothesis believes that the paleo-Pacific plate had an oceanic plateau subducting northwestwards to the southern lithospheric plate, causing the deformation, metamorphism as well as the pluton emplacement migrating towards northwest part of the South China, and hence the formation of southern fold belt. In 190Ma, the subduction plate broke off, signaling the end of orogeny and the beginning of post-orogenic extension, as well as the emplacement of A-type granites. After 150Ma, the subduction slab rolled back to the subduction zone, leading to the migration of granite emplacement towards the southeast coast area.

This hypothesis accounts for the macro age-spatial structure of Late Mesozoic granites in South China and the geochemical evolutionary characteristics, but further consideration should be made to explain some detailed geological phenomena, for example, the Early Cretaceous deformation in Fujian coastal areas which has been widely accepted as the result of strike-slip regime (Charvet et al., 1990; Xu et al., 1990; Tong and Tobisch, 1996; Wang and Lu, 1997a, b, 2000).

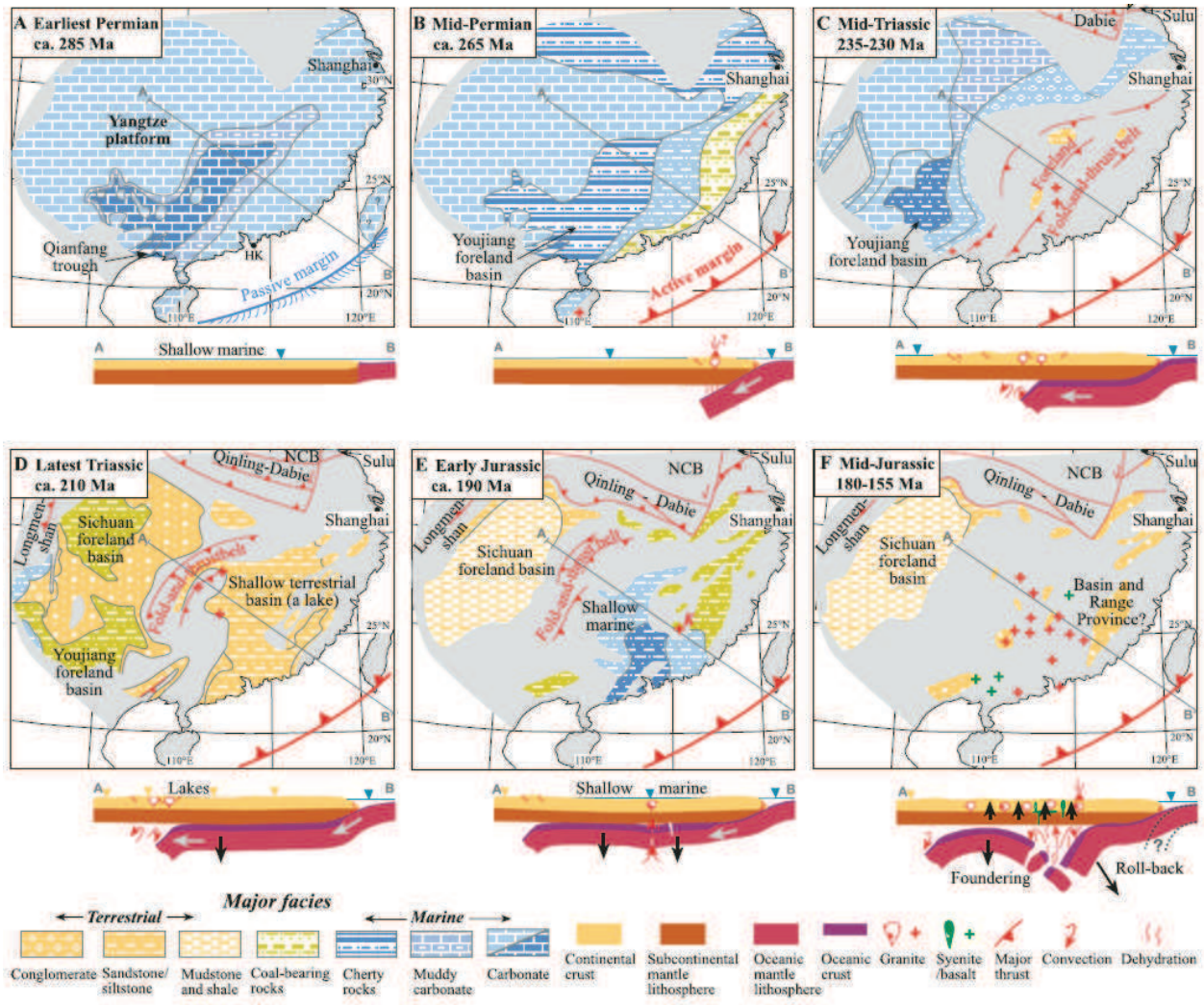

Figure 1 2: Hypothesis of flat subduction and subduction slab roll back

After (Li and Li, 2007)

1.2.3 Hypothesis of Mid-Ocean Ridge Subduction

The hypothesis of flat subduction and subduction zone retreat has another problem. In the Lower Yangtze Area, there is a NW-SE magmatic belt. 400 km long, 100 km wide, the belt developed between 150 Ma and 120 Ma, perpendicular to the subduction zone, but the magmatism of this granite belt does not show any polarity of migration to the coast (Ling et al., 2009; Wu et al., 2012). The belt contains a variety of granites, including I-type granites, A-type granites and adakites, symmetrically distributed on both sides of the axis of the magmatic belt (Sun et al., 2007; Ling et al., 2009). Considering that there might have been two oceanic plates in the Paleo-Pacific Ocean: the Kula plat on the north which subducted NNW to Eurasia, and the Pacific plate on the south which subducted SW to Eurasia, thus, the Mid-Ocean Ridge between

them probably subducted beneath the Lower Yangtze Area, thus accounting for the distribution of magmatic rocks in this region. This is the hypothesis of Mid-Ocean Ridge Subduction (Ling et al., 2009; Sun et al., 2007). Nevertheless, even if the kinematics of Pacific plate can be discovered based on the age and order of guyot, more tectonic evidence needs to be found on the South China plate to find whether the Pacific plate has affected the South China plate. For example, unlike the single paleo-Pacific plate subducting beneath towards East Asia, dual oceanic plates subducting toward East Asia northwards and southward respectively, brings about different kinematics modes. It is most likely to prove the hypothesis of Mid-Ocean Ridge subduction in such regions as the Lower Yangtze Area and the Fujian coastal area, the former is the location of the Mid-Ocean Ridge Subduction and the latter is closest to the subduction zone, respectively.

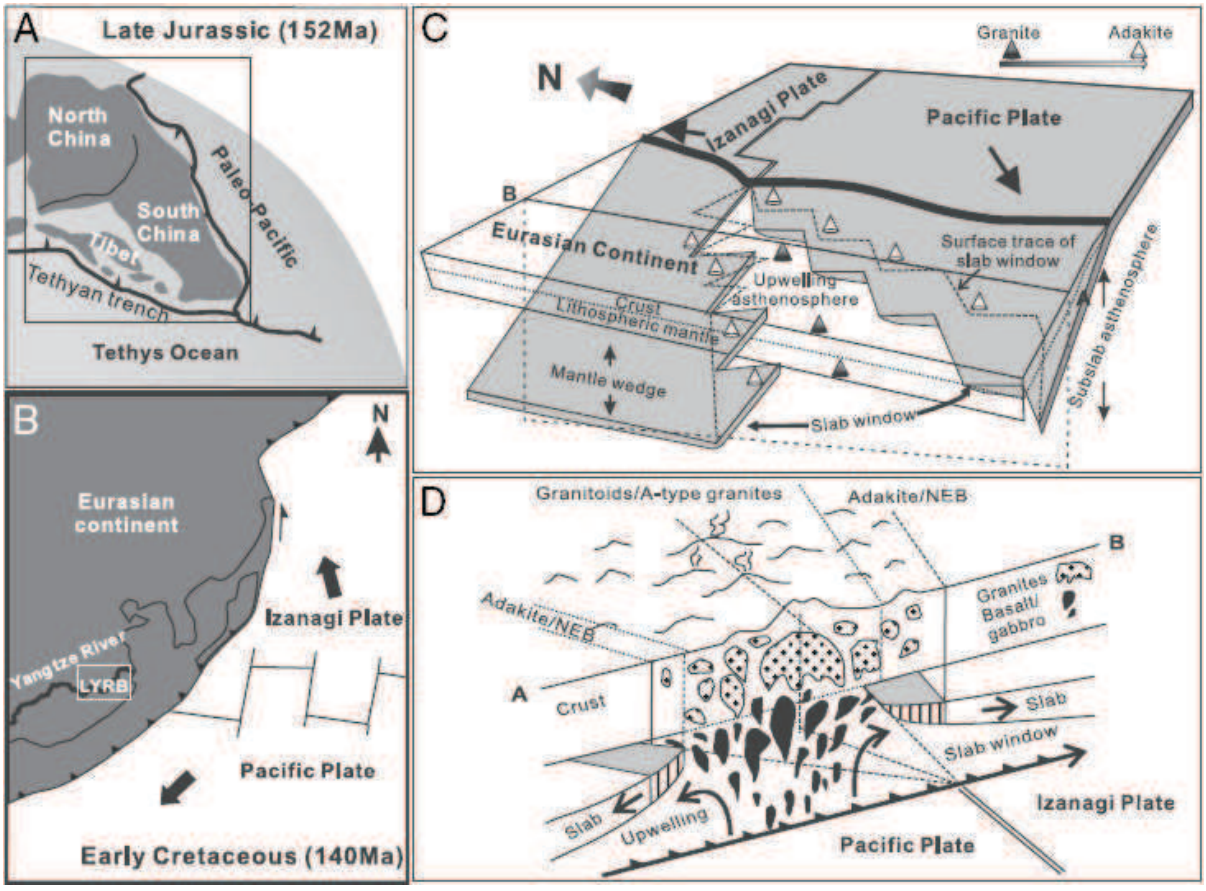

Figure 1 3: hypothesis of Mid-Ocean Ridge subduction

After (Ling et al., 2009)

1.2.4 Hypothesis of Plateau collapse

There are different interpretations concerning the causes of A-type or adakitic plutons in the magmatic belt of the Lower Yangtze Area. Since the thickened crust can also produce the magma with such chemical composition, some researchers assume that there used to be a plateau in East China (Zhang et al., 2008)； the plateau collapses, causing a series of extensional structures, and the crust thickness changed from 50 km (suggested by adakitic plutons) to 30 km (suggested by Seismic reflection data now) (Schmid et al., 2001). Despite other supporting evidence, the most important proof, adakitic plutons, can be caused by other possibilities, one of which is the differentiation of mantle magma in the normal crust. In addition, the reason why the crust thickened also remains unsolved.

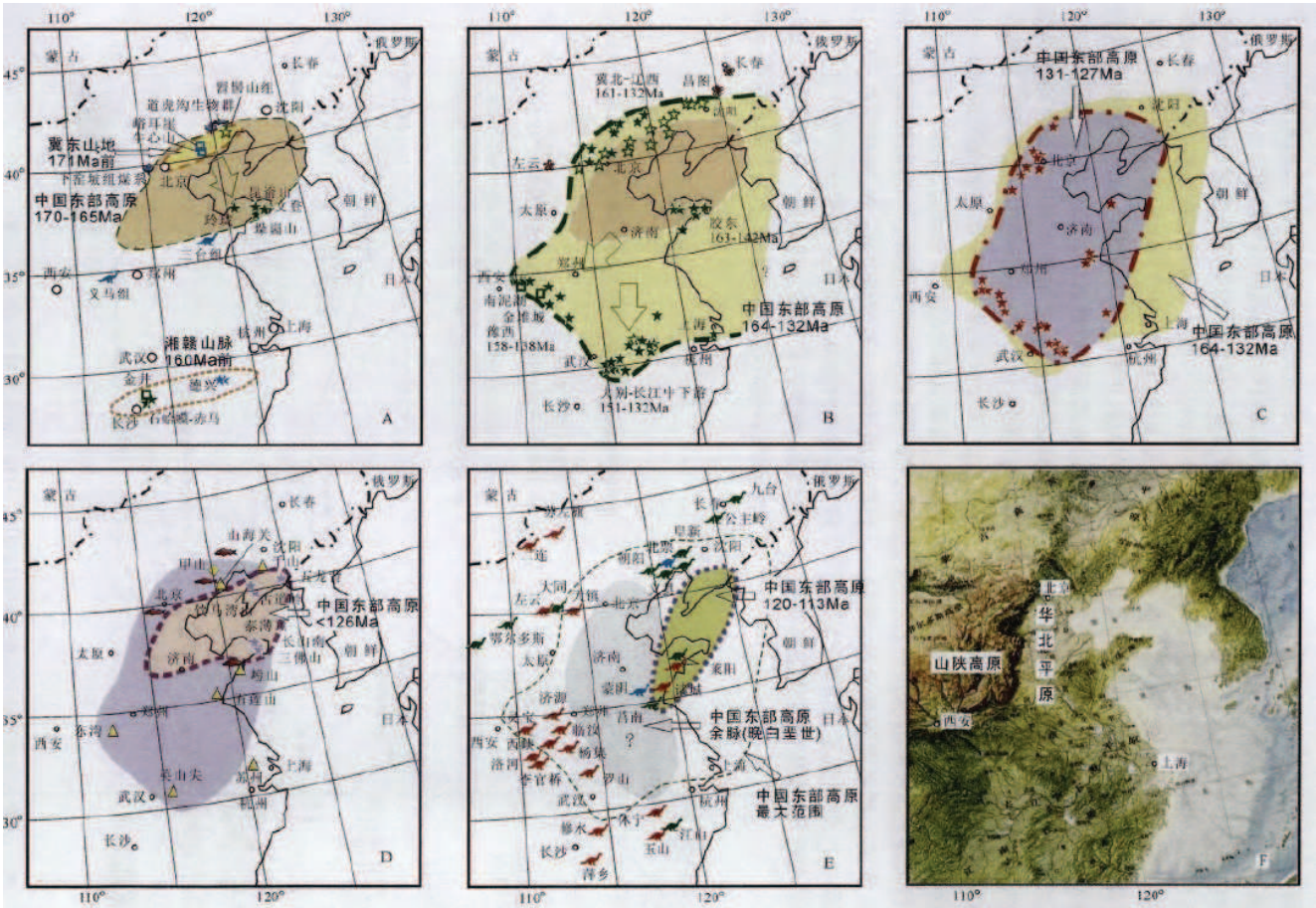

Figure 1 4: Hypothesis of plateau collaps

After (Zhang et al., 2008)

1.2.5 Hypothesis of Strike-Slip and Pull-Apart

Some researchers emphasize the role of the strike-slip tectonic regime in their Late Mesozoic geodynamic models of South China (Xu et al., 1987a; Charvet et al., 1990; Xu et al., 1990; Tong and Tobisch, 1996; Wang and Lu, 1997b, 2000; Li et al., 2001). In the most typical model, the Paleo-Pacific plate is represented by the northward subducting Kula plate. Its movement resulted in large shear displacement on the margin of East Asian continent, giving rise to the development of the sinistral strike-slip fault system featured by a series of NE-SW faults, such as Tancheng-Lujiang fault and Changle–Nan'ao fault (Xu et al., 1987a). The eastern edge of South China Block, therefore fell into the control of strike-slip and pull-apart tectonic regime, causing large pluton emplacements and the formation of pull-apart basins (Gilder et al., 1996). The recent structural analysis shows that Tancheng-Lujiang fault, the major representative of strike-slip regime, experienced ephemeral strike-slip movement, but existed mostly in the form of normal fault during the Late Mesozoic (Faure et al., 2003; Mercier et al., 2007). In addition, the hypothesis can hardly explain the massive emergence of NE-SW semi-graben basins formed on the land and under the sea in the South China Block (Shu et al., 2009b; Cukur et al., 2011).

Despite the controversy, current research still can not invalidate the hypothesis of strike-slip regime in the Late Mesozoic South China. The Tancheng-Lujiang fault is only one of the faults included in the hypothetical NE-SW strike-slip fault system. The other faults may have slipped enough to take in the important South China shear deformation resulted from the northward subduction of Kula plate. The Changle–Nan'ao fault and the strike-slip fault system in mid-Hunan and Jiangxi areas are examples of this kind (Charvet et al., 1990; Xu et al., 1990; Wang and Lu, 1997b; Li et al., 2001).

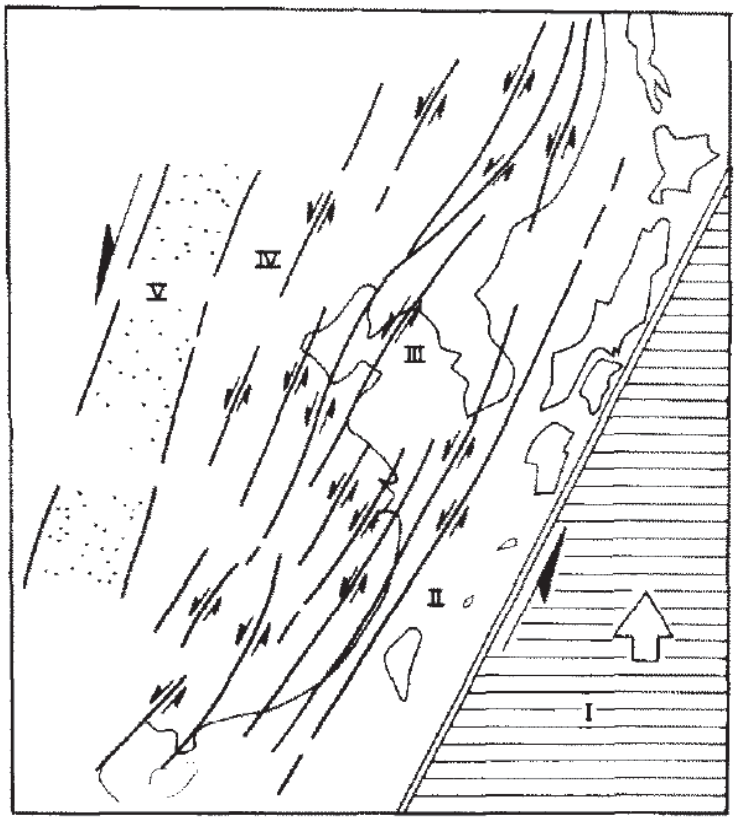

Figure 1 5: Hypothesis of Strike-Slip and Pull apart

After (Xu et al., 1987)

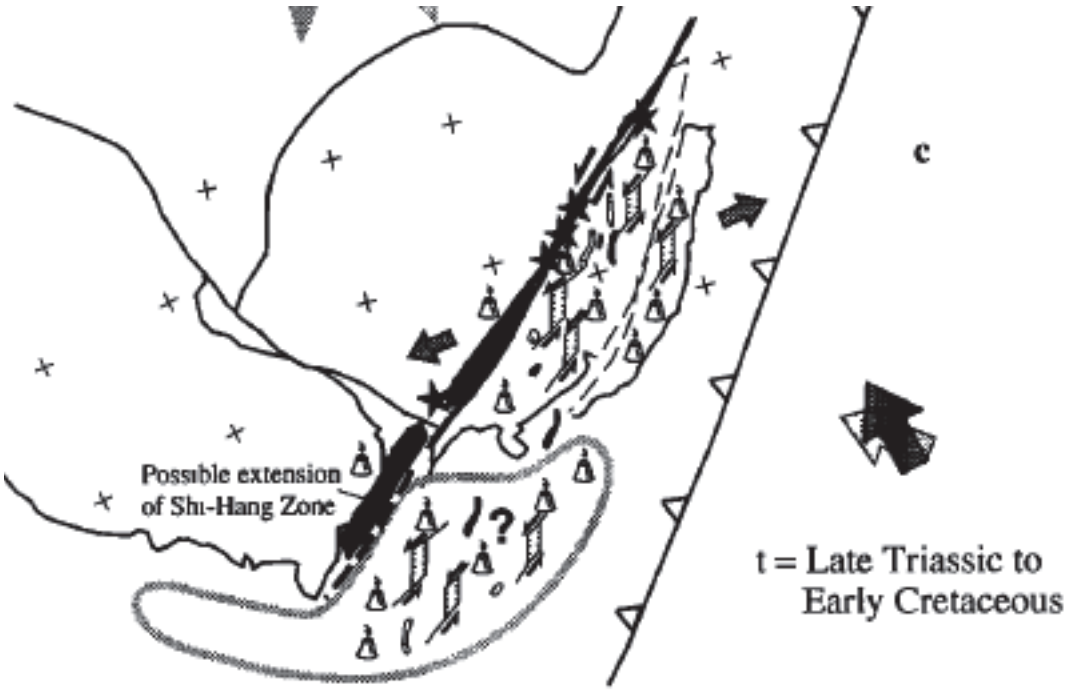

Figure 1 6: Hypothesis of Strike-Slip and Pull apart

After (Gilder et al., 1996)

2 Overview of the Study

2.1 Research Purpose and Contents

As mentioned above, in the late Mesozoic, a large crustal deformation occurred in South China, resulting in the formation of a large number of extensional basins, as well as pluton and dyke emplacements. However, there is no consensus on the dominating tectonic regime and geodynamic background in this region. Some researchers argue that the extensional regime plays a leading role in the tectonic evolution of South China in the Late Mesozoic (Gilder et al., 1991a; Goodell et al., 1991; Zhou et al., 2006; Shu et al., 2009b), while others believes in the importance of strike-slip regime (Xu et al., 1987a; Charvet et al., 1990; Xu et al., 1990; Tong and Tobisch, 1996; Wang and Lu, 1997b, 2000; Li et al., 2001).

Previous studies concentrate in the geochemical characteristics of granitic plutons in the South China, some of which have made relatively systematic analyses on basins and their structures. However, few have touched upon the regional tectonic information based on the processes of pluton emplacement.

The emplacement process is usually constrained by regional tectonic regime, and thus the investigation on such processes can offer some insights into the tectonic regime in the region. The large amount of Late Mesozoic granites in South China makes it possible to define and compare the tectonic regimes of various regions. Therefore, it is effective to understand the Late Mesozoic tectonic evolution in South China by investigating pluton emplacement. In this study, the important scientific issue in earth science - Late Mesozoic tectonic evolution in the South China - is divided into four separate, but interrelated and progressive questions:

（1）what were the emplacement mechanisms of the Late Mesozoic plutons in the South China?

（2）what were the regional tectonic regimes of pluton emplacement?

（3）what were the similarities and differences of tectonic regimes between individual regions in the same period?

（4）how did the tectonic regimes of various regions evolve throughout the Late Mesozoic?

The exploration of the questions above would shed some new light on a macroscopic

problem:

（5）what was the Late Mesozoic geodynamic background in South China?

2.2 Research Design and Methodology

The effective solution to the questions above is to investigate and analyze the tectonic regimes of typical regions in South China and then, through comparison and combination, establish a geodynamic model which can be compatible with multi-disciplinary data. Although previous studies have different understandings on the definition of paleo-Pacific, the direction of its subduction and the way it affects the tectonic evolution in South China, most of them agree on the effects of paleo-Pacific subduction on the Late Mesozoic tectonic evolution in South China (Jahn, 1974; Zhou and Li, 2000; Chen et al., 2002; Li and Li, 2007; Sun et al., 2007; Ling et al., 2009). Thus, we select the typical regions of different tectonic positions in the South China subduction system as the research targets. The first region is the Fujian coastal areas which have developed the Changle-Nan'ao belt. Closest to the paleo-Pacific subduction zone, the belt is thought to be a 200km strike-slip fault caused by the NNW subduction of paleo-Pacific plate. The second region is the Lower Yangtze Area (or Lower Yangtze Drainage Basin Area). It is believed to be the region where the Paleo-Pacific Mid-Ocean Ridge subducted westwards to Eurasia, resulting in the development of symmetrical I-type, A-type and adakitic pluton belts. This region is also thought to have the thickened crust where the gradual collapse of Late Mesozoic occurred. Furthermore, there is a NW-SE magmatic belt developed around 145Ma, a period of magma emplacement quiescence. Hunan, the third region, is close to the edge of the 1300km deformation belt caused by paleo-Pacific subduction, and close to the starting point of the coastal ward migration of pluton emplacement in the Jurassic-Cretaceous period in the South China, and hence it is a typical region with Cretaceous extensional structure. Also, of all the three regions, Hunan is the farthest tectonic position to the paleo-Pacific subduction zone. Several target plutons in Fujian, the Qingyang-Jiuhua Massif (or the Qingyang-Jiuhua composite plutons) in Southern Anhui, Hengshan composite plutons in Hunan are selected for multi-disciplinary study. Research methods include: field structural observation, lab microscopic observation, magnetic fabric (AMS) measurement, Paleomagnetism method, gravity modeling, Al-total content in Amphibole geobarometrical calculation, monazite U-Th-Pb microprobe

analysis, etc.

2.3 Workload of the Study

This research is sponsored by the Ministry of Land and Resources grant (201211024-04), NSFC(41225009), National Science and Technology Major Project（Grant 2011ZX05008 -001）, and Major Project of Chinese Academy of Sciences (Grant KZCX1-YW-15-1). In this study, a number of regions in South China have been selected to investigate the tectonic evolution in the Late Mesozoic from a multi-disciplinary perspective. The PhD candidate is also sponsored by Sino-Europe Joint Doctoral Promotion Program (DPP) Scholarship of Chinese Academy of Sciences. The detailed workload is listed in Table 1-1.

Table 1 1 Workload of the Study

NO.	Tasks	UNIT	Fujian	Qingyang-Jiuhua massif	Hengshan Massif	Total
1	observation sites	piece	429	169	81	679
2	fabric acquired	piece	167	84	44	295
3	hand samples acquired	piece	77	70	47	194
4	Identification of rock thin sections	piece	112	65	35	212
5	AMS sampling sites	piece	109	93	33	235
6	AMS test samples	piece	885	652	282	1819
7	IRM test samples	piece	44	7	2	53
8	Thermomagnetic curve test samples	piece	38	9	0	47
9	Hysteresis loop test samples	piece	23	7	2	32
10	Paleomagnetic tests samples	piece	69	55	0	124
11	Gravity modeling profile	piece	0	6	0	6
12	Density sample test	piece	3	15	32	50
13	Hornblende geobarometer thin sections	piece	0	3	0	3
14	Monazite SEM experiment samples	piece	9	0	3	12
15	monazite electron-probe microanalysis samples	piece	2	0	1	3

2.4 Major Findings and Innovations

The study has a series of valuable data and discoveries, providing insights into the regional tectonics. The major findings include:

（1） The Changle-Nan'ao belt experienced NW thrust mainly between 130 Ma - 110 Ma. The NW thrust may be associated with the collision between the Philippine micro-continent and the South China Block. The belt, coupled with the Ophiolitic suture zone in the West Philippines, formed a thrust-back thrust dual belt on the Andean-type continental margin of the South China Block;

（2） The emplacement of Qingyang-Jiuhua plutons during 140 Ma – 130 Ma was permissive. This region was under the control of NW-SE weak extensional regime during this time, and it has not experienced any strong strike-slip displacement since then.

（3） Of all the Hengshan Granitic Massif, the Baishifeng Two-Mica Granitic Pluton experienced a permissive emplacement with vertical magmatic injection in 150 Ma. All through the Cretaceous, this region was influenced by WNW-ESE extensional regime.

（4） After 105Ma, Changle-Nan'ao belt began a weak NW-SE regional extensional regime, signaling the start of extensional regime's control across the entire South China.

（5） Combined with previous studies and the new findings above, this study attempts to propose a geodynamic model of Cretaceous tectonic evolution in South China.

These findings shed new light on the Late Mesozoic structural events in the South China Block, providing further understandings of regional tectonic regime. The multi-disciplinary research methodology proves to be practical and effective in geological research, enriching to some degree the methodology in geological studies.

2.5 Structure of the Study

The paper consists of 7 chapters. Chapter one introduces the evidence of Late Mesozoic extensional events in South China and the major geodynamic hypotheses on this issue. This chapter also includes the research purpose, methods, work load and the major findings of this study. Chapter two describes the history of geological evolution in the South China from the Proterozoic to the Mesozoic. Chapter three investigates the Late Mesozoic deformation and

granite emplacement mechanism in the Changle-Nan'ao belt along the Fujian coast, attempting to discuss the regional tectonic regime's connection with the deformation and emplacement in this period. Chapter Four explores the Qingyang-Jiuhua emplacement mechanism of the plutons in Southern Anhui in order to reveal the regional tectonic regime during the process of emplacement. Chapter Five discusses the emplacement of Hengshan Granitic Massif, the movement of the fault on the western margin of Hengshan, as well as the opening of Zhajiang basin which is coupled with the Hengshan Granitic Massif, so as to reconstruct the regional tectonic evolution there from the transition period of the Jurassic and the Cretaceous to the Late Cretaceous. Chapter six summarizes and discusses the features and similarities of the Late Mesozoic tectonic evolution of the three regions in the South China Block, and then incorporates the collected data and observations into a geodynamic model. Chapter seven includes the major findings and conclusions as well as the implications for further study.

Chapter 2 The Multi-Stage Tectonic Background of South China Block

This chapter focuses on the geological background of South China Block in different evolution stages and the current studies in this regard. From the Precambrian to Late Mesozoic, a series of important tectonic events occurred on the South China Block. The preexisting structures formed by these tectonic events, in various degrees, constitute the background of the Late Mesozoic extensional events in this study. We first set forth the basic geological features in the South China Block, and then sort the important tectonic events in the order of geological time.

1 Geological Features of South China

The South China, as its name implies, is the southern part of China. In the geographic studies, the South China refers to the south of Qingling-Dabie Mountains-Huaihe River, east of the Tibean Plateau, and west of the coastline of East China Sea and South China Sea. The South China Block (SCB), in the sense of geology, covers a similar area. It is separated from the North China Block by the Qingling-Dabie orogen, the Tancheng-Lujiang fault and Sulu orogen to its north, the Songpan-Ganzi Block by the Longmenshan fault to its northwest, and the Indochina Block by the Songma-Songchay suture zone to its southwest (Fig. 2-1). The continental shelf along the Southern coast is also part of the South China Block. The current SCB only covers the southern area of China, but in Cretaceous and the earlier periods, West Philippines and some islands with ancient basements in the South China Sea were also part of the SCB. These segments were broken off from the main body of SCB in Cenozoic due to the opening of the South China Sea.

SCB is composed of Yangtze plate and Cathaysia Block. Unlike other Precambrian cratons, it experienced a long and complex tectonic evolution in the Phanerozoic. The tectonic movements in Neoproterozoic, Early Paleozoic, Triassic, Jurassic and Cretaceous periods resulted in conspicuous crust deformation (Mattauer et al., 1985b; Charvet et al., 1996; Faure et

al., 2003, 2008, 2009; Shu et al., 2008c). Almost the entire SCB was involved in the deformation events except for the Sichuan basin. The previous tectonic events tend to influence the later ones, and the structure distribution of the later tectonic events is also subjected to the pre-formed structures in the previous tectonic events. For instance, the Late Mesozoic "Ganhang rift" basin developed along the Neoproterozoic ophiolitic mélange, because this was the weakest zone in the South China Block. Hence, the effects of inherited structures should be taken into consideration in the exploration of the later tectonic events. In the meantime, it is difficult to study the previous tectonic events, because their structures have been transformed by the later tectonic events. These complications pose a challenging situation in the study of South China tectonics. The following is the introduction of geological evolution of SCB in different stages.

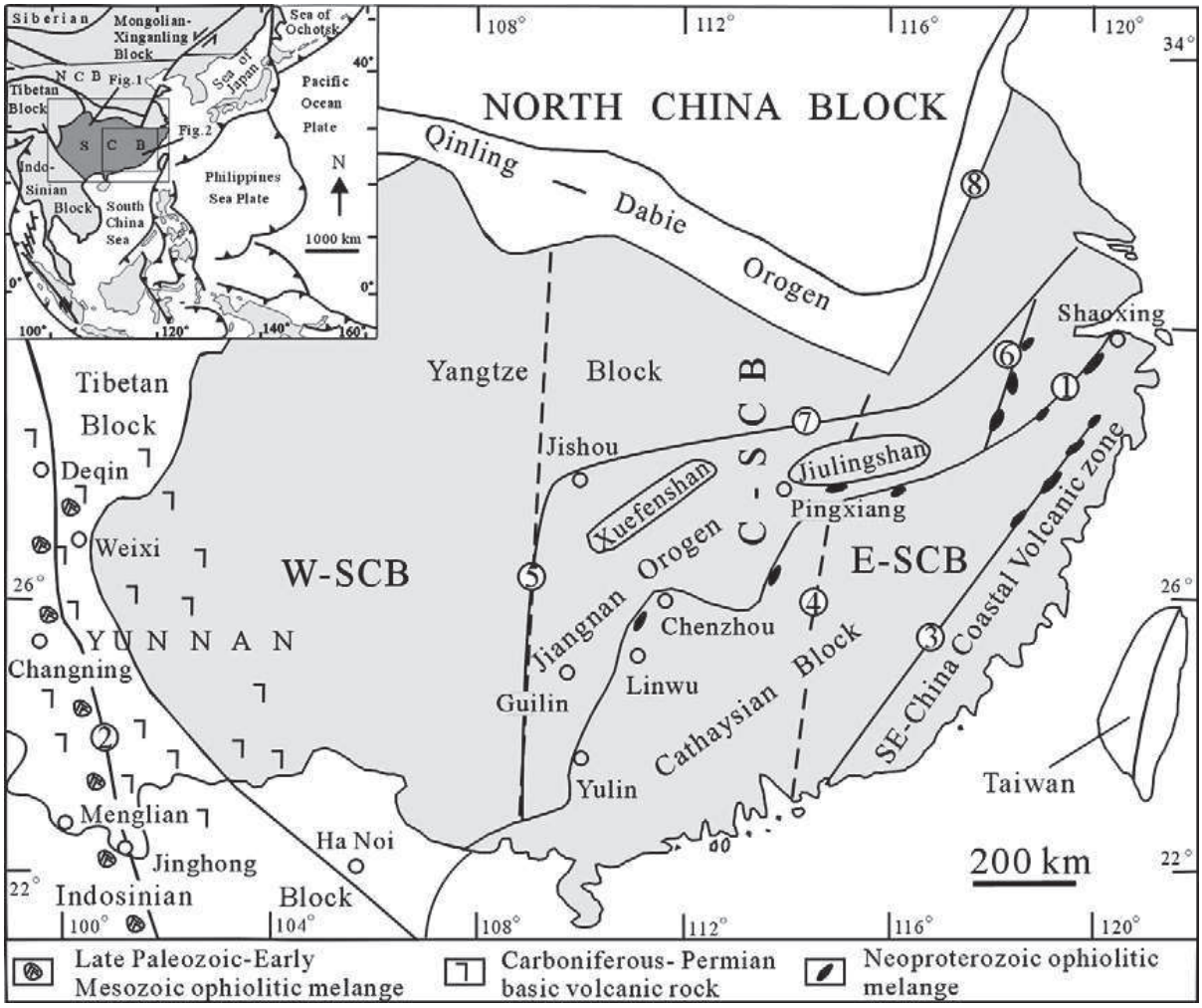

Figure 2 1: The South China Tectonic Map

After (Shu et al., 2008c)

2 The Multi-stage Tectonic Events in the South China Block

2.1 Precambrian

The oldest rocks in the South China Block are a combination of TTG gneisses and associated metamorphosed mudstones along the Kongling Group in the Yangtze plate. According to the Sm-Nd age test, this set of rocks were separated from the mantle and formed the crust in ca. 3 Ga, constituting the oldest continental nucleus of the SCB (Qiu and Gao, 2000). The oldest rocks of the Cathaysia block are mainly distributed in the northern Wuyi Mountain and the Yunkaidashan - Nanling areas. Hu Xiongjian (1994) points out that the age of diagenetic in the Badu group is around 2.0-2.4Ga. According to Li Xianhua, the zircon dating shows that the gneissic granite in northwestern Fujian is at the age of 2.6-1.9Ga（Li et al., 2011）. These are the oldest Cathaysia rocks (Hu, 1994; Li et al., 2011). The Neo Archean basement is expected to lie under the Neoproterozoic cover of the Wuyi Mountain, and the ancient substances in the Yunkai-Nanling area may stem from the other older continents (Yu et al., 2006a). Shu Liangshu has made systematic detrital zircon chronological study on the Paleozoic sandstones in the Jinggangshan and Nanling areas of Cathaysia plate. The study shows the growth periods of Cathaysia are concentrated in 2.56-2.38 Ga, 1.93-1.52 Ga, 1.3-0.9 Ga, 0.85-0.73 Ga and 0.68-0.55 Ga, and it has also been found magmatic zircon at the age of up to 3Ga (Xiang and Shu, 2010; Yao et al., 2011). Thus, the early Cambrian crust substances worked as continental nucleus in South China, and then grew and expanded based on the nucleus.

The most significant event in the Neoproterozoic period should be the formation of Jiangnan orogen and its subsequent participation in the global continental breakup event as a part of Rodinia supercontinent (Charvet et al., 1996; Shu et al., 2011; Wang et al., 2012; Zheng et al., 2007)). The Jiangnan orogeny is also known as the Jinning Orogeny or the Sibao Orogeny. The ultramafic and siliceous rock combinations were spread continually along the Shaoxing-Jiangshan-Pingxiang belt and the Dongxiang-Dexing-Shexian belt. They are considered as Ophiolites fragments, mostly as old as 0.9-1.0Ga (Li et al., 1994; Shu et al., 2006). The northeastern Jiangxi also grew blue schist, with a large amount of I-tyep granites along the area (Guo et al., 1996; Shu et al., 1993). This boundary, therefore, represents the suture zone of

the Yangtze and Cathaysia plates and the location of island arc (Li et al., 1994; Shu and Charvet, 1996; Wu et al., 2005; Shu et al., 2006; Gao et al., 2009). The detrital zircons study of the basement of the Jiangnan Orogen shows that the lower age limit of the orogeny is 1.0 Ga (Wang et al., 2007a), while the study of post-orogeny granite suggests that the upper age limit of this tectonic movement is 819-826Ma (Li, 1999).

With the formation of the Jiangnan Orogeny and the breakup of Rodinia supercontinent, the South China started the cleavage stage in the Nanhua period. From 800 to 760Ma, there were a lot magmatism associated with rifting events, which reflects the geochemical features of continental rifts. These magmatism were mostly emerging mantle materials in the continental crust (Li et al., 2003; Zheng et al., 2007; Shu et al., 2011; Wang et al., 2012). As the lithology is concerned, these igneous rocks were mostly bimodal magmatic rocks. Take the example of bimodal volcanites in East Zhejiang, their basalt is 794Ma, and the rhyolite 792Ma (Wang and Li, 2003). This breakup formed a broad passive continental margin, and a period of tectonic stability began (Wang and Li, 2003; Yan et al., 2004).

2.2 Early Paleozoic

The South China Block entered into a period of tectonic stability since the Neoproterozoic breakup. Yangtze plate developed a passive continental margin, and the Cathaysia block was split into Wuyi, Nanling, Yunkai blocks. The entire Southern basement is covered by thick marginal sedimentary of carbonate-clastic rocks from Sinian, Cambrian and Ordovician periods, but contemporary volcanic rocks and mafic intrusive rocks are missing (Shu et al., 2008b).

The South China revived in the Silurian. The revival is marked by the absence of the Silurian in the Cathaysia block. The strata after the Silurian overlie unconformably above the Sinian-Ordovician marginal sedimentary (Faure et al., 2009; Shu et al., 2009b). This orogeny formed the Wuyishan, Nanling, Yunkai fold belts, with most tectonic lines going along E-W or NE-SW strikes. The tectonic style is presented as closed, inverted, asymmetric, recumbent folds, with the highest shortening rate of 67%, which suggests how strong the tectonic movement was (Shu et al., 2008b). The kinematics study shows that in this orogeny, Wuyi Mountain thrusted in a fan-shaped style, its rock slices on the NW side thrusting northwestward and those on the SE side thrusting southwestward (Charvet et al., 2010). Evidence from Yukai Mountains also

suggests that there was a top-to-the-NW deformation in this tectonic movement (Lin et al., 2008). Therefore, it is quite likely that a NE-SW orogenic belt with a NW polarity existed along the Wuyi Mountain-Yunkai Mountains (Li et al., 2010c). The orogenic belt was present from 460 Ma to 440 Ma, and then, after the orogeny, entered into the stage of post orogenic extension, resulting in migmatization and magmatism (Faure et al., 2009; Charvet et al., 2010). With regard to the nature of this orogeny, some researchers believe that this was an intra-continental orogeny (Wang et al., 2007b; Faure et al., 2009; Charvet et al., 2010; Wang et al., 2010); others think that there was a collision of plates and closure of oceanic basins (Liu, 1994).

2.3 The Early Mesozoic

After the late Paleozoic, peace returned to the South China Block. The paleogeographic patterns of Yangtze and Cathaysia lithofacies began to converge. At this time, the marginal clastic sediments in the Devonian and Carboniferous transformed to a combination of Middle Triassic epeiric shallow marine carbonate and siliceous rocks, filling in multiple sedimentary belts between faults. The thickness of these sediments was relatively stable. There were neither large volcanite interlayers nor sediments of deep-water facies, demonstrating the stable coastal-shallow water sedimentary characteristics from the Late Devonian to middle Triassic (Shu et al., 2008a).

In the Late Devonian, the South China again developed under the influence of convergent tectonic regime. The Paleo-Tethys Ocean in East Asian began to close, followed by strong deformation and magmatism. The Upper Triassic, therefore, unconformably overlies the strata of Middle Triassic and the earlier periods (GXBGMR, 1984; YNBGMR, 1984; FJBGMR, 1985; HNBGMR, 1987; GDBGMR, 1988). Meanwhile, in the southwest and west of southern China, there were a series of northward collages and accretion along the southwest border in South China by several terranes, such as the Songchay terrane, and eventually led to the suturing of the Indochina and South China Block, and left ophiolite fragments in the suture zone (Carter et al., 2001; Lepvrier et al., 2004, 2011). The ^{40}Ar-^{39}Ar dating on the collision-related ductile shear zone shows that the tectonic deformation occurred at the age of 250 Ma - 240 Ma (Lepvrier et al., 2004). The collision is known as the Indo-China Orogeny. On the southern margin of South

China, the kinematics of the Yunkai terrane indicates a contemporary top-to-the NE shear sense, which can be seen as a response to the collision (Lin et al., 2008; Lin et al., 2011;). In the west, Songpan-Ganzi terrane thrusted to the South China Block along the Longmenshan fault in the period of Indo-China Orogeny (Harrowfield and Wilson, 2005). The adakite characteristics of the plutons around 220 Ma suggest the existence of thickened crust, probably resulted from the thrust in the Indo-China Orogeny (Zhang et al., 2006; Zhang et al., 2007). In this thrusting belt, the undeformed granites cut through the geological structure of Indo-China Orogeny. The age of these granites is from 197 Ma to 153 Ma, indicating that the compaction had been ended in the Jurassic (Roger et al., 2004). On the northern margin of the South China, the Qinling-Dabie orogenic belt, separating the North China Block and the South China Block, is known for the high-ultra high pressure metamorphic caused by deep continental subduction (Hacker et al., 1998a; Wang and Cong, 1999). According to the results of U-Pb zircon test and monazite U-Th-Pb test on ultrahigh pressure terranes, the ultrahigh pressure metamorphic mostly occurred in 236 Ma – 244 Ma and 230 Ma – 220 Ma. In 220 Ma – 205 Ma, the beginning of amphibolite facies metamorphism marked the end of ultrahigh pressure metamorphism. The deep subduction of Dabie Mountain gave rise to the southward foreland fold-thrust belt in the South China Block, the Yangtze fold belt and Jiangnan orogenic belt thus forming a series of anticline / dome structures (Faure et al., 1998; Schmid et al., 1999; Li et al., 2010a). Currently, there are different views on the nature of Qingling-Dabie orogen in the Triassic. Some researchers point out that the North and South Blocks virtually collided and sutured in the Triassic, so the Qinling-Dabie orogenic belt was the result of an inter-plate orogeny (Schmid et al., 1999). Other researchers, however, believe that the North and South Blocks already finished the collision in the Paleozoic, and thus the Qinling-Dabie orogenic belt was an intra-continental orogen (Mattauer et al., 1985a).

How to understand the deformation across the entire South China Block? Was it an intra-continental or an inter-plates orogeny? The biggest controversy, in fact, still consists in the collision of Yangtze and Cathaysia plates. Though there is an absence of Triassic Ophiolites belt between the Yangtze and Cathaysia plates, the overall deformation in the South China conforms to the tectonic facies caused by inter-plate collisions, in view of the macroscopic deformation style. Kenneth Hsu et al, thus, interpret the Triassic South China as the alpine-type orogenic belt.

The Cathaysia plate thrusted to the Yangtze plate from a distance, resulting a series of klippes and structural windows (Hsu et al., 1988).

But in any case, be it an inland orogen or an inter-plate collision, the Indo-China Movement played a significant role in the tectonic evolution in the South China Block. It has established the boundaries and framework of this block. Since then, the marine environment ended in the South China and the stage of continental sedimentation began (Shu et al., 2009a; Shu et al., 2009b).

2.4 The Late Mesozoic

Compressional tectonic movement in the Triassic continued until the early Jurassic, leading to the development of numerous foreland basins and forming an unconformable contact between Late Jurassic and Early Jurassic strata in the Yangtze River region (Shu et al., 2009b). From a global point of view, Jurassic is an era of tectonic regime transformation. The Late Jurassic rifting activities in Nanling area symbolize the dominance of extensional regime in the Late Mesozoic, and the E-W tectonic line in the Indo-China Movement gradually changed into the NE-SW trend typical in the Late Mesozoic (Zhou et al., 2006). Certainly, the previous systematic studies on the Jurassic basalt in SCB questioned the existence of NW subduction of paleo-Pacific in the Jurassic (Chen et al., 2008). The most distinct feature from Jurassic to Cretaceous in the Late Mesozoic is the coastal ward migration of magmatic activities (Li and Li, 2007; Zhou and Li, 2000). The migration began from the end of the quiescence period of magmatism in South China, and lasted to the Late Cretaceous, with the front of magmatic activities moving to the Fujian and Taiwan coasts (Fig. 2-2; Lan et al., 1996; Qiu et al., 2000, 2008; Lan et al., 2008; Yui et al., 2009; Li et al., 2012). It is most feasible to interpret this evolutionary trend with deeper subduction angle of the Pacific/Paleo-Pacific to the South China Block or the roll back retreat of its flat subduction (Li and Li, 2007; Zhou and Li, 2000).

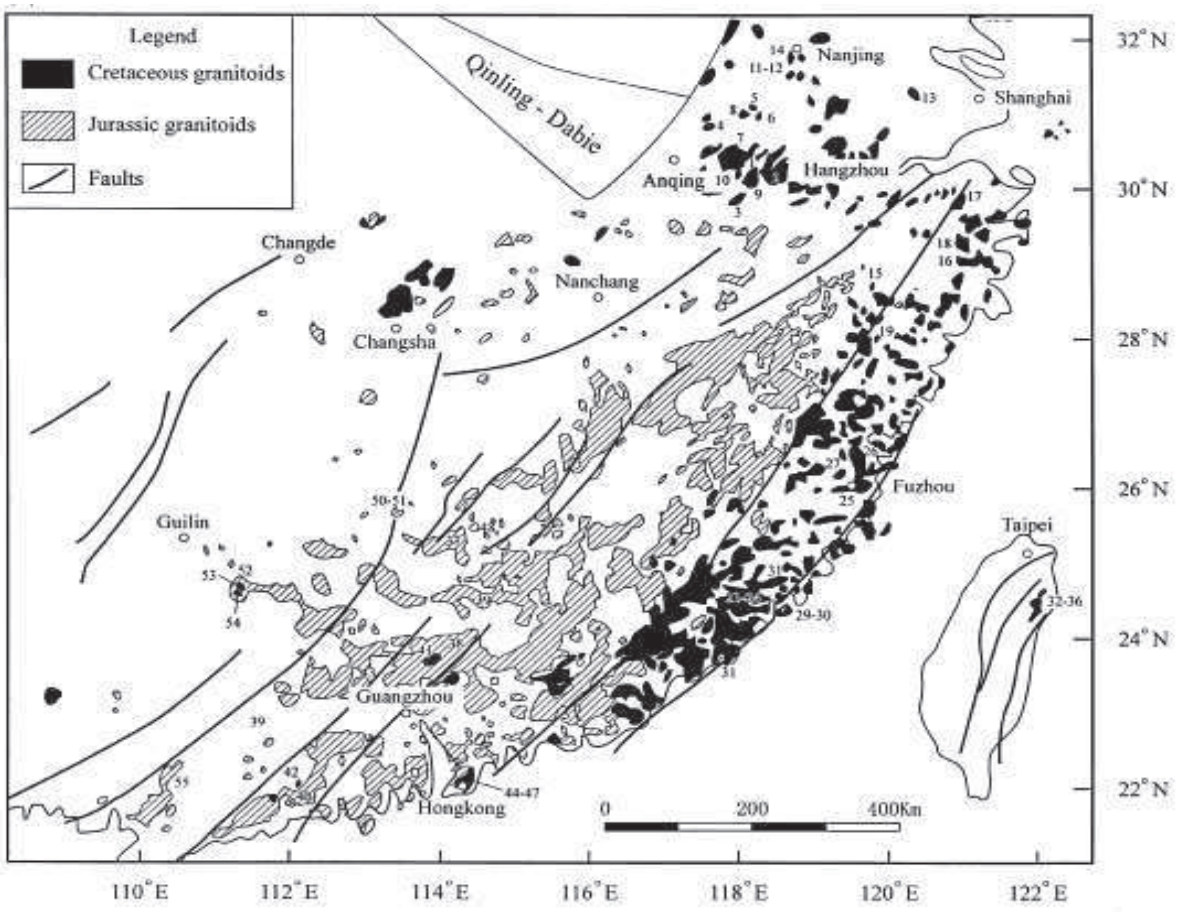

Figure 2 2: Distribution of Late Mesozoic Plutons in the South China

After (Li, 2000)

In the Late Mesozoic, the extensional tectonic dominated the entire South China Block. The Nanling area was the first area to begin the extension. With the eruptions of bimodal volcanites, it developed three E-W magmatic belts in the Late Jurassic (Zhou et al., 2006). By the time of Cretaceous, a number of normal faults had taken shape in the whole area. Some of the earlier strike-slip faults, such as the famous Tancheng–Lujiang fault, had developed into a normal fault in the early Cretaceous, which is believed to be caused by a deeper NW subduction angle of the Pacific (Mercier et al., 2007; Zhu et al., 2010). From inland Hunan to the Wuyi Mountain in Fujian, opened a series of red continental sedimentary graben / half-graben basins filled by coarse clastic sediments along these normal faults (Shu et al., 2009b). In Zhejiang and Jiangxi areas in particular, the graben basins along the earlier Neoproterozoic suture zone, also known as the "Ganhang rift", were filled with large amount of bimodal volcanites (Gilder et al., 1991a; Goodell et al., 1991). The geological bodies superimposed by several earlier tectonic events have

not escape the extension in the Late Mesozoic, neither. The NW-SE lineation runs throughout the Dabie Mountains, pointing at a top-to-the-NW direction. This is interpreted as the result of the detachment developed in an extensional regime in the Cretaceous. The ductile detachment fault of this orogeny was bent afterwards by the migmatite dome that the mid-Dabie terrane developed later (Faure et al., 2003). When the migmatite exhumed upwards, many syntectonic granites intruded in it and their marginal facies were ductile deformed. The lineation and kinematics of these granites suggest that they were moving under the NW-SE extensional background (Hacker et al., 1998; Faure et al., 2003). In Lushan Mountain and Wugong Mountain, the domes formed by compression in the Triassic also developed extensional tectonics in the Cretaceous. In 140 Ma, Lushan grew top-to-the-NW detachment faults, and Wugong Mountain developed granites of the same extensional structures (Faure et al., 1996; Lin et al., 2000; Zhu et al., 2010). In the southeast end of southern China, the Changle-Nan'ao belt in Fujian coastal areas grew a NE-SW A-type granite belt with miarolitic structure in the Late Cretaceous, indicating a rapid superficial emplacement. The contemporary NE-SW dyke swarms and the bimodal volcanite sequence sandwiched in Shimaoshan Formation also illustrate the existence of an extensional environment (Qiu et al., 1999, 2000; Dong et al., 2006; Qiu et al., 2008; Dong et al., 2010). The effects of extension did not stop at the coastline of South China Block. Seismic investigations show that there is an extensive distribution of late Cretaceous graben and semi-graben basins in the East China Sea continental shelf. The NE-SW trend of these basins and their peripheral faults also point to the NW-SE extension (Cukur et al., 2011).

2.3 Summary

This chapter describes the important tectonic events of various geological periods in the South China Block. Whether it is the formation of the Neoproterozoic Jiangnan Orogenic Belts and the subsequent break up or the Early Paleozoic Orogen, strong deformation and magmatic activities in the Early Mesozoic (the famous Indo-China Orogeny in the Triassic), or the widespread extensional tectonic movement in the Late Mesozoic, all of them have left significant imprints on the tectonic development and evolutionary history of the South China Block. Previous tectonic events have inevitably influenced the later tectonic events; the later events developed based on the previous events in varying degrees. The following chapters will further

discuss their relations based on the exploration of specific events.

Chapter 3 Back-thrusting in an active continental margin: Early Cretaceous NW-directed thrusting in the Changle-Nan'ao belt of the SE China coastal area

1 Introduction

The Late Mesozoic tectonic regime of the East Asia Continental Margin (EACM), and its relationship with the Paleo-Pacific subduction has long been debated in the geological community. The NNW subduction of the Paleo-Pacific slab or a NW drift Okhotomorsk Block were viewed as the cause of the development of a sinistral strike-slip regime responsible for continental-scale faults, such as the Tanlu fault system, Median Tectonic Line in Japan, and the Changle-Nan'ao fault zone in SE China (e.g. Xu et al., 1987; Faure and Natal'in, 1992, Sengor and Natal'in, 1993; Yang et al., 2013). Changing subduction direction of the Pacific slab could influence the tectonic features of the upper plate (Sun et al., 2007). An NW Paleo-Pacific (Izanagi?) flat subducting slab with variable dip angles or a retreating subduction zone could produce an extensional regime, and coastward migration of magmatic activities (Zhou and Li, 2000; Li and Li, 2007).

However, these interpretations are mostly based on granite geochemistry, and structural information is rarely provided. Since the Paleo-Pacific slab disappeared, the Cretaceous tectonics evidence from the continental crust of E. Asia margin is crucial to document the geodynamics of this area.

The Changle-Nan'ao belt (CNB), being the easternmost structure zone close to the assumed subduction trench along the coastal area of SE China, has been considered as a sinistral intracontinental strike-slip fault whose displacement attends 227 km (Xu et al., 1989; Charvet et al., 1990; Tong and Tobish, 1997;) or as a collision zone with a shear sense shifting from sinistral to dextral due to

microcontinent accretion (Hsu et al., 1990; Wang and Lu, 1997b). This zone has been also invoked to accommodate the Cretaceous continental deformation of Asia in response to the subduction and collision of the West Philippines Microcontinent before the Cenozoic opening of the S. China sea (Faure et al., 1989). Based on the $^{40}Ar/^{39}Ar$ dating, it was proposed that thrusting regime played an important role in exhuming the high temperature metamorphic rocks exposed to the SE of the CNB (Chen et al., 2002). Though attractive, this hypothesis was not substantiated by any structural proofs.

Structural analyses and Anisotropy of Magnetic Susceptibility (AMS) measurements have been conducted in order to answer following questions: 1) What is the Late Mesozoic tectonic regime of the CNB? 2) When did the displacement occur? 3) What is the geodynamic setting of EACM?

2 Geological Setting

Located on the SE. coast of SCB, the CNB is a NE-SW striking ca. 400 km long and 40-60 km wide ductile zone (Cui et al., 2013, Fig. 3-1a). It is an important geophysical anomaly belt such as bouguer gravity anomaly (Fig. 3-2). On the basis of lithology and structural analyses, we divide CNB into five units, namely 1) J_3 and K_1 pervasively deformed Gneiss Unit; 2) J_3 and K_1 Deformed Volcanite Unit; c) K_1 syntectonic granitoid intruded into the deformed rocks; d) K_2 undeformed isotropic plutons intruding into the previous rocks; e) K_2 undeformed volcanite, which unconformably overly the deformed rocks (Fig. 3-1b).

In the Gneiss Unit the granitoids and their sediment country rocks were ductilely deformed and metamorphosed in amphibolite facies to orthogneiss and micaschist (Tong and Tobisch, 1996) .

The Deformed Volcanite Unit which is on the NW side of CNB experienced a weak metamorphism (Tong and Tobisch, 1996). Several mylonitic zones developed in the J_3 and K_2 dacite, rhyolite and andesite (Douling and Nanyuan formations, respectively). Previous investigations indicate a NE-SW striking foliation (Charvet et

al., 1990; Wang and Lu, 2000). Some syntectonic granitoid intruding into the two deformed units are characterized by a magmatic foliation defined by the preferred orientation of biotite, feldspar, and amphibole, in particular on the pluton boundary. Microgranular mafic enclaves included in the syntectonic granitoid were stretched and oriented, but neither of them exhibit a post-solidus deformation (Li et al., 2003).

Numerous undeformed isotropic granitoid intruded into the previous rocks. Coeval NE-SW striking mafic and acidic dykes intruded and the Late Cretaceous andesite, rhyolite and bimodal volcanic series (Shimaoshan formation), covers the previous rocks.

In the past decades, hundreds of ^{40}Ar-^{39}Ar and U-Pb datings have been performed in order to assess the timing of the tectonic and magmatic events (Tab. 3-1). This geochronological dataset shows that the ^{40}Ar-^{39}Ar ages of the deformed rocks range from 133 Ma to 84 Ma (Wang and Lu, 1997a, 2000; Chen et al., 2002). The results of U-Pb zircon dating indicate that the micaschist and deformed granitoid are older than 130 Ma while the isotropic granitoids are younger than 100 Ma and the ages of the syntectonic granitoid are in between (Li et al., 2003; Liu et al., 2012; Cui et al., 2013; Fig. 3-3a; Tab. 1). The ages of the NE-SW striking dykes are ca. 90 Ma (Dong et al., 2006). The J_3 and K_1 volcanic rocks which were involved in the ductile deformation erupted from 168 to 130 Ma, whilst the undeformed Late Cretaceous volcanic rocks erupted during 104-95 Ma (Guo et al., 2012). Between 130 Ma and 104 Ma, there was a volcanic quiescence (Fig. 3-3b). Several geochemical studies show that the volcanic rocks and many granitic plutons, regardless of deformed or not, have magmatic arc affinities (Guo et al., 2012; Xu et al., 1999). Alkaline plutons emplaced at ca. 90 Ma are interpreted as intraplate extension-related bodies (Li et al., 2013b).

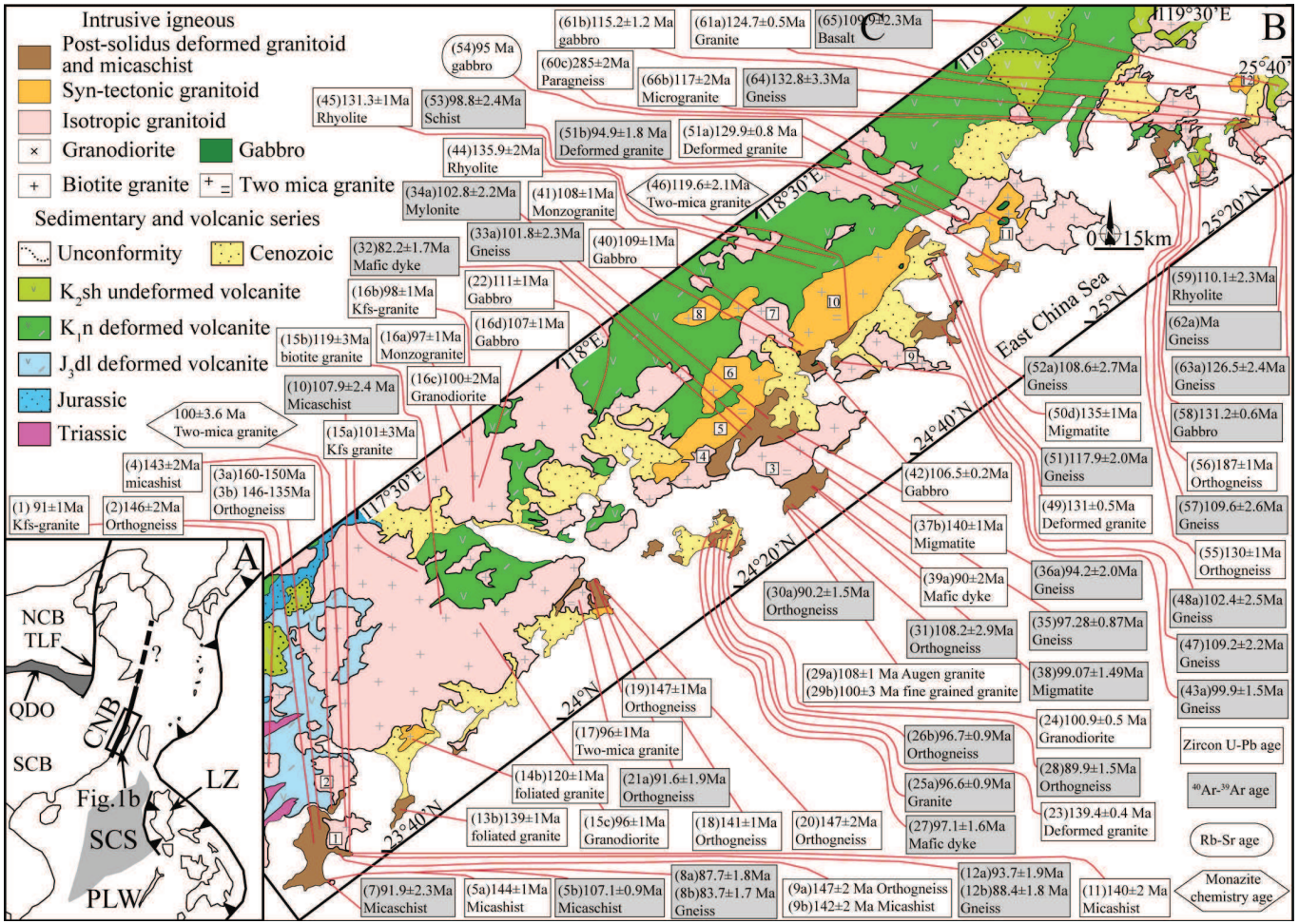

Figure 3 1: The sketch geologic map of the Changle-Nan'ao Belt and the age of the emplacement of plutons

a: Sketch tectonic map of east Asia during Cretaceous, b: the sketch geologic map of the Changle-Nan'ao Belt and the age of the emplacement of plutons. NCB: North China Block, SCB: South China Block, QDO: Qinling-Dabie Orogen, CNB: Changle-Nan'ao Belt, PPS: Paleo-Pacific Subduction Zone, SCS: South China Sea, LZ: Luzong Island, PLW: Palawan Island.

Table 3 1 Geochronology data of igneous and micaschist in Changle-Nan'ao Belt

number of location	location	lithology	age	bearing	method	mineral	reference
	Nanao island	Gneissic granite	160-155	*	U-Pb	Zircon	Cui et al., 2013
	Nanao island	Gneissic granite	136±1	†	U-Pb	Zircon	Cui et al., 2013
	Nanao island	Weakly deformed granite	133-123	§	U-Pb	Zircon	Cui et al., 2013
	Nanao island	weakly deformed granite	124±1	†	U-Pb	Zircon	Cui et al., 2013
1	Jingangshan	Alkali-feldspar granite	91±1	†	U-Pb	Zircon	Li et al., 2014
2	Lingyuan	gneissic granite	146±1	†	U-Pb	Zircon	Liu et al., 2012
3a	Jiaotou	gneissic granite	160-150	†	U-Pb	Zircon	Cui et al., 2013
3b	Jiaotou	gneissic granite	146-135	#	U-Pb	Zircon	Cui et al., 2013
4	Chendai	Micaschist	143±2	†	U-Pb	Zircon	Liu et al., 2012
4	Tongling	two-mica granite	100±3.6	†	U-Pb chemistry	Monazite	This study
5a	Aojiao	Micaschist	144±1		U-Pb	Zircon	Liu et

							al., 2012
5b	Aojiao	Mica schist	107.1±0.9		40Ar/^{39}Ar	Biotite	Wang and Lu 2000
7	Dongshan	Schist	91.9±2.3		40Ar/^{39}Ar	Muscovite	Chen et al., 2002
8a	Dongshan	Gneiss	87.7±1.8		40Ar/^{39}Ar	Biotite	Chen et al., 2002
8b	Dongshan	Gneiss	83.7±1.7		40Ar/^{39}Ar	K-fieldspar	Chen et al., 2002
9a	Jinshan	gneissic granite	147±2		U-Pb	Zircon	Liu et al., 2012
9b	Jinshan	Micaschist	142±2		U-Pb	Zircon	Liu et al., 2012
10	Donggu	Mica schist	107.9±2.4		40Ar/^{39}Ar	Muscovite	Wang and Lu, 2000
11	Yanya	Micaschist	140±2		U-Pb	Zircon	Liu et al., 2012
12a	Dongshan	Gneiss	93.7±1.9		40Ar/^{39}Ar	Muscovite	Chen et al., 2002
12b	Dongshan	Gneiss	88.4±1.8		40Ar/^{39}Ar	Biotite	Chen et al., 2002
13a	Guleishan	gneissic granite	160-150	*	U-Pb	Zircon	Cui et al., 2013
13b	Guleishan	gneissic granite	139±1	†	U-Pb	Zircon	Cui et al., 2013
13c	Guleishan	gneissic granite	137±1	†	U-Pb	Zircon	Cui et al., 2013

13d	Guleishan	gneissic granite	125±2	§	U-Pb	Zircon	Cui et al., 2013
14a	Duxun	weakly deformed granite	126-124	*	U-Pb	Zircon	Cui et al., 2013
14b	Duxun	weakly deformed granite	120±1	†	U-Pb	Zircon	Cui et al., 2013
14c	Duxun	weakly deformed granite	117±1	§	U-Pb	Zircon	Cui et al., 2013
15a	zhangpu-Chengxi	Alkali-feldspar granite	101±3	†	U-Pb	Zircon	Qiu et al., 2012
15b	zhangpu-Changqiao	Biotite granite	119±3	†	U-Pb	Zircon	Qiu et al., 2012
15c	zhangpu-Huxi	Granodiorite	96±1	†	U-Pb	Zircon	Qiu et al., 2012
16a	Gunong	Monzogranite	97±1	†	U-Pb	Zircon	Chen et al., 2013
16b	Xincun	Alkali-feldspar granite	98±1	†	U-Pb	Zircon	Chen et al., 2013
16c	Changtai granites	Granodiorite	100±2	†	U-Pb	Zircon	Chen et al., 2013
16d	Changtai gabbro	gabbro	107±1	†	U-Pb	Zircon	Chen et al., 2013
17	Taiwushan	two-mica granite	96±1	†	U-Pb	Zircon	Zhao et al., 2012
18	Baikeng	gneissic granite	141±1	†	U-Pb	Zircon	Cui et al., 2013
19	Gangwei	Gneissic granite	147±1	†	U-Pb	Zircon	Cui et al., 2013
20	Shenwo	augen granite	147±2	†	U-Pb	Zircon	Liu et al., 2012
21a	Shenwo	Gneiss	91.6±1.9		$^{40}Ar/^{39}Ar$	Hornblende	Chen et

							al., 2002
21b	Shenwo	Gneiss	86.9±1.8		40Ar/^{39}Ar	K-fieldspar	Chen et al., 2002
22	Huacuo	gabbro	111±1	†	U-Pb	Zircon	Li et al., 2012
23	Jinmen island	deformed granite	139.4±0.4	†	U-Pb	Zircon	Yui et al., 1996
24	Jinmen island	granodiorite	100.9±0.5	†	U-Pb	Zircon	Yui et al., 1996
25a	Jinmen	Granite	96.6±0.9		40Ar/^{39}Ar	Biotite	Lo et al., 1993
25b	Jinmen	Granite	83.5±0.3		40Ar/^{39}Ar	K-fieldspar	Lo et al., 1993
26a	Jinmen	Gneiss	100.8±0.6		40Ar/^{39}Ar	Hornblende	Lo et al., 1993
26b	Jinmen	Gneiss	96.7±0.6		40Ar/^{39}Ar	Biotite	Lo et al., 1993
26c	Jinmen	Gneiss	86.0±0.3		40Ar/^{39}Ar	K-fieldspar	Lo et al., 1993
27	Jinmen	Mafic dyke	97.1±1.6		40Ar/^{39}Ar	Hornblende	Chen et al., 2002
28	Jinmen	Gneiss	89.9±1.5		40Ar/^{39}Ar	Biotite	Chen et al., 2002
29a	Weitou	augen granite	108±1	†	U-Pb	Zircon	Liu et al., 2012
29b	Weitou	fine grain granite	100±3	†	U-Pb	Zircon	Liu et al., 2012
30a	Weitou	Gneiss	90.2±1.5		40Ar/^{39}Ar	Biotite	Chen et al., 2002

30b	Weitou	Gneiss	87.2±1.4		40Ar/^{39}Ar	K-fieldspar	Chen et al., 2002
31	Weitou	Gneiss	108.2±2.9		40Ar/^{39}Ar	Biotite	Wang and Lu 2000
32	Shidaoshan	Mafic dyke	82.2±1.7		40Ar/^{39}Ar	whole rock	Chen et al., 2002
33a	Shidaoshan	Gneiss	101.8±2.3		40Ar/^{39}Ar	Biotite	Chen et al., 2002
33b	Shidaoshan	Gneiss	87.0±1.8		40Ar/^{39}Ar	K-fieldspar	Chen et al., 2002
34a	Shidaoshan	Mylonite	102.8±2.2		40Ar/^{39}Ar	Hornblende	Chen et al., 2002
34b	Shidaoshan	Mylonite	88.0±1.8		40Ar/^{39}Ar	K-fieldspar	Chen et al., 2002
35	Lingxiushan	Gneiss	97.28±0.87		40Ar/^{39}Ar	Muscovite	Fu et al., 1989
36a	Lingxiushan	Gneiss	94.2±2.0		40Ar/^{39}Ar	Biotite	Chen et al., 2002
36b	Lingxiushan	Gneiss	86.0±0.8		40Ar/^{39}Ar	K-fieldspar	Chen et al., 2002
37a	Shenhu	Migmatitic gneiss	160-145	*	U-Pb	Zircon	Cui et al., 2013
37b	Shenhu	Migmatitic gneiss	140±1	#	U-Pb	Zircon	Cui et al., 2013
38	Shizhen	Migmatite	99.07±1.49		40Ar/^{39}Ar	Biotite	Fu et al.,

							1989
39a	Jinjiang	mafic dyke	90±2	†	U-Pb	Zircon	Dong et al., 2006
39b	Jinjiang	mafic dyke	87±2	†	U-Pb	Zircon	Dong et al., 2006
41	Quanzhou	Monzogranite	108±1	†	U-Pb	Zircon	Li et al., 2012
40	Quanzhou	gabbro	109±1	†	U-Pb	Zircon	Li et al., 2012
42	Taohuashan	gabbro	106.5±0.2	†	U-Pb	Zircon	Li et al., 1995
43a	Houtsu	Gneiss	99.9±1.5		$40Ar/^{39}Ar$	Biotite	Chen et al., 2002
43b	Houtsu	Gneiss	89.5±1.4		$40Ar/^{39}Ar$	K-fieldspar	Chen et al., 2002
44	Huian	rhyolite	135.9±2	†	U-Pb	Zircon	Guo et al., 2012
45	Huian	rhyolite	131.3±1	†	U-Pb	Zircon	Guo et al., 2012
46	Huian	two-mica granite	119.6±2.1	†	U-Pb chemistry	Monazite	This study
47	Duchuo	Gneiss	109.2±2.2		$40Ar/^{39}Ar$	Hornblende	Wang and Lu 2000
48a	Huian	Gneiss	102.4±2.5		$40Ar/^{39}Ar$	Hornblende	Chen et al., 2002
48b	Huian	Gneiss	101.4±2.5		$40Ar/^{39}Ar$	Biotite	Chen et al., 2002
48c	Huian	Gneiss	98.4±2.4		$40Ar/^{39}Ar$	K-fieldspar	Chen et al.,

							2002
49	Quanggang geshan	deformed granodiorite	131±0.5	†	U-Pb	Zircon	Li et al., 2003
50a	Liucuo	Fine-grained granite	142±2	*	U-Pb	Zircon	Cui et al., 2013
50b	Liucuo	Fine-grained granite	132±1	†	U-Pb	Zircon	Cui et al., 2013
50c	Liucuo	Garnet-bearing leucogranite	145±3	*	U-Pb	Zircon	Cui et al., 2013
50d	Liucuo	Garnet-bearing leucogranite	135±1	#	U-Pb	Zircon	Cui et al., 2013
50e	Liucuo	Garnet-bearing leucogranite	130-120	§	U-Pb	Zircon	Cui et al., 2013
50	Geshan	Gneiss	117.9±2.0		$^{40}Ar/^{39}Ar$	Biotite	Wang and Lu 2000
51a	Putian sucuo	deformed granodiorite enclave	129.9±0.8	†	U-Pb	Zircon	Li et al., 2003
51b	Sucuo	Microgranitic enlave	94.9±1.8		$^{40}Ar/^{39}Ar$	Hornblende	Li et al., 2003
52a	Putian	Gneiss	108.6±2.7		$^{40}Ar/^{39}Ar$	Hornblende	Chen et al., 2002
52b	Putian	Gneiss	106.7±2.6		$^{40}Ar/^{39}Ar$	Biotite	Chen et al., 2002
52c	Putian	Gneiss	94.5±2.3		$^{40}Ar/^{39}Ar$	K-fieldspar	Chen et al., 2002
53	Putian	Schist	98.8±2.4		$^{40}Ar/^{39}Ar$	Muscovite	Chen et al., 2002

54	Daiqianshan	gabbro	95	†	Rb-Sr	Zircon	wang 2002
55	Niutouwei	augen granite	130±1	†	U-Pb	Zircon	Liu et al., 2012
56	Jincheng	deformed granite	187±1	†	U-Pb	Zircon	Liu et al., 2012
57a	Gaoshan	Gneiss	109.6±2.6		$^{40}Ar/^{39}Ar$	Hornblende	Chen et al., 2002
57b	Gaoshan	Gneiss	105.3±2.1		$^{40}Ar/^{39}Ar$	Biotite	Chen et al., 2002
57c	Gaoshan	Gneiss	100.7±2.1		$^{40}Ar/^{39}Ar$	K-fieldspar	Chen et al., 2002
58	Lianhuoshan	Gabbro	131.2±0.6		$^{40}Ar/^{39}Ar$	Hornblende	Chen et al., 2002
59	Gaoshan	Rhyolite	110.1±2.3	†	$^{40}Ar/^{39}Ar$	whole rock	Chen et al., 2002
60a	Nanwuli	Paragneiss	1827±23	†	U-Pb	Zircon	Cui et al., 2013
60b	Nanwuli	Paragneiss	637±6	†	U-Pb	Zircon	Cui et al., 2013
60c	Nanwuli	Paragneiss	285±2	†	U-Pb	Zircon	Cui et al., 2013
61a	Pingtan	dioritic grabbro	115.2±1.2	†	U-Pb	Zircon	Dong et al., 1997
61b	Pingtan	granite	124.7±0.5	†	U-Pb	Zircon	Dong et al., 1997
62a	Pingtan	Gneiss	126.5±3.1		$^{40}Ar/^{39}Ar$	Biotite	Chen et al., 2002

62b	Pingtan	Gneiss	111.6±2.7		40Ar/^{39}Ar	K-fieldspar	Chen et al., 2002
63a	Pingtan	Gneiss	126.5±2.4		40Ar/^{39}Ar	Biotite	Chen et al., 2002
63b	Pingtan	Gneiss	116.3±2.4		40Ar/^{39}Ar	K-fieldspar	Chen et al., 2002
64	Pingtan	Gneiss	132.8±3.3		40Ar/^{39}Ar	Hornblende	Chen et al., 2002
65	Pingtan	Basalt	109.9±2.3	†	40Ar/^{39}Ar	whole rock	Chen et al., 2002
66a	Qiulu	Microgranite	138±3	*	U-Pb	Zircon	Cui et al., 2013
66b	Qiulu	Microgranite	117±2	†	U-Pb	Zircon	Cui et al., 2013
	Danyang	Monzogranite	100±5	†	U-Pb	Zircon	Lin et al., 2011
	Gushan	Biotite granite	107±5	†	U-Pb	Zircon	Lin et al., 2011
	Kuiqi	Peralkaline granite	95±3	†	U-Pb	Zircon	Lin et al., 2011
	Jiantian	Granodiorite	110±4	†	U-Pb	Zircon	Lin et al., 2011
	Nanzhen	granite	96.1±2.7	†	U-Pb	Zircon	Qiu et al., 2008
	Dacengshan	granite	93.1±2.4	†	U-Pb	Zircon	Qiu et al., 2008
	Sansha	granite	91.5±1.5	†	U-Pb	Zircon	Qiu et al., 2008
	Dajing	granite	93.8±1.8	†	U-Pb	Zircon	Qiu et

al., 2008

*, age of inherit zircon, †, zircon age of emplacement or eruption, §, zircon age of later thermal event, #, zircon age of migmatite. The locations of ages refer to Fig. 3-1.

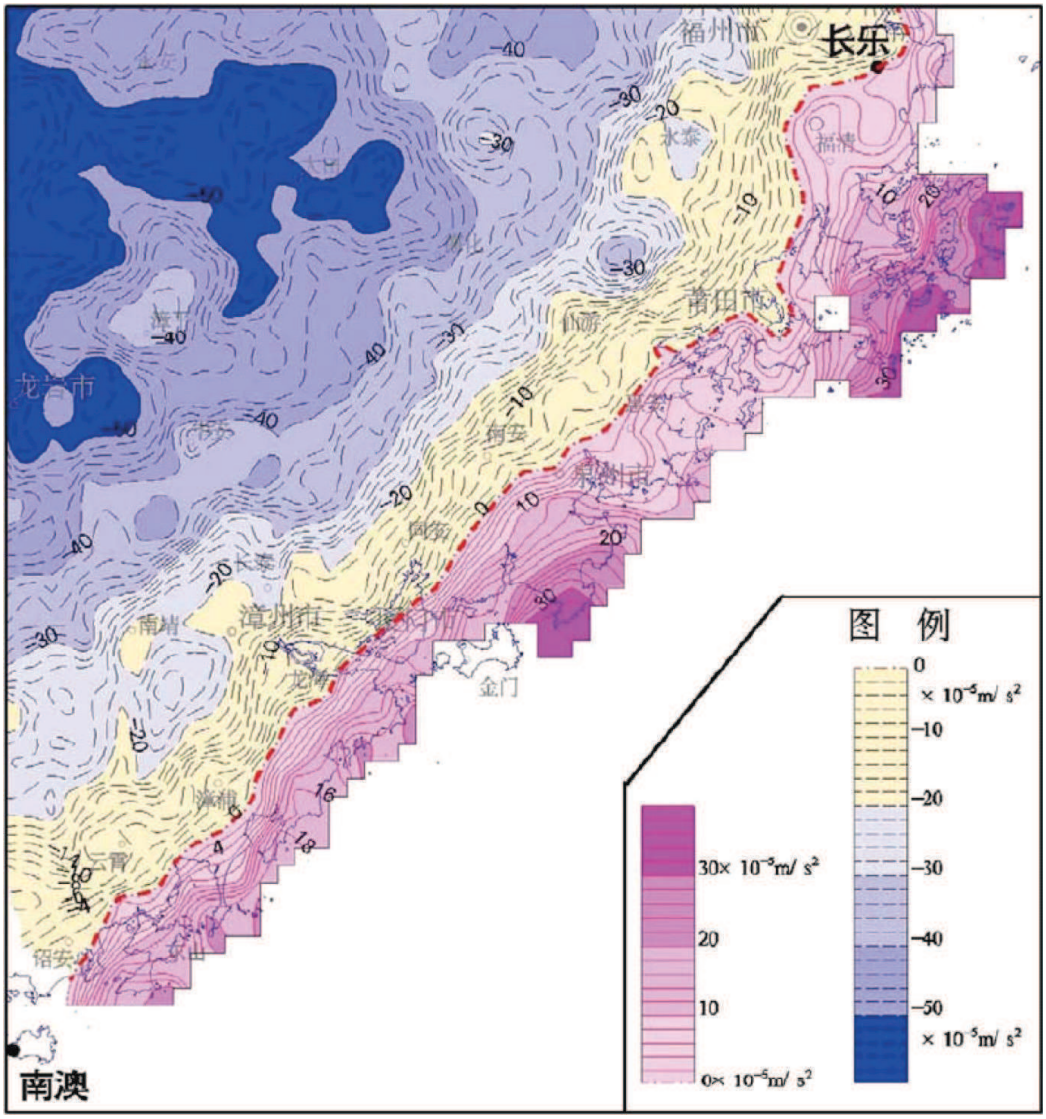

Figure 3 2: Bouguer Anomaly map of Changle-Nan'ao Belt and its adjacent area. (Shi, 2010)

3 New structural insights

For achieving the general view on the deformation style and fabric mode of CNB, we conducted a systematic structural investigation.

3.1 Gneiss Unit

All through the CNB, There develops folds and pervasive foliation in the migmatite, the pervasively post-solidus deformed granitoids (the orthogneiss) and micaschist of the Gneiss Unit. The foliation is formed by stretched quartz, micas and oriented feldspar (Fig. 3-4a, b, c, d, e). The foliation of the rocks in the Gneiss Unit is predominantly striking NE-SW with a variable dip indicating a fold effect after the formation of foliation (Fig. 3-5b, 1c1). NE-SW striking fold axes can be widely observed (Fig. 3-4b, 3-5b, 3-5c1). The stretching mineral and magnetic lineations are scattered (Figs. 3-5c3). They commonly strike NW-SE when the foliation is flat or moderate. When the foliation is steep, the lineation is down dip or NE-SW with nearly a horizontal dip. Most of the NE-SW lowly inclined lineation occurs in the Dongshan Island (location 1 in Fig. 3-5b). In this area, their developed NW-verging asymmetric folds in the mica schist (Fig. 3-4b). In the outcrop of such asymmetric fold, the NE-SW lowly inclined lineation and the NE-SW axis of fold are present together (Fig. 3-4b). Field observations of sigmoidal Quartz and K-feldspar (Fig. 3-4c) indicate a top-to-the-NW shear sense when the lineation is striking between NNW-SSE and WNW-ESE with a small dip angle. When the foliation is steep and lineation is down dip, the kinematic indicators show that the SE side is moving upward. For the NE-SW horizontal lineation, no shear sense can be established. The orientation of newly formed amphibole in the gneiss indicates a amphibolites phase metamorphism coeval to the deformation (Fig. 3-4d).

3.2 Deformed Volcanite Unit

As shown by systematic field work investigation, there developed several mylonite and hyper mylonite shear zone accommodating the main displacement of the J_3 and K_1 lavas in the Deformed Volcanite Unit (Fig. 3-4f and g), while the main body of the J_3 and K_1 lavas was not deformed (Fig. 3-4h). The deformed volcanite share the same planar and linear fabric as the Gneiss Unit, although the deformation is

heterogeneous (Fig. 3-5b, 3-5c1, 3-5c2, 3-5c3, 3-5c4 and 3-5d). the variation of dips of the deformed volcanite indicates a fold effects after the formation of the foliation which can be also observed in the outcrop (Fig. 3-4 f and g). Field observations of shear bands, sigmoidal, and SC fabric of quartz, indicate a top-to-the-NW shear sense when the lineation is shallow dipping, or NW side down/SE side up shear sense when the lineation is steeply dipping (Fig. 3-4i and j). The folding of the foliation indicates a top-to-the-NW vergence that complies with the ductile kinematics. In the Jiangyin island of Fuqing area (location 7 in Fig. 3-5b), a cleavage crosscuts the bedding of the sediments interbedded in the volcanic rock series. The bedding-cleavage relationships indicate also a NW-verging folding.

The boundary between the Gneiss and the Deformed Volcanite Units is not exposed, however, in the Fuqing area, on the Deformed Volcanic Unit near the boundary, an ultramylonite layer with, down dip lineation with shear bands and asymmetric folds is observed. These criteria indicate that the NW and SE sides are moving downward and upward, respectively (Fig. 3-4i andj; location 8 in Fig. 3-5b). On the Gneiss Unit side of this boundary, the orthogneiss foliation trends N70E, NW85 and the stretching lineation strikes NE60 with a 60° dip angle. The NW side-moving-downward sense of shear indicated by asymmetric tails around K-feldspar is consistent with that documented in the ultramylonitic volcanite (location 8 in Fig. 3-5b).

3.3 Syntectonic granitoids

In agreement with previous workers, several syntectonic granitoid with ages coincident with the 130-104 Ma volcanic quiescence, are recognized in the CNB (Li et al., 2003; Guo et al., 2012; Liu et al., 2012; Cui et al., 2013). The sny-tectonic granitoids are predominant spindle shaped with a NE-SW strike (Fig. 3-1b, location 5, 6, 8, 10, 11, 12). On the southeast coast of the Dongshan island (location 1 in Fig. 3-1b), the margin of a Two-Mica granite is foliated in accordance with the micaschist country rocks foliation, while inside the pluton, the preferred orientation is represented by NE-SW striking schlierens. The similar trend of schlieren, magmatic

fabric, metamorphic foliation of the country rock argue for a syntectonic pluton. Near Duxun (location 4 in Fig. 3-5b), a two-mica granite yielding a 120 Ma age (Cui et al., 2013) also exposes an isotropic core and a foliated boundary oriented N60E, SE70 (Fig. 3-1b). On the coast of Weitou and Niutouwei (locations 5 and 8 in Fig. 3-1b), magmatically foliated augen granodiorites are dated at108±1 Ma and 130±1 Ma, respectively (Liu et al., 2012). In these areas, the main parts of the plutons are covered by sea. The boundary between the syn-tectonic granitic dykes and the country rocks are wavy and parallel to the foliation of the country rocks, indicating the emplacement was in ductile deformation domain and coeval to the deformation (Fig. 3-4l). Many syn-tectonic plutons include numerous microgranitoids enclaves which was considered as mafic magma injection during the emplacement of the syn-tectonic granitoids (Dong et al., 1998; Li et al., 2003a; Xing et al., 2010). In this study, the observation of tails developed in the enclaves argues that during the mafic magma injection, the host magma had not been fully crystallized (Fig. 3-4m). These syn-tectonic microgranitoids enclaves also recorded the regional strain. For example, the shape of these enclaves is oblate and the ab surfaces are parallel to the magmatic foliation of the host rocks (Fig. 3-4m). For example, the orientation of ab surface of the syn-tectonic microgranitoids enclave is N35E, NW70, while the magmatic foliation of the host rocks is N45E, NW70.

3.4 Isotropic Granitoids and Undeformed Volcanite

Isotropic granitoids, younger than 100 Ma, intrude the CNB extensively (Fig. 3-1b and 3-3). These plutons are undeformed and featured by massive structure and magmatic texture (Fig. 3-4n). Their emplacement did not alter the previous fabric in the gneiss and micaschist (e.g. location 2 in Fig. 3-5b). Coevally with the emplacement of the isotropic granitoids, the volcanic activity is represented by undeformed lava flows that unconformably overly upon the previously deformed units (Fig. 3-5b and d).

3.5 Late Narrow strike-slip shear zones

In field, several NE-SW dextral strike-slip shear zones have been observed in a few of outcrops. Due to the scarcity of their outcrops, they can hardly be mapped. These shear zones are only several cm in width, which is totally different with the pervasive deformation of the Gneiss and the Deformed Volcanite Units. Field observation shows that the narrow dextral strike-slip shear zone crosscut the undeformed isotropic granitoid (Fig. 3-4p; location 8 in Fig. 3-5b), indicating a late deformation event in the evolution of the CNB. In the following, these shear zones will not be considered.

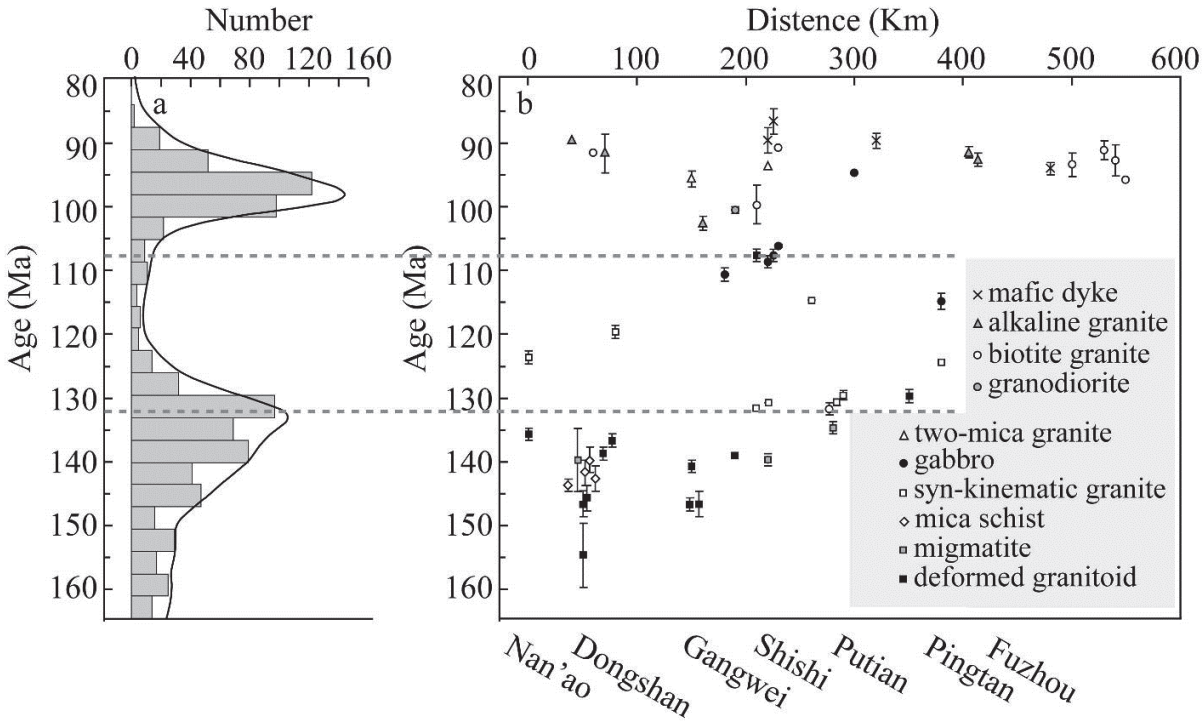

Figure 3 3: The geochronology framework of Changle-Nan'ao Belt

a: age distribution of volcanite in CNB (Guo et al., 2012), b: age distribution of granitoid and micschist (part of data after Yang's unpublished data)。

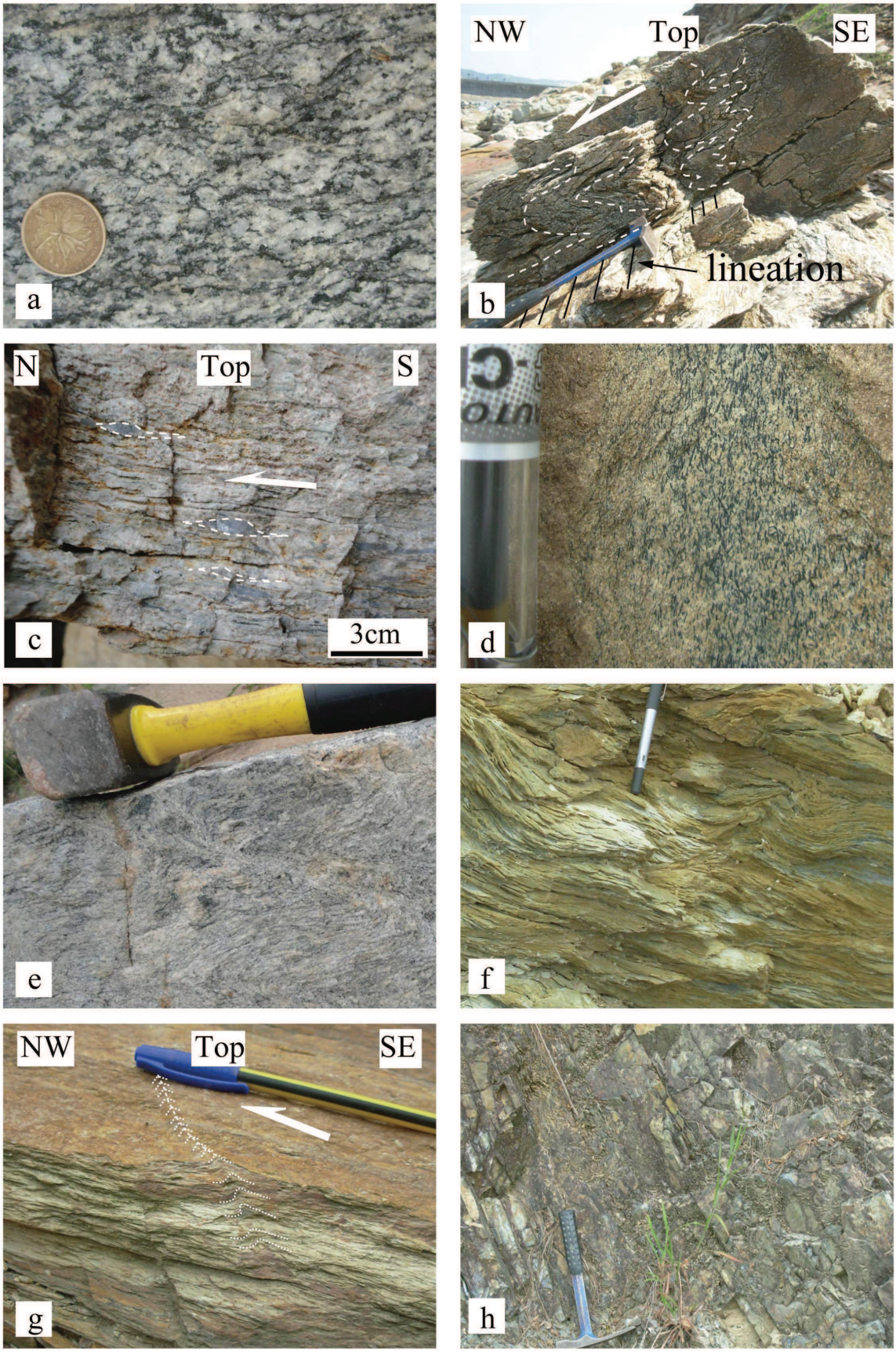
a
NW
Top
SE
lineation
b
N
Top
S
3cm
c
d
e
f
NW
Top
SE
g
h

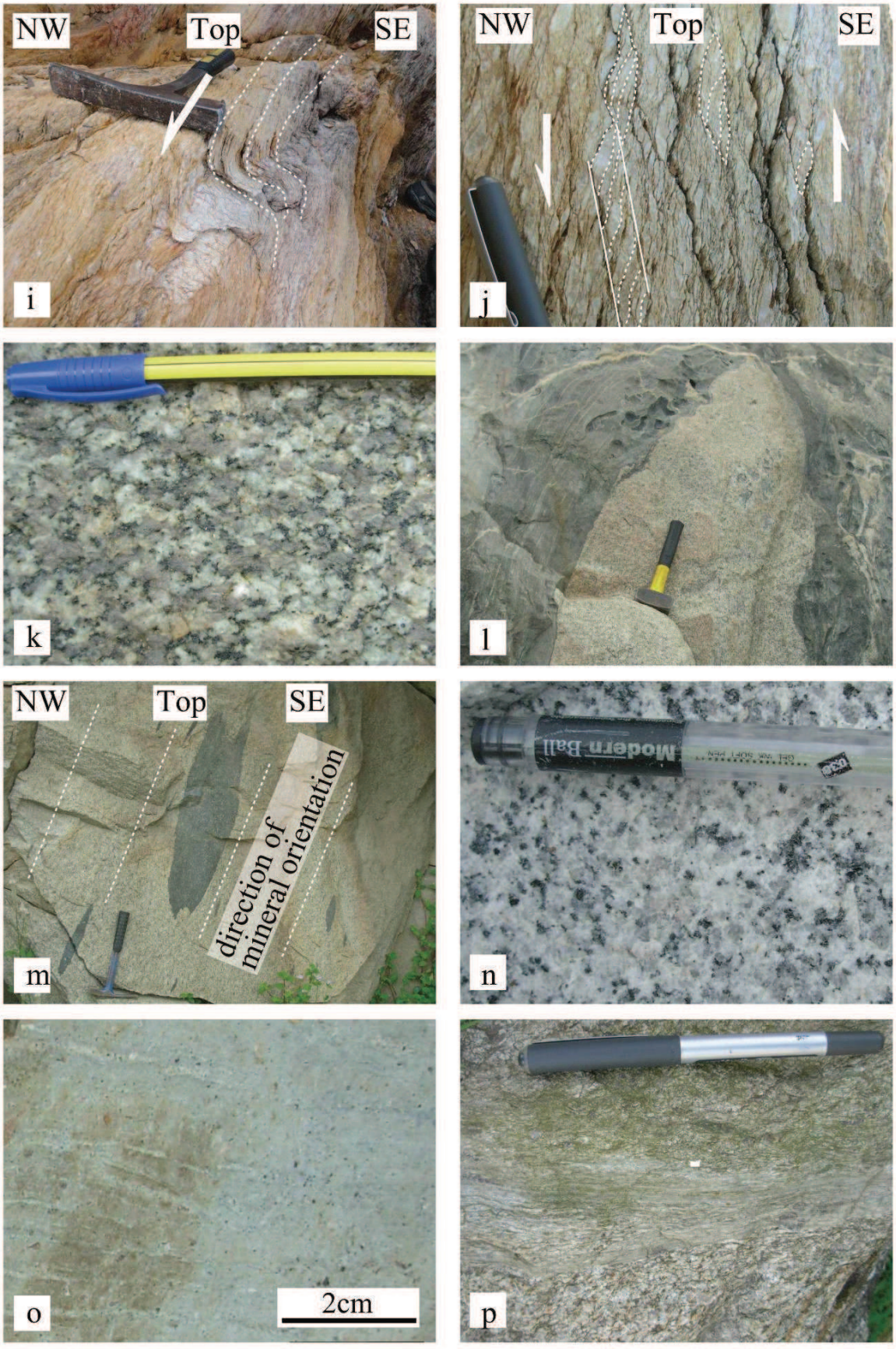

Figure 3 4: Photos of macro structural observation in field

a: pervasively post-solidus deformed granitoids in the Gneiss Unit, b: NW-verging asymmetric NE-SW striking fold in the Dongshan island, the fold axis and the lineation is parallel with each other and can be observed simultaneously, indicating a related origion (location 2 in Fig. 3-5), c: along the direction which is parallel to the NW-SE or N-S lineation and perpendicular to the foliation, "sigmoidal" quartz indicates a top-to-the-N shear sense (location 5 in Fig. 3-5), d: newly formed amphibole in amphibolites are oriented indicating the deformation occurred in a amphibolites metamorphic phase (location 29 in Fig. 3-5), e: the magmatic foliation of the migmatite was folded (location 3 in Fig. 3-5), f: the foliation of the deformed volcanites was folded (location 28 in Fig. 3-5), g: the bending of the foliation in deformed volcanites indicates a top-to-the-NW shear sense (location 30 in Fig. 3-5), h: not all of the Early Cretaceous volcanites of the Nanyuan Formation was deformed by mylonites (location 7 in Fig. 3-5), i: near the boundary of the Deformed Volcanites Unit and the Gneiss Unit, the foliation of the deformed volcanites is vertical and the asymmetric folds indicates the NW-side-down, SE-side-up (location 27 in Fig. 3-5), j: near the boundary of the Deformed Volcanites Unit and the Gneiss Unit, the foliation of the deformed volcanites is vertical and the shear bends indicates the NW-side-down, SE-side-up (location 27 in Fig. 3-5), k: the minerals in the Early Cretaceous syn-tectonic granitoids is oriented without deformation (location 26 in Fig. 3-5), l: the boundary between deformed volcanites and syn-tectonic granitic dykes is wavy and parallel to the foliation, and the foliation did not crosscut the boundary and the syn-tectonic dykes, that indicates during the emplacement of dykes, the deformation is still active (location24 in Fig. 3-5), m: the microgranitoids enclaves in the Early Cretaceous syn-tectonic granitoids forms "fish swarm structure", the ab surfaces of the enclaves are parallel to the magnetic foliation of the host rocks (location 22 in Fig. 3-5), n: the Late Cretaceous granitoids were not deformed (location 31 in Fig. 3-5), o: the Late Cretaceous volcanites were not deformed (location 32 in Fig. 3-5), p: the late NE-SW striking narrow mylontic zone crosscut the Late Cretaceous undeformed isotropic granitoids (location 22 in Fig. 3-5).

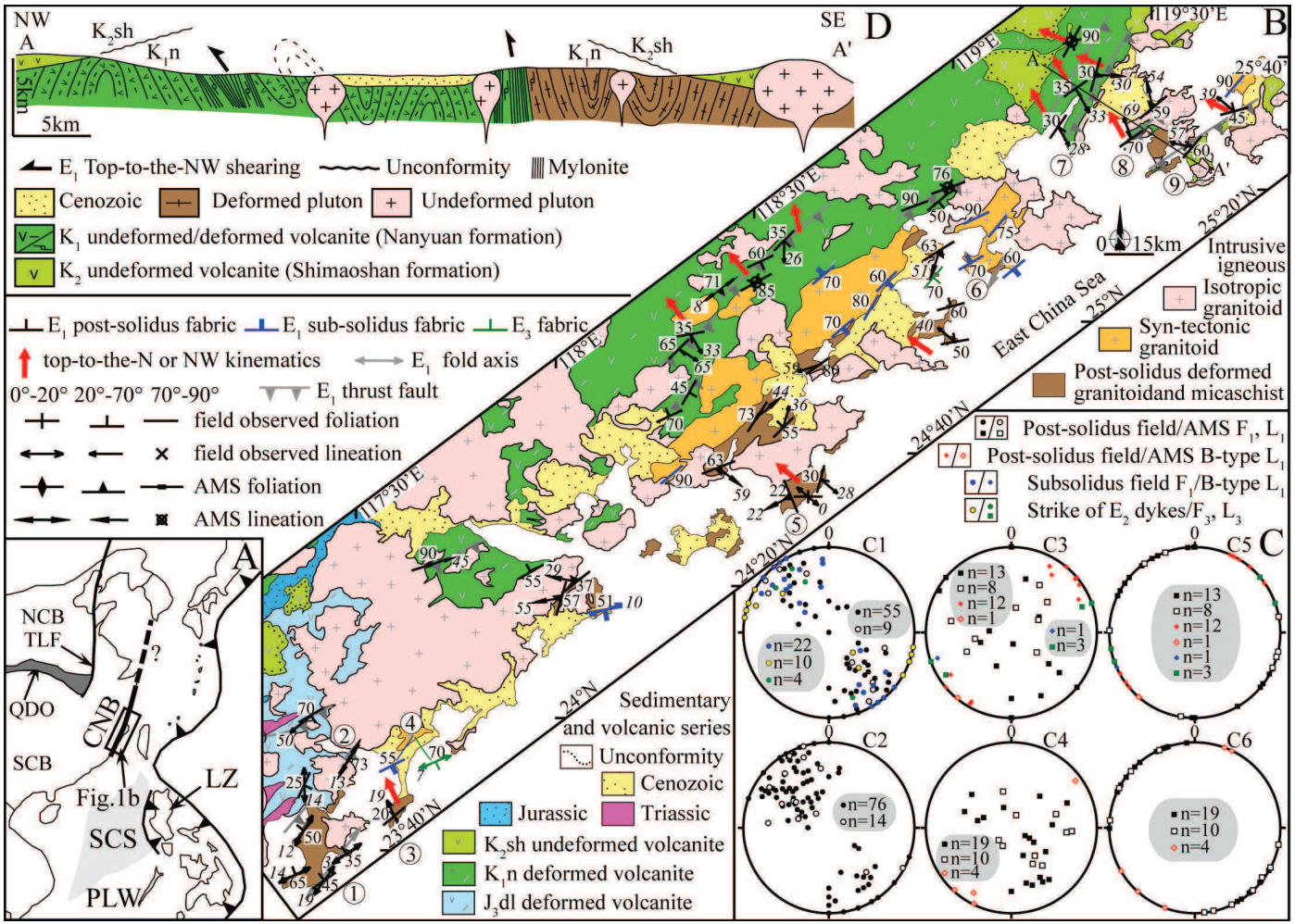

Figure 3 5: structural geologic map of the Changle-Nan'ao Belt

A: Sketch map of the present East Asia Margin geodynamics. NCB: the North China Block: TLF: the Tan-Lu fault; QDO: the Qinling-Dabie Orogen; SCB: South China Block; CNB: Changle-Nan'ao Belt; SCS: South China Sea; LZ: Luzon Island; PLW: Palawan Island. B: Sketch geologic map of the Changle-Nan'ao Belt. Fabric drawn in black, blue and green represent for post solidus, sub solidus deformation of E_1 and post solidus deformation of E_3. C: Equal-area projections of total fabrics in lower hemisphere of the Changle-Nan'ao Belt. c1, foliation pole of gneiss, syn-tectonic granitoid, E_3 narrow shear zone, strike of dykes, c2, foliation pole of deformed volcanite, c3, lineation of gneiss, E_3 narrow shear zone; c4, lineation of deformed volcanic rocks; c5, lineation of gneiss, E_3 narrow shear zone after correcting foliation to flat; c6, A-type lineation of deformed volcanic rocks after correcting foliation to flat. Solid and open samples represent for field observed and AMS fabric. black, blue, green and yellow colors represent for fabrics of post solidus, sub solidus of E_1, post solidus of E_3 and strikes of dykes of E_2.

4 Monazite U-Th-Pb microprobe dating

4.1 Methodology

Contrary to Zircon, the amount of initial Pb in Monazite during its forming is very little and can be neglected. Therefore, all the content of Pb contained in Monazite can be treated as isotropic origin (Parrish, 1990). Practically, the decay age of monazite can be calculated by U, Th, Pb contents determined by microprobe. Monazite U-Tn-Pb microprobe dating method is gifted with many advantages. Firstly, thanks to the high closure temperature, later thermal event can hardly exert effect on monazite and cause Pb lose (Cocherie et al., 1998). Secondly the size of the microprobe beam is tiny therefore enclaves or other impurities can be escaped in order to guarantee exactness of the determined age. Lastly, this method can be conducted in situ, at a fast speed and with a low running cost. All these advantages make this method an effect and popular method in determination of metamorphism

and magma crystallization age.

There are two procedures to conduct such method. The first is to crack samples and concentrate monazite, then fix acquired monazite on the target and then conduct measurement. The second method is using scanning electron microscope (SEM) to distinguish monazite from apatite and zircon on a thin section directly and then conduct measurement. In the photograph of SEM, monazite, the brightness of apatite and zircon are much higher than other minerals and monazite can be distinguished from apatite and zircon by its characteristic element spectrum. After preparing the target or thin section, the prepared monazite is measured by microprobe along the pre-settled profiles. The diameter of the beam of microprobe is 1 um, the distance between two sites for measuring should be no less than 5um. If the size of monazite is large, for example the diameter is large than 50 um, the distance between two site should be enhanced. In order to acquire a high quality of measurement, all the monazite should be larger than 20 um. The profiles should be kept away from inclusion and away from the edge of monazite. The acquired data were processed by a excel macro named "Macro Monazite" to get an apparent age of one site. With software named "Isoplot", the ages of one site are statistic in order to get an age in Th/Pb-U/Pb diagram or get a average age. The former is suitable for the sample with large variance of Th/U (Cocherie and Albarede, 2001) .

The standard mineral using in monazite U-Th-Pb microprobe dating are as follows: Pb: PbS; U: UO_2; Th: (ThO_2); REE and Y: synthesized XPO_4; P: apatite; Si and Ca: andradite.

4.2 Sample description

In order to acquire the representative ages of syn-tectonic and isotropic granitoids, Huian two-mica granite (syn-tectonic granitoid) and Dongshan two-mica granitoid were choosed to conduct monazite U-Th-Pb microprobe dating. The sample SC236 was acquired on the boundary of the Huian two-mica granite. In the outcrop, the orientation of biotite and muscovite was observed. In microscopic observation, the mineral paragenesis is Qtz (20%), Kfs (30%), Pl (30%), Bio (10%), Mus (5%).

Sample SC396 was acquired in Dongshan two-mica granite. In outcrop, it is observed that the minerals are idiomorphic, without orientation and deformation. The texture of the rock is typical igneous. The mineral paragenesis is Qtz (30%), Kfs (25%), Pl (25%), Bio (10%), Mus (5%).

4.3 Experiment course

After over glid of carbon, these two thin sections were observed by SEM for finding monazite. As a result, 17 homogenous monazite with 30-50 um in diameter has been found in SC236 while 18 homogenous monazite with 20-60 um in diameter has been found in SC396. All the monazite found in these two thin sections are igneous origin and exist as inclusion in biotite (Fig. 3-6). Cameca SX50 microprobe (jointly raised by Orleans University and BRGM) was used to perform the measurement on the monazite above 20 um in diameter. The distance between two individual sites is 5-10 um depending on the size of measured monazite. Accelerating voltage was 20 kv, current is 100nA. Both contents of Th and U are above 7500 ppm, in this case, in order to avoid error induced by high U content, the detection limit for U, Tn and Pb is set by 150 ppm.

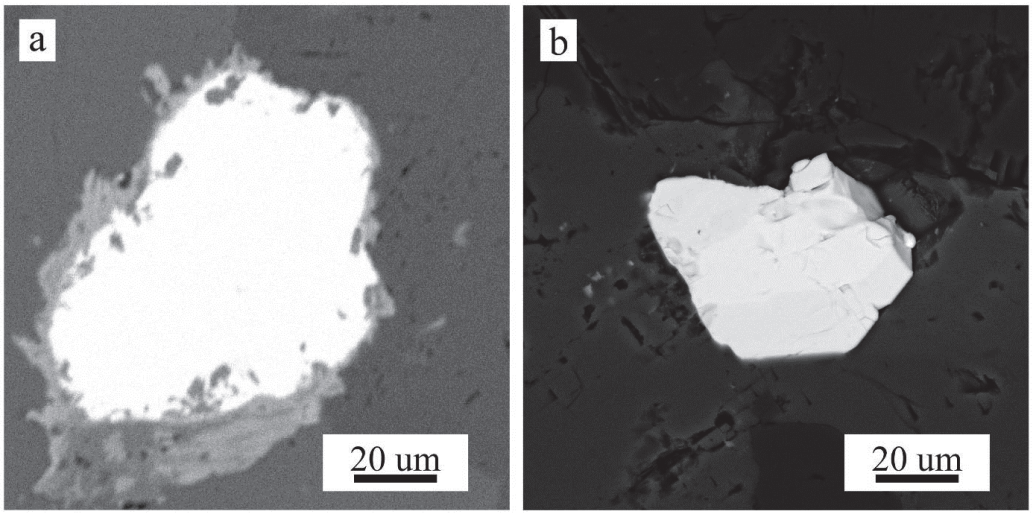

Figure 3 6: The BSE photos of monazite acquired in the granite in CNB

a: SC236, syn-tectonic granite; b: SC396 isotropic granite

4.4 Experiment result

As result shows, owing to the young age, low Pb content and narrow variance of Th/U, both data of SC236 and SC396 can not be plotted in Th/Pb-U/Pb diagram (Cocherie and Albarede, 2001). However, the average ages of these two thin sections provide good quality result (Fig. 3-7). The average age of SC236 is 119.6±2.1Ma (Fig. 3-7a), while the average age of SC396 is 100±3.6Ma (Fig. 3-7b). The Huian two-mica granite is feature by a boundary with mineral orientation and an isotropic core which indicate a syn-tectonic granite. Whilst the Dongshan two-mica granie is generally isotropic which indicate a post-orogenic granite. Therefore, these two ages indicate that in 120 Ma during the crystallization of Huian two-mica granite, the deformation was ongoing, while in 100 Ma, during the crystallization of Dongshan two-mica granite, the tectonic event was already finished. These results are consistent with the geochronology framework (Fig. 3-3b).

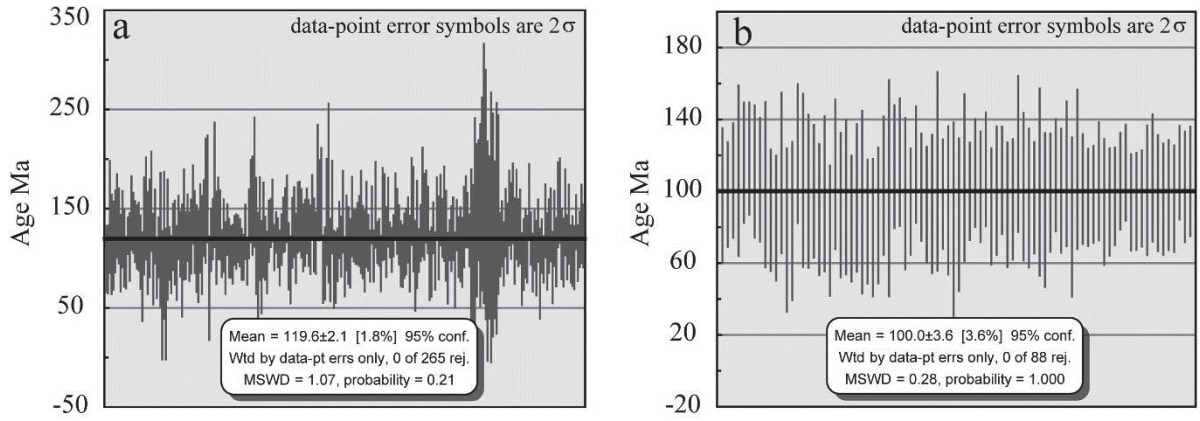

Figure 3 7: Average ages of monazite in plutons of CNB

a: SC236, syn-tectonic granite; b: SC396 isotropic granite

5 Rock Magnetism Study

5.1 A brief introduction to AMS study

In the weak deformation domain, it is very difficult to acquire fabric vie the traditional field observation. In this situation, the anisotropy magnetic susceptibility (AMS) is a effective method to illustrate fabric by measuring the orientation of magnetic minerals (Tarling and Hrouda, 1993). In the ductile deformed rocks, as indicated by previous works, the lineation and the pole of the foliation of the deformd rocks are well represented by the magnetic lineation and the pole of the magnetic foliation (Zhang and Zhu, 1989). Therefore, in the case of only foliation develops in the ductile deformed rocks, the AMS measurement is a good choice to determine the lineation. At the same time, in the granite emplacement study, the AMS mode of a pluton can well illustrate the emplacement mechanism and its tectonic regime. As previous studies show, the magnetic lineation of the granite emplacing during extension regime is well oriented, whose direction indicate the regional extension direction (Talbot et al., 2000; Joly et al., 2007; Turrillot et al., 2011; Lin et al., 2013). The magnetic foliation of the pluton emplacing during compression regime is well oriented and steep inclined. In this situation, the magnetic foliation is perpendicular to the compression direction (Bouchez and Gleizes, 1995; Charles et al., 2009). In the strike-slip regime, the magnetic fabric is without an obvious mode (Olivier and Ameglio, 2002; Neves et al., 2003). In the pluton emplacing in a post-tectonic or a very weak tectonic regime, the magnetic foliation is apt to be co-concentric representing the upward magma upwelling (de Oliveira et al., 2010; Wei et al., 2013).

5.2 Sampling and test

Owing to the weak deformation in many places of the CNB, only foliation was available in our field structural observations in some outcrops. In order to acquire lineation, in the lab, oriented specimen from 23 site were cut into 2cm×2cm×2cm standard cubic to conduct the AMS measurement. Besides, AMS samples have been

carried out by gasoline driller on isotropic granitoids, syn-tectonic granitoids and pervasive post solidus deformed granitoids (orthogneiss) in 86 sites (Tab. 3-2). In each pluton, the sites are regular distributed and the neigboring sites are at least 2 km away from each other. In each sites, 5-6 AMS standard cores with 2.5 cm in diameter were acquired. Each core is oriented by compass. If the weather permits, the orientation was corrected by sun compass. In the lab, all cores were cut into standard cylinder specimen with 2.2 cm hight. At last, 154 standard cubic and 731 standard cylinder specimens were acquired.

Table 3 2 The AMS measurement results of the Changle-Nan'ao Belt

	Coordinates				Km			K_1				K_3			
Site	Lat. (°N)	Long. (°E)	lith	N	(10^{-6}SI)	P_j	T	Dec (°)	Inc (°)	a_{95max} (°)	a_{95min} (°)	Dec (°)	Inc (°)	a_{95max} (°)	a_{95min} (°)
FJ01	25.15	119.05	DG*	8	11400	1.624	0.687	320	63	23	4	129	27	9	5
FJ02	25.16	119.12	*	8	3510	1.129	0.093	284	50	14	11	166	21	13	10
FJ03	25.13	119.15	*	7	851	1.108	0.05	65	36	53	23	328	10	29	13
FJ04	25.24	119.10	*	8	12000	1.457	0.362	294	47	11	9	175	24	10	5
FJ05	25.26	119.06	DG§	10	29100	1.554	0.075	187	55	17	7	329	29	24	8
FJ06	25.24	119.10	§	10	22700	1.427	0.319	167	64	22	8	306	20	15	9
FJ07	25.24	119.11	§	10	26300	1.451	0.129	283	59	9	5	175	10	6	4
FJ08	25.24	119.12	§	12	29400	1.54	0.088	319	58	9	3	142	32	14	3
FJ09	25.26	119.26	§	12	34200	1.092	0.083	120	22	4	2	351	57	4	2
FJ10	24.92	118.89	*	8	17800	1.152	0.241	290	7	41	10	110	83	10	9
FJ11	24.88	118.92	*	7	4130	1.108	-0.199	315	4	9	6	55	67	13	6
FJ12	24.89	118.92	*	7	13000	1.086	-0.216	321	7	18	7	202	76	28	10
FJ13	24.89	118.93	*	9	17400	1.175	0.044	309	3	7	4	44	61	11	4
FJ14	24.89	118.96	*	9	11800	1.177	0.489	143	18	21	6	21	59	9	5
FJ15	24.89	118.97	*	8	21000	1.099	-0.154	103	33	17	14	212	27	36	12
FJ16	24.87	118.95	*	11	28400	1.142	-0.183	114	1	14	4	207	78	21	7
FJ17	24.91	118.87	*	11	21600	1.147	0.172	268	4	10	3	175	42	6	3
FJ18	24.90	118.84	*	7	1530	1.954	0.32	255	21	28	14	54	68	31	12
FJ19	24.89	118.79	*	10	15200	1.238	-0.047	138	18	11	8	275	66	10	6

FJ20	24.88	118.73	†	11	7990	1.109	0.233	282	11	12	5	14	11	10	6
FJ21	25.00	118.75	†	11	9590	1.509	0.289	55	18	12	2	321	13	8	3
FJ22	24.63	118.25	†	11	6850	1.204	0.199	237	31	17	3	139	13	9	3
FJ23	24.63	118.29	†	10	248	1.062	0.272	127	73	9	7	328	16	15	7
FJ24	24.60	118.30	§	7	25600	1.209	0.396	235	61	21	12	140	3	16	6
FJ25	24.61	118.34	*	10	14500	1.156	0.391	279	9	23	7	140	78	8	4
FJ25D	24.61	118.34	MD	8	20700	1.032	-0.563	122	9	11	4	30	12	20	10
FJ26	24.61	118.34	*	7	10700	1.102	0.227	273	13	26	6	102	77	10	7
FJ26	24.61	118.34	#	8	28200	1.023	-0.402	97	62	11	3	313	23	27	11
FJ27	24.62	118.38	*	10	17600	1.102	0.17	87	23	59	12	259	66	14	9
FJ28	24.63	118.41	DG	10	10300	1.194	0.503	128	59	21	10	339	27	14	7
FJ29	24.67	118.39	*	7	9530	1.082	-0.01	56	38	58	15	277	44	19	15
FJ30	24.70	118.39	§	8	23100	1.334	0.115	310	46	8	5	107	42	6	2
FJ31	24.68	118.49	†	6	10400	1.078	0.129	274	3	27	10	181	41	17	5
FJ32	24.67	118.55	†	9	22500	1.17	0.378	322	20	9	5	160	70	6	4
FJ33	24.65	118.57	†	10	14900	1.148	0.076	322	23	6	4	107	63	23	6
FJ34	24.64	118.58	†	7	28700	1.096	0.268	321	3	53	19	228	43	24	10
FJ35	24.56	118.60	Mig	11	6610	1.286	0.189	242	22	39	9	67	68	17	10
FJ36	24.56	118.60	*	11	8770	1.214	0.006	286	12	9	7	77	77	11	6
FJ37	24.57	118.62	Mig	8	7660	1.166	0.246	279	10	16	10	74	79	22	5
FJ38	24.56	118.64	*	6	8210	1.36	-0.041	321	7	4	2	153	83	4	1
FJ38	24.56	118.64	DG*	4	10300	1.223	0.132	-	-	-	-	-	-	-	-
FJ39	24.69	118.62	†	6	11400	1.231	0.109	293	4	15	2	69	84	6	4
FJ40	24.71	118.60	†	10	6110	1.121	0.134	295	13	16	4	132	77	9	6
FJ41	24.89	118.66	DG*	10	17700	1.4	-0.014	247	43	6	2	150	8	8	5
FJ42	24.96	118.65	†	6	15900	1.221	0.505	199	40	10	4	310	23	6	2
FJ43	24.97	118.64	†	9	17200	1.3	0.593	143	62	12	4	307	27	4	4
FJ44	24.96	118.56	*	8	17900	1.133	0.758	320	7	47	3	183	81	6	2
FJ45	24.89	118.45	†	6	2190	1.109	-0.007	123	70	12	3	296	20	7	5
FJ46	24.91	118.45	†	8	1590	1.085	-0.18	134	70	11	7	284	18	13	9
FJ47	25.00	118.34	†	8	4650	1.098	-0.046	161	60	25	9	293	21	22	11
FJ48	25.02	118.30	†	6	4990	1.065	0.217	194	1	60	9	285	51	21	12
FJ49	25.45	119.51	DG*	8	1810	1.31	0.328	65	62	11	5	322	7	9	3
FJ50	25.44	119.53	DG*	6	4900	1.5	0.119	10	66	7	2	142	17	5	4

FJ51	25.37	119.49	DG*	7	140	1.1	0.427	31	36	11	4	139	23	11	5
FJ52	25.58	119.69	OG*	8	14000	1.382	0.432	223	61	7	4	128	3	6	4
FJ53	25.54	119.71	DG†	9	11800	1.36	0.582	240	17	19	7	142	26	10	3
FJ54	25.47	119.58	DG*	12	32900	1.341	0.451	225	45	6	5	118	17	6	2
FJ55	25.18	118.97	Mig	10	19500	1.571	0.483	198	51	7	5	327	27	9	5
FJ56	25.16	118.95	†	13	17800	1.377	0.566	241	23	20	6	341	21	6	4
FJ56	25.16	118.95	*	5	22500	1.399	0.68	250	5	35	1	342	19	5	1
FJ57	25.00	118.65	†	8	6910	1.21	0.362	151	70	6	4	321	20	6	4
FJ58	25.05	118.62	†	7	18600	1.129	0.618	221	26	29	7	322	22	7	5
FJ59	25.09	118.64	†	6	3260	1.066	0.632	249	48	22	8	356	15	10	5
FJ60	25.08	118.64	†	8	8790	1.118	0.479	237	13	7	4	333	23	5	4
FJ61	25.11	118.67	†	8	13100	1.129	0.145	257	4	6	5	348	9	8	4
FJ62	25.02	118.67	†	10	13400	1.132	0.488	231	5	14	4	322	10	8	5
FJ63	25.00	118.73	†	8	6560	1.178	0.308	236	2	9	3	326	20	4	2
FJ64	25.09	118.71	§	7	7440	1.146	0.105	137	25	8	1	231	8	7	2
FJ65	25.04	118.79	†	7	2130	1.124	0.368	65	27	8	2	328	13	8	5
FJ66	25.07	118.80	†	8	5460	1.197	0.344	254	13	20	7	350	28	8	5
FJ67	25.10	118.84	*	9	7560	1.285	-0.011	181	33	6	3	318	49	10	3
FJ68	25.15	118.89	*	8	15100	1.263	0.46	189	49	34	8	333	35	11	6
FJ69	24.96	118.82	*	7	14600	1.087	0.564	276	1	70	7	180	85	10	7
FJ70	23.88	117.39	*	7	592	1.081	0.067	83	38	45	14	224	45	74	29
FJ71	23.86	117.42	*	7	13300	1.088	0.528	99	6	21	6	202	67	7	5
FJ72	23.87	117.45	*	7	188	1.02	-0.225	356	5	55	17	144	85	33	15
FJ73	23.86	117.44	*	6	14600	1.094	0.636	86	10	19	4	199	65	8	4
FJ74	23.83	117.47	*	5	382	1.02	0.5	301	3	27	3	206	58	17	5
FJ75	23.85	117.48	*	7	17600	1.079	0.185	94	11	8	4	209	66	9	2
FJ76	23.69	117.34	Mig	8	185	1.143	0.213	221	12	29	8	128	17	34	14
FJ77	23.74	117.51	†	7	345	1.076	0.337	289	26	20	9	187	22	31	20
FJ78	23.75	117.51	†	6	24400	1.282	0.176	240	15	4	2	134	45	2	2
FJ79	23.75	117.49	†	7	617	1.06	0.186	299	35	16	5	188	27	11	3
FJ80	23.74	117.45	†	6	14100	1.1	0.526	285	28	12	3	153	52	8	3
FJ81	23.74	117.43	†	9	4210	1.057	0.382	299	11	37	15	171	73	23	17
FJ82	23.71	117.43	†	7	8610	1.099	0.474	304	37	47	13	142	51	19	11
FJ83	23.67	117.44	†	6	4380	1.119	-0.002	294	7	53	21	31	46	45	34

FJ84	24.29	118.13	DG§	6	720	1.251	0.626	249	10	19	4	348	39	5	2
FJ85	24.34	118.05	DG§	6	204	1.114	0.325	281	29	12	4	142	53	5	4
FJ86	24.31	118.01	DG*	6	2250	1.323	0.314	260	55	20	9	106	33	18	8
SC393	23.67	117.46	DG*	6	1930	1.208	-0.191	217	28	3	2	127	0	4	1
SC416	24.34	118.08	DG§	4	5030	1.506	0.208	-	-	-	-	-	-	-	-
SC435	24.76	118.51	DG*	9	2570	1.314	0.714	50	44	4	1	303	17	3	2
SC457	25.54	119.26	DV	7	18.7	1.05	-0.169	306	33	40	7	177	44	35	12
SC458	25.54	119.25	DV	11	9.45	1.179	0.433	222	2	24	4	318	72	15	5
SC484	25.71	119.30	DV	7	51.8	1.014	0.512	21	77	32	4	119	2	10	6
SC487	25.64	119.31	DV	5	29	1.047	0.114	140	55	10	4	352	31	5	4
SC500	25.58	119.28	DV	6	6	1.033	0.171	150	49	16	6	274	30	79	5
SC501	25.54	119.26	DV	7	-4.08	1.059	-0.22	297	38	7	2	206	1	9	3
SC506	25.49	119.27	DV	6	36.3	1.053	0.871	141	42	44	2	307	47	4	1
SC509	25.49	119.30	DV	7	39.7	1.131	0.689	95	35	11	3	308	50	4	1
SC513	25.62	119.36	DV	9	29.7	1.057	0.457	93	30	3	3	286	60	5	2
SC517	25.54	119.50	DV	7	3750	1.189	0.61	347	54	5	3	140	33	3	2
SC528	25.31	118.98	DV	4	4	59.9	1.102	0.583	-	-	-	-	-	-	-
SC530	25.33	118.96	DV	14	38	1.045	0.279	206	71	4	2	340	14	4	2
SC535	25.30	118.92	DV	3	3	24.2	1.017	-0.028	-	-	-	-	-	-	-
SC551	25.10	118.51	DV	8	52.9	1.109	0.885	225	73	11	2	331	5	2	1
SC560	25.09	118.43	DV	6	37.7	1.046	0.62	54	8	8	2	321	19	4	2
SC595	23.90	117.48	DV	8	1050	1.367	0.57	210	13	10	5	304	17	6	3
SC659	23.72	117.40	OG*	8	1600	1.388	0.338	219	2	9	3	309	5	8	3
SC668	24.39	117.70	DV	5	705	1.046	0.493	73	45	8	1	343	0	5	1
SC669	24.37	117.93	DV	4	4	9.21	1.092	0.009	-	-	-	-	-	-	-
SC671	24.40	117.95	DV	3	3	26.6	1.11	0.872	-	-	-	-	-	-	-

Lat: latitude, long: longitude, lith: lithology, Km: average magnetic susceptibility, P_J and T: the anisotropy degree and the shape parameter of AMS ellipsoid, K_1 and K_3: magnetic lineation and the pole of magnetic foliation, Inc: inclination, Dec: declination, α_{95}max and α_{95}min: the long and short axis of error ellipsoid, DV: deformed volcanite, DG: pervasive post-solidus deformed granitoids, OG: granitoids with oriented minerals, MD: mafic dykes, Mig: migmatite, *:biotite granite, †: two-mica granite, §: granodiorite, #: gabbro.

In Laboratoire de Magnétisme des Roches d'Orléans, IRM experiments were carried out on different lithologies by IM30 pulse magnetizer and JR5 magnetometer. Coupled with a CS3 furnace, KLY3 was used to perform the thermal-susceptibility experiments on powders of different lithologies. The KLY3 kapabridge was used to perform the AMS and bulk susceptibility measurements. The results were processed by ANISOFT (offered by AGICO) to calculate the main magnetic anisotropic axes (K_1 for lineation and K_3 for the pole of foliation), the shape parameter (T) and the anisotropy degree (P_J). Morover, hysteresis curves were obtained by AGM and VSM electromagnetic inductometer on different lithologies in the Paleomagnetic laboratory of Institut de Physique du Globe de Paris. The micromag VSM software has been used to processing the hysterosis loops data.

5.3 Magnetic mineralogy

The species and size of the magnetic meanerals determine that whether the AMS ellipsoid represents the strain ellipsoid (Tarling and Hrouda, 1993; Borradaile and Henry, 1997). For example, contrary to normal situation, the K_1 and K_3 of the magnetic ellipsoid of the anti-magnetic mineral and the single domain of the magnetite represent c and a axes of the strain ellipsoid, respectively. Thus, in order to reach a correct interpretation of AMS mode, it is necessary to determine the specials of magnetic minerals.

The measurements show that the bulk susceptibility of volcanite is usually small, ranging from 0.1×10^{-3}SI to 1×10^{-3}SI, some individuals with big values could attend 4×10^{-3}SI whilst a single individual is negative with value of -4×10^{-6}SI. The bulk susceptibilities of the migmatite and pervasively sub-solidus deformed granitoids are large, ranging from 1×10^{-3} to 30×10^{-3} SI (Fig. 3-8a). Regardless the individual lithology, both bulk susceptibilities of the syn-tectonic granitoids and isotropic granitoids are large, usually ranging from 1×10^{-3}SI to 35×10^{-3}SI (Fig. 3-8b).

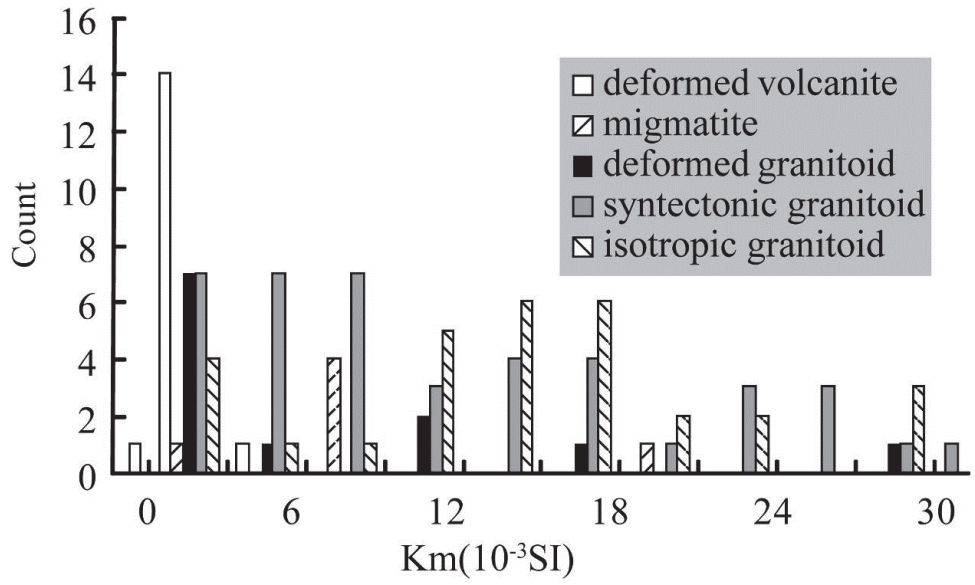

Figure 3 8: The bulk susceptibility mode of the granitoids in the Changle-Man'ao Belt

Thermal-susceptibility curves indicate that at the temperature of 580°C, the susceptibilities of the migmatite, pervasively sub-solidus deformed granitoids, syn-tectonic granitoids, isotropic granitoids drastic decrease (Fig. 3-9a-k), indicating that magnetite is predominant in the magnetic carriers. In some specimens, the susceptibilities continue to decrease after 580°C indicating the existence of hematite. The thermal-susceptibility curves of majority specimens of deformed volcanite show that the susceptibilities decrease slowly with the increased temperature without an apparent curie temperature, considering the low susceptibility value of this kind of specimens, the paramagnetic mineral is considered as the main magnetic carriers (Fig. 3-9l). In some specimens of the deformed volcanite, although the susceptibility is very low, the thermal-susceptibility drastic decrease at 580°C indicating the existence of tiny amount of magnetite (Fig. 3-9m).

The shapes of hysterosis loops of migmatite, pervasively sub-solidus deformed granitoids, syn-tectonic granitoids, isotropic granitoids are featured by "sigmoidal" shape indicating that the main magnetic carrier is magnetite (Fig. 3-9n-x). In the hysterosis loops of deformed volcanite, the induced magnetism varies in proportion to

exerted magnetic field (eg. Fig. 3-9ab). The hysterosis loops of some individual specimens show a mélange of a main linear shape with a small fraction of sigmoidal shape (Fig. 3-9c and aa). The features of hysterosis loops of deformed volcanite indicate that the main magnetic carrier is paramagnetic minerals such as biotite and in some individual specimens, small amount of magnetite also exist. Differ with majority specimens of volcanites, there is one specimen whose susceptibility is negative (SC501). In this specimen, the induced magnetism decreases during the increases of exerted magnetic field (Fig. 3-9ac) indicating that the magnetic carrier is anti-magnetic minerals. In such situation, the magntic fabric is anti-fabric whose K_1 and K_3 represent c and a axis of strain ellipsoid, respectively. So before interpreting, a correction should be conducted on the magnetic fabric in which, K_1 represents the pole of the foliation and K_3 represents the lineation.

IRM curves show that in the exerted magnetic field under 100mT, the induced magnetism increase drastic and near to saturation (Fig. 3-9ad-10) indicating the predominant magnetic carriers are magnetite in migmatite, pervasively sub-solidus deformed granitoids, syn-tectonic granitoids, isotropic granitoids.

5.4 AMS result

5.4.1 The quality of AMS measurement and the shape of AMS ellipsoid

The AMS data of the CNB is listed in Table 3-2. As this table shows, the α_{95max} and α_{95min} (Jelinek, 1981) of K_1 and K_3 are both lower than 20°, thus, the quality of the AMS data in this study is satisfactory and can be used in the structural interpretation (Tab. 3-2).

In the P_J-T diagram, most T values are above zero, indicating the AMS ellipsoids are predominant oblate. The P_J values of pervasively sub-solidus deformed granitoids are mostly above 1.2 while the P_J values of deformed volcanites are mostly beneath 1.2 indicating that the deformation degree of pervasively sub-solidus deformed granitoids is higher than deformed volcanites (Fig. 3-10a and b). The P_J values of most syn-tectonic granitoids specimens are higher than 1.2 while the P_J values of most

isotropic granitoids specimens are lower than 1.2 indicating during the emplacement, the syn-tectonic granitoids experienced higher strains than isotropic granitoids (Fig. 3-10c and d). In the the P_J-Km diagram, the P_J values of syn-tectonic granitoids are in proportion to Km value while in the isotropic granitoids, no similar trend is found. At the condition of same Km, the P_J value of syn-tectonic granitoids is higher than isotropic granitoids indicating a higher regional strain during the emplacement of syn-tectonic granitoids.

5.4.2 The magnetic fabric mode

The lab measured magnetic foliation is well consistent with the field observed structural foliation (Fig. 3-11a-e). In some observation site where both structural lineation and magnetic lineation are available, the magnetic lineation is also consistent with structural lineation (Fig. 3-11e). As puts it by the previous works, the AMS fabric can be treated as structural fabric (Zhang and Zhu, 1989), we used magnetic lineation to substitute where the structural lineation was not available. Plotting the magnetic fabric in the same stereotype projection diagram of the structural fabric, the similar trend is found between two kinds of fabrics (Fig. 3-5c1-4). In the whole CNB, the magnetic foliations of syn-tectonic granitoids are predominantly highly inclined, NE-SW striking while the magnetic lineations scatter (Fig. 3-11a-f, 12a-f, 13). The magnetic foliations of the isotropic granitoids are predominantly shallow inclined and the magnetic lineations concentrate on NW-SE direction (Fig. 3-11a-f, 12a-f, 13).

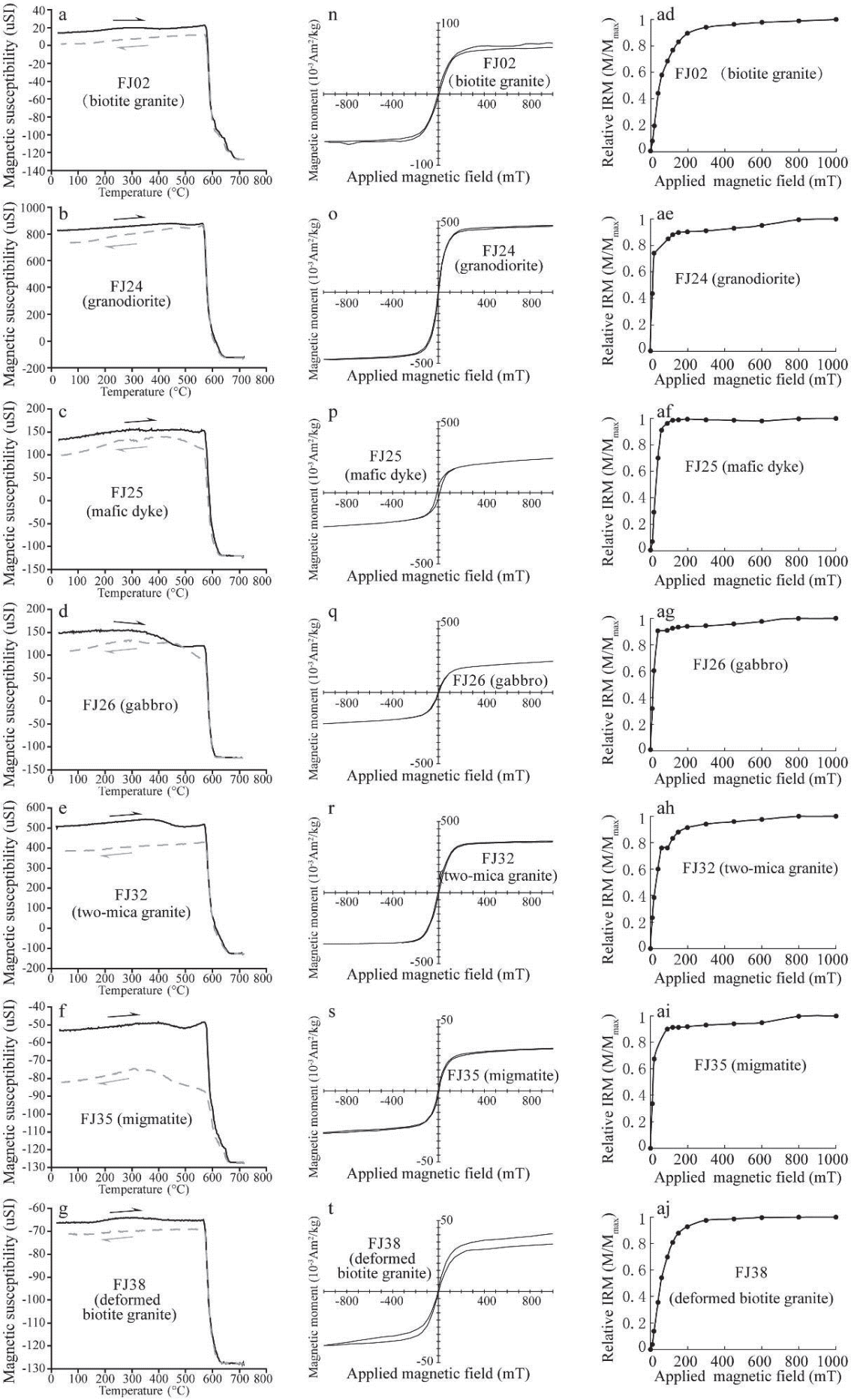
a
FJ02
(biotite granite)
Magnetic susceptibility (uSI)
Temperature (°C)
n
FJ02
(biotite granite)
Magnetic moment (10⁻³Am²/kg)
Applied magnetic field (mT)
ad
FJ02 (biotite granite)
Relative IRM (M/M_max)
Applied magnetic field (mT)
b
FJ24
(granodiorite)
o
FJ24
(granodiorite)
ae
FJ24 (granodiorite)
c
FJ25
(mafic dyke)
p
FJ25
(mafic dyke)
af
FJ25 (mafic dyke)
d
FJ26 (gabbro)
q
FJ26 (gabbro)
ag
FJ26 (gabbro)
e
FJ32
(two-mica granite)
r
FJ32
(two-mica granite)
ah
FJ32 (two-mica granite)
f
FJ35 (migmatite)
s
FJ35 (migmatite)
ai
FJ35 (migmatite)
g
FJ38
(deformed
biotite granite)
t
FJ38
(deformed
biotite granite)
aj
FJ38
(deformed biotite granite)

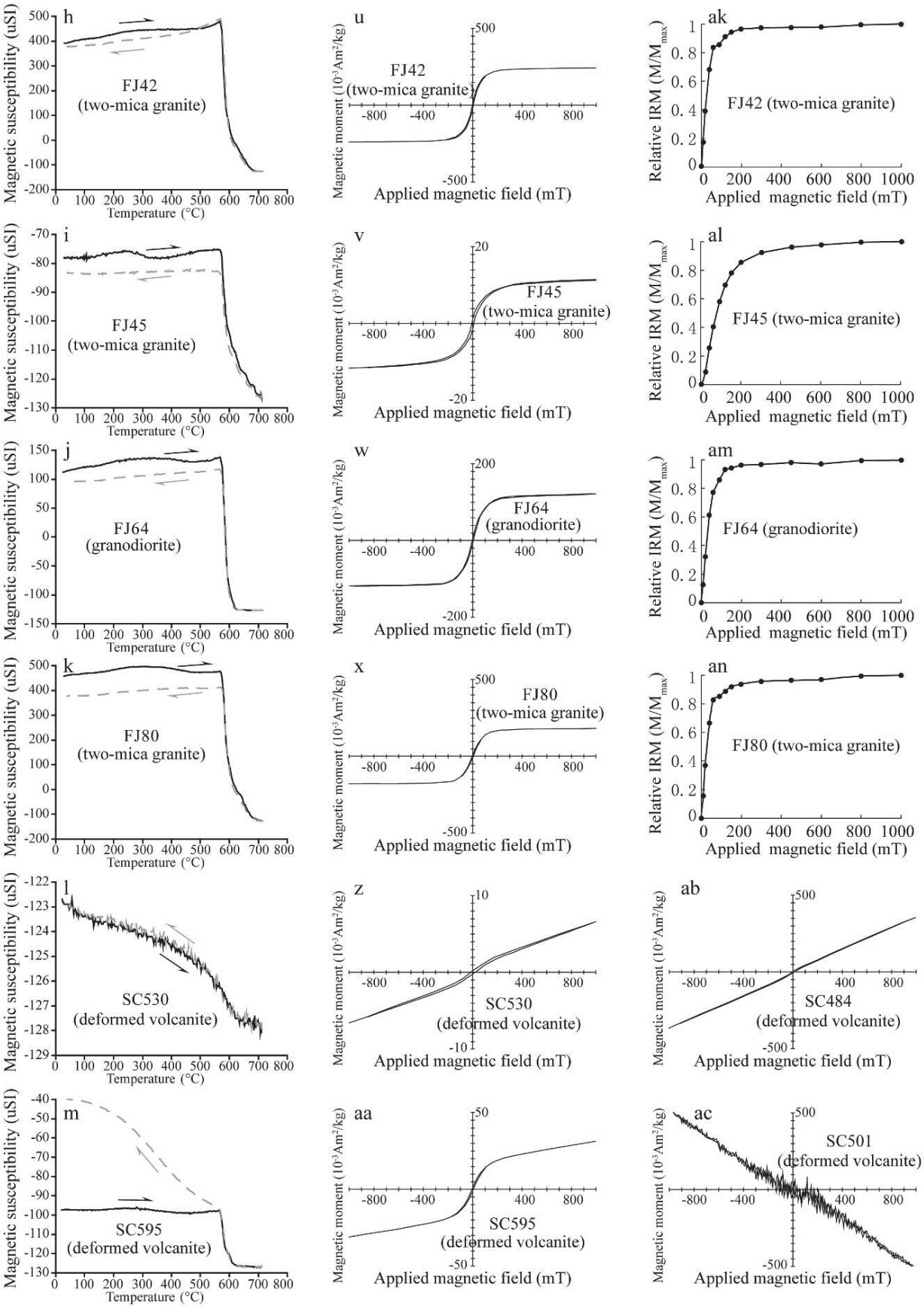

Figure 3 9: The magnetic minerals specials in the Changle-Nan'ao Belt

a- m: Thermal-susceptibility curves and curie temperature, n-ac: hysterosis loops, ad-an: Iso Temperature Remnant (IRM) curves.

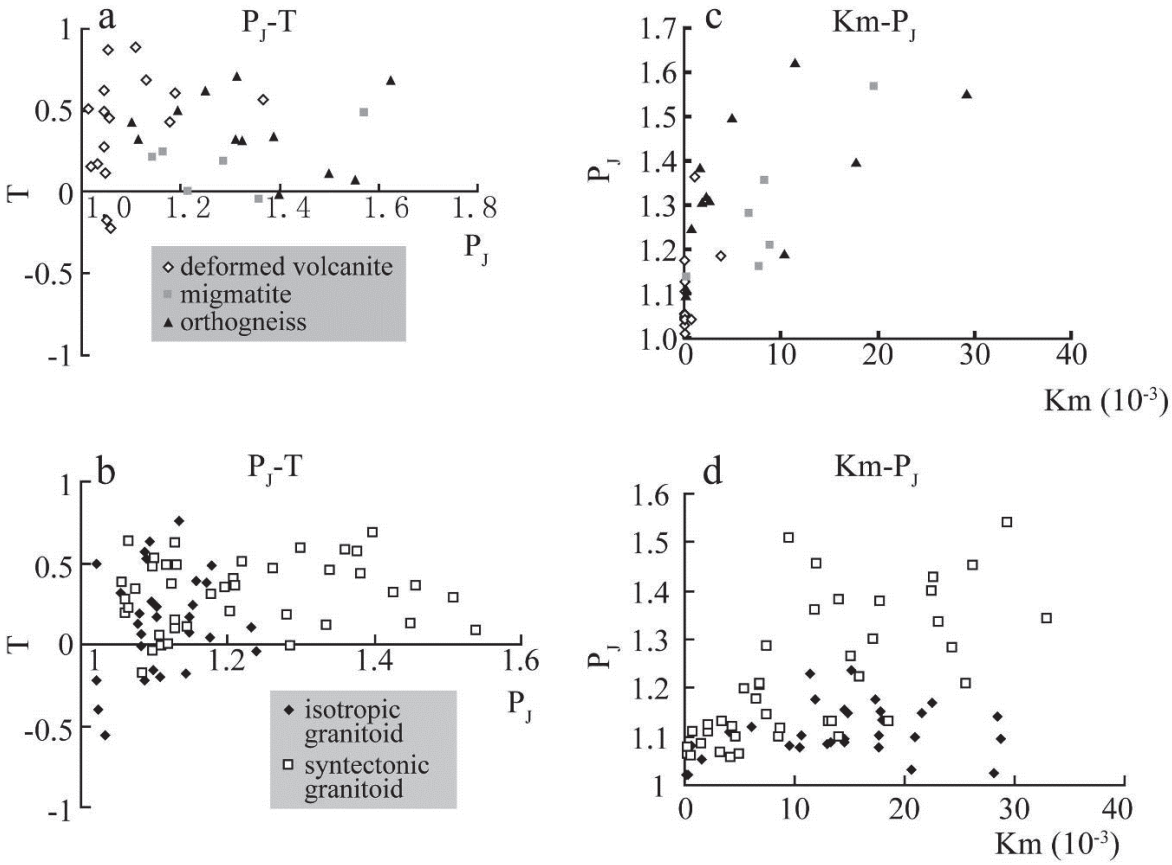

Figure 3 10: The characteristics of AMS ellipsoid of the granitoids in the Changle-Nan'ao Belt

a: P_J-T diagram of the deformed rocks (pervasively sub-solidus deformed granitoids and deformed volcanites), b: P_J-T diagram of the syn-tectonic granitoids and isotropic granitoids, c: the Km-P_J diagram of the deformed rocks, d: the Km-P_J diagram of the syn-tectonic granitoids and isotropic granitoids.

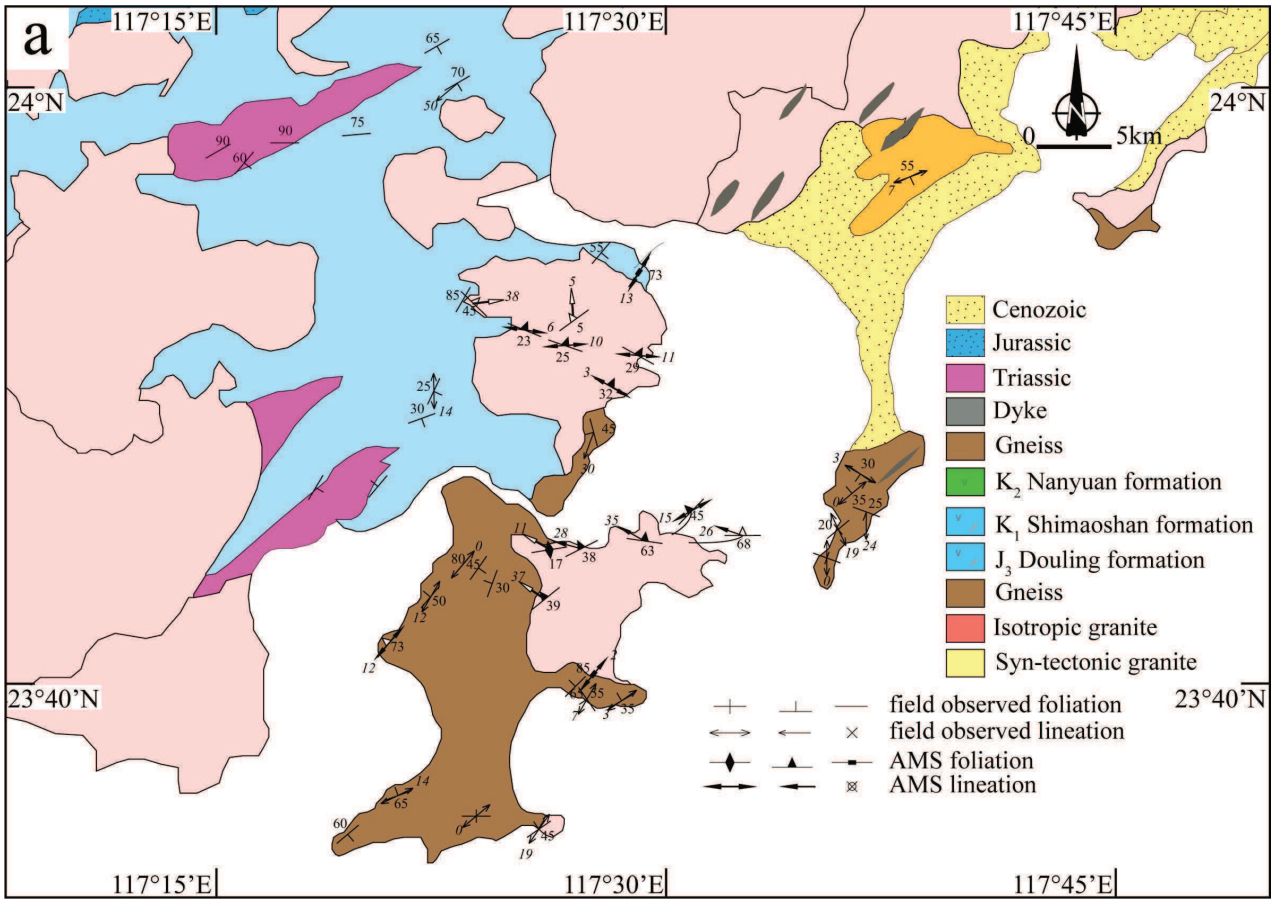

Figure 3 11: The field observed structural fabric and the lab measured AMS fabric geologic map of the CNB

a: the Yunxiao-Dongshan area, b: the Longhai-Gangwei area, c: the Jinjiang-Shishi area, d: the Quanzhou-Huian area, e: the Fuqing-Pingtan area

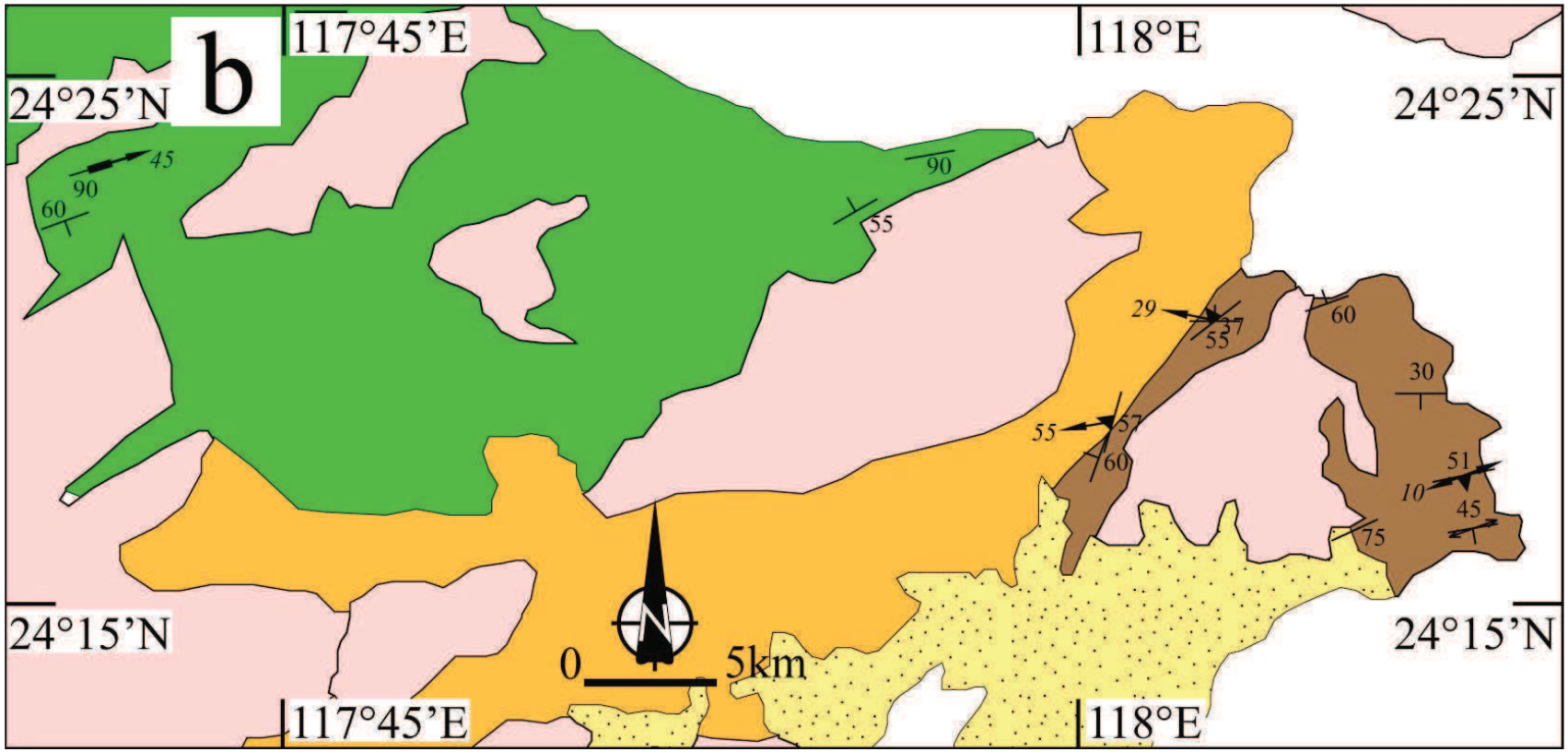
b
117°45'E
118°E
24°25'N
24°15'N
45
90
60
90
55
29
37
55
60
30
55
57
60
51
10
45
75
N
0
5km

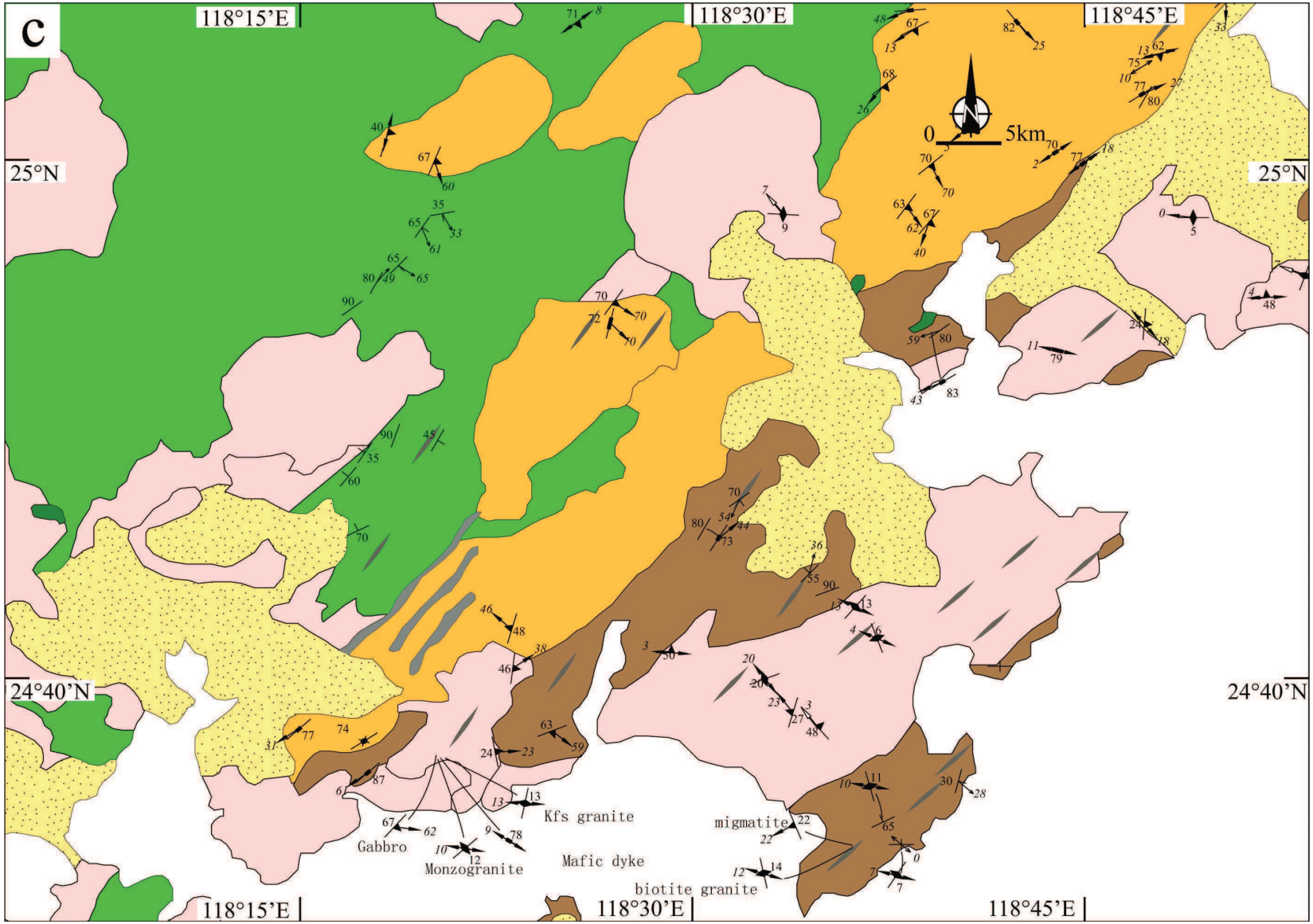
C
118°15'E
118°30'E
118°45'E
25°N
24°40'N
0
5km
Kfs granite
migmatite
Gabbro
Monzogranite
Mafic dyke
biotite granite

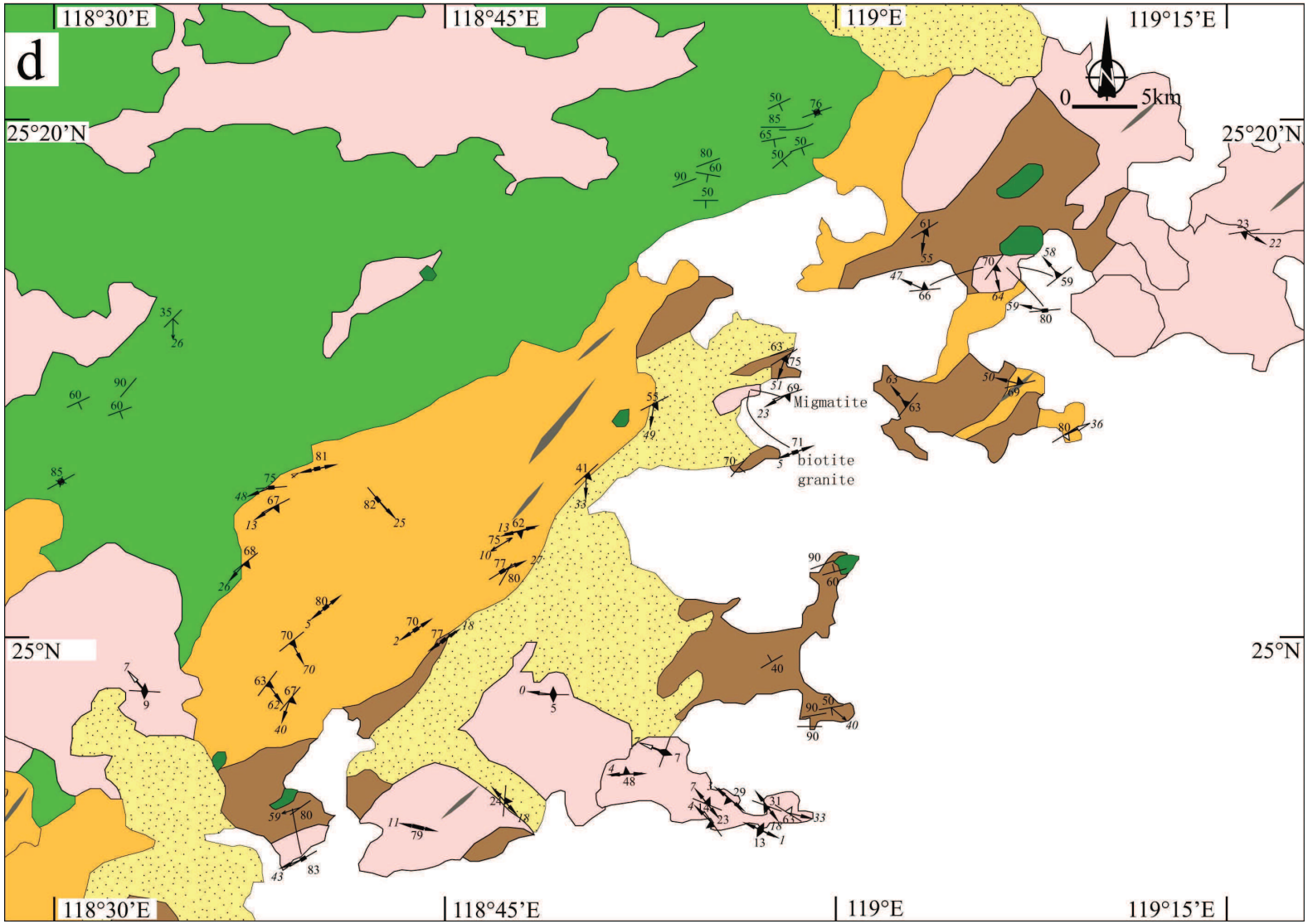
d
118°30'E
118°45'E
119°E
119°15'E
25°20'N
25°N
0
5km
Migmatite
biotite
granite

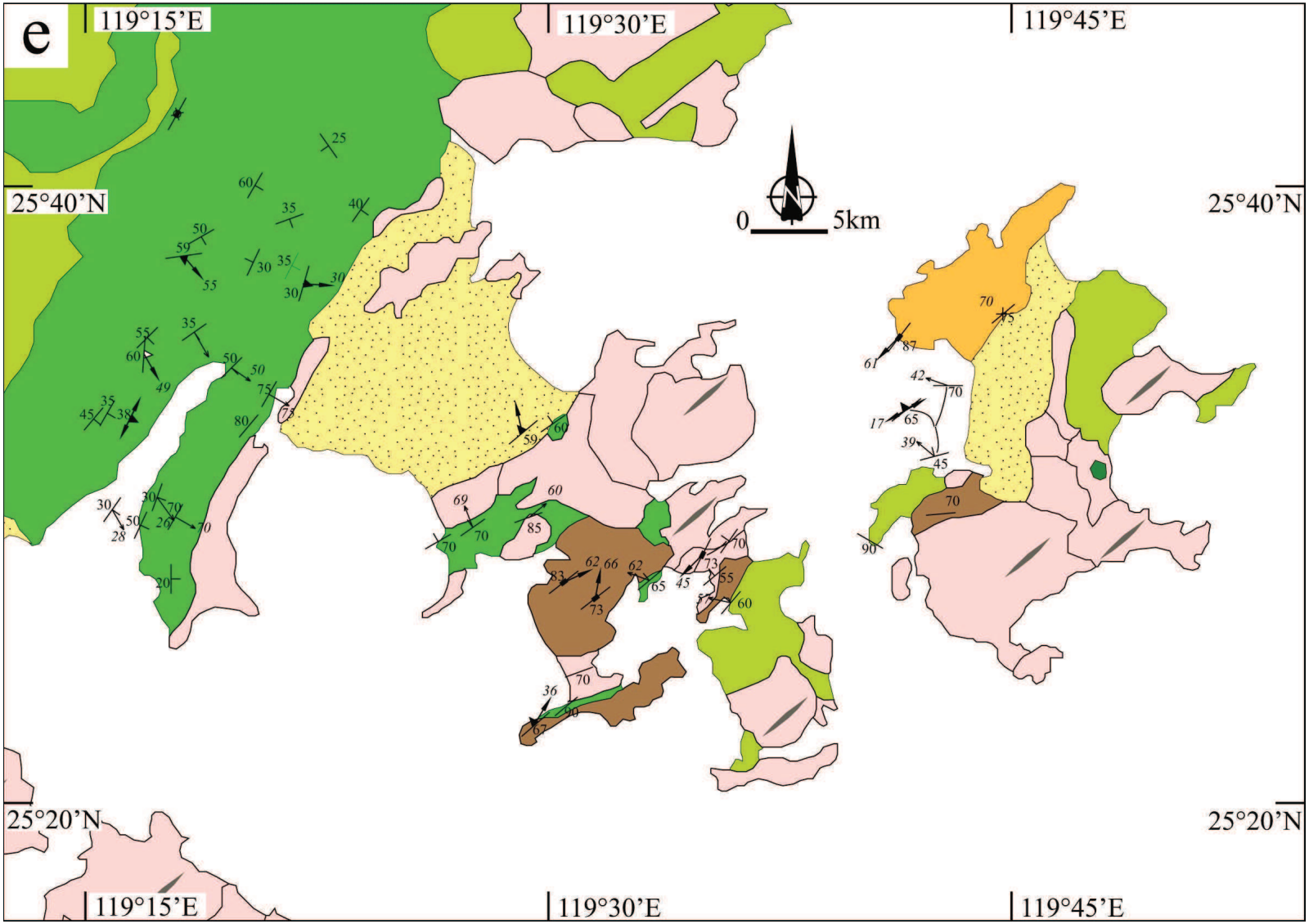
e
119°15'E
119°30'E
119°45'E
25°40'N
25°20'N
0
5km
N

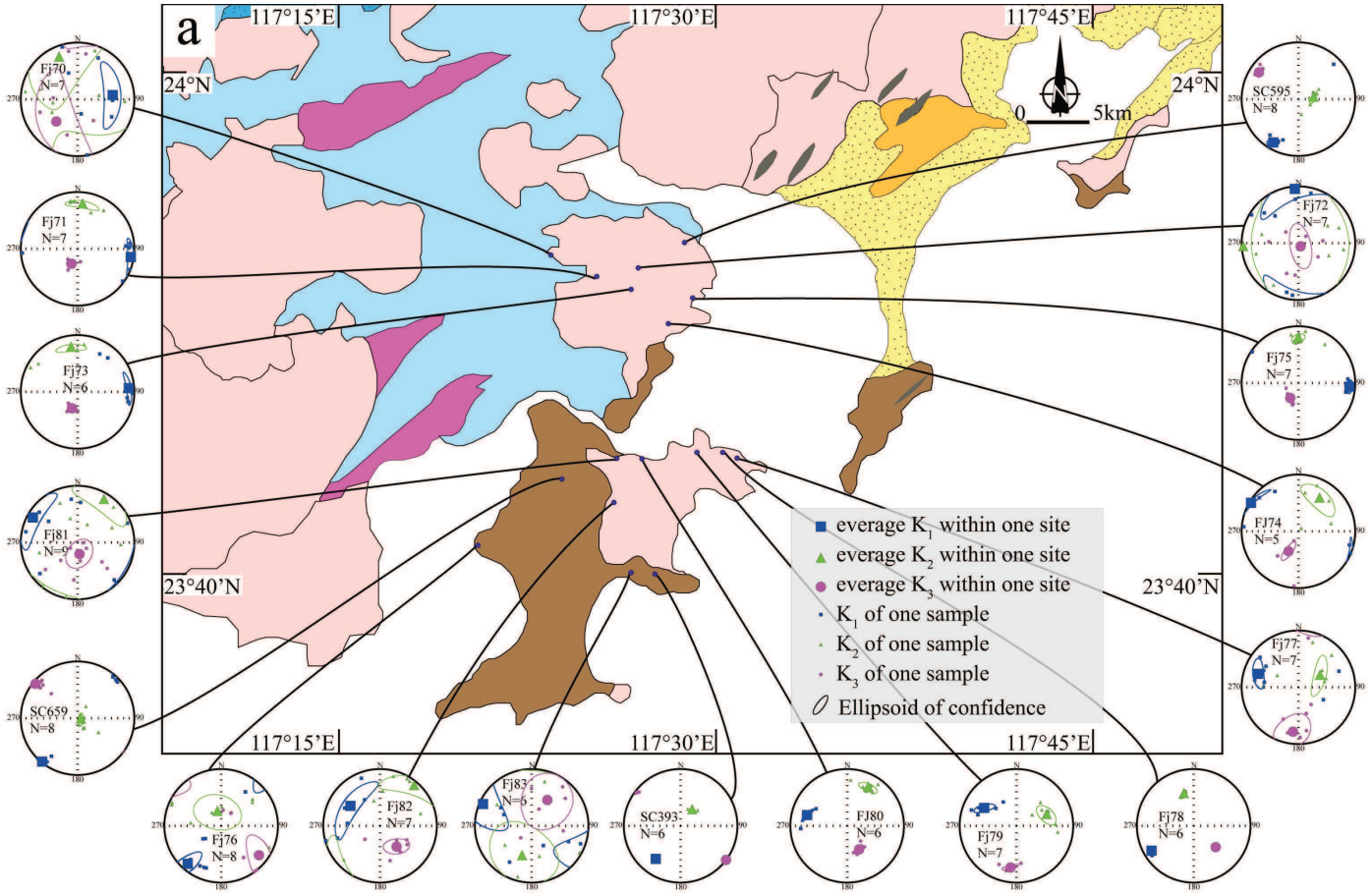

Figure 3 12: The steoro projection diagrams of AMS data of the CNB

a: the Yunxiao-Dongshan area, b: the Longhai-Gangwei area, c: the Jinjiang-Shishi area, d: the Quanzhou-Huian area, e: the Fuqing-Pingtan area

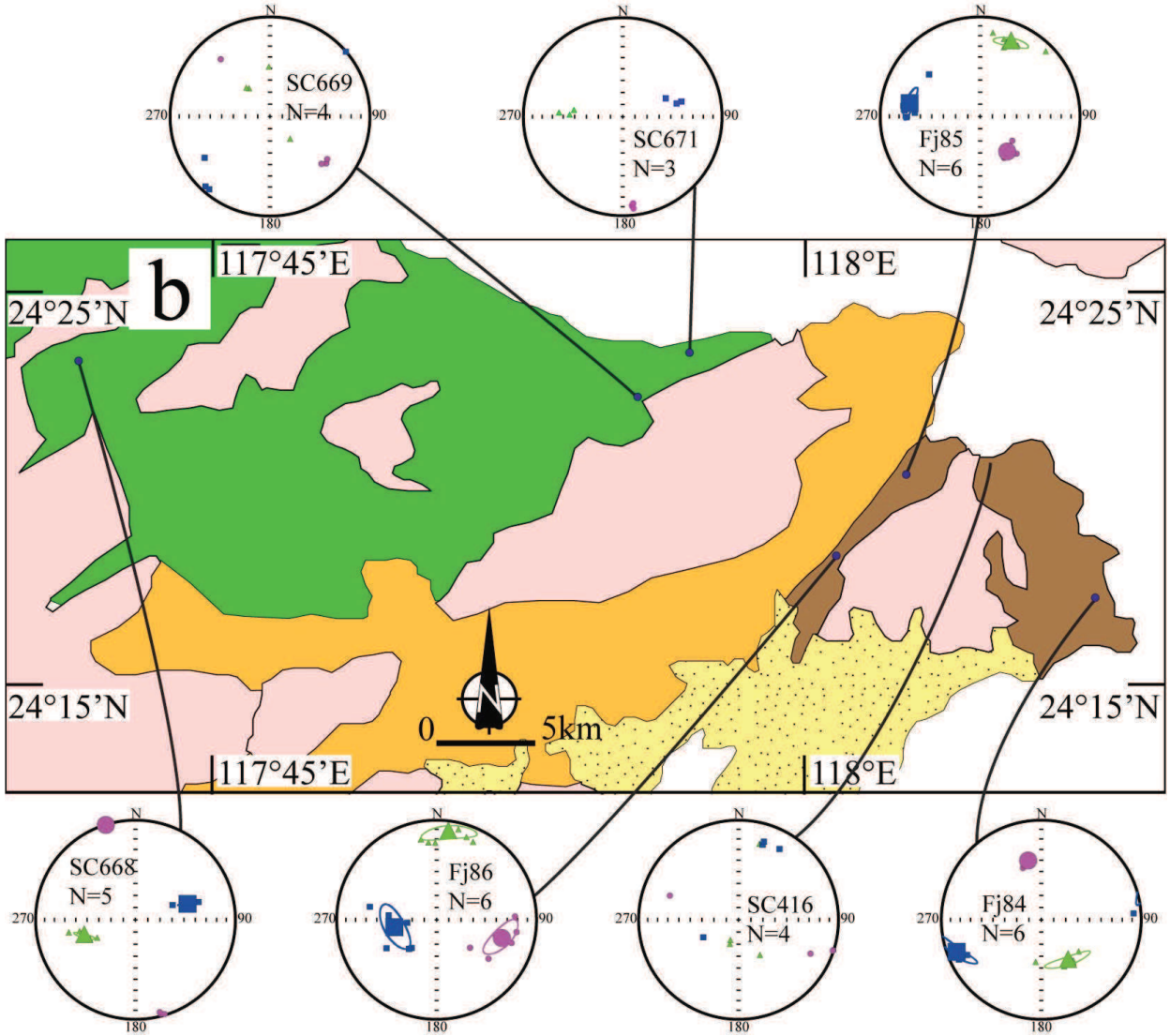
SC669
N=4
SC671
N=3
Fj85
N=6
b
117°45'E
118°E
24°25'N
24°15'N
0
5km
SC668
N=5
Fj86
N=6
SC416
N=4
Fj84
N=6

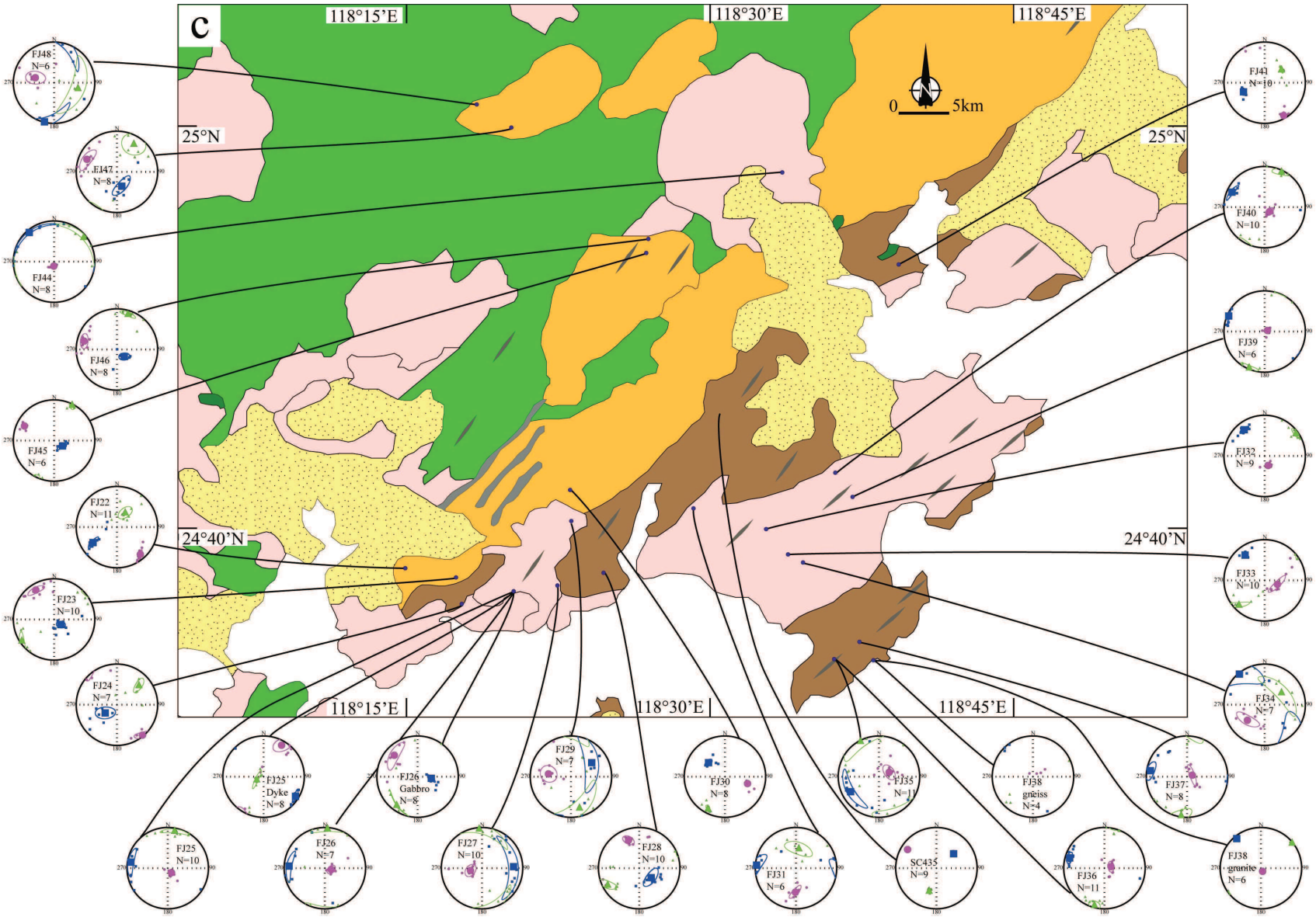
c
118°15'E
118°30'E
118°45'E
25°N
24°40'N
0
5km
FJ48 N=6
FJ47 N=8
FJ44 N=8
FJ46 N=8
FJ45 N=6
FJ22 N=11
FJ23 N=10
FJ24 N=7
FJ41 N=10
FJ40 N=10
FJ39 N=6
FJ32 N=9
FJ33 N=10
FJ34 N=7
FJ25 Dyke N=8
FJ26 Gabbro N=8
FJ29 N=7
FJ30 N=8
FJ35 N=11
FJ38 gneiss N=4
FJ37 N=8
FJ25 N=10
FJ26 N=7
FJ27 N=10
FJ28 N=10
FJ31 N=6
SC435 N=9
FJ36 N=11
FJ38 granite N=6

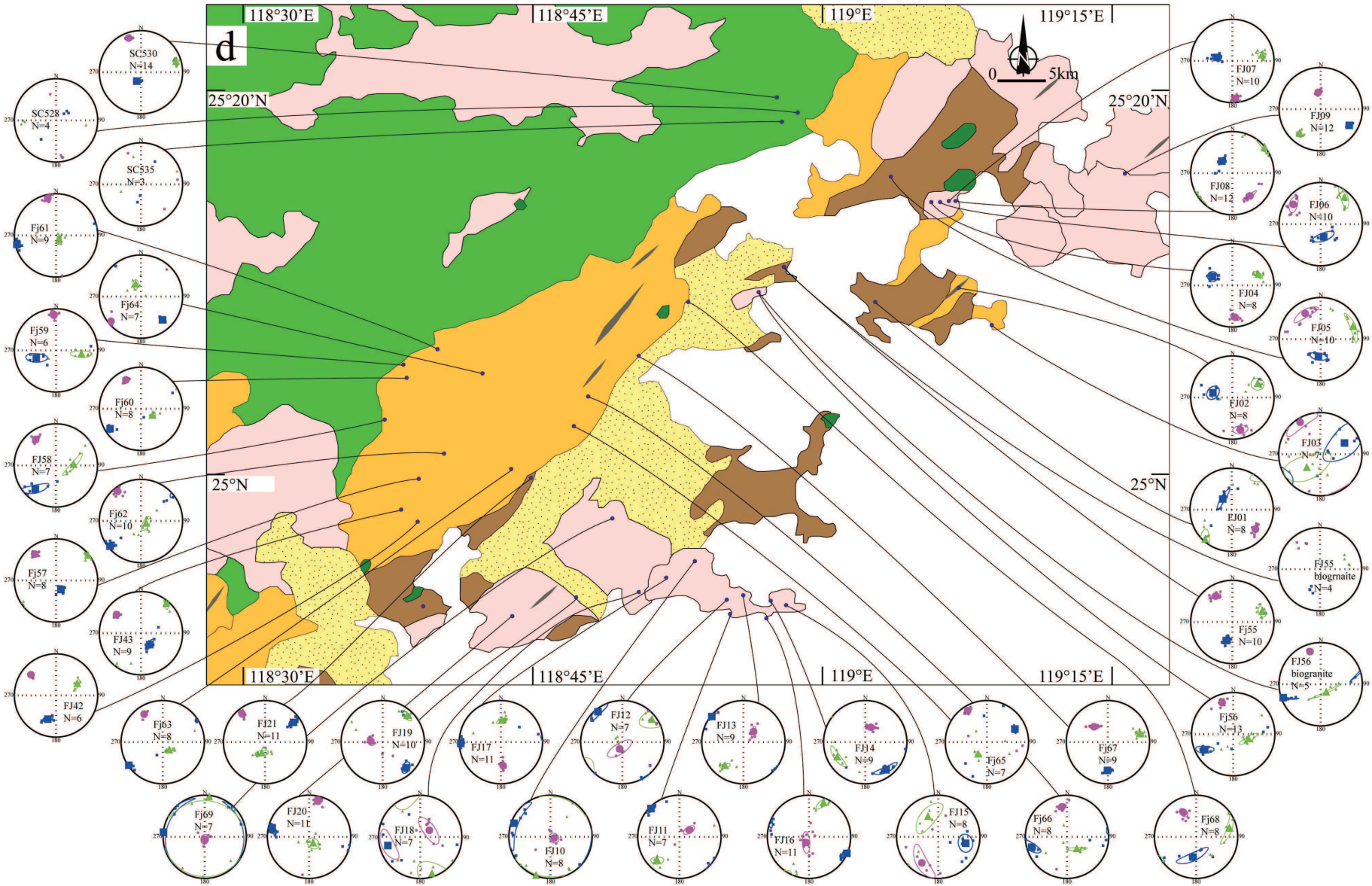
d
118°30'E
118°45'E
119°E
119°15'E
25°20'N
25°N
0
5km
SC530 N=14
SC528 N=4
SC535 N=3
Fj61 N=9
Fj64 N=7
Fj59 N=6
Fj60 N=8
FJ58 N=7
Fj62 N=10
Fj57 N=8
FJ43 N=9
FJ42 N=6
FJ07 N=10
FJ09 N=12
FJ08 N=12
FJ06 N=10
FJ04 N=8
FJ05 N=10
FJ02 N=8
FJ03 N=7
EJ01 N=8
FJ55 biogrnaite N=4
Fj55 N=10
FJ56 biogranite N=5
Fj56 N=13
Fj63 N=8
FJ21 N=11
FJ19 N=10
FJ17 N=11
FJ12 N=7
FJ13 N=9
FJ14 N=9
Fj65 N=7
Fj67 N=9
Fj69 N=7
FJ20 N=11
FJ18 N=7
FJ10 N=8
FJ11 N=7
FJ16 N=11
FJ15 N=8
Fj66 N=8
Fj68 N=8

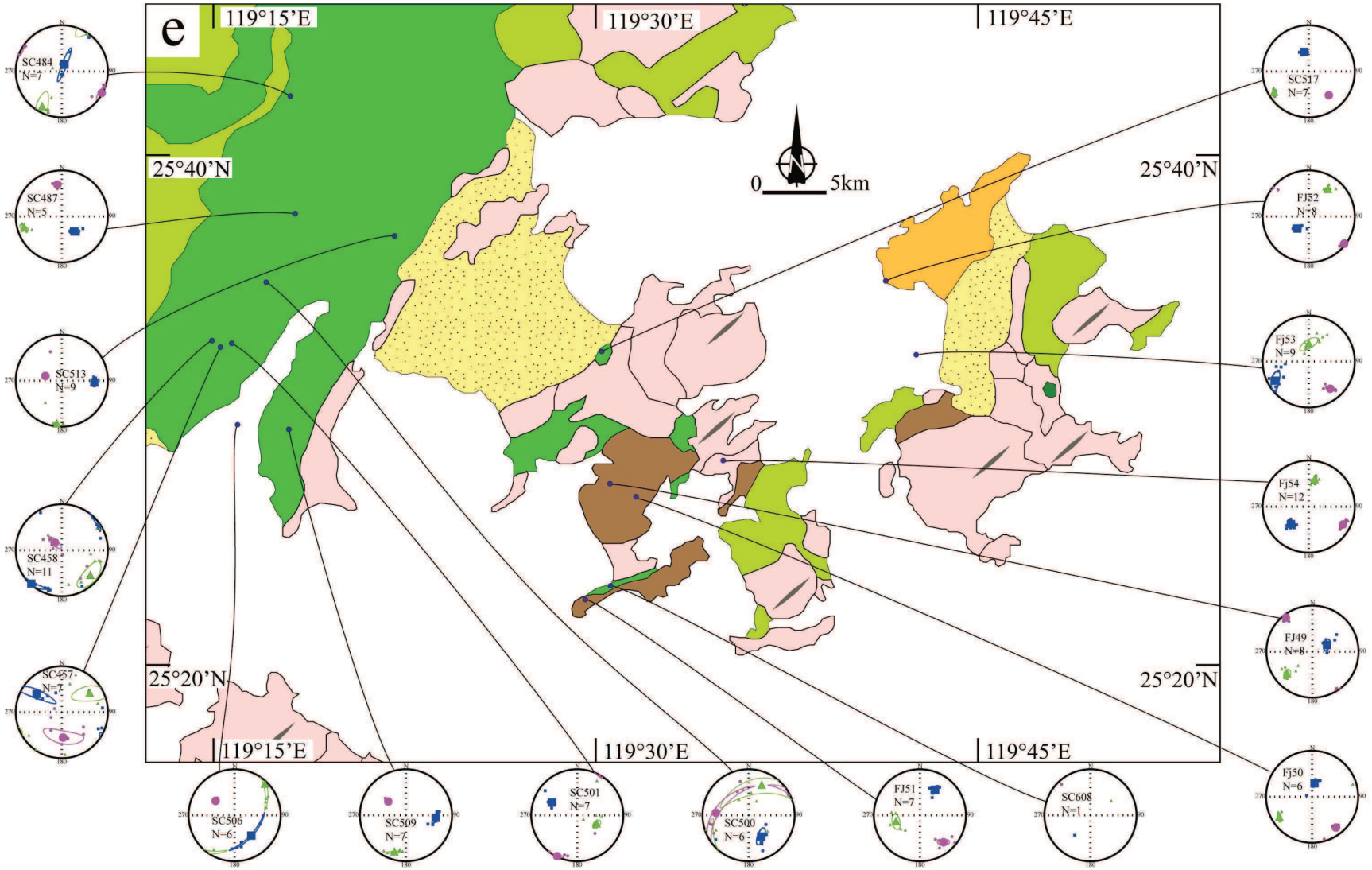
e
119°15'E
119°30'E
119°45'E
25°40'N
25°20'N
0
5km
SC484 N=7
SC487 N=5
SC513 N=9
SC458 N=11
SC457 N=7
SC506 N=6
SC509 N=7
SC501 N=7
SC500 N=6
FJ51 N=7
SC608 N=1
SC517 N=7
FJ52 N=8
Fj53 N=9
Fj54 N=12
FJ49 N=8
Fj50 N=6

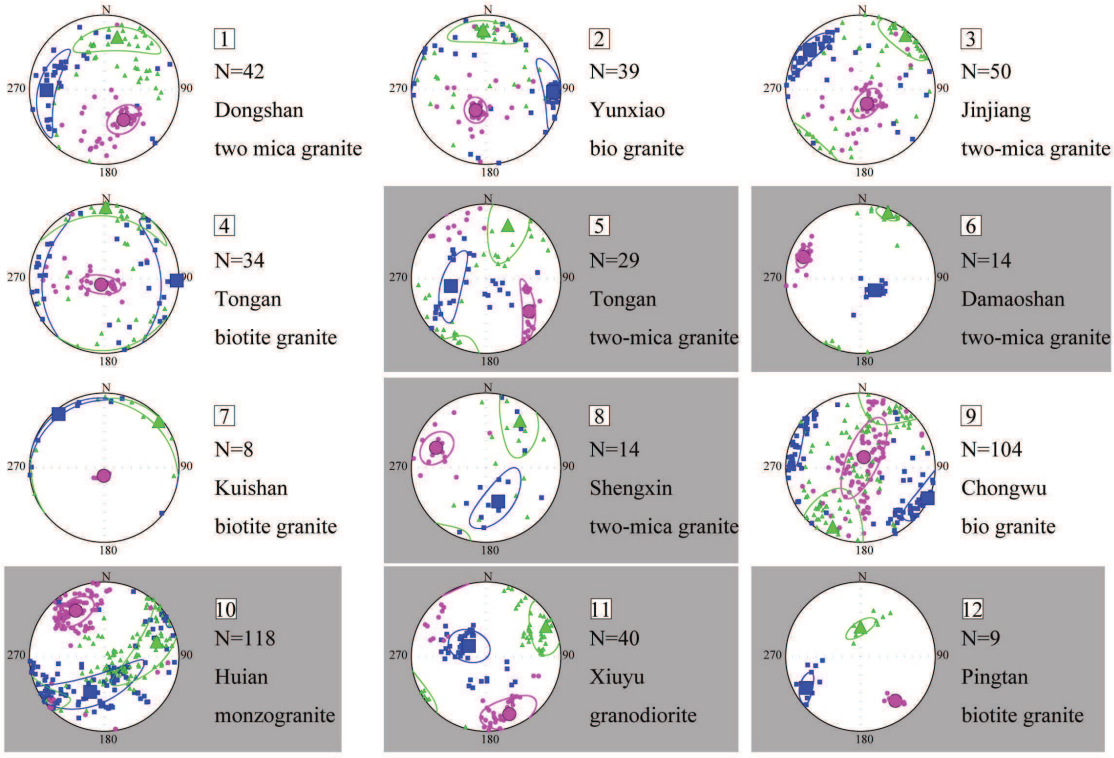

Figure 3 13: The total steoro projection of AMS data of the CNB

1,2,3,4,7,9: isotropic granitoids, 5,6,8,10,11,12:syn-tectonic granitoids. The locations of the plutons refer to Fig. 3-1. Big and small blue rectangle represent average K_1 of the pluton and individual K_1 of specimen, respectively, big and small green triangle represent average K_2 of the pluton and individual K_2 of specimen, respectively, big and small red circle represent average K_3 of the pluton and individual K_3 of specimen, respectively,

6 Microscopic observations

6.1 Oriented thin-section making

In order to observe the deformation style and determine the shear sense, oriented thin-sections have been made along the direction which is parallel to the lineation/magnetic lineation and perpendicular to the foliation/magnetic foliation from the oriented hand specimens acquired in the field work and the AMS standard column specimens, respectively. Besides, for those specimens in which NE-SW shallow inclined lineation develops, the oriented thin-sections

perpendicular to the lineation/magnetic lineation and perpendicular to the foliation/magnetic foliation were also made.

6.2 Deformation style

The deformation style of pervasively sub-solidus deformed granitoids and micaschist of the gneiss unite are described as follows: in the oriented thin-sections made from the specimens with NW-SE or highly inclined lineations, feldspars and micas are oriented. Some big grains of feldspar were cracked (Fig. 3-14a). The quartz were stretched, some grains even developed "sigmoidal" shape, or sub-grains which formed oblique foliation (Fig. 3-14b). In the case of lowly inclined foliation/magnetic foliation, the shear sense is top-to-the-NW, while the foliation/magnetic foliation is highly inclined, the shear sense is NW side down and SE side up. In the oriented thin-sections made from the specimens with NE-SW lowly inclined lineation/magnetic lineation, along the direction which is parallel to the lineation/magnetic lineation and perpendicular to the foliation/magnetic foliation, it is to observe that the micas were oriented, quartz grains are stretched, wavy extinction, developing sub-grains. However, no shear sense has been observed (Fig. 3-14c). Along the direction which is perpendicular to the lineation/magnetic lineation and perpendicular to the foliation/magnetic foliation, folded foliation has been observed (Fig. 3-14d).

In the oriented thin-sections made from deformed volcanites, along the direction which is parallel to the NW-SE lineation/magnetic lineation and perpendicular to the foliation/magnetic foliation, the deformed volcanite is featured by porphyritic tecture. The phenocrysts are usually plagioclase and quartz. Plagioclase grains are featured by wavy extinction, cracks, necking and asymmetric pressure shadow developing in the shear (Fig. 3-14e). Sericite is oriented to form shear bend (Fig. 3-14f). Quartz is featured by wavy extinction, sub-grains, and developed "sigmoidal" shape. In the case of lowly inclined foliation/magnetic foliation, such shear senses indicate a top-to-the-NW motion while in the case of highly inclined foliaton/magnetic foliation, the shear sense is NW side down and SE side up. In the oriented thin-sections along the direction which is parallel to the NE-SW lowly inclined magnetic lineation and perpendicular to the magnetic foliation, cracked plagioclase, wavy extinction and sub-grains of quartz were observed, however, no shear sense was found.

In the oriented thin-sections, the syn-tectonic granitoids were featured by orientation of plagioclase along the direction of magnetic lineation. The plagioclase developed factures which are mostly perpendicular to the magnetic foliation and was further more infilled by quartz (Fig. 3-14g). Along the edge of plagioclase which is parallel to the magnetic foliation, there developed myrmikites (Fig. 3-14h). Plagioclase and micas are usually bended (Fig. 3-14i and j). Quartz developed wavy extinction and sub-grains. All of these phenomenons indicate that during the crystallization, the magma experienced a compression along the direction perpendicular to the magnetic foliation.

The isotropic granitoids are featured by automorphic plagioclase, micas, and anhedral quartz infill in the space between plagioclase and mica. No minerals orientation and deformation developed. The texture of rocks is typical magmatic (Fig. 3-14k). Along the edge of plagioclase which is parallel to the horizontal magnetic foliation, there developed myrmikit indicating a vertical compression (Fig. 3-14l).

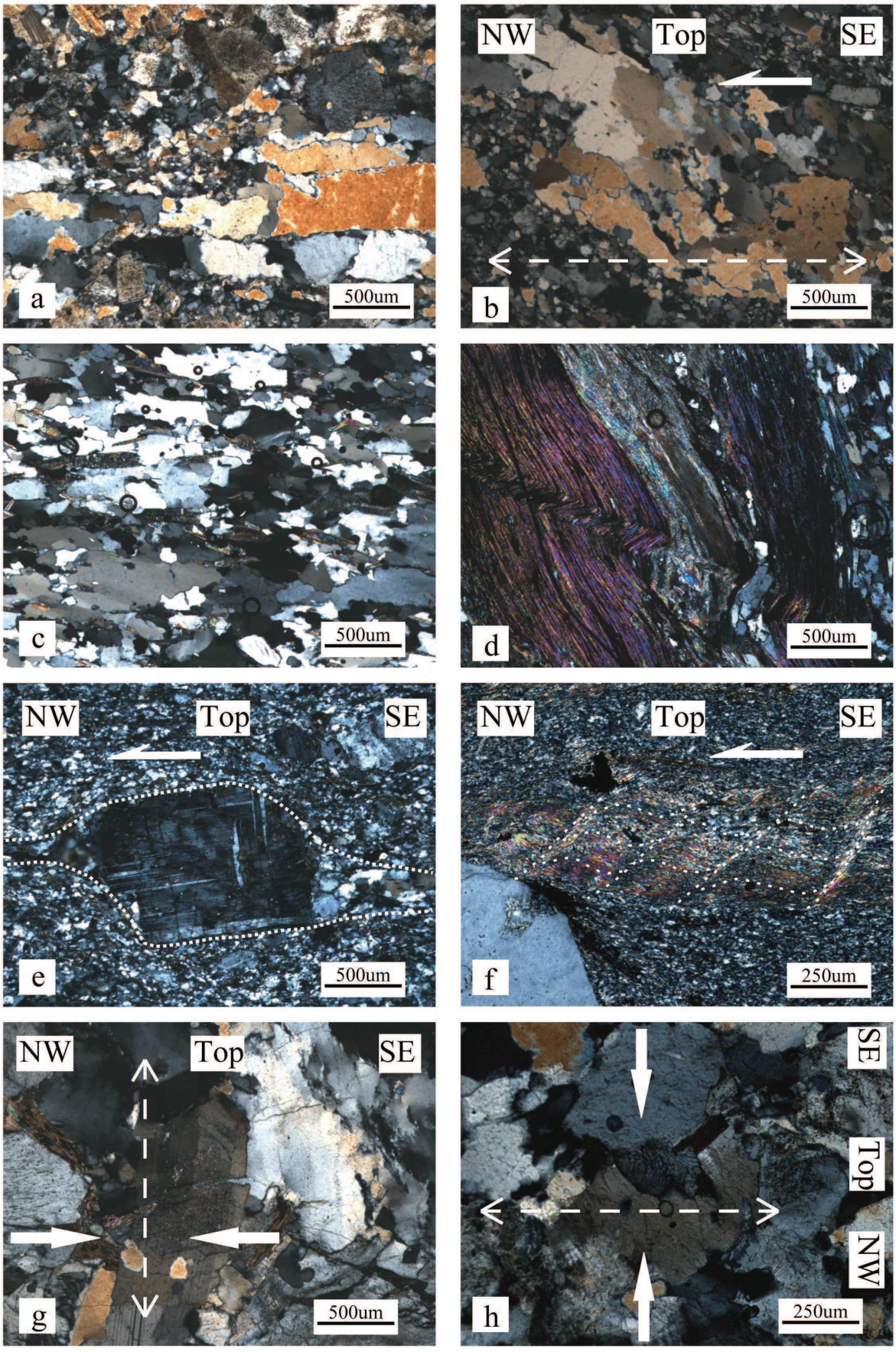
a
500um
NW
Top
SE
b
500um
c
500um
d
500um
NW
Top
SE
e
500um
NW
Top
SE
f
250um
NW
Top
SE
g
500um
SE
Top
NW
h
250um

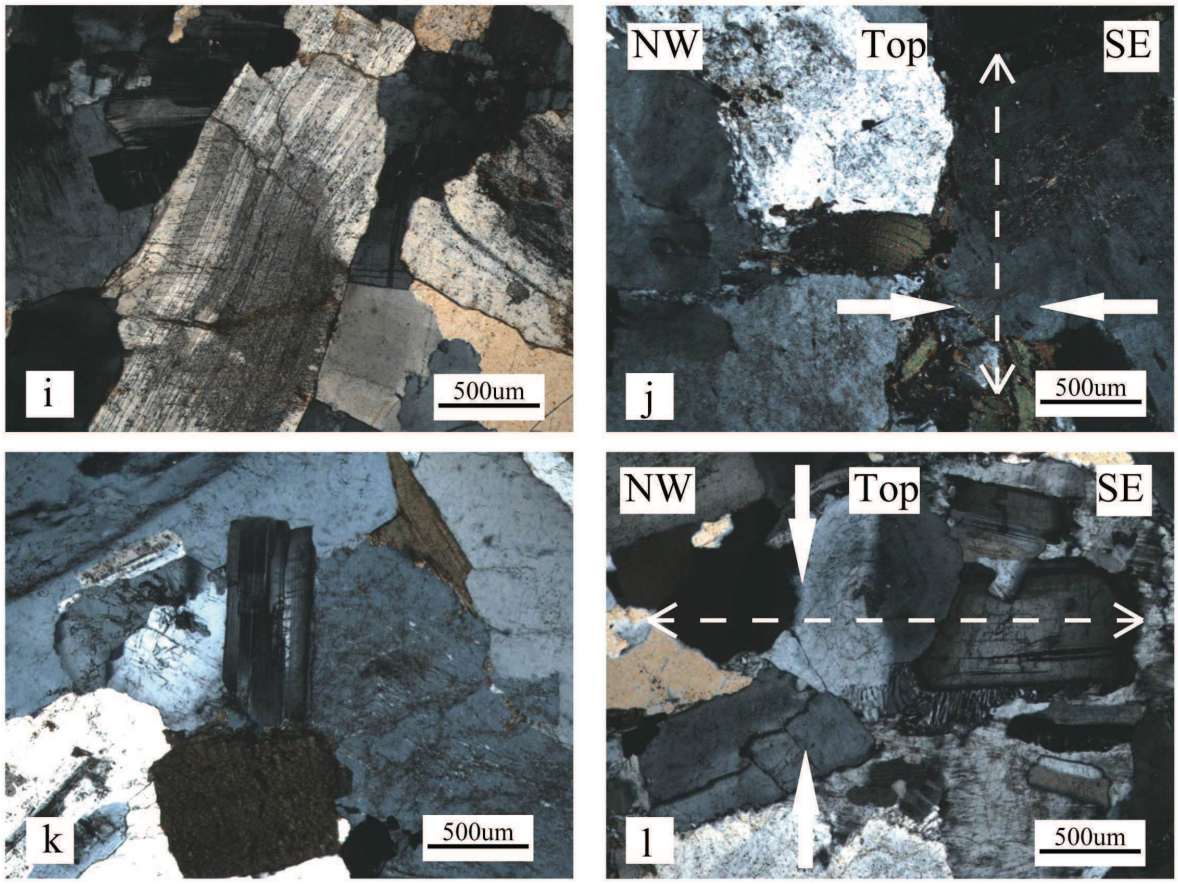

Figure 3 14: Microscopic photo of the granitoids in the CNB

All the microscopic photo were taken from the thin-sections parallel to the lineation/magnetic lineation and perpendicular to the foliation/magnetic foliation except for f which is along the direction perpendicular to the lineation and perpendicular to the foliation. White dashed line represents direction of foliation. a: quartz was stretched in the pervasively sub-solidus deformed granitoids, b: stretched quartz grains formed oblique foliation indicating top-to-the-NW shear sense, c: along the direction which is parallel to the NE-SW lowly inclined lineation, no shear sense was found, d: along the direction perpendicular to the NE-SW lowly inclined lineation, folds of foliation can be observed, e: in the deformed volcanites, the asymmetric pressure shadow indicates a top-to-the NW shear sense, f: in the deformed volcanites, shear bend indicates a top-to-the-NW shear sense, g: in the syn-tectonic granitoids, along the direction perpendicular to the highly inclined NE-SW magnetic foliation, plagioclase developed cracks indicating a NW-SE shortening, h: in the syn-tectonic granitoids, along the edge of plagioclase which is parallel to the highly inclined magnetic foliation, there developed myrmikit, i: in the syn-tectonic granitoids,

the plagioclase was ductile bended indicating a high temperature deformation above solidus of magma, j: in the syn-tectonic granitoids, along the direction which is perpendicular to the magnetic foliation, the long axis of biotite was bended indicating a NW-SE shortening, k: the isotropic granitoids is featured by magmatic texture, l: in the isotropic granitoids, along the edge of plagioclase which is parallel to the horizontal magnetic foliation, there developed myrmikit indicating a vertical shortening.

7 Discussion

7.1 Summaries on observation and measurement

The magnetic carriers of the rocks of the Gneiss Unit (the pervasively sub-solidus deformed granitoids and migmatite), the syn-tectonic granitoids, the isotropic granitoids are mainly magnetite while the magnetic carriers of the deformed volcanites are mainly paramagnetic minerals. Hematite only occurred in some specimens of volcanites and there is just one site are featured by anti-magnetic minerals. Thus a conclusion can be reached that except for the only one site of volcanites, all the magnetic fabrics acquired in the CNB is normal magnetic fabric whose AMS ellipsoid represent strain ellipsoid and can be directly used in structural interpretation. As for the only one site featured by anti-magnetic minerals, in the process of structural interpretation, it should be kept in mind that, the K_1 of AMS ellipsoid represent c axis of strain ellipsoid and the K_3 of AMS ellipsoid represent a axis of strain ellipsoid.

The Gneiss Unit and the Deformed Volcanites Unit of the CNB stretch along NE-SW direction. Both of the foliations/magnetic foliations of these two units strike along the NE-SW direction which is parallel with the stretching direction of these two units. The variation of the foliation/magnetic foliation indicates a later folding alteration on these two unites. The lineations/magnetic linations scatter. According to whether it is parallel to the strike of the foliation or not, the lineation/magnetic lineation can be divided into A-type and B-type. The former developed coeval with the foliation while the latter developed coeval with the fold. In order to acquire the original lineation mode, it is necessary to restore the foliation to horizontal.

After the restoration, the B-type lineation does not change obviously and retain NE-SW direction, while the A-type lineation concentrates on NW-SE direction. At the same time, all of the indicators of shear sense concentrate on top-to-the-NW motion.

The syn-tectonic granitoids in the CNB are usually spindle shaped. The long axe of these granitoids are NE-SW directioned. In the field work, it is observed that NE-SE striking magmatic foliation usually developed along the boundary of these granitoids. The microgranitoids enclaves included in these plutons are oblate whose ab plates are parallel with the magmatic foliation. The magnetic foliation of the syn-tectonic granitoids is predominantly highly inclined and striking NE-SW while the magnetic lineation scatters. Microscopic observations indicate that on the thin-sections parallel to the magnetic lineation and perpendicular to the magnetic foliation, the plagioclase and micas are bended, oriented. Along the NW-SE direction, the plagioclase was cracked and infilled by quartz. Along the edge of plagioclase which is parallel to the highly inclined magnetic foliation, there developed myrmikit. All of these phenomenons indicate a NW-SE compression.

Field observations show that in the isotropic granitoids, the minerals are undeformed and not oriented. Microscopic observations show that the rocks are featured by magmatic texture. Amphibole, plagioclase, micas are automorphic, quartz is semi automorphic. Along the edge of plagioclase which is parallel to the horizontal magnetic foliation, there developed myrmikit indicating vertical compression. The magnetic lineation of all the isotropic granitoids is well oriented along the NW-SE direction.

7.2 Polyphase tectonics in the CNB

As the previous studies showed, the amphibolites metamorphic phases had been attended during the deformation of the Gneissic Unit while the Deformed Volcanites Unit only experienced the green schist metamorphic phase (Chen, 1997; FJBGMR, 1985; Tong and Tobisch, 1996). Owing to the big gap of the metamorphism between the two units, Wang and Lu (Wang and Lu, 2000) attributed the different metamorphic facies: amphibolite in the Gneiss Unit, and low green schist in the Deformed Volcanic Unit, to two different tectonic events, namely, the formation of the basement of the Min-Tai microcontinent recorded by the gneissic rocks, and the

collision between the Min-Tai microcontinent and the Min-Zhe volcanic arc recorded by the deformed volcanites indicating a strike-slip displacement.

The previous studies divided the lineation of the CNB into two type, the former is NE-SW lowly inclined lineation which is parallel to the strike of the NE-SW foliation (Tong and Tobisch, 1996; Shu et al., 2000; Wang and Lu, 2000), the latter is the lineation ranging from ENE-WSW to NNE-SSE which is oblique to the strike of the foliation (Charvet et al., 1990). Both of these two types of lineations have been interpreted as the evidences of the strike-slip displacement. Besides, there are also some narrow mylonitic shear zone with tens of centimeter or several meters in width crosscutting the gneissic rocks (Tong and Tobisch, 1996). Further more, these narrow shear zones were NE-SW and NW-SE conjugated (Wang and Lu, 1997b), and deformed in the green schist metamorphic phase condition (Wang and Lu, 2000). Thus, the displacement of the CNB was interpreted as a two stage deformation, a older N-S compression featured by sinistral strike-slip displacement and a later E-W compression featured by a dextral strike-slip displacement, respectively (Wang and Lu, 1997b).

However, a single tectonic event can leave different footprints at different crustal depths. The gneissic rocks may just represent a deeper and hotter deformation level comparing to the shallow-crust deformed volcanic rocks (Fig. 3-15). The structural consistency, i.e. the fabric attitude, and shear sense in both units supports this argument (Fig. 3-5b and c). In the Shijing village of the Jianjiang county, NE-SW striking foliation of amphibolites and NW-SE amphibole stretching lineation indicate that coeval to the amphiboles metamorphic phase, the deformation of the CNB was also active (Fig. 3-4d). The kinematics of the CNB should be determined by the shear sense in the foliation of the gneiss and the deformed volcanites. The narrow shear zones were just products of late stage local event which does not represent the whole CNB. The fact that the deformation in the Gneiss Unit was more pervasive than that in the Deformed Volcanite Unit indicates a SE-ward strain increase.

Based on field and laboratory observations, the Late Mesozoic tectonics of CNB can be subdivided into E_1, E_2 and E_3 phases. The E_1 phase, responsible for the development of the foliation in the Gneiss and Deformed Volcanite Units, can be further divided into an E_{1a} and an E_{1b} events in terms of structural superimposition, however, as they present a continuity of a same tectonic event, E_{1b} can be considered as a late increment of E_1 phase.

The E_1a event that controls the architecture of the CNB is responsible for the formation of S_1 foliation, L_1 lineation and related kinematics observed in both Gneiss and Deformed Volcanite Units (Fig. 3-5B and 3-5C). In spite of a consistent strike of S_1, L_1 scatters both in strike and dip (Fig. 3-5C1-C4). This dispersion is due to the E_{1b} event that folded the S_1 foliation and rotated L_1. In order to retrace the original L_1 orientation, it is necessary to restore S_1 to its initial geometry. It is reasonable to assume a subhorizontal E_{1a} foliation attitude. Thus after restoring the S_1 to horizontal, most of L_1 mineral or magnetic lineations concentrate along the NW-SE direction, except only a few NE-SW horizontal ones (Fig. 3-5C5 and 3-5C6). Representing 26% of the total amount of the measured lineation, the NE-SW lineation is mostly exposed in the Dongshan Island (Fig. 3-5B). In the Aojiao and Sufeng villages, a NE-SW mineral lineation is parallel to axes of NW-verging fold axes (Fig. 3-4b, location 1 in Fig. 3-5B). Along this NE-SW lineation, kinematic indicators are absent, either in the field or in the thin section, though a minor amount of stretching do exist, as indicated by elongated and recrystallized quartz grains. Thus a coaxial strain regime can be determined along the NE-SW lineation that is therefore interpreted as a B-type structure, i.e. perpendicular to the transport direction, formed during the folding, and does not represent a regional shearing direction.

The E_1b event is responsible for the folding of S_1 in the gneiss, volcanites. The NW fold vergence is consistent with the E_1a kinematics (Fig. 3-4b, e, f, g and i). The E_1b event produced an important variation in dip of both foliation and lineation.

To summarize, the deformation in Gneiss and Deformed Volcanite Unites argue a NW-directed thrust. On the rims of K_1 syntectonic plutons, the NE-SW striking highly inclined magmatic foliation also argues a NW-SE compression.

The E_2 phase is coeval with the opening of NE-SW striking brittle cracks filled by dykes (e.g. Dong et al., 2006). The oldest age of the Late Cretaceous volcanites of Shimaoshan Formation which was not involved in the deformation of the Changle-Nan'ao Belt is 104 Ma. All of the granitoids emplaced after 100 Ma are isotropic granitoids, such as the fine grain granite in weitou is 100.9±0.9Ma (Liu et al., 2012), the Dongshan two-mica granite is 100±3Ma (this study). The emplacement of isotropic granitoids usually did not alter the E_1 fabric of country rocks. For example, the Yunxiao biotite granite in Yunxiao county (Fig. 3-11a), the Taiwushan two-mica granite in Longhai county (Fig. 3-11b) and the Jinjiang two-mica granite in Jinjiang

county (Fig. 3-11c). These indicate that the emplacement of these granitoids were permissive, and the room occupied by the plutons were offered by the regional extension (Pitcher, 1979b). It is worth to note that these kind of granitoids, regardless their emplacement location, whether in the Gneiss Unit or in the Deformed Volcanites Unit, whether in the north part or in the south part of the CNB, the magnetic foliations and lineations in each site in the pluton are predominantly horizontal and NW-SE directing, respectively (Fig. 3-11a-e, 12a-e,13). As previous studies showed, in those plutons which emplaced during extension, the magnetic lineation concentrated and was parallel to the regional extension direction (Talbot et al., 2000; Joly et al., 2007; Turrillot et al., 2011; Lin et al., 2013). This phenomenon is caused by that, during the crystallization of the magma, the crystallizing velocity of minerals is highest along the regional extension direction (Talbot et al., 2000; Joly et al., 2007; Turrillot et al., 2011; Lin et al., 2013). Thus it is logic to interpret that after 105 Ma the CNB experienced a NW-SE extension event as indicated by the NW-SE magnetic lineation. And the predominant horizontal magnetic foliation indicates a vertical magma upwelling which occupies the room opened by such extension (Wei et al., 2013). The NW-SE extension summarized by the NW-SE magnetic lineation is also favored by the regional distributed NE-SW dykes whose age is ca 90 Ma (Dong et al., 2006). Although a series evidences exist, this E_2 extension is rather weak in which just crustal tension gashes opened to accommodate granite and dykes, no obvious regional scaled ductile fault developed.

The E_3 event is featured by late NE-SW shear zones. Since the scarcity of this kind of outcrops, in the following, this structure that cut the isotropic granites will not be considered.

Since a long time, the CNB has been regarded as a ductile strike-slip fault due to the observation of a NE-SW lineation parallel, in Dongshan island, or oblique, in the rest of CNB, to the strike of the foliation, and discovery of cm-wide mylonitic shear zones (Charvet et al., 1990; Tong and Tobisch, 1996; Wang and Lu, 2000). Our field investigation and AMS study acknowledge the previous observations, however our interpretation differs as follows. 1) The flat-lying foliation with a NW-SE lineation in many sites does not support the existence of a NE-SW strike-slip fault (e.g. location 3 and 4 in Fig. 3-5B); 2) After restoring S_1 to horizontal, the oblique lineation strikes NW-SE, and the shear sense is consistently top-to-the-NW (Fig. 3-5C5, C6); 3) regardless of the origin of the NE-SW horizontal lineation, its rare abundance, local occurrence (mainly in Dongshan island), and absence of shear sense, reduce the possibility

of a significant strike-slip faulting; 4) the E_3 mylonitic shear zones belong to a late event.

7.3 Deformation age of the Changle-Nan'ao belt

Biotite, muscovite, amphibole yield ^{40}Ar-^{39}Ar ages between 133 and 84 Ma (Wang and Lu, 2000; Chen et al., 2002). However, owing to the extensive occurrence of the late magmatism, the ^{40}Ar-^{39}Ar chronometer may have been reset and may not always represent the age of the E_1 phase (Li et al., 2003). For example, the zircon age of the migmatite in the Jinjiang coast area is 140±1Ma (Cui et al., 2013), the biotite and muscovite ^{40}Ar-^{39}Ar age is 98-99Ma (Fu et al., 1989), the U-Pb zircon age of the mafic dykes in the same area is 90±2Ma and 87±2Ma (Fig. 3-1b) (Dong et al., 2006); the U-Pb zircon age of gneiss in Shen'ao is 141-147Ma(Cui et al., 2013; Liu et al., 2012), the amphibole ^{40}Ar-^{39}Ar age is 91.6±1.9Ma, the k-feldspar ^{40}Ar-^{39}Ar age is 86.9±1.8Ma (Chen et al., 2002), the U-Pb zircon age of the adjacent Taiwushan two-mica granite is 96.9±1.3Ma (Fig. 3-1b) (Zhao et al., 2012); the U-Pb zircon age of the Donggu micaschist is 142±2Ma (Liu et al., 2012), the biotite ^{40}Ar-^{39}Ar age is 107.9±2.4Ma (Wang and Lu, 2000), the adjacent monazite U-Pb chemistry age of the Dongshan two-mica granite is 100±3Ma (Fig. 3-1b and 3-7b). Apparently, the ^{40}Ar-^{39}Ar clock has been reset and thus, the deformation age of CNB should be determined by U-Pb zircon age whose closure temperature is higher. Recent zircon U-Pb datings of granite and volcanite in the study area show that the youngest ages of the volcanites involved in E_1 is 130 Ma, and the oldest age of the undeformed volcanites is 104 Ma (Guo et al., 2012). This late K_1 period is also the emplacement age of the Duxun (120 Ma), Weitou (108 Ma), Geshan (131 Ma), Sucuo (130 Ma), and Niutouwei (130 Ma) syntectonic granitoids (Li et al., 2003; Liu et al., 2012; Cui et al., 2013; locations 4, 5, 6, 9 in Fig. 3-5B). Thus a ca 130-105 Ma age is proposed for the E_1 phase.

7.4 Geodynamic context of the Changle-Nan'ao Belt

In the Late Mesozoic, the EACM experienced several tectonic events accommodated by the Paleo-Pacific-Eurasia convergence. The SW Japan nappes, the blueschists of the Tananao complex in Taiwan and the ophiolite-melange complex in the West Philippines argue for subduction and closure of the Paleo-Pacific ocean basin (Faure et al., 1987, 1989; Wintsch et al., 2011). The coeval magmatic belt in Zhejiang-Fujian area is featured by arc affinity (Lapierre et

al., 1997). In this period, the EACM was considered as a andean type active continental margin (Li et al., 2012). In the Philippines, South-directed ophiolite nappe thrusting due to the collision of the WPM with SCB is documented (Faure et al., 1989; Faure and Natal'in, 1992). Because the south china sea was opened in the Tertiary (Huchon et al., 1998; Hutchison, 2004), so in the Cretaceous, the West Philippines was besides South China Block (Faure et al., 1989). Given that the West Philippines experienced a clockwise rotation due to the opening of the South China Sea during the Cenozoic (Zhou et al., 1995; Almasco et al., 2000), in Early Cretaceous, the West Philippines Suture (WPS) was featured by a SE-directed nappe. Before Early Cretaceous, the WPM was to the SE of the CNB (Hall, 2012). Thus the top-to-the-NW shear sense in the CNB could be interpreted as a back-thrust with respect to the WPS (Fig. 3-15). After the E_1 event, the E_2 one, coeval with granitoid emplacement, including A-type plutons throughout the study area (Li et al., 2013b), suggests an extensional regime, though structural data to support this view remain to be documented.

7.5 The relationship between the Deformed Volcanites Unit and the Gneiss Unit

Owing to the metamorphic phase gap between the low green schist deformed volcanites unit and the amphibolite phase Gneiss Unit, their structural relationship is a interesting topic among the geology society. Zhu et al. (Zhu et al., 1993) argued that the deformed volcanites were unconformity overlain on the gneiss. Other researchers considered that there was an ophiolitic suture zone between the Deformed Volcanites Unit and the Gneiss Unit (Hsu et al., 1990; Lu et al., 1994; Wang and Lu, 1997b). However, the unconformity is hard to account the difference of the metamorphic phases between the two units. The scattered gabbros which are used to be considered as the member of Changle-Nan'ao suture zone are not usually deformed, and the geochemistry characteristics of these gabbros does not match the gabbro of ophiolite (Xu et al., 1999; Zou, 1995). By calculating Al^{total} in amphibole geobarometer, Tong and Tobisch (1996) indicated that the syn-tectonic granite intruding into the Gneiss Unit emplaced at 16 km depth. Now, these syn-tectonic granites expose in the surface, thus there is an exhumation process of the

Gneiss Unit. After calculating the cooling rate by using ^{40}Ar-^{39}Ar data, Chen et al. (2002) assumed that thrust may play a role in the exhumation of the Gneiss Unit. However, this hypothesis needs more structural data.

In this study, the boundary between the Gneiss Unit and the Deformed Volcanites Unit was observed in the Fuqing area. On both sides of the boundary, the shear senses indicate NW side descend and SE side ascend. This geometry has two different interpretations: 1, the two units contact with each other by a normal fault in which the Deformed Volcanites Unit is the hanging wall and the Gneiss Unit is the foot wall; 2. The two units contact with each other by a thrust fault in which the Deformed Volcanites Unit is the foot wall and the Gneiss Unit is the hanging wall. Considering the extension event occurred during E_2, if the contact relationship is a normal fault, it should be active during E_2. However, the E_2 event is featured by tension gash opening and emplacement of plutons and dyke swarm without developing normal fault, we prefer the contact relationship is a thrust fault. In this model, the gneiss was thrust on the deformed volcanites in E_1a, and the contacting surface was folded and became highly inclined in E_1b.

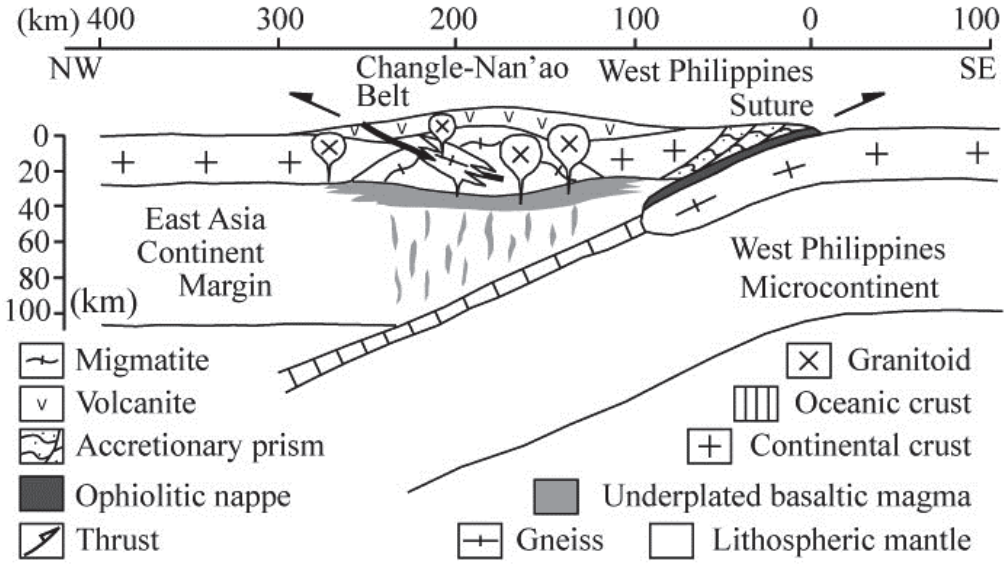

Figure 3 15 tectonic model of southeast margin of the South China Block during the Late Messozic

8 Summary

In this chapter, combined with previous geochronological studies, this detail structural analysis of CNB, AMS measurement, monazite U-Pb chemistry dating allows us to reappraise the tectonic scenario of the SE. coast area of SCB. Our model, at variance with previous ones, poses that during the E_1 event between 130-105 Ma, a NW-directed thrust developed, forming a NE-SW striking low-angle foliation and a NW-SE directed stretching lineation with a top-to-the-NW shear sense. The foliation was subsequently folded during the same tectonic phase. This thrust is considered as a back-thrust towards the East Asia continent due to the collision of the West Philippines Microcontinent with SCB. During the 104-90 Ma period, lava flows, post-orogenic granitoid and dykes emplaced probably in an extensional regime (E_2). Our results suggest that the Late Mezosoic tectonics in the East Asia Continental Margin were controlled by microcontinent collision and subsequent extension rather than by continental scale strike-slip faulting. The West Philippines Suture Zone and the Changle-Nan'ao Belt formed a thrust and back thrust couple on the Early Cretaceous Andean type East Asia Continent Margine.

Chapter 4 A multidisciplinary study on the emplacement mechanism of the Qingyang-Jiuhua Massif in Southeast China and its tectonic bearings.

In this chapter, the emplacement mechanism of the Qingyang-Jiuhua Massif, the regional tectonic regime of South Anhui area and their relation ship are discussed. This chapter is divided into two parts. These two parts have been accepted as Jounal of Asian Earth Sciences as research articles. In the first part, a systematic field observation, microscopic observation, magnetic fabric measurement, paleomagnetic study have been conducted in order to describe and analys the deformation style in different scope ranging mineral, field outcrop, massif and block. Based on the result acquired, a possible emplacement mechanism is proposed. The second part focuses on the emplacement depth and the 3D shape of the massif. The Al^{total} in amphibole geobarometer calculation and 2D gravity modeling has been conducted in order to determine the emplacement depth and the 3D shape of the massif. Based on the results of second part, the possible emplacement mechanism proposed in the first part is carefully exmamined and the relationship between emplacement mechanism and the syn-emplacement regional tectonic regime is discussed.

Part I

A multidisciplinary study on the emplacement mechanism of the Qingyang-Jiuhua Massif in Southeast China and its tectonic bearings. Part I: structural geology, AMS and paleomagnetism

W. Wei[a,b,c,d,e], Y. Chen[b,c,d], M. Faure[b,c,d], Y.H. Shi[f], G. Martelet[d], Q.L. Hou[a], W. Lin[e*], N. Le Breton[b,c,d], Q.C. Wang[e]

[a] University of Chinese Academy of Sciences, Beijing 100049, China

[b] Univ d'Orléans, ISTO, UMR 7327, 45071, Orléans, France

[c] CNRS/INSU, ISTO, UMR 7327, 45071 Orléans, France

[d] BRGM, ISTO, UMR 7327, BP 36009, 45060 Orléans, France

[e] Institute of Geology and Geophysics, Chinese Academy of Sciences, Beijing 100029, China

[f] Hefei University of Technology, Hefei 230009, China

[*]Corresponding author: linwei@mail.iggcas.ac.cn

Abstract

During the Cretaceous, the South China Block (SCB) experienced a widely distributed extensional event including numerous plutons emplacement and basin opening. Investigations on the tectonic regime coeval with pluton emplacement, and emplacement mechanism of the pluton remain relatively rare in the SCB. In order to address these questions, a multidisciplinary approach, including field structural and petrographic observations, anisotropy magnetic susceptibility (AMS) and paleomagnetic analyses, was carried out on the Qingyang-Jiuhua granitic massif which intrudes into the Lower Yangtze fold belt in the northeastern part of SCB. The Qingyang-Jiuhua massif is composed of the granodioritic Qingyang and monzogranitic Jiuhua plutons dated by zircon U-Pb method at ca. 142 Ma, and ca. 131 Ma, respectively. Our structural observations show that the intrusion of the Qingyang-Jiuhua massif does not modify the fold strike. A weak ductile deformation of the country rocks and granitoid can be only observed in the boundary zone with limited contact metamorphism. In the contact aureole of the

massif, the foliation follows the pluton contour, and the mineral lineation is rare. When present, it exhibits a down-dip attitude. Field and microstructural observations indicate isotropic magmatic textures in most parts of the massif. The AMS analysis of 93 sites reveals weak values for the anisotropy degree (P_J<1.2) and oblate magnetic fabric dominance (T>0) for most of the measured samples. Two principal foliation patterns are identified: horizontal foliations in the center of the plutons, and vertical foliations on the boundaries. Magnetic lineation strike is largely scattered, and weakly inclined at the scale of the entire massif. The paleomagnetic investigations indicate that (a) the younger Jiuhua pluton did not produce a remagnetization in the older Qingyang pluton, (b) no relative movement can be observed between these two plutons, (c) the entire massif did not experience any important relative movement with respect to South China, considering the paleomagnetic uncertainties. Integrating the newly obtained results with previous observations, our study favors a permissive emplacement mechanism for the two plutons, i.e. vertical magma intrusion into an opening space controlled by the NW-SE brittle stretching of the upper crust, which is in agreement with a weak extensional regional tectonic framework of the SCB.

Keywords

South China Block; Pluton emplacement mechanism; Anisotropy of Magnetic Susceptibility; Paleomagnetism; Cretaceous tectonic extension.

1 Introduction:

The Late Mesozoic geology of South China Block (SCB) is featured by a large number of graben or half-graben basins coupled with numerous plutons and related ore deposits (Gilder et al., 1991b; Goodell et al., 1991; Zhou et al., 2006; Li et al., 2010b; Mao et al., 2011). The plutons and the adjacent contemporary basins are often connected by normal faults (Shu et al., 2009b; Shu et al., 2007). Besides the plutons and basins, many other features, such as bimodal volcanic rocks, widely distributed dyke swarms, and development of normal faults systems, also argue for an extensional tectonic regime during the Late Mesozoic (Zhao et al., 2004; Zhou et al., 2006; Yu et al., 2007). Numerous geochronologic and geochemical studies have been conducted to

document the source and evolution of the Mesozoic magmatism (Liu et al., 2012; Wu et al., 2012). Presently, it is widely accepted that the Late Mesozoic volcanic rocks in SCB shows an obvious magmatic arc affinity (Zhou et al., 2006 and references therein), and the plutons have a mixed provenance containing juvenile mantle material to some extent (Zhao et al., 2004; Yu et al., 2005; Xu et al., 2010). Moreover, the age of the plutonism reveals a coastward polarity (Zhou and Li, 2000; Li and Li, 2007). These facts were synthesized into the several speculative and incompatible geodynamic models, considering an increase of the subduction angle of the Paleopacific plate (Zhou and Li, 2000) and a retreat of the Paleopacific slab (Li and Li, 2007). Moreover, it is worth to note that an NW-SE striking granitoid belt of ca. 400 km in length and 100 km in width was developed from 150 Ma to 120 Ma, without any coastward polarity, in the lower Yangtze area in the northeast part of the SCB (Ling et al., 2009; Wu et al., 2012). Due to its variable composition of I-type, A-type granitoids and adakites, this belt is controversially interpreted as a result of Ocean Ridge Subduction (Ling et al., 2009; Sun et al., 2007) or a collapse of thickened crust (Zhang et al., 2008).

To better understand the geodynamic context of this extensional event, the assessment of the contemporary regional tectonics, and the mechanisms of pluton emplacement are also crucial. Although the geochemistry data is abundant in the Lower Yangtze area, the detailed structural analyses, such as structural observations to recognize the different scales of deformation, and extension direction, are still rare. Available regional deformation data in this area are derived from several scattered locations with ductile deformation and the regional extension direction are still controversial (Lin et al., 2000; Faure et al., 2003; Zhu et al., 2010b).

Among the rare existing structural studies, the Late Mesozoic extensional regime of SCB is the main feature for some authors (Gilder et al., 1991b; Faure et al., 1996; Faure et al., 2003; Zhou et al., 2006; Shu et al., 2009b), while the importance of a Late Mesozoic strike-slip regime has been emphasized by others (Xu et al., 1987b; Gilder et al., 1996; Li et al., 2001;). A sinistral transcurrent faulting during the Middle to Late Cretaceous is reported along the Tan-Lu fault (Mercier et al., 2007), and also in the SE coastal region of SCB (Wang and Lu, 2000).

In the present state of knowledge, structural studies on pluton emplacement and their bearings on the interpretation of regional tectonics are not available in the study area. In this study we choose the Qingyang-Jiuhua massif in the central part of the Lower Yangtze area as

target to answer following questions: 1) What is the tectonic regime during the emplacement of this massif at ca. 140 Ma-130 Ma? 2) Is there an obvious strike-slip regime after the crystallization of this massif? 3) What is the emplacement mechanism of this massif, and 4) Is there a relationship between the emplacement mechanism and the regional tectonic regime? A multidisciplinary approach has been applied in this study emphasizing i) the deformation of the granitic massif and its country rock at the micro, macro and regional scales, ii) the anisotropy of magnetic susceptibility (AMS) fabrics, and iii) the paleomagnetic analysis. Integrating newly obtained data with previous ones, the emplacement mechanism of the massif, and their relationship with the regional tectonic framework are discussed.

2 Geological setting

2.1 Geologic framework of the Lower Yangtze area

The Lower Yangtze area is located in the southeast of China and can be divided into three parts: the Dabie-Sulu massif in the north, the lower Yangtze fold belt in the middle, and the Jiangnan orogenic belt in the south (Fig. 4-1).

The Dabie-Sulu massif, separating the North China Craton from the Lower Yangtze fold belt, was well studied during last 3 decades because of its ultra high pressure metamorphism (Cong and Wang, 1999). This massif was formed by the Paleozoic collision between the North China and South China Blocks (Mattauer et al., 1985b; Faure et al., 2008), followed by a Middle Triassic intracontinental subduction (Faure et al., 2008). During the Early Cretaceous, a migmatitic dome characterized by an NW-SE maximum stretching direction developed in the Dabie area (Lin et al., 2007). Several syn-kinematic granitoid plutons intruded into this dome (Faure et al., 2003). Lastly, the eastern border of the Dabie dome is represented by the Tanlu normal fault, along which half-graben basins were filled by the Late Cretaceous continental red beds (Mercier et al., 2007).

The lower Yangtze fold belt is composed of sandstone, siltstone, mudstone and carbonate series, deposited from Neoproterozoic (Sinian) to Triassic (AHGBMR, 1987). During the Middle Triassic, the main body of these marine sedimentary rocks were folded and thrust to the SE

(Schmid et al., 1999) while in the southern part of this belt, folds and thrusts may be due to the activity of the Jiangnan belt during this period (Li et al., 2010b). Upper Triassic conglomerate and sandstone unconformably deposited upon the older series (Shu et al., 2009b). In the Jurassic time, the deposits are predominantly terrigeneous, volcanic and volcano-clastic. A Late Jurassic unconformity argues for a tectonic event (Yang et al., 2011). Since the Early Cretaceous, the extensional tectonic regime predominates in the lower Yangtze fold belt, as shown by the formation of continental red bed basins, and the emplacement of granitic plutons, including the Qingyang-Jiuhua massif investigated in this study (Fig. 4-1; Mercier et al., 2007; Shu et al., 2007, 2009; Zhu et al., 2010b).

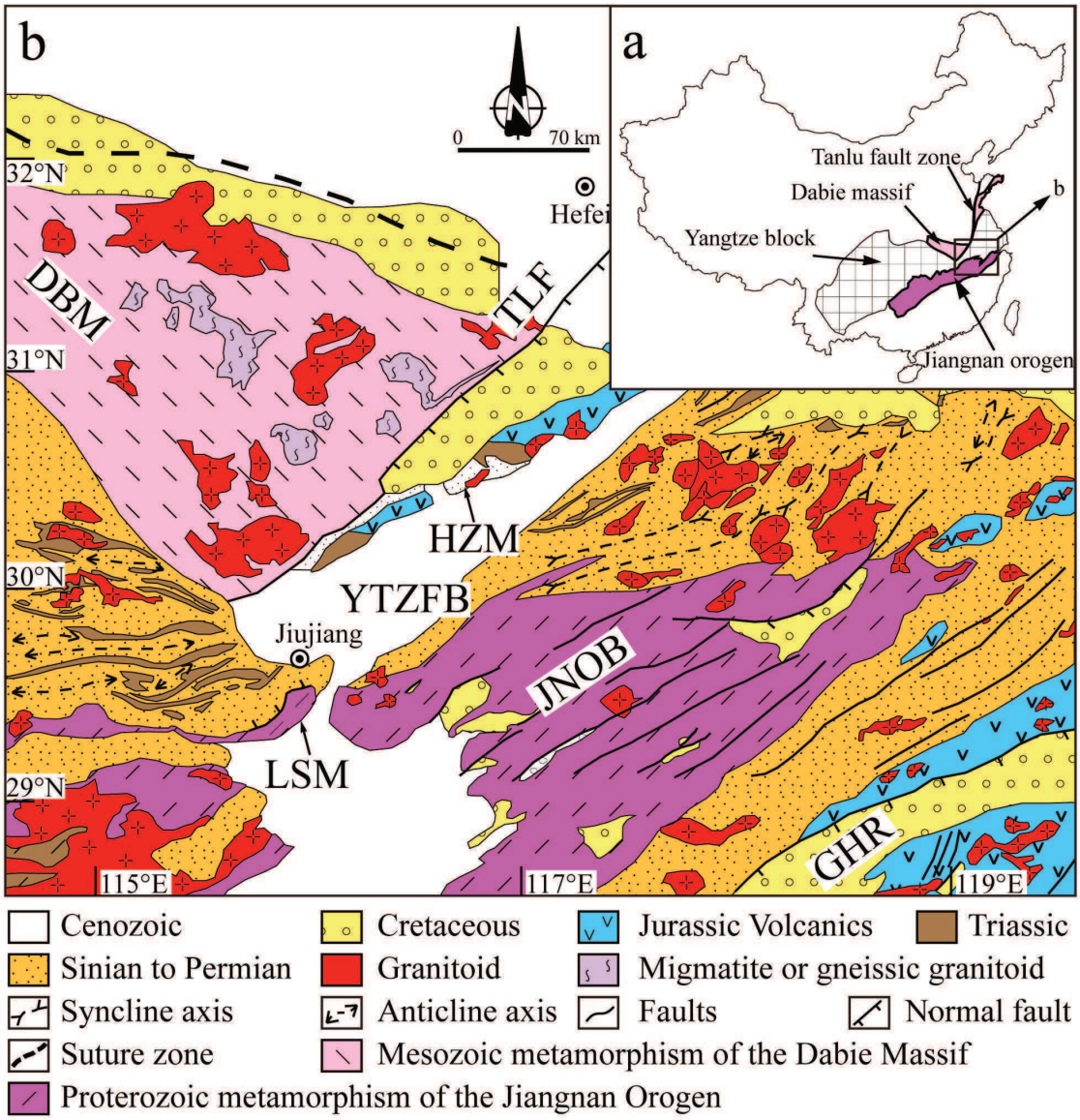

Figure 4 1: Regional geological map.

DBM: the Dabie massif, LYTZFB: the Lower Yangtze fold belt, JNOB: the Jiangnan orogenic belt, TLF: the Tanlu fault, HZM: the Hongzhen massif.

The Jiangnan orogenic belt is a Neoproterozoic collision belt, where several ophiolitic masses are recognized (e.g. Shu et al., 2006). During the Early Paleozoic, an E-W fault system indicating an N-S shortening developed (Yu et al., 2007). In the Cretaceous, NE striking normal faults, are believed to control the Late Mesozoic red bed basin opening, and granitic pluton emplacement (Yu et al., 2007).

2.2 Qingyang-Jiuhua massif

The Qingyang-Jiuhua massif, located in the southern part of Anhui Province, Southeast China, is one of Late Mesozoic granitic massifs intruding into the Lower Yangtze fold belt. The massif crops out approximately on ~750 km^2 (Xu et al., 2010; Wu et al., 2012;). Lithologically, this massif is divided into the Qingyang pluton and the Jiuhua pluton (Fig. 4-2). The Qingyang pluton, consisting of 4 subplutons, is formed mainly by granodiorite with a diorite rim on its northeastern boundary. Lithologically, the Jiuhua pluton is divided into an ENE-WSW elongated monzogranitic facies, to the east, and a N-S striking K-feldspar granite to the west.

Several dating have been carried out on three facies by the U-Pb zircon method. The granodiorite of the Qingyang pluton is dated at 144.8±0.7Ma (Chen et al., 2005a), 140±1.1Ma (Xu et al., 2010) and 139.4±1.8 to 142.0±1.0Ma (Wu et al., 2012), the monzogranite of the Jiuhua pluton at 133.2±1.3 Ma (Xu et al., 2010) and 130.3±1.8 to 131.0±2.6Ma (Wu et al., 2012). The K-feldspar granite of the Jiuhua pluton is dated by zircon and monazite at 127±1.6 Ma and 129±10 Ma, respectively (Xu et al., 2010). So the Qingyang-Jiuhua massif is probably formed by two magmatic events within about 10Ma (Wu et al., 2012). Geologic investigations have also indicated that the Jiuhua pluton intrudes the Qingyang pluton, and then, the whole massif is intruded by NE-SW or N-S microgranite dykes (Fig. 4-2; AHBGMR, 1987).

The Sm-Nd isotopic analyses show that the isotopic characteristics, and the Nd model age of granitoid near the Jiangnan orogenic belt, including the Qingyang-Jiuhua massif, are very similar to the surrounding Proterozoic metamorphic rocks (Chen et al., 1993). It is therefore argued that these granitoids originated from crustal melting without significant input of mantle material (Chen et al., 1993). The crustal anatexis is confirmed by the occurrence of inherited Archean

zircons (Xu et al., 2010). The trace elements geochemistry suggests a magmatic arc affinity similar to the arc magmatism developed in the southeastern coast of China. The petrological, geochronological and geochemical features argue that the Qingyang-Jiuhua massif was also related to the Late Mesozoic Paleo-Pacific subduction (Xu et al., 2010).

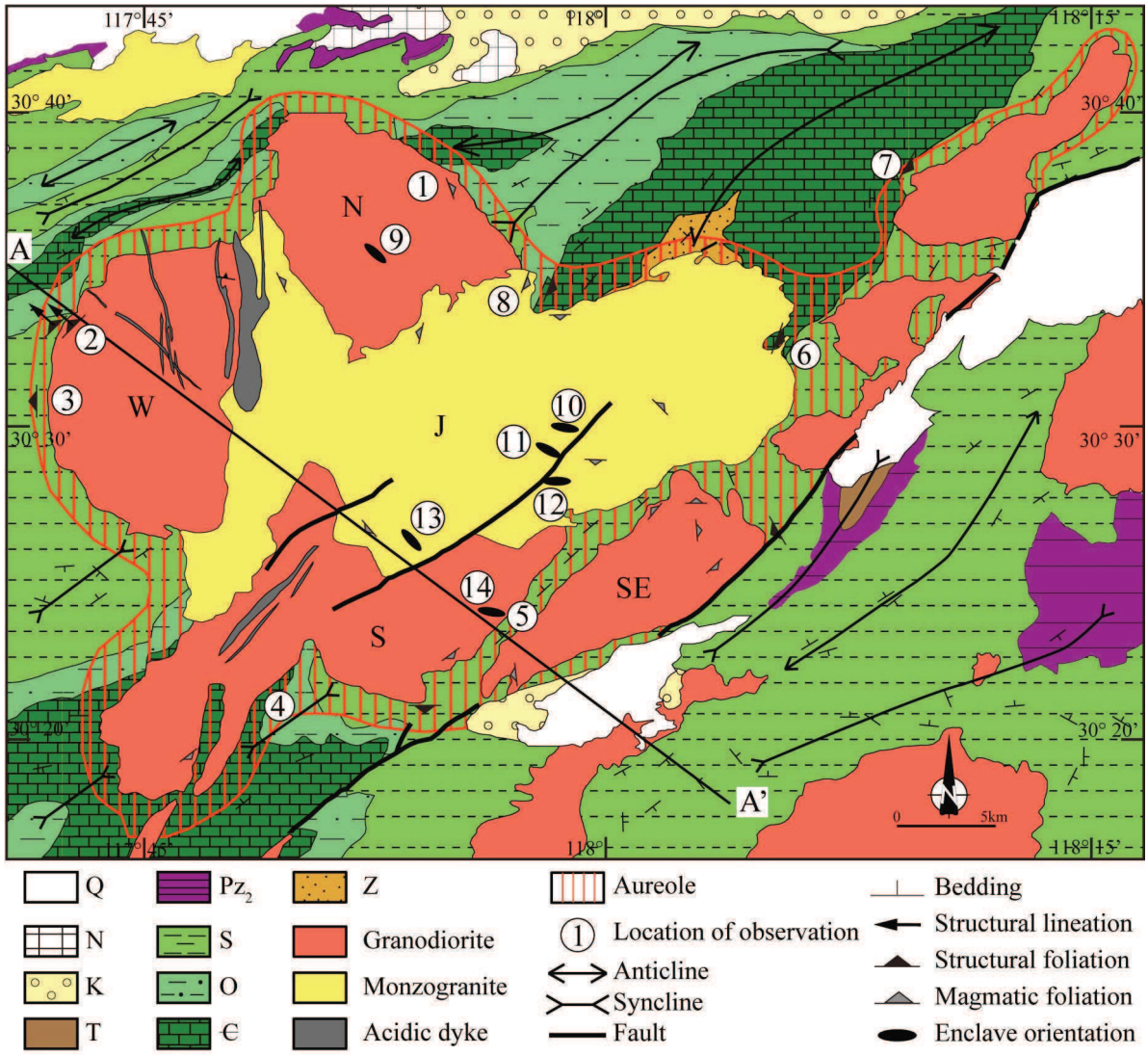

Figure 4 2: Simplified geological map of the Qingyang-Jiuhua massif area.

Q: Quaternary, N: Tertiary, K: Cretaceous, T: Triassic, S: Silurian, O: Ordovician, ∈: Cambrian, Z: Sinian, GD: Granodiorite of the Qingyang pluton, MG, Mongzogranite of the Jiuhua pluton, AD: Acidic dyke, J, N, W, S and SE represent for the Jiuhua pluton, the northern, western, southern and southeastern subplutons of the Qingyang pluton, respectively.

3 Structural analysis of the Qingyang-Jiuhua massif

3.1 Macroscopic fabrics in granite and contact metamorphic rocks

The rock forming minerals of the Qingyang granodiorite are mainly quartz, K-feldspar, plagioclase, biotite and amphibole. The Jiuhua monzogranite consists of quartz, red K-feldspar, plagioclase and biotite. In both rocks, K-feldspar occurs as cm-sized megacrysts within an mm-sized matrix. Microgranite dykes are mainly composed of K-feldspar megacrysts with a minor amount of quartz and biotite.

Based on our field observation, the Qingyang and Jiuhua granitoids appear as isotropic rocks (Fig. 4-3a). The main parts of these two plutons are undeformed, the plagioclase, K-feldspar and quartz have euhedral to sub euhedral habits. The platy minerals, such as biotite, and needle minerals, such as amphibole, are randomly distributed without any preferred orientation. Deformation structures occur only on the boundary of the massif. In particular, along the northeastern boundary of the massif, biotite and amphibole form a well-developed preferred orientation with an N160E E65, and N20E E55 foliation in locations ① and ⑧, respectively (Fig. 4-2). In location ⑧, the granite foliation is subparallel both to the strike of the granite-host rock boundary and the foliation (N20E 90) measured in the adjacent marble in the metamorphic aureole. On the western boundary, both the pluton and its adjacent country rock experienced a ductile deformation with an N35E W55 foliation and N130E NW lineation (location ② in Fig. 4-2). There, a mylonitic fabric develops in the granite (Fig. 4-3b). Quartz and feldspar grains are deformed into sigmoidal shapes that indicate a top-to-the-NW shear sense. This ductile shear zone is a normal fault indicating the rising up of the pluton with respect to its country rock.

The Qingyang-Jiuhua massif is surrounded by a metamorphic aureole of several hundred meters to 1 km in width (Fig. 4-2). Marble and andalusite hornfels are the dominant rock-types. The marble is formed by coarse grain calcite (locations ④, ⑥ and ⑧ in Fig. 4-2), while the andalusite hornfels is composed of very fine grain quartz, feldspar, muscovite, phyllite and andalusite (locations ②, ③, ⑤ and ⑦ in Fig. 4-2). These contact metamorphic rocks are well foliated. The foliations are roughly parallel to the granite boundary (locations ②, ③, ⑤, ⑥, ⑦ and ⑧ in Fig. 4-2). In location ③ which is in the aureole zone near the west boundary

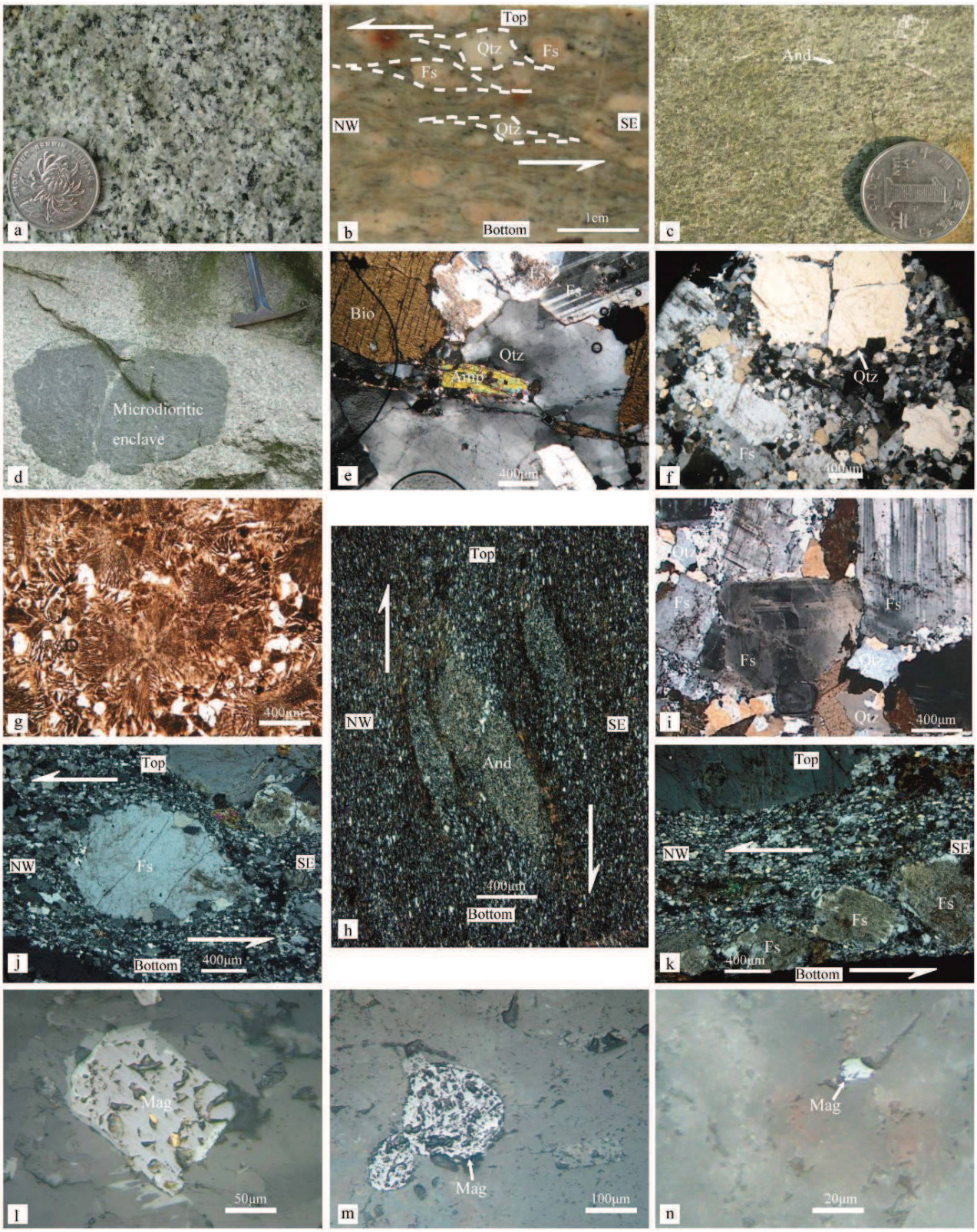

Figure 4 3: Macro- and micro- structures of the Qingyang-Jiuhua massif

(a) Isotropic granodiorite of the Qingyang pluton. (b) Top-to-the NW ductile shearing on the NW boundary of the Qingyang granodioritic pluton (Location ② in Fig. 4-2). (c) Andalusite

porphyroblasts aligned in the aureole hornfels of the massif (Location ⑥ in Fig. 4-2). (d) Crack filled by granite in the microgranitoids enclave in Jiuhua pluton. (e) The sharp extinction of Quartz, polysynthetic twins of Plagioclase, Biotite without bend in granodiorite show a magmatic texture. (f). The sharp extinction of Quartz in monzogranite shows magmatic texture. (g). Microscopic photo of acidic dyke show magmatic texture. (h) Sigmoidal andalusite porphyroblasts developed in the south eastern boundary of the Qingyang pluton showing a downard motion of the SE part (Location ⑤ in Fig. 4-2). (i) Weak post-solidus ductile deformation in the granite on the NE boundary (Location ① in Fig. 4-2). (j) Sigmoidal shape of feldspar on the NW boundary (Location ② in Fig. 4-2). (k) Domino structure of feldspar on the NW boundary of the Qingyang-Jiuhua Massif (Location ② in Fig. 4-2). (l). Magnetite in granodiorite. (m). Magnetite in monzogranite. (l). Magnetite in acidic dyke.

3.2 Microgranitoid enclave orientation

Microgranitoid enclaves are widespread in the Qingyang-Jiuhua massif. Most enclaves have been stretched and some enclaves were cracked and injected by magma indicating magma flowing during emplacement (Fig. 4-3d). The limited outcrop conditions allowed us to measure only the 2D fabrics of these microgranitoid enclaves. The enclave long axis orientation in each site indicates a dominant NW-SE to E-W preferred orientation more or less consistent with the magmatic fabrics illustrated in the 1:200000 geologic map of the studied massif (Figs. 4-2 and 4-4).

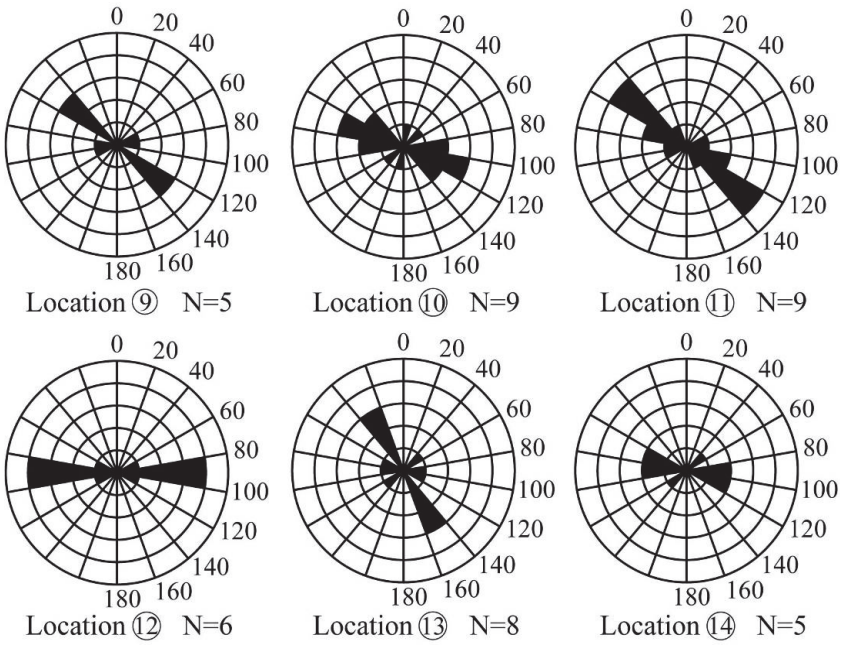

Figure 4 4: Preferred orientation of microgranitoid enclaves (Sample locations shown in Figure 2).

3.3 Microscopic structures

Field observations indicate that the main body of the massif appears as isotropic. The ductile deformation only locally occurs in the granite and its country rocks near the pluton boundary. In order to better constrain the deformation mechanics and shear sense of the boundary of the massif, structural observations were conducted at the microscope-scaled thin sections from both granite and country rock. Several oriented thin sections were prepared from hand samples and AMS cores (see below). The thin sections were cut perpendicular to the foliation and parallel to the lineation when recognized in hand sample, or magnetic foliation and lineation for AMS cores. Three types of microstructures have been recognized, namely granitic structure, weak ductile deformation, and intense ductile deformation.

Firstly, the magmatic structure is found in the main parts of both Qingyang and Jiuhua plutons. In thin sections parallel to the AMS lineation and perpendicular to the AMS foliation, post solidus deformation features are absent. The amphibole occurs as euhedral crystal habit (Figs. 3e). The plagioclase is characterized by igneous zoning, polysynthetic twins， euhedral to semi euhedral crystal habits (Figs. 3e, 3f and 3g). The K-feldspar contains flame microperthite and

Carlsbad twins are well developed in many grains. Biotite exhibits a sharp extinction and no cleavage bend (Fig. 4-3e). Quartz has anhedral shape, which indicates that it crystallized from a melt (Figs. 4-3e and 4-3f). Many quartz grains have subgrain boundaries and both quartz and feldspars are characterized by a weak undulose extinction showing that the rock experienced a limited deformation at the end of the crystallization of the melts, and thus the magmatic texture is not altered (Paterson et al., 1989).

Secondly, a weak ductile deformation is found in the country rock on the southeastern and northeastern boundaries of the massif. Along these margins, the country rocks are represented by andalusite hornfels in which the andalusite forms dark needles of 1 or 2 mm in size of (Fig. 4-3c). In the northwestern boundary of the septum (location ⑤ in Fig. 4-2), the foliation in the hornfels is oriented at N60E NW75, which is parallel to the sedimentary bedding and the granite boundary. The andalusite lineation is nearly vertical. The observation of oriented thin section shows that in hornfels, andalusite aggregates exhibit a sigmoidal shape with tiny quartz tails (Fig. 4-3h). The shear sense shows that the NW side (pluton side) rises up and the SE side (country rock side) moves down.

On the northeastern boundary, the granitoid rocks are still weekly ductilely deformed. The plagioclase is magmatically zoned and euhedral. Many tiny grains due to dynamic crystallization develop around plagioclase clasts (Fig. 4-3i). K-feldspar has a flame microperthite texture and an euhedral shape. On the grain boundary, myrmekite texture replaces K-feldspar. The quartz is anhedral with sutured grain boundaries and subgrains boundary (Fig. 4-3i). These three minerals have a undulose extinction. Biotite is sometimes bended and undulose. Amphibole shows a sharp extinction and a euhedral habitus without deformation.

Thirdly, intense ductile deformation is only found on the northwestern boundary (location ② in Fig. 4-2). In oriented thin sections, stretched quartz grains form polycrystalline ribbons. K-feldspars deformed into a sigmoidal shape are sigma-type porphyroclasts (Fig. 4-3j). Some feldspar grains are crushed and rotated as dominos or book shelf microstructure (Fig. 4-3k). The shear sense indicators show a top-to-the- NW motion that can be related to the pluton side rise with respect to the country rock.

3.4 Regional fold geometry and pluton emplacement

The Qingyang-Jiuhua massif intrudes into the Yangtze fold belt. In agreement with previous works, our study shows that, the fold geometry developed in the country rocks is abruptly interrupted by the granitic intrusion. The strike of fold axis is not defected by the plutons. Moreover, in the metamorphic aureole, folds that might be considered as the result of a shortening effect of the country rock during the emplacement of the pluton are absent.

4 Rock magnetism

4.1 Sampling and measurement

As illustrated by numerous case studies during past decades, AMS fabric pattern of a pluton may reflect the tectonic regime during its emplacement while the paleomagnetic records are easily to be influenced by the tectonic event after the crystallization of the pluton (Bouchez and Gleizes, 1995; Talbot et al., 2005b; Joly et al., 2007; Charles et al., 2011; Lin et al., 2013a). These two methods are applied to investigate different scaled deformation and tectonic characteristics of the study area.

In order to obtain a general view of the AMS features of the Qingyang-Jiuhua massif, AMS sampling is performed with 93 sites covering this massif by gasoline drill (Table 4-1). These sites are ca. 2 km away with a relatively homogeneous spatial distribution within the pluton (Fig. 4-9). For each site, 5 to 6 cores of 2.5 cm in diameter with an interval of about 2 meters are drilled and oriented by both magnetic and, when possible, solar compasses. The cores are cut into standard AMS specimens with a length of 2.2 cm in the laboratory. As a result, 5 to 11 specimens were obtained for each site and a total of 652 specimens for the whole massif.

In order to constrain the relative movement of the Jiuhua pluton with other 4 subplutons of the Qingyang pluton during and after their crystallization (Fig. 4-2), 15 specimens from the Jiuhua pluton (J), 12 specimens from the west subpluton (W), 11 specimens from the south subpluton (S), 10 specimens from the north subpluton (N), 12 specimens from the southeast subpluton (SE) of the Qingyang pluton were taken for the paleomagnetic measurements.

In Laboratoire de Magnétisme des Roches d'Orléans, IRM experiments were carried out on

different lithologies by IM30 pulse magnetizer and JR5 magnetometer. Coupled with a CS3 furnace, KLY3 was used to perform the thermal-susceptibility experiments on powders of different lithologies. The KLY3 kapabridge was used to perform the AMS and bulk susceptibility measurements. The results were processed by ANISOFT (offered by AGICO) to calculate the main magnetic anisotropic axes (K_1 for lineation and K_3 for the pole of foliation), the shape parameter (T) and the anisotropy degree (P_J) using Jelinek statistics (Jelinek, 1981). To get the paleomagnetic record, both progressive AF and thermal demagnetizations were used to clean the magnetic remanence with about 15 steps. JR5 magnetometer was used to measure the magnetic remanence. Moreover, hysteresis curves were obtained by an electromagnetic inductometer on different lithologies in the Paleomagnetic laboratory of Institut de Physique du Globe de Paris.

4.2 Magnetic mineralogy

To better interpret the AMS and magnetic remanence measurements, it is essential to recognize their carriers because the magnetic record depends on the magnetic mineralogy, relative abundance and size (e.g. Tarling and Hrouda, 1993).

Figure 4-5 presents the distributions of bulk magnetic susceptibility of measured specimens. The granodiorite and monzogranite show a unimodal and large distribution with an average of Km higher than $15x10^{-3}$ SI, while the acidic dykes reveal a narrow distribution centered at about $4x10^{-3}$ SI. It is worth noting that most of the specimens show relatively high bulk susceptibilities in order of 10^{-3} SI with few exceptions, such as Site CZ63 and CZ14 composed of acidic dykes (Table 4-1).

The thermal experiments show that a sharp drop of the magnetic susceptibility has been observed for all measured samples at ca. 580°C (Figs. 4-6a, 4-6b, 4-6c, 4-6d and 4-6e), indicating the dominance of magnetite in the magnetic mineral composition of collected samples. In detail, some samples show a slow decrease of magnetic susceptibility to zero until to at ca. 700°C (Figs. 4-6a, 4-6b, 4-6d and 4-6e), implying the existence of hematite.

The IRM acquisition diagram shows a rapid increase of the induced magnetization before 100 mT (Figs. 4-6f, 4-6g, 4-6h, 4-6i and 4-6j) and all measured samples are saturated before 200 mT (Figs. 4-6g, 4-6h, 4-6i and 4-6j), except for the acidic dyke (Fig. 4-6f), which is only saturated at 80% at this field. This observation indicates that the weak coercive minerals, such as

magnetite, are dominant regardless of their differences in lithology.

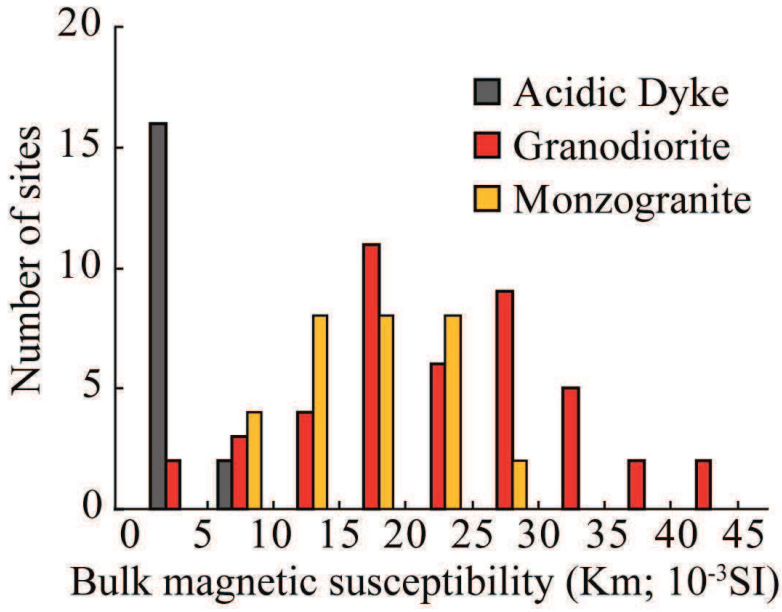

Figure 4 5: Distribution of bulk magnetic susceptibility of the Qingyang-Jiuhua massif.

Table 4 1 The AMS results of granotoids from the Jiuhua-Qingyang massif.

site	Coordinates		Lith	n	Km	P_J	T	K_1				K_3			
	Long (°E)	Lat (°N)			(10^{-4}SI)			Dec (°)	Inc (°)	a_{95max} (°)	a_{95min} (°)	Dec (°)	Inc (°)	a_{95max} (°)	a_{95min} (°)
CZ01	117.846	30.633	AD	10	15	1.032	-0.151	68.7	11.9	13.6	7.3	162.5	17.3	24.9	7.1
CZ02	117.817	30.612	GD	8	202	1.122	0.117	336.6	25.9	18.2	5.7	163.5	63.9	7.7	5.4
CZ03	117.807	30.582	AD	8	4.74	1.027	0.665	102.7	84.5	19.1	8.7	268.1	5.4	14.2	9.6
CZ04	117.793	30.578	GD	9	245	1.078	0.359	311.6	26.3	16.5	2	188.9	47.6	8.5	2.2
CZ05	117.799	30.539	AD	5	7.39	1.007	0.206	99.7	67	17.4	6	254.8	21	12.1	1.9
CZ06	117.799	30.509	AD	6	73.1	1.054	0.262	14.9	12.7	19.1	8.7	280	20.9	13	4.2
CZ07	117.807	30.502	AD	9	16.9	1.023	0.14	2.2	20.3	39.9	10.1	94.3	5.9	21	9.6
CZ08	117.795	30.505	GD	8	257	1.071	0.063	263.5	12.6	12.7	5.8	157.3	51.3	10.6	7.3
CZ09	117.795	30.495	GD	9	198	1.138	-0.208	195.5	2	12.8	3.3	2.7	87.9	19.6	7.1
CZ10	117.799	30.489	GD	7	266	1.066	-0.039	205	31.9	35.5	7	356.1	54.6	8.9	7.5
CZ11	117.799	30.485	MG	5	134	1.07	0.05	198.5	10.2	17.1	7.7	94.9	52.5	19.1	8.4
CZ12	117.802	30.470	AD	5	3.84	1.024	-0.08	357.2	1.7	19.4	10.5	267	7.8	53.7	5.1

CZ13	117.799	30.450	AD	6	10.5	1.041	0.177	174.1	28.2	60.3	18.6	341.6	61.2	28.8	15.1
CZ14	117.799	30.437	AD	6	1.16	1.016	0.167	178.4	37.8	44	9.1	268.6	0.2	21.9	1.4
CZ15	117.790	30.474	GD	10	219	1.079	-0.324	195.8	29.3	10.5	8	33	59.6	30.1	10.3
CZ16	117.699	30.515	MG	8	108	1.21	0.039	222.4	69	4.4	1.8	46.6	20.9	5	1.9
CZ17	117.706	30.514	MG	11	106	1.042	0.739	267.1	35.7	11.8	3.1	170.2	9.6	3.7	2.2
CZ18	117.754	30.502	GD	8	278	1.123	0.047	172.6	17.3	21.1	4.3	55.8	55.3	12.2	8.6
CZ19	117.758	30.486	GD	10	194	1.053	0.184	184.4	14.8	14.8	9.4	18.4	74.8	17	8.1
CZ20	117.759	30.476	MD	9	496	1.015	0.249	36.3	64.8	32	8.2	250.1	21.3	24.4	9.7
CZ20	117.759	30.476	GD	11	179	1.035	-0.15	167.5	23	31.2	14.1	70.2	16.8	52.3	27.7
CZ21	117.747	30.508	GD	11	268	1.12	-0.106	162.5	15.7	10.8	5	54.6	47.6	12	3.4
CZ22	117.741	30.532	GD	7	197	1.081	0.109	137	8	41.1	11	39.2	43.9	13.7	10.3
CZ23	117.953	30.541	MG	7	153	1.055	0.143	9.9	12	24.5	2.9	111.5	43.4	11.9	5.8
CZ24	117.961	30.547	MG	10	182	1.102	0.639	212.4	1.6	61.2	5.7	119.1	64	7	3.1
CZ25	117.978	30.554	MG	9	194	1.109	0.49	288.6	45.1	50.3	1.8	126.1	43.6	8.2	3.7
CZ26	117.980	30.557	MG	7	79.1	1.077	0.099	189.2	5.4	64.7	2.7	95.4	34.7	10.3	3.1
CZ27	117.923	30.500	MG	6	84.2	1.049	0.147	166.7	3	13.9	3.7	74.8	32.3	10.8	5.1
CZ28	117.907	30.489	MG	6	130	1.059	0.278	292.7	56.9	32.6	24.3	133.6	31.3	62.5	19.9
CZ29	117.923	30.423	GD	6	33.9	1.082	0.098	223.2	3.9	13.4	5.2	317.2	46.3	18.5	8.1
CZ30	117.894	30.380	GD	5	187	1.06	0.023	267.8	12.3	36.9	15.3	359.5	7.7	37.6	8.1
CZ31	117.901	30.357	GD	8	249	1.087	0.489	260.1	28.9	51.4	5.2	163.3	12.2	11.8	5.6
CZ32	117.937	30.399	GD	7	2.83	1.146	0.112	38.9	6.7	18.6	4.7	129.2	2.7	6.4	5.3
CZ33	117.942	30.403	GD	6	314	1.173	0.39	39	7.9	25.4	6	308.8	1.9	8.8	5.4
CZ34	117.940	30.560	MG	6	210	1.112	0.64	275.7	6.9	41	6.8	170.4	65.5	10.1	6.1
CZ35	117.942	30.568	MG	8	178	1.12	0.242	316.2	37.7	28.5	6.3	151.7	51.3	17.2	2.5
CZ36	117.866	30.588	GD	9	353	1.103	0.209	339.3	4.1	37.8	5.9	215.1	82.8	18.7	6.7
CZ37	117.880	30.549	AD	9	1.82	1.036	0.638	185.3	20.7	38.5	8.3	77.9	38.3	29.7	10.6
CZ38	117.873	30.538	MG	5	2.32	1.081	0.187	53.9	3.2	53.7	9.3	148.6	55.8	26.1	11.4
CZ39	117.861	30.523	AD	7	43.7	1.057	-0.028	40.4	43.1	44.4	22.8	260.2	39.4	29.9	22.4
CZ40	117.857	30.516	AD	5	27.5	1.069	-0.126	115.2	29.3	82.2	23.3	256.5	54.3	32	15.8
CZ41	117.845	30.515	MG	5	1.35	1.036	0.236	62	32.9	29.6	5.8	185.5	40.5	21	6
CD42	117.871	30.520	AD	6	23.4	1.074	0.019	90.7	53.5	22	4.7	353.5	5.3	19	58
CZ43	117.879	30.509	MG	5	156	1.088	0.266	252.4	29.8	22	4.5	106.6	55.2	18.4	4.4
CZ44	117.885	30.492	MG	6	240	1.088	0.242	338.2	20.5	23	4.1	105.6	58.4	8.5	4.1
CD45	117.885	30.478	MG	8	104	1.049	-0.036	175.1	3.8	44.8	10.4	84.5	8.9	44.6	7.3
CZ46	117.883	30.435	MG	5	166	1.074	0.148	305.1	6.9	16	10.3	38.8	28.4	22.2	8.3

CZ47	117.890	30.421	GD	6	236	1.161	-0.528	21.6	0.9	4.6	1.8	291.2	25.1	27	3.3
CZ48	117.862	30.414	GD	8	134	1.233	0.615	188.8	64.6	28.4	4.5	293.6	6.9	6.1	4.2
CZ49	117.818	30.402	GD	5	319	1.064	0.311	156.5	15.2	20.8	9.2	51.2	44.2	10.1	5.9
CZ50	117.822	30.419	GD	5	260	1.08	0.476	233.5	11	42	8.3	57.8	79	11.4	2.4
CZ51	117.827	30.435	GD	5	298	1.095	0.566	275.9	17.8	22.2	5.6	57.5	67.7	6.6	2.8
CZ52	117.832	30.448	GD	6	177	1.092	0.553	286.2	12.5	7.4	5.4	55.7	70.7	15.8	5.6
CZ53	117.815	30.386	GD	5	349	1.173	0.302	278.5	6.4	14.8	2.7	186.4	18.8	4.1	2.7
CZ54	117.799	30.414	AD	6	15.6	1.029	-0.095	289.6	54.4	63.7	21.8	52.7	21.3	55.9	24.2
CZ55	117.800	30.398	GD	7	400	1.13	-0.005	316.4	13.9	8.5	3.7	47.8	5.8	17	4.1
CZ56	117.828	30.388	GD	8	286	1.132	-0.156	255.2	16.1	9.6	2	349.2	13.7	8.2	3.8
CZ57	117.808	30.353	GD	5	65	1.076	-0.294	103.9	3.2	25.1	8.6	12.2	27.9	9.2	3.1
CZ58	117.911	30.435	GD	6	252	1.113	-0.01	193.6	28.6	8.9	2.9	301.5	29.5	8.2	2.4
CZ59	117.944	30.457	MG	5	139	1.057	-0.081	86.7	27.8	15.7	10.5	197.9	34.4	35.5	7.4
CZ60	117.961	30.459	MG	5	231	1.068	-0.375	94.6	6	19	2.8	258.8	83.8	27.4	3.4
CZ61	117.969	30.470	MG	8	252	1.075	-0.244	97.6	18.3	12.9	6.2	210.1	49.2	28.6	11
CZ62	117.974	30.499	MG	5	183	1.088	-0.275	111.6	0.4	18.3	1.5	21.1	52.3	22.1	5.1
CZ63	117.916	30.559	AD	5	0.33	1.239	0.438	275.2	46.9	31.6	1	127.7	38.3	3	5
CZ64	117.911	30.547	AD	5	17.4	1.057	-0.073	2.2	4	13.7	6.9	244	81.5	29.8	4
CZ65	117.883	30.646	DIO	11	564	1.041	0.448	260	3.1	23.7	10.9	169.3	13.1	22.5	12
CZ66	117.754	30.541	AD	6	65.6	1.041	0.232	129.7	61.2	31.9	5.7	243.6	12.5	19	5.4
CD67	117.760	30.530	AD	6	4.13	1.032	0.56	337.9	31.8	17.6	2.4	245.4	4.1	7.4	2.6
CZ68	117.763	30.522	GD	7	96.8	1.202	-0.134	111.9	3.3	61.1	18.3	222.6	80.8	60.6	13
CZ69	117.727	30.551	GD	6	223	1.09	0.161	33.8	41.4	12.9	11.1	132.6	9.8	27.9	11
CZ70	117.706	30.527	AD	6	6.22	1.109	0.413	179.6	28.3	8.1	3	66.9	35.7	7.5	3.2
CZ71	117.971	30.391	GD	7	137	1.15	0.081	208	1.4	12.2	6.6	117.1	33.6	12.4	6.9
CZ72	117.986	30.417	GD	5	172	1.313	-0.456	40.5	27	4.5	2.8	131.2	1.5	8.2	4.4
CZ73	117.997	30.429	GD	6	156	1.274	-0.253	47.5	30.5	6	3.6	166.3	39.2	5.4	3.7
CZ74	117.970	30.439	GD	6	159	1.105	0.157	16.4	4.4	25.4	11.2	107.7	16.3	28.8	3.4
CZ75	117.984	30.395	GD	5	123	1.286	-0.182	21.5	19.8	6.1	2.8	113.7	6.2	8.6	2.6
CZ76	117.996	30.384	GD	6	39	1.117	-0.368	190.9	17.6	10.9	3.2	300.1	46	13.4	7.3
CZ77	30.558	117.997	MG	7	191	1.146	0.446	41	16.6	38.4	4.7	137	19.4	20.6	3.4
CZ78	30.543	118.003	MG	7	58.3	1.119	0.69	47.6	17.3	37.4	4.5	171.3	60.8	9.5	2.9
CZ79	30.523	117.990	MG	7	240	1.13	0.648	145.7	10.4	25.8	5	20.2	72.4	5	3
CZ80	30.507	117.986	MG	10	201	1.08	0.542	109.6	1.32	21.2	14.5	208.1	32.2	33.4	18
CZ81	30.533	118.003	MG	7	79	1.093	0.384	106.5	1.7	77.4	4.9	9.5	76.4	8.5	2.6

CZ82	30.458	118.021	GD	10	53.4	1.205	0.052	343	37.1	24.5	8.6	116.6	42.4	10.9	9
CZ83	30.411	118.037	GD	6	159	1.163	0.025	9.9	13.6	3.1	1.6	255.4	59.7	8.3	3
CZ84	30.436	118.035	GD	7	109	1.11	-0.03	346	31.4	12.5	6.4	205.7	51.6	10.2	7.1
CZ85	30.442	118.058	GD	5	171	1.165	0.585	349.4	22.8	40.6	3.7	228.6	50.6	4.6	3.8
CZ86	30.547	118.056	MG	9	255	1.146	0.438	165.1	1.8	6.1	4.1	259.4	67.4	7.5	4.1
CZ87	30.562	118.066	MG	7	227	1.157	0.612	350.4	3.2	14.2	2.6	251.7	69.5	3.5	2.5
CZ88	30.553	118.013	MG	7	229	1.143	0.538	303.2	33.2	44.8	4.9	180.7	39.3	8.1	5.9
CZ89	30.557	118.030	MG	7	136	1.126	0.413	292.7	1.6	15	3.9	201.2	42.7	5.5	3.7
CZ90	30.616	118.188	GD	5	347	1.119	0.046	169.5	22.9	31.3	5.5	52.8	46.8	12.8	4.4
CZ91	30.618	118.171	GD	10	411	1.122	0.171	345.8	33.9	21.5	5.6	102.5	33.7	9.9	5.8
CZ92	30.618	118.153	GD	6	409	1.305	0.052	209.5	4.8	9.2	5.3	300	5.5	6.7	1.8
CZ93	30.616	118.204	GD	6	302	1.077	0.19	189.8	17.9	8.7	5.7	4.6	72	24	5

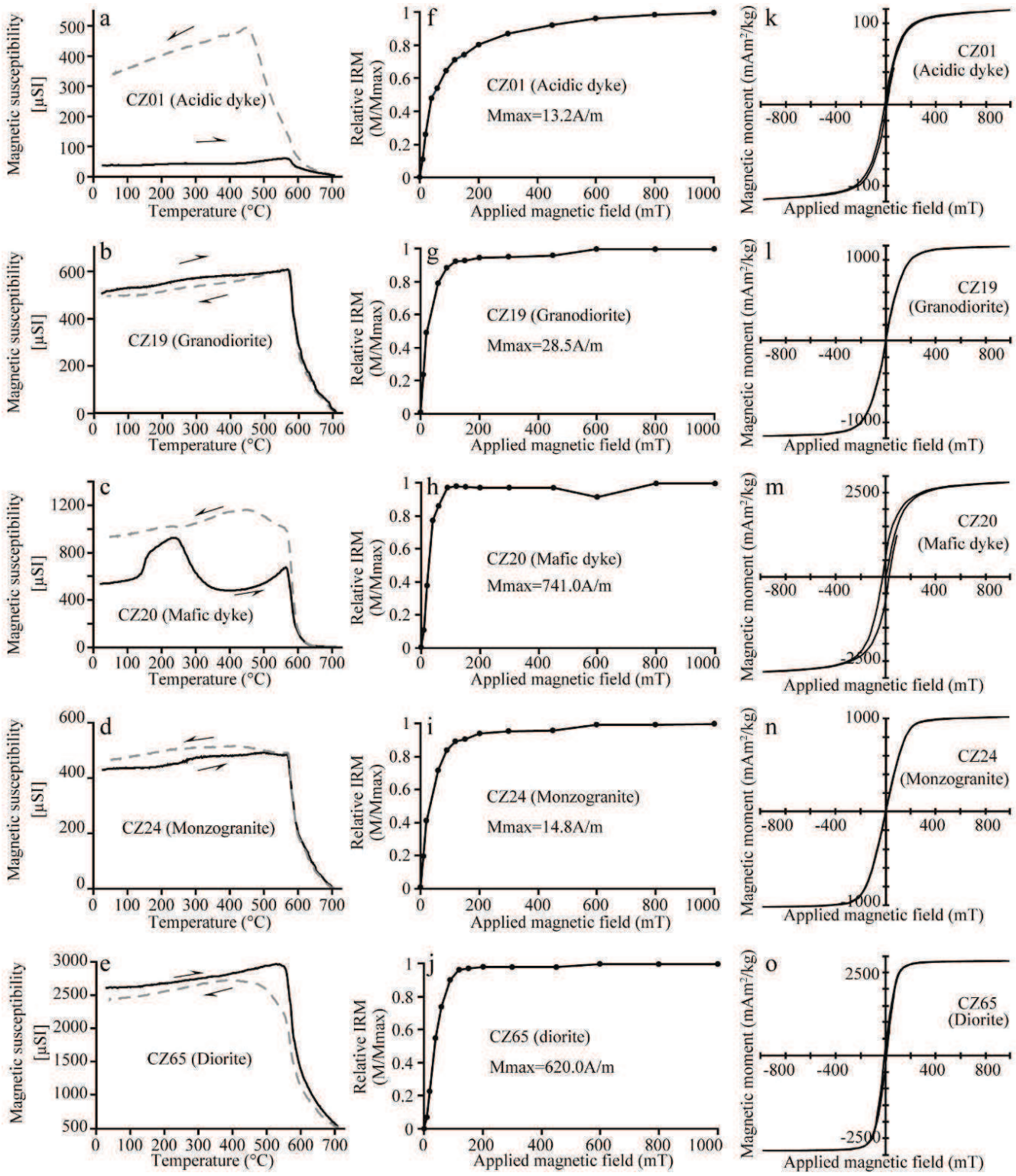

Figure 4 6: Thermal-Susceptibility, Isothermal Remanent Magnetization (IRM), Hysteresis Loop diagram of the Qingyang-Jiuhua massif.

The hysteresis loops present shaped sigmoidal shapes, indicating the existence of magnetite (Figs. 4-6k, 4-6l, 4-6m, 4-6n and 4-6o). According to these measurements, the magnetite sizes have been estimated, revealing the pseudo-single domain and multi-domain for the magnetite

(Fig. 4-7; Dunlop, 2002)

In summary, the pseudo-single domain and multi-domain magnetites that have been documented can be considered as the main carriers for the magnetic susceptibility and remanence for investigated lithotologies of this study. This conclusion is consistent with microscopic observations shown in Figures 4-3l, 4-3m and 4-3n. Therefore, the magnetic fabrics may be directly correlated with magmatic or tectonic fabrics (e.g. Tarling and Hrouda, 1993).

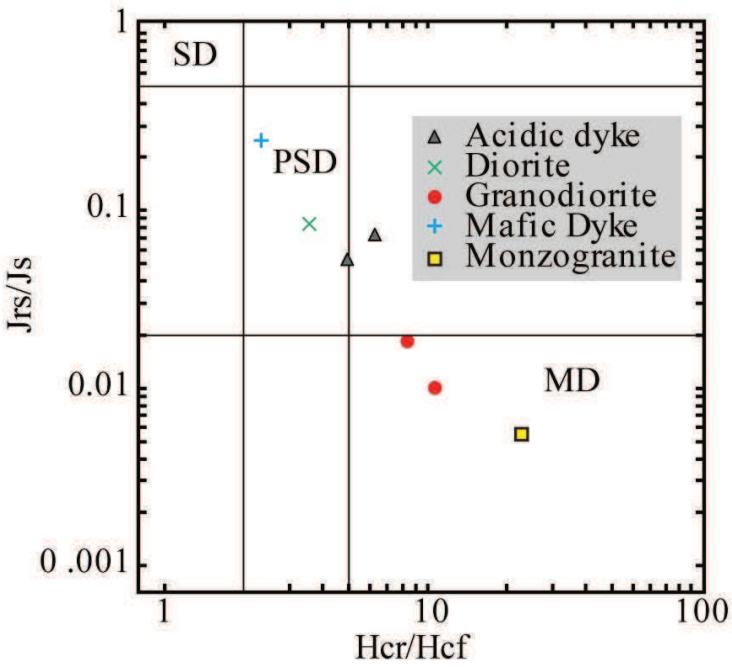

Jrs/Js versus Hcr/Hc for samples from the Qingyang-Jiuhua pluton, with the boundaries of SD and MD behaviours for magnetite taken from the values of Dunlop(2002)

Figure 4 7: Jrs/Js versus Hcr/Hc diagram from measured samples of the Qingyang-Jiuhua massif to define the magnetite size.

Jrs: remanence, Js: saturation remanence, Hcr: coercivity of remanence, Hc: coercivity, SD: single domain, PSD: pseu-single domain, MD: multi-domain, respectively.

4.3 AMS results

4.3.1 Anisotropy degree and shape parameter

The statistical results of AMS measurement of the Qingyang-Jiuhua massif are presented in

Table 4-1. For each site, the coordinate data of a sampling location, the mean bulk susceptibility (Km), the anisotropy degree (P_J), the shape parameter (T), the mean direction of declination and inclination of K1 and K3 axes as well as their corresponding confidence ellipse (α_{95}) are provided (Jelinek, 1981). In the P_J-Km diagram (Fig. 4-8a) most sites (90%) show a Km value below 40×10^{-3}SI with a P_J value below 1.2. Moreover, there seems to exist a trend of P_J vs Km (the shadowed zone in Fig. 4-8a). Few sites (CZ16, CZ48, CZ63, CZ68, CZ72, CZ73, CZ75, CZ82, CZ92; location see Fig. 4-9) show high P_J values (> 1.2) and are far away from the P_J vs Km trend. This may be due to their close spatial relationship with country rocks. Most sites show a positive value for their shape parameter (T), revealing the foliation dominance for the magnetic fabrics. No obvious relationship between T and P_J parameters can be observed (Fig. 4-8b).

4.3.2 AMS fabrics

Figures 4-9a and 4-9b present the mean directions of magnetic lineation (K_1) and pole of magnetic foliation (K_3) of each site from the Juhua pluton and the Qingyang pluton, respectively. It can be found that the magnetic fabrics are well defined for most sites, and the magnetic foliation of both the Jiuhua pluton (Fig. 4-9a) and the Qingyang pluton (Fig. 4-9b) are better constrained than the magnetic lineation for most individual sites. The magnetic lineations of both plutons are characterized by weakly inclined and largely scattered orientations (Figs. 4-9 and 4-10). Near the boundary between the massif and the country rocks, the magnetic lineation of most sites is more or less parallel to the strike of the boundary (Figs. 4-9 and 4-10). The foliation orientations are more complicated. Two main groups may be defined: flat and highly inclined foliations. The sites that present highly inclined magnetic foliations are principally localized near lithological boundaries (dyke-pluton, pluton-pluton, pluton-country rock). For instance, Sites CZ47 and CZ58 are localized on the boundary of two plutons (Fig. 4-9b), CZ16, CZ72 and CZ 92 are close to the country rocks (Fig. 4-9b), and CZ03 and CZ05 are dykes (Fig. 4-9a). The directions of these foliations are generally parallel to the boundaries (Fig. 4-9). The remained magnetic foliations observed from the central parts of plutons can be characterized by a flat pattern (Figs. 4-9, 4-10 and 4-11).

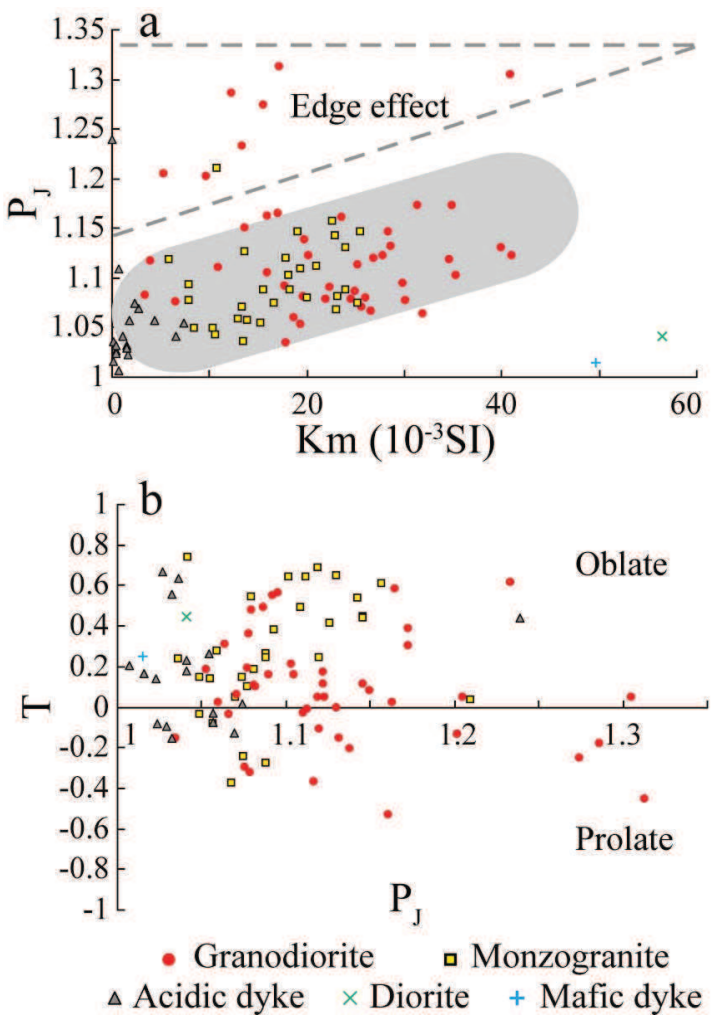

Figure 4 8: AMS scalar parameters of each site and main lithologies.

(a) T (shape parameter) vs. P_J (corrected anisotropy degree), (b) P_J vs. Km (mean bulk magnetic susceptibility in 10^{-3} SI). The calculations of T and P_J can be found in Jelinek (1981).

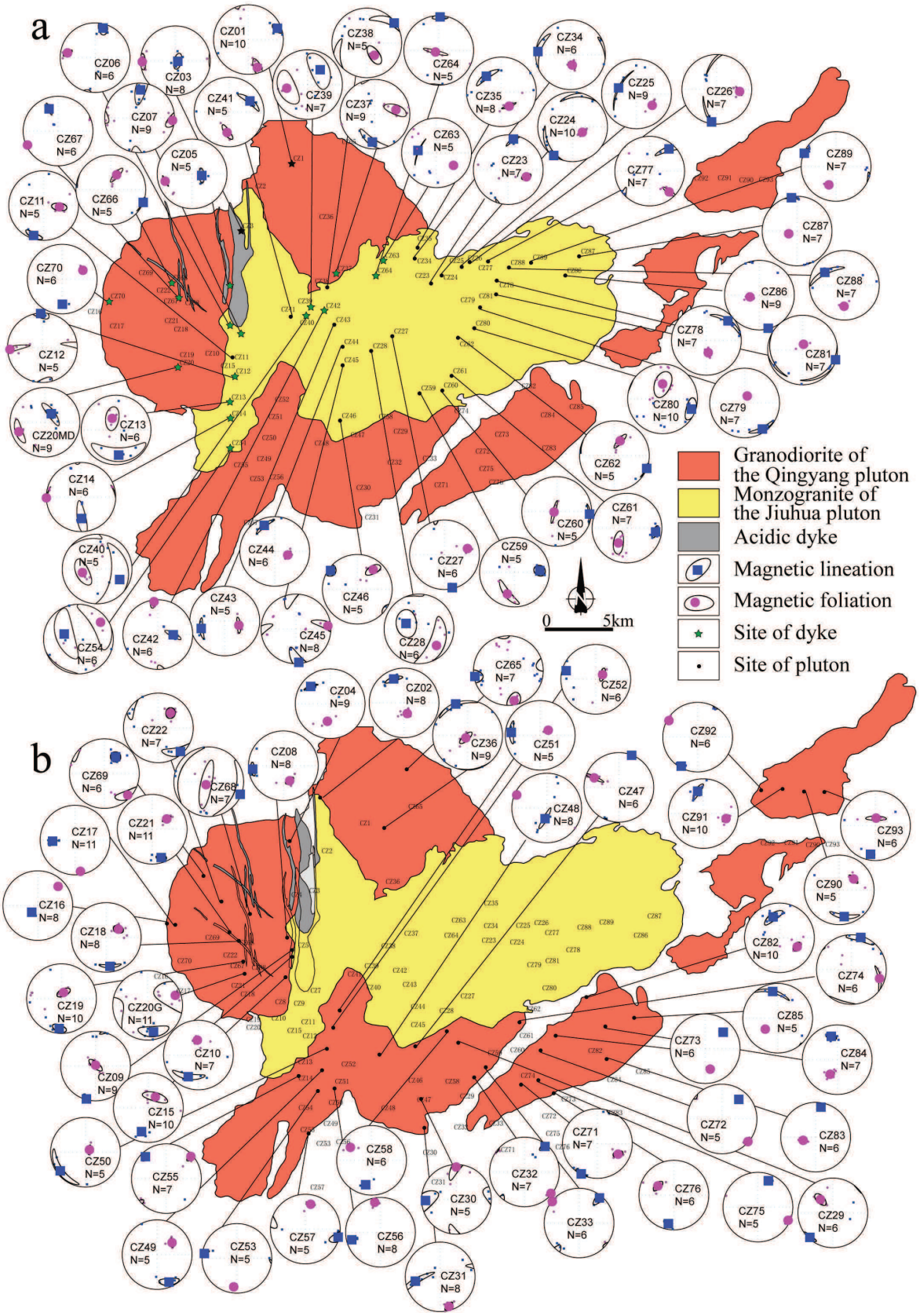

Figure 4 9: The equal area lower hemisphere projection of each site from the Qingyang-Jiuhua massif

Squares and circles stand for K1 (magnetic lineation) and K3 (pole of magnetic foliation), respectively. Small grey and larger black squares or circles represent individual specimen and site-mean direction, respectively with their confidence ellipses at 95% level.

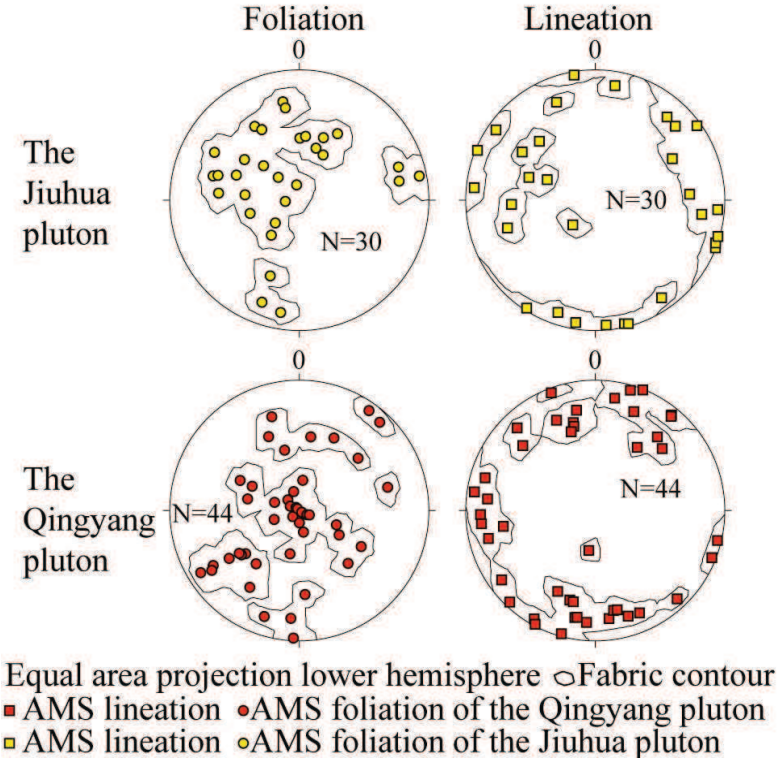

Figure 4 10: Total fabrics projection (equal area lower hemisphere) of the Qingyang-Jiuhua massif.

In this diagram, each solid square and circle represent one site. Data of 18 acidic dykes and 1 mafic dyke are not included in the statistics.

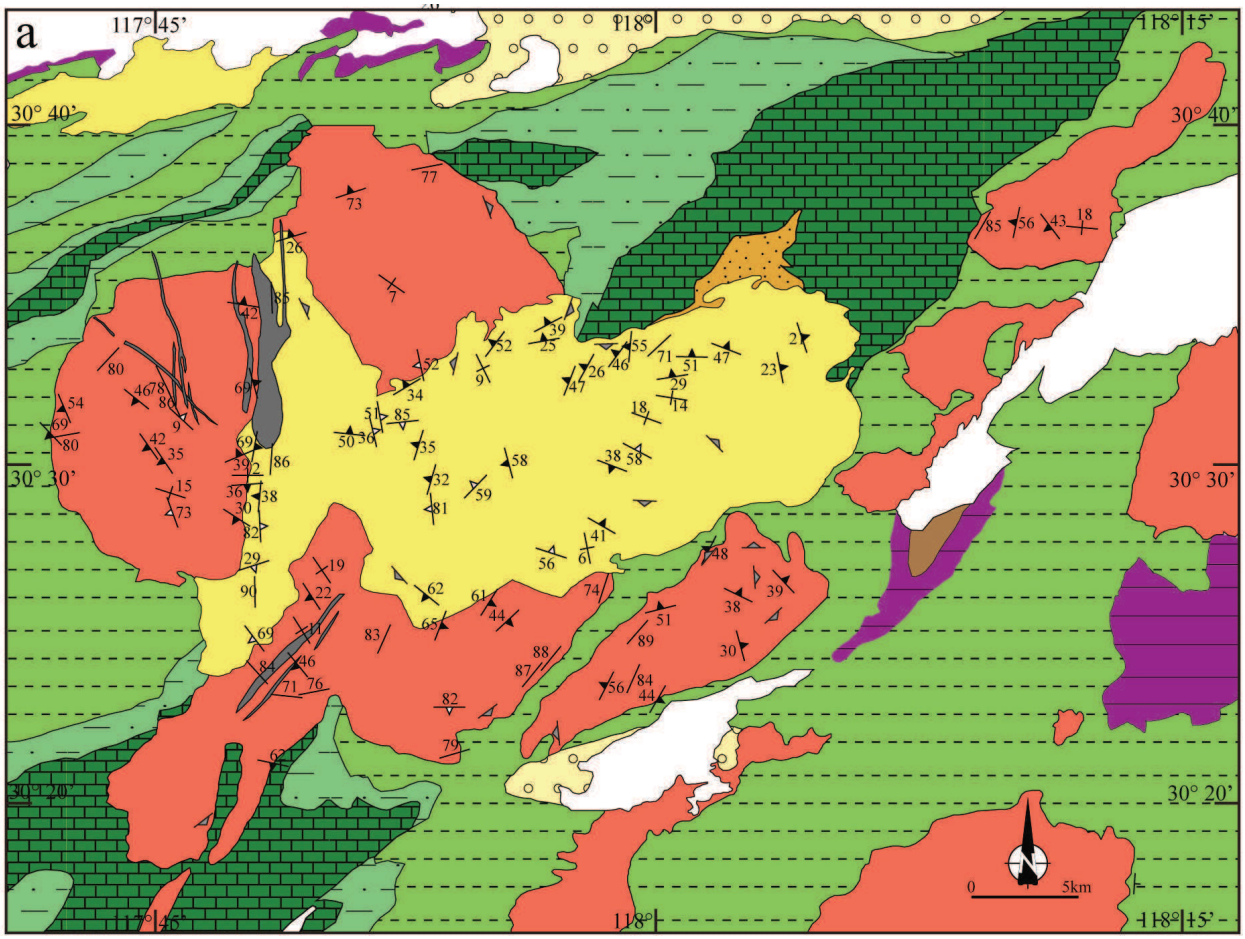

Figure 4 11: Magnetic foliation (a) and lineation (b) of the granitic rocks in the Qingyang-Jiuhua massif.

Q: Quaternary, N: Tertiary, K: Cretaceous, T: Triassic, Pz_2: upper Paleozoic, S: Silurian, O: Ordovician, ∈: Cambrian, Z: Sinian.

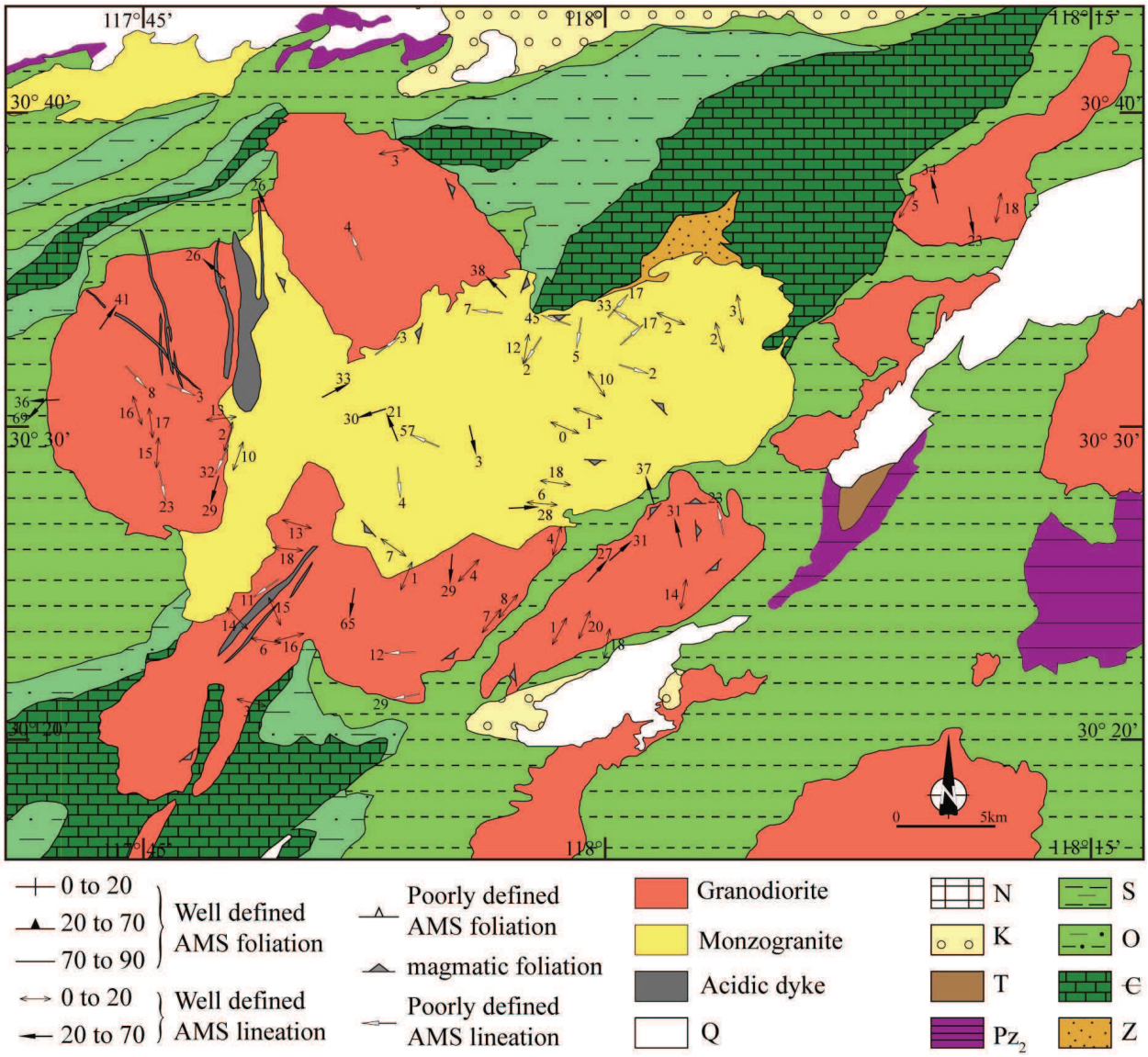

4.4 Paleomagnetic results

Among the 60 specimens selected for the paleomagnetic study, 55 have been successfully measured (Table 4-2; 14 from the Jiuhua pluton and 41 from the 4 subplutons of the Qingyang pluton; others were broken during the heating). Twenty of them have been progressively demagnetized by the AF technique and the remained 35 specimens are treated by thermal demagnetization with about 15 steps. Magnetic remanence directions were determined by a principal component analysis (Kirschvink, 1980). Inclinations and declinations obtained by progressive demagnetization were plotted on orthogonal vector diagrams (Zijderveld, 1967). Site-mean (the Jiuhua pluton and the subplutons of the Qingyang pluton) directions were

computed with Fisher statistics (Fisher, 1953). Paleomagnetic software packages of J.P. Cogné (Cogné, 2003) and R. Enkin (unpublished) were used for the data analysis.

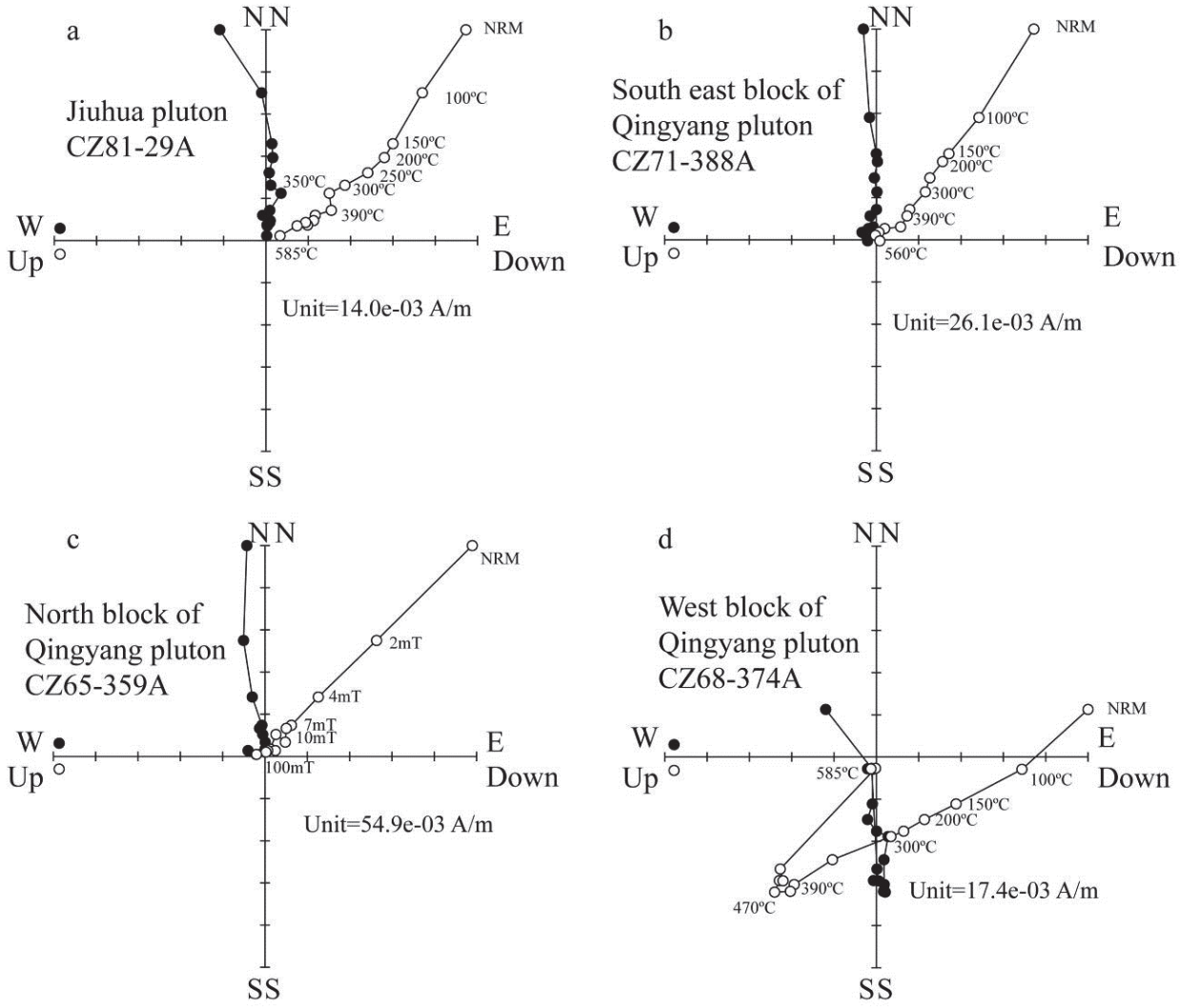

Figure 4 12: Zijderveld diagrams (1967) of the thermal and AF demagnetization for the representative samples.

The Jiuhua pluton (CZ81-29A) and the Qingyang pluton (others). Solid and open circle stand for horizontal and vertical plan, respectively.

Most specimens show a single component after having removed the viscous magnetization at lower temperature (100°C; Figs. 4-12a and 4-12b) or magnetic field (2mT; Fig. 4-12c). The magnetic remanence can be cleaned up at about 585°C or about 10 mT, reconfirming the

magnetite as the main remanence carrier. The reversed magnetic direction has been also observed on several specimens (Fig. 4-12d). For the specimens showing a single direction, the component may be isolated between 150 and 585°C or 2 to 10mT. Concerning the specimens presenting both normal and reversed directions, the normal component can be isolated from 150 to 470°C and the reversed one from 470 to 585°C.

To compare the directions among the subplutons within the Qingyang pluton and those between the Qingyang and Jiuhua plutons, the mean magnetic directions have been calculated from high temperature/AF components for the Jiuhua pluton and each subpluton of the Qingyang pluton, showing a good consistence (Fig. 4-13a and Table 4-2). It is worth noting that both normal and reversed directions have been observed in the older Qingyang pluton, but only single normal one in the younger Jiuhua pluton (Table 4-2).

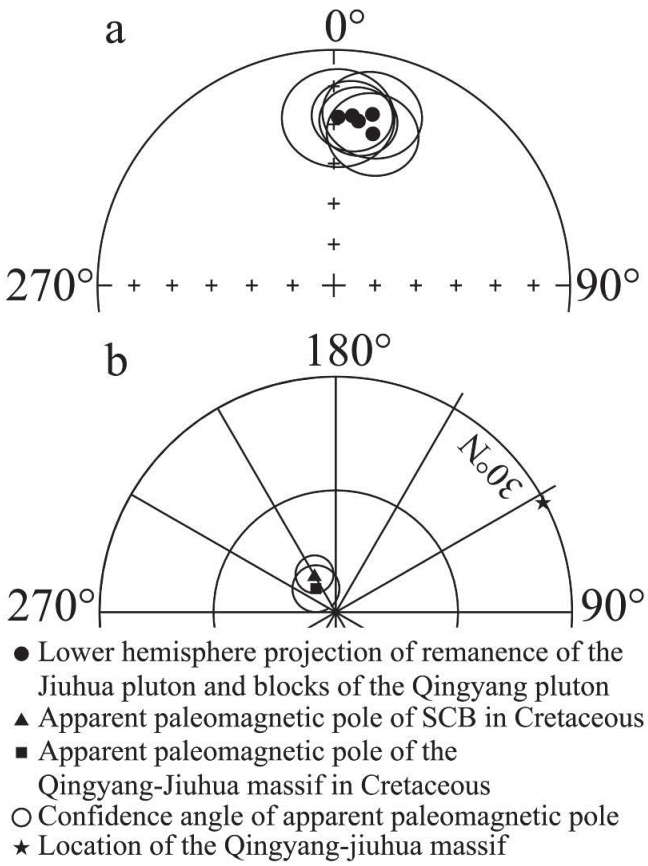

Figure 4 13: Paleomagnetic results of the Qingyang-Jiuhua massif.

(a) site-mean directions of the Jiuhua and blocks of the Qingyang pluton; (b) Paleomagnetic poles for the Qingyang-Jiuhua massif (■) and South China Block (▲) with sampling locality (★).

Table 4 2 Paleomagnetic results of high temperature magnetic components from the Qingyang-Jiuhua massif

Subpluton	Coordinates		N	P	Direction				Pole			
	Lat. (°N)	Long. (°E)			D (°)	I (°)	k	a_{95} (°)	l (°)	f (°)	dp (°)	dm (°)
W	30.5	117.7	10	N and R	6.2	43.2	17.3	11.3	82.3	250.5	8.7	14.0
S	30.4	117.9	11	N and R	12.7	46.3	19.3	11.3	78.6	218.1	9.3	14.5
N	30.6	117.9	8	N	358.2	47.4	17.8	14.7	87.4	335.5	12.4	19.1
SE	30.4	118.0	12	N	11.4	49.4	22.3	9.0	80.2	205.9	7.9	11.9
J	30.5	117.9	14	N	13.5	50.2	23.6	8.1	78.4	202.1	7.3	10.9
Average	**30.5**	**117.9**	5		**8.3**	**47.4**	**251.4**	**4.8**	**82.5**	**220.1**	**A_{95} = 5.7°**	
SCB									**79.4**	**209.0**	**A_{95} = 4.6°**	

N: specimen number, D: declination, I: inclination, k: precision parameter, α_{95} and A_{95}: statistic confidence of paleomagnetic direction and paleomagnetic pole at 95% level, respectively, l , f , dp and dm: latitude and longitude of paleomagnetic pole and its half radius of confidence in latitude and longitude, respectively, J: the Jiuhua pluton, W, S, N, SE: west, south, north, southeast subpluton of the Qingyang pluton.

5 Discussion

To understand the tectonic context and the mechanism of the Qingyang-Jiuhua massif emplacement, the deformation in different scales has been investigated in this study by different methods: microscopic observation on thin section, AMS, field structural observation and paleomagnetism. In order to provide a clear vision on the results from both field observation and laboratory measurements, in this discussion, we will firstly summarize these observations and then interpret them in terms of deformation within the massif, the regional tectonic context and the mechanism of the massif emplacement.

5.1 Summary of observations

In the field, the observation on this massif of 750 km^2 shows that igneous rocks have an isotropic fabric in most parts of the pluton. Along the contact zone between the pluton and country rocks locally developed, foliation and lineation are parallel to the contact, and downward plunging, respectively. However, in most places no visible deformation can be observed along the contact between the pluton and host rocks. Long axes of enclaves indicate a dominant NW-SE to E-W preferred orientation, more or less consistent with the magmatic fabrics illustrated in the 1:200000 geologic map of the studied massif (Fig. 4-2). In the country rocks, a regional ductile shear zone is absent. The ductile deformation only occurs in the aureole zone in which the foliation is consistent with the geometry of the contact, and the stretching lineation is vertical when it occurs. In the laboratory, microscopic observations indicate a predominant magmatic texture, while the post-solidus deformation texture only occurs on a few sites along the boundary between the massif and its country rocks. AMS measurements on 652 specimens of 93 sites present a weak anisotropy degree (P_J), and positive values of shape parameter (T) for the majority of sites. Globally, at the scale of the entire massif, the magnetic fabric is characterized by horizontal and scattered lineation, when it is located on the boundary of the massif, it follows the boundary contour; a flat and vertical foliation in the central part and the border of plutons, respectively. The paleomagnetic investigation on 55 samples from the Qingyang-Jiuhua massif statistically reveals coherent paleomagnetic directions with both normal and reversed magnetic polarities in four subplutons of the older Qingyang pluton and only normal one in the younger Jiuhua one.

5.2 Deformation within the massif

Structural and textural observations, acquired both in the field and laboratory, provide the direct data to argue for the emplacement mechanism. The microscopic observations on thin sections indicate magmatic textures, while the outcrop-scaled macroscopic observations in the field indicate that the main body of the massif is isotropic. The microgranitoid enclaves may be considered as passive strain markers and their preferred orientation may reflect the magmatic

process although it is not universally accepted (Paterson et al., 2004). Throughout the magmatic process, due to the higher content of mafic minerals in enclave than its host granitic rocks which lead to the earlier crystallization of the former than latter, the viscosity contrast between these two kinds of rocks is low in the initial stage; high in the second stage in which the enclave is highly crystallized while the host granite is still lowly crystallized; and low again in the last stage in which the host granitic rocks is highly crystallized same as the enclave. So in these tree stage, the enclave may deformed due to the magma flow to form a stretched shape and preferred orientation in the first stage, act as rigid objects transported, rotated and cracked in the magma by convection in the second stage, and deformed together with host granitic rock again in the last stage, respectively (Caricchi et al., 2012). In this course, the shape fabric of the enclave becomes statistically oriented parallel to magmatic fabrics (Vernon and Collins, 1988). In this study, numerous microgranitoid enclaves exhibit an angular shape and boudinage (Fig. 4-3d). Near the contact zone, the preferred orientation of these microgranitoid enclaves is parallel to both the magmatic foliation and the contact interface (Fig. 4-2). AMS samples were collected from both host granitoid rocks and enclaves within one site to compare their magnetic fabrics (Site CZ61; Fig. 4-14). The results show that the magnetic fabrics of host granites and enclaves are undistinguishable, and that their anisotropy degrees and shape parameters are also comparable. The susceptibility of enclaves higher than that of granitoids can be accounted by the high content of mafic minerals in the former rocks. The consistency of the shape fabric and AMS fabric between enclave and its host granitic rocks mainly reveal a magmatic course, thus in the studied massif the post-solidus deformation is rather weak.

Ductile deformation only occurs on the boundary of the massif and the nearby metamorphic aureole as well. On the both the NW and SE boundaries, the shear sense deduced from the ductilely deformed igneous and country rocks indicates that the massif side rises up with respect to the country rocks (Figs. 4-3b,4- 3c, 4-3f and 4-3g).

The significance of an AMS fabric may be multiple (e.g. Tarling and Hrouda, 1993; Borradaile and Henry, 1997). According to various parameters, such as susceptibility carrier, mineral size, anisotropy degree, shape parameter, the magnetic fabric may reflect either the mineral shape preferred orientation formed during the magmatic crystallization stage, or the mineral deformation fabric acquired during a later tectonic stage. In these two different cases, the

interpretation of the AMS fabrics is not the same. For the former, the fabric can be due to either magma flow or regional tectonics which exerts an influence on the melt before its final consolidation (e.g. Joly et al., 2009), while for the latter, the fabric results from regional tectonic events, after final crystallization of the pluton, which cause the deformation of the pluton as well as its country rocks (e.g. Bouchez and Gleizes, 1995).

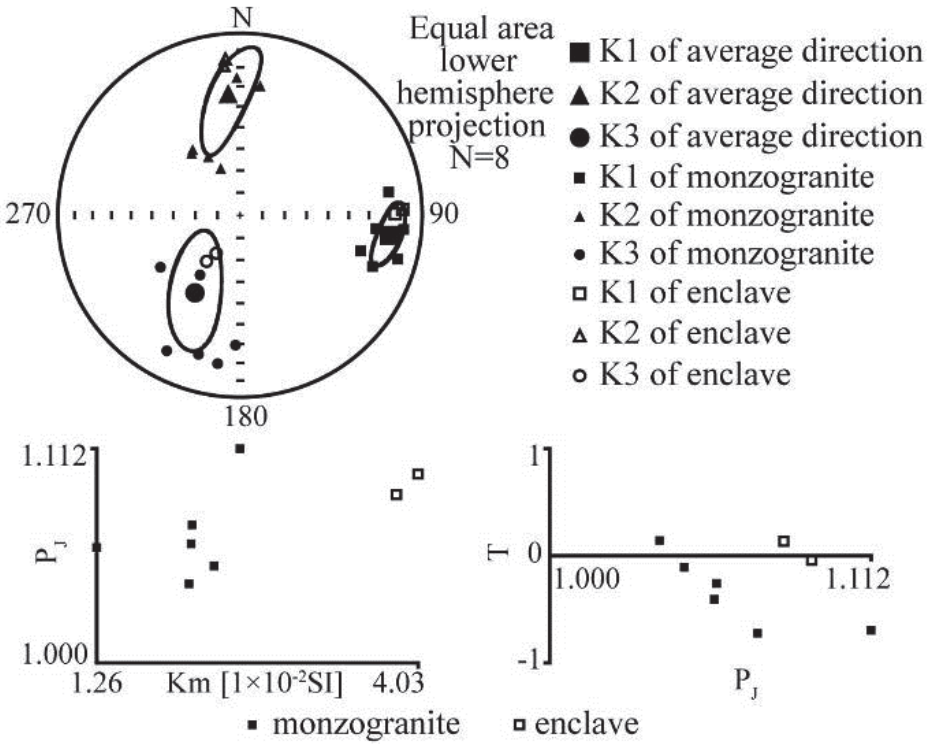

Figure 4 14: Comparison of AMS fabrics of the microgranitoid enclave with the host monzogranite.

In this study, the AMS fabric may be ascribed to the primary magmatic fabrics for several following reasons (Tarling and Hrouda, 1993). Firstly, our microscopic observations on thin sections, which are cut perpendicularly to the AMS foliation and parallel to the AMS lineation, do not reveal any post-solidus deformation (Figs. 4-3e, 4-3f and 4-3g); Secondly, the P_J values of most specimens are below 1.2, indicating that the anisotropy did not originate from a post-solidus deformation. For a few exceptional cases, P_J values above 1.2 can be explained by a border effect since these sites are located close to the pluton boundary (Figs. 4-8a, 4-9a and 4-9b). Thirdly, except for those specimens in the contact zone, all other specimens show that P_J values

varies in function of Km. This fact shows that the AMS ellipsoid can be reasonably correlated to the magnetite concentration instead of a posterior deformation (Charles et al., 2009). Consequently, the AMS fabric of the Qingyang-Jiuhua massif is ascribed to the magmatic flow, and/or regional tectonics event during syn-emplacement and late magmatic crystallization.

The paleomagnetic investigation also shows that a negligible deformation occurred within the pluton after the crystallization. The paleomagnetic directions from the Jiuhua pluton and 4 subplutons of the Qingyang pluton are statistically undistinguishable (Fig. 4-13a), implying that the younger Jiuhua intrusion did not produce any significant rotation among these subplutons. One might suspect this consistency of both elder and younger magnetic directions due to the remagnetization by the younger pluton emplacement. As described in Section 4.4, both normal and reversed directions have been isolated from the elder Qingyang pluton, however, only normal magnetic directions from the younger Jiuhua one (Figs. 4-12a, 4-12b, 4-12c and 4-12d). Therefore, the remagnetization possibility can be ruled out.

In summary, the results obtained by different methods, and at different observation scales, converge to point the same conclusion: the Qingyang-Jiuhua massif did not experienced a significant deformation either during or after its emplacement.

5.3 Implications on regional tectonics

In the vicinity of the Qingyang-Jiuhua massif, no continuous ductile shear zone has been documented. The ductile deformation has been only observed on the boundary of the massif. This suggests that the study area experienced a weak deformation including the during the emplacement time of the Qingyang-Jiuhua massif.

AMS is often considered as an efficient tool to study weak deformation such as that developed in plutons (e.g. Tarling and Hrouda, 1993; Bouchez and Gleizes, 1995). Nevertheless, the significance of granitic fabrics of plutons depends on the competition between magma dynamics and regional tectonic strain (Faure and Pons, 1991). If the crystallization is fast, the regional tectonics does not have the possibility to leave its imprint on the AMS fabric of igneous rocks (e.g. Callot et al., 2001). On the contrary, if the pluton crystallization time is long enough, the characteristics of this tectonic event may be revealed by the AMS fabric (e.g. Archanjo and

Bouchez, 1997; Archanjo et al., 1999; Neves et al., 2003; Zak et al., 2005, 2008;). Thus, when the tectonic strain is very weak, the pluton AMS fabric pattern will be controlled by magma flow (e.g. de Oliveira et al., 2010).

A good example is provided by AMS studies from granites in the Variscan French Massif Central. The well-grouped NW-SE striking magnetic lineation records well the NW-SE late-orogenic extension developed at the end of the Variscan orogeny, also documented by structural analysis of regional ductile normal faults, and pluton metamorphic aureoles (Joly et al., 2009; Talbot et al., 2005a). However, in our study, the shallow inclination scattered orientation of the magnetic lineation (Figs. 4-10 and 4-11b) might be due to the granitic magma flow under a weak regional tectonic influence during the late stage of crystallization (e.g. de Oliveira et al., 2010).

Several authors have emphasized the importance of the tectonic activity in the lower Yangtze area during the Cretaceous period, with contrasting directions (Lin et al., 2000; Faure et al., 2003; Mercier et al., 2007; Zhu et al., 2010b). An NE-SW extension, at ca. 145 Ma, is reported in the Hongzhen "metamorphic core complex" (Zhu et al., 2010b); an Early Cretaceous NW-SE stretching is recognized in the Lushan, Dabieshan, and along the Tanlu fault (Faure et al., 2003; Wu et al., 2007); a ca. 126 Ma NE-SW stretching is recognized in the Lushan massif (Lin et al., 2000), and a sinistral transcurrent motion developed from ca. 127 Ma to ca. 105 Ma along the Tanlu fault (Mercier et al., 2007). In order to clarify this controversy, we try to find if there is a relative movement of the study area with respect to its surrounding zones. As all the paleomagnetic directions from the Qingyang subplutons and the Jiuhua pluton show a good consistency, we can calculate a paleomagnetic pole at 82.5°N, 220.1°E, A_{95}=5.7° with n=5 (Table 4-2; square in Fig. 4-13b). We take SCB as reference and its Cretaceous pole for the comparison (see Wu et al., 1998 for details of this average pole). The weak angular difference (3.5°±7.3°) between these two paleomagnetic poles indicates that no paleomagnetically detectable relative movement occurred between the study area and SCB after the massif crystallization. Though keeping the weak resolution of the paleomagnetism in mind, we can conclude the intensive deformation observed in some zones, such as in the Dabie and Lushan massifs, concerns just local and limited areas. Moreover, if any strike-slip movement took place in the region, it could not be very important.

5.4 Hypothesis on the emplacement mechanism of the massif

The emplacement mechanism of granitoid can be divided into forceful and permissive types according to the manners of room creation (Pitcher, 1979). This can be identified by the impact exerted on country rocks by the granitoid emplacement. In the former type, granitic magma occupy the room created by pushing away the country rock during the pluton emplacement. In this case, the previous structures of the country rock, such as folds and faults, are modified, and several pluton emplacement-related structures such as folds, foliation, and mineral lineation develop around the massif in response to the pressure created by the crystallizing magma. While in the latter type, the emplacement of pluton has more links to the regional tectonics context because the room is created by a regional deformation coeval with the magma intrusion.

Based on the above discussion, our structural observations and the AMS fabric pattern favor a permissive mechanism by vertical magmatic injection, as illustrated in Figure 4-15.

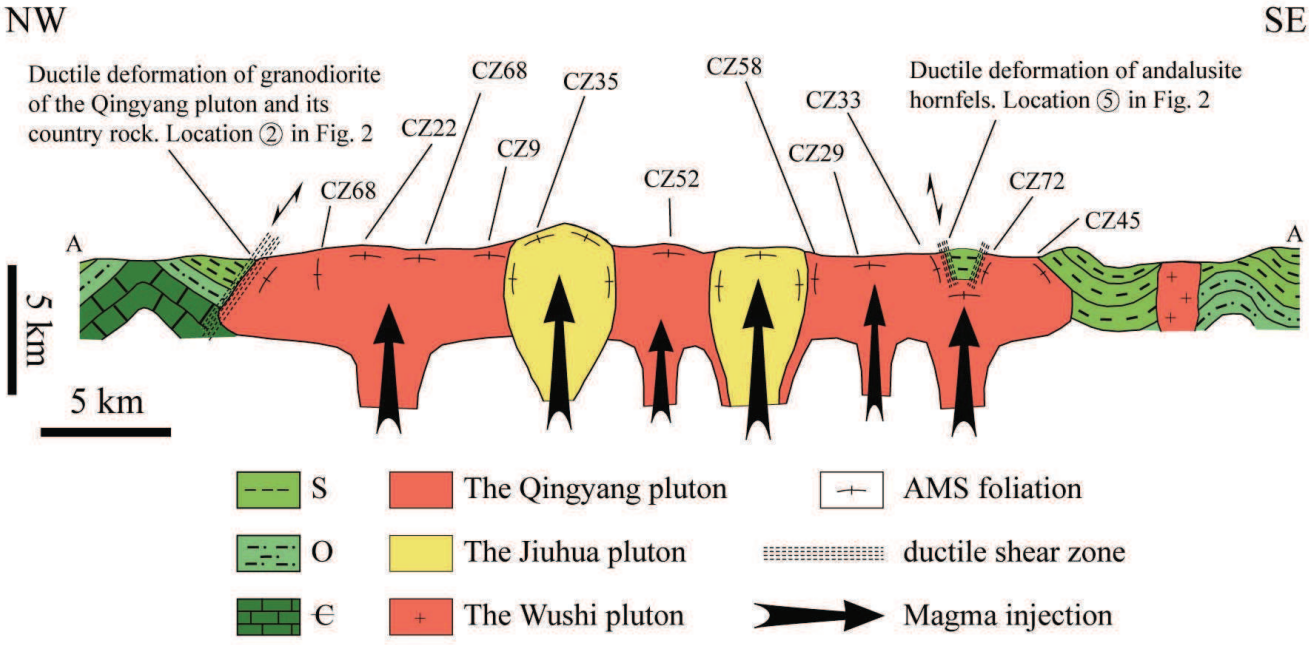

Figure 4 15: Emplacement model of the Qingyang-Jiuhua massif along AA' line (Fig. 4-2).

S: Silurian, O: Ordovician, ∈: Cambrian, CZ refers to the site number shown in Figs. 4-9a and 4-9b.

1) The main body of the Qingyang-Jiuhua massif is isotropic both at macroscopic and microscopic scales, e.g. quartz and feldspars show only an undulose extinction. This means that during the granite crystallization, the massif recorded a weak pressure effect that was unable to induce a significant structural effect on the country rocks, since there is neither modification of the previous fold geometry developed in the whole Yangtze fold belt (Fig. 4-2), nor creation of fold in the aureole. The magma emplacement just caused the local ductile shearing along the boundary surface, which could imply the ascent of the magma relatively to its country rocks (Figs. 4-2 and 4-15). This means that the space occupied by the massif was probably created by regional tectonics during the magma intrusion.

2) The fact that the emplacement of the younger Jiuhua pluton did not make any significant tilt of the Qingyang pluton, as shown by our paleomagnetic study (Fig. 4-13a) argues that the space was not created by pushing away the country rocks during the emplacement of the Jiuhua pluton.

3) The fabric distribution pattern supports a permissive emplacement mechanism of vertical magma injection.

Usually, when a vertically ascending magma stops near its final location, due to the blocking of the overlying country rocks and the pressure from the successive extruding magma beneath (arrows in Fig. 4-15), the foliation in the localities near the roof and side vertical surface of the pluton would be parallel to the boundary between the pluton and its country rocks. This generally leads to a flat foliation near the roof of the pluton and a boundary-concordant arrangement of the steep foliation near the pluton margins. When magma reaches the roof of the massif, in its central part, it will flow horizontally. This mechanism explains the flat lying foliation, and the low inclined scattered magnetic lineation in the central part of the massif. While near the boundaries between the pluton/massif and its country rocks, the magnetic lineation will be horizontal and parallel to the boundary (Fig. 4-11).

Field observations show that the exposures of the Qingyang-Jiuhua massif are close to the pluton roof. There exists a NE-SW oriented narrow strip of sedimentary country rock zone in the southeastern part of the Qingyang pluton (location ⑤ in Fig. 4-2). Considering its narrow shape, it could be interpreted as septum with the igneous rock joint together beneath.

The shape parameter T values of most specimens are above 0, presenting a dominance of

oblate shapes for AMS fabrics. Together with microscopic observations of the undulose extinction of quartz and feldspar by indicate magma crystallization under the pressure produced by subsequent magma injection.

The most obvious feature of AMS foliation is that the majority of the magnetic foliations is weakly inclined (Fig. 4-11a; e.g. CZ22, CZ68, CZ9, CZ35 and CZ29 in Fig. 4-15), and the highly inclined ones dominate along the massif boundaries where they are oriented parallel to the boundaries (Fig. 4-11a; e.g. CZ58, CZ 33 and CZ72 in Fig. 4-15). Enclave preferred orientation observed in this study, and the magmatic fabrics described by previous investigations shown in the 1:200000 geologic map of the Qingyang-Jiuhua massif (Fig. 4-2) also show a tendency to this accordance of the granite foliation with the massif boundary. This suggests an existing room when magma intrudes into.

According to the observations of deformation in different scales and the above discussion, it seems that the study region experienced a relatively weak deformation during the Cretaceous, even if the regional tectonics seems to play the most important role in the massif emplacement with respect to the internal magma dynamics.

6 Conclusions

For the purpose of understanding the tectonic context and mechanism of the emplacement of the Qingyang-Jiuhua massif, a multidisciplinary study has been carried out to investigate different scaled deformations from magnetic mineral fabric and petrographic texture to granitoid pluton and regional scale tectonics. The principal results are the following.

1. The composite Qingyang-Jiuhua massif mainly recorded an isotropic magmatic fabric, although a weak ductile deformation has been observed in the rocks of the border zone between the massif and country rocks. Both field observation and AMS measurement reveal flat or highly inclined foliations in the central or border zones of the massif, respectively.

2. The good consistency of the fold orientation in the study area around the massif with respect to the regional fold belt indicates that the granite emplacement did not modify the original tectonic framework.

3. The newly obtained paleomagnetic results confirm this observation, since no significant relative movements have been paleomagnetically detected either within the different parts of the massif or with the surrounding areas.

4. A possible emplacement mechanism involving a vertical and permissive intrusion of the Qingyang-Jiuhua massif accommodated by a relatively weak regional deformation during Late Mesozoic can be put forward.

This emplacement mechanism, based on surface structural observations and AMS analyses, remains a working hypothesis that needs further assessment. In order to improve this interpretation and the understanding of the contemporaneous regional tectonic framework, more information, such as the depth of emplacement and the 3D geometric characteristics of the massif, is needed. These additional data will allow us to better understand the textural features of AMS results and magma feeding processes.

Acknowledgements

The first author benefited a scholarship from the Sino-European Joint Doctoral Promotion Program (DPP) of the Chinese Academy of Sciences for his Ph.D. stay at ISTO (Orléans University-CNRS, France). This study was funded by the Chinese National 973 Project (2009CB825008), National Natural Science Foundation of China (41225009), the Innovative Project of the Chinese Academy of Sciences (Grant No. KZCX1-YW-15-1), the Major National Science and Technology Project (No. 2011ZX05008-001), and the Ministry of Land and Resources grant (201211024-04). Dr. Bernard Henry and Dr. Sanzhong Li are thanked by there constructive comments to improve the manuscript.

Part II

A multidisciplinary study of the emplacement mechanism of the Qingyang-Jiuhua Massif in Southeast China and its tectonic bearings.

Part II: Al^{total} in amphibole geobarometry and gravity modeling

Wei Wei[a,b,c,d,e], Guillaume Martelet[d], Nicole Le Breton[b,c,d,], Yonghong Shi[f], Michel Faure[b,c,d,], Yan Chen[b,c,d,], Quanlin Hou[a], Wei Lin[e*], Qingchen Wang[e]

[a] University of Chinese Academy of Sciences, Beijing 100049, China

[b] Univ d'Orléans, ISTO, UMR 7327, 45071 Orléans, France

[c] CNRS/INSU, ISTO, UMR 7327, 45071 Orléans, France

[d] BRGM, ISTO, UMR 7327, BP 36009, 45060 Orléans, France

[e] SKL, Institute of Geology and Geophysics, Chinese Academy of Sciences, Beijing 100029, China

[f] Hefei University of Technology, Hefei 230009, China

[*]Corresponding author: linwei@mail.iggcas.ac.cn

Abstract

The Late Mesozoic geology of the Lower Yangtze area in South China is characterized by the opening of sedimentary basins, the emplacement of numerous granitic plutons and the formation of several world-class ore deposits. The contemporary tectonic and geodynamic framework remains inadequately investigated. In order to provide a possible comprehensive understanding of the granitoid emplacement mechanism and its regional tectonic context, a multidisciplinary study has been performed to explore the emplacement mechanism of the Qingyang-Jiuhua massif. This massif consists of the granodioritic Qingyang and the monzogranitic Jiuhua plutons, dated at 142±1.0 Ma and 131±2.6 Ma, respectively. The results deduced from field structural observation, petrographic and magnetic fabrics, paleomagnetism (presented in Part I of this study, in the same volume) show that this massif was probably vertically emplaced by a permissive intrusion mechanism coeval with weak regional tectonics. However, detailed information on the characteristics of this tectonic event and its emplacement

depth could need to be documented. Therefore, further investigations on Al^{total} in amphibole geobarometry and a gravity modeling have been carried out to improve this hypothesis and acquire details of the emplacement depth of the studied massif and the primary deformation direction. The amphibole geobarometry data show that the Qingyang-Jiuhua massif is emplaced in the upper crust between 5 and 12 km. The gravity modeling indicates that the shape of the massif corresponds to a laccolith, characterized by several NE-SW-striking linear thickened zones that may be interpreted as the feeder roots of the massif, from where the magma is injected in the brittle upper crust. The integration of these results leads us to conclude that (1) the Qingyang-Jiuhua massif is fed by vertical and NE-SW striking tension gashes; (2) the late Early Cretaceous tectonics in the study area is characterized by a NW-SE directed extension.

Keywords

South China; Late Mesozoic extension; Al^{total} in amphibole geobarometry; gravity modeling.

7 Introduction

As a part of the South China Block (SCB), the Lower Yangtze area experienced similar Cretaceous tectonics than the SE part of SCB, namely: granitic pluton emplacement, continental sedimentary basin opening, and ore deposits formation (Gilder et al., 1991a; Goodell et al., 1991; Mercier et al., 2007; Li et al., 2010b; Mao et al., 2011). Numerous geochronological and geochemical works have been performed in order to illustrate the evolution and provenance of these igneous activities. Now it is well accepted that most of the Early Cretaceous magmatism took place between 145 Ma and 120 Ma (Wu et al., 2012) with a wide diversity of geochemical characters, namely I type, A type and adakitic signatures (Ling et al., 2009; Wu et al., 2012). However, the understanding of the geodynamic context of the pluton emplacement remains problematic. It was at first interpreted as a result of the thinning of a previously thickened crust (Zhang et al., 2008), from >50 km, as suggested by the presence of adakites (Wang et al., 2006), to the present 30 km, as documented by seismic reflection data (Schmid et al., 2001). However, Ling et al. (2009) argued that the hypothesis of a previously thickened crust was not consistent

with the development of extensional basins during the Late Jurassic to Cretaceous (Ling et al., 2009). Furthermore, the presence of adakites can also be explained by fractional crystallization of mantle-derived magmas within a normal crust (Li et al., 2009a). In the Lower Yangtze area, the NW-SE striking igneous belt is perpendicular to the subduction zone and the symmetric distribution of the A-type and adakite zones relative to the axis of this igneous belt, a slab window model was consequently proposed (Ling et al., 2009). But this model also faces the problems of the synchronous formation of the adakitic rocks and the development of rift basin in the whole Lower Yangtze area (Li et al., 2010b). Based on the arc-affinity of the REE and the trace element distribution patterns of plutons, it has been also proposed that the Lower Yangtze area corresponded to a back-arc environment (Xu et al., 2010).

Compared to the abundance of geochemical work, the structural data are rare and only performed in a few localities with ductile deformation. Consequently, the regional tectonic context of the Cretaceous magmatism is still in dispute (Lin et al., 2000; Faure et al., 2003; Zhu et al., 2010b). For instance, according to the structural analysis conducted in the Lushan and Dabie massifs, it is argued that a NW-SE extension took place in the beginning of the Cretaceous (Lin et al., 2000; Faure et al., 2003;). This feature is interpreted as the start of the steep subduction of the Paleo-Pacific slab (Zhu et al., 2010a). Throughout the study of quartz c-axis preferred orientation, a NE-SW extension direction was also proposed for the same Cretaceous time span (Zhu et al., 2010b). Therefore, more investigations are needed to clarify the regional tectonic context during the Early Cretaceous, and for this purpose, contemporaneous plutons can be considered as good markers of crustal deformation.

In Part I of these twin papers, we documented a multidisciplinary study, including the structural observation, Anisotropy Magnetic Susceptibility (AMS) and paleomagnetism of the Early Cretaceous Qingyang-Jiuhua massif. The results of these investigations indicate that the emplacement of the granitic massif did not alter the pre-emplacement structure of the country rocks, as folds axes were not disturbed around the massif. The ductile deformation only developed locally at the boundary between the massif and its country rocks. The AMS fabric, characterized by a vertical or sub-vertical foliation near the pluton boundary, and a horizontal or sub horizontal one in the center of the massif, only recorded the magma flow. The scattered AMS lineation did not recorded any syn-emplacement regional deformation. The paleomagnetic pole

of the Qingyang-Jiuhua massif, overlaps with the mean paleomagnetic pole of SCB indicating that the hypothesis of important strike-sip motion of this the Lower Yangtze area with respect to SCB can be ruled out. According to these results, yet reported in Part I, a permissive emplacement mechanism with vertical magma injection, coeval with a weak regional deformation, can be inferred. However, the shape of the granitic massif, details of the emplacement mechanism, as well as the regional tectonic setting of the magmatic emplacement remain unknown.

As unveiled by several previous studies, the determination of pluton shape and the understanding of emplacement mechanism can give insights on the regional tectonic framework (Pitcher, 1979b; Talbot et al., 2005b; Turrillot et al., 2011). Moreover, it should be pointed out that the emplacement depth could also impact on the shape of the pluton (Pitcher, 1979). Therefore the emplacement depth must be considered when interpreting the regional tectonic bearings of a pluton shape.

An Al^{total} in amphibole geobarometry and a gravity modeling have been performed in the already structurally studied Qingyang-Jiuhua massif (cf. Wei et al. 2013, Part I in this volume). This study aims to answer several unsolved questions, including: (1) What is the shape of the granitic massif? (2) Does this shape comply with the permissive emplacement mechanism suggested in Part I? (3) What is the regional tectonic context coeval with the pluton emplacement? (4) Is there a relationship between the emplacement mechanism and the regional tectonic context?

8 Geological setting

8.1 The geological framework of the Lower Yangtze area

The Lower Yangtze area, located in the northeastern part of the SCB, is composted of the Dabie Massif, the Lower Yangtze fold belt and the Jiangnan orogenic belt from north to south, respectively (Fig. 4-16).

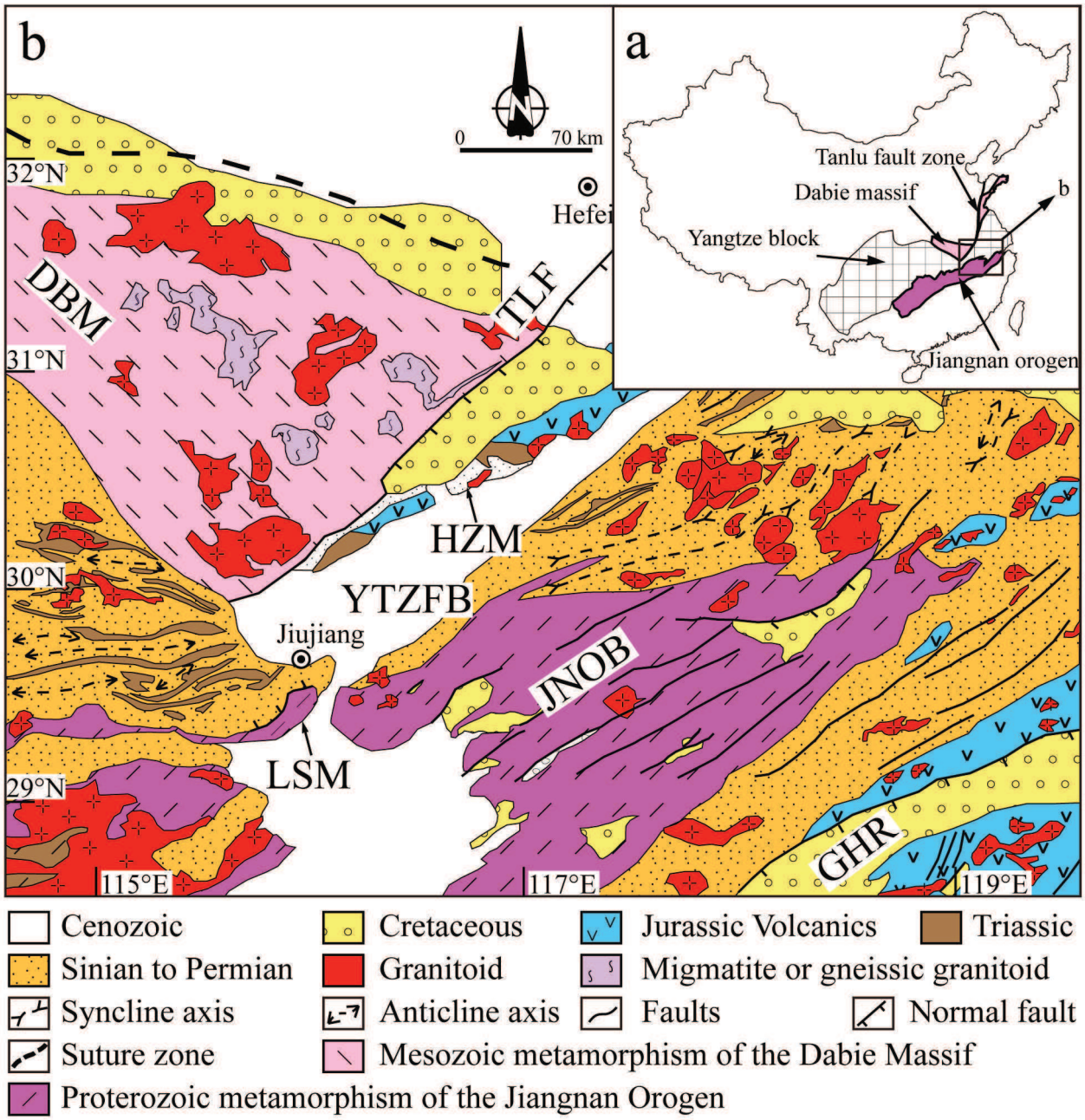

Figure 4 16: Regional geological map of the Lower Yangtze area.

TLF: the Tanlu fault, YTZFB: the Lower Yangtze fold belt, JNOB: the Jiangnan orogenic belt, GHR: the Ganhang rift basin, DBM: the Dabie massif, LSM: the Lushan massif, HZM: the Hongzhen massif.

The Dabie massif separates the North China Craton (NCC) from the SCB, which collided in Paleozoic time (Mattauer et al., 1985b; Faure et al., 1999; Mingram et al., 2004). In the Triassic, the Dabie domain experienced an intracontinental deformation responsible for high to ultra-high

pressure metamorphism (Cong and Wang, 1999). During the Cretaceous, an extensional tectonic event gave rise to a migmatitic dome in the North Dabie massif with a pervasively distributed NW-SE stretching lineation and a top-to-the-north ductile shearing (Faure et al., 2003). During the exhumation of the North Dabie massif, numerous syn-kinematic plutons emplaced with ductilely sheared boundaries also indicating a NW-SE extension (Hacker et al., 1998b; Faure et al., 2003). In the last stage, the Dabie massif was bounded by brittle normal faults leading to the formation of Cretaceous half graben basins infilled by red continental sediments (Mercier et al., 2007).

The Lower Yangtze fold belt, which was intruded in the Early Cretaceous by the Qingyang-Jiuhua massif consists of a Neoproterozoic to Early Triassic marine sedimentary series. This series was deformed by south-directed folds and thrusts belt in response to the intra-continental subduction of the Dabie massif (Schmid et al., 1999). It is also proposed that to the south part of this belt, some folds and thrusts may relate to the reactivation of the Neoproterozoic Jiangnan orogenic belt during the Triassic to Jurassic times (Li et al., 2010a). Except numerous graben and half-graben basins opened inside the Lower Yangtze fold belt (AHBGMR, 1987), the structure and evolution of the Cretaceous extensional event are still poorly constrained.

The Jiangnan orogenic belt is a Neoproterozoic orogen characterized by ophiolitic suture and high-pressure metamorphism, which led to the formation of the SCB (Charvet et al., 1996; Li et al., 2009b; Shu et al., 2006). In the Triassic, a series of antiforms were developed there in response to the deep continental subduction of the Dabie Massif in order to accommodate the continuing convergence between NCC and SCB (Faure et al., 1996; Faure et al., 1998; Lin et al., 2001). During the Cretaceous, the Jiangnan orogenic belt is characterized by extensional structures, such as the Wan-Zhe-Gan NE-SW striking normal fault system and intracontinental half-graben basins (Gilder et al., 1991a; Goodell et al., 1991; Yu et al., 2007).

8.2 The Qingyang-Jiuhua massif

The Qingyang-Jiuhua massif, located in the Lower Yangtze fold belt, mainly consists of the granodioritic Qingyang and the monzogranitic Jiuhua plutons. They are mainly composed of

granodiorite with a diorite rim around the northeast boundary and monzogranite together with some alkali feldspar granite, respectively. Geologic investigations indicate that along its boundary, the Jiuhua pluton captured several blocks from the Qingyang pluton. The entire massif is intruded by NE-SW or N-S striking microgranite dykes (Fig. 4-17; AHBGMR, 1987).

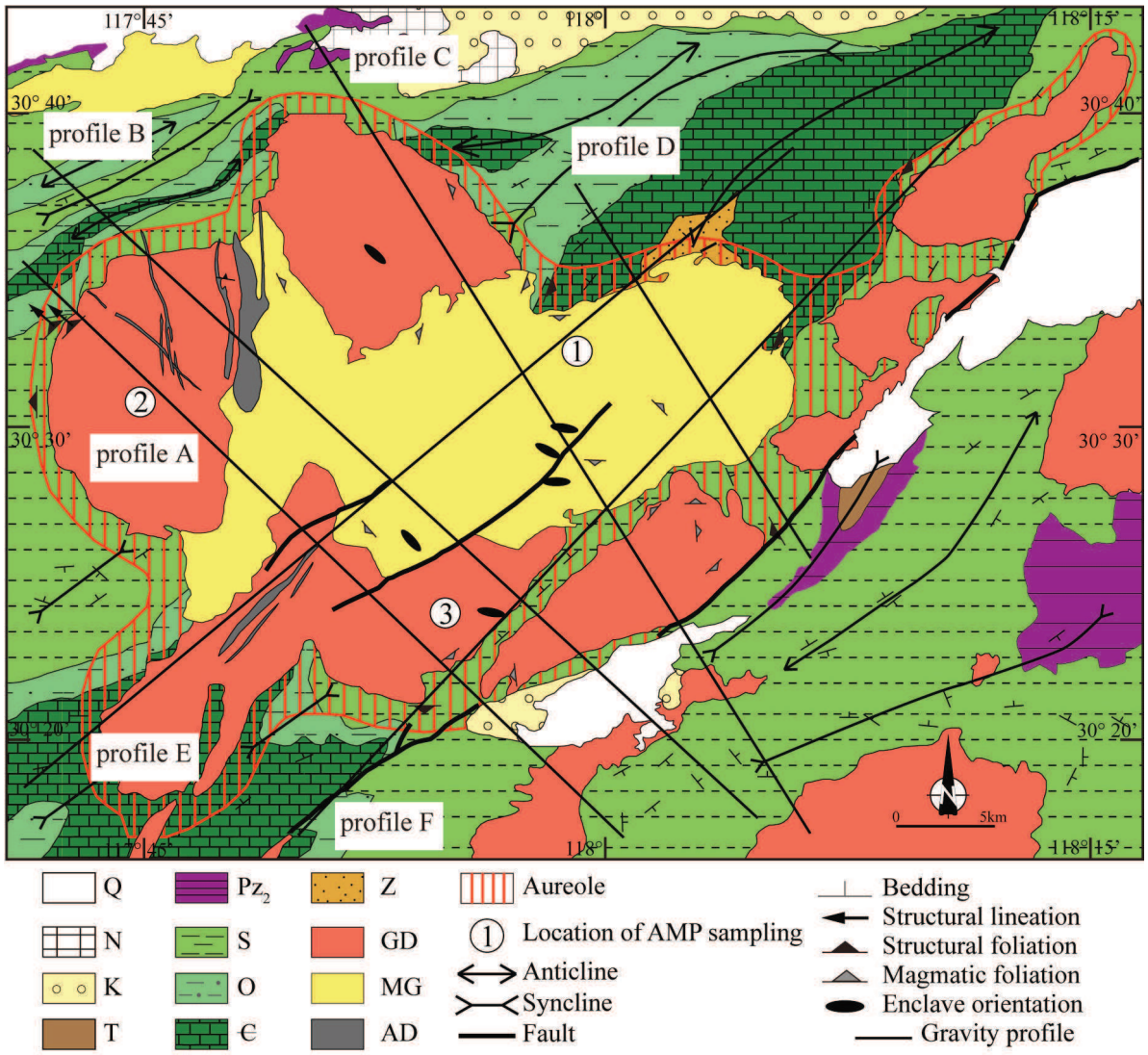

Figure 4 17: Simplified geological map of the Qingyang-Jiuhua massif and its surrounding area with gravity modeling profiles (Fig. 4-23).

Q: Quaternary, N: Tertiary, K: Cretaceous, T: Triassic, Pz_2: Upper Paleozoic, S: Silurian, O: Ordovician, ∈: Cambrian, Z: Sinian.

In the Qingyang pluton, amphibole and biotite yield similar Ar-Ar ages at 137.1±1.4 Ma,

and in the Jiuhua pluton, biotite yields 122.7±1.2 Ma (Chen et al., 1985). These ages suggest a fast cooling of the massif. Recently, several zircon U-Pb geochronological studies have been performed on the Qingyang-Jiuhua massif in order to acquire precise emplacement ages. The Qingyang granodiorite is variously dated at 144.8±0.7Ma (Chen et al., 2005a), 140±1.1Ma (Xu et al., 2010) and 139.4±1.8 to 142.0±1.0Ma (Wu et al., 2012). The Jiuhua monzogranite yields zircon U-Pb ages at 133.2±1.3 Ma (Xu et al., 2010), and 130.3±1.8 to 131.0±2.6Ma (Wu et al., 2012). The alkali feldspar granite of the Jiuhua pluton is dated by zircon and monazite U-Pb methods at 129Ma and 127Ma, respectively (Xu et al., 2010).

Several geochemical works have also been performed in order to track the magma provenance. According to the Sm-Nd isotopic signature, and similarity of the Nd model age with plutons in the adjacent Jiangnan orogenic belt, it was argued that the granitoids originated from the melting of the SCB Proterozoic basement without significant mantle material input (Chen et al., 1993). REE and trace element analyses on the Qingyang-Jiuhua massif suggest an arc affinity of the massif that would be related to the subduction of the Paleo-Pacific slab. Magma mixing between crustal and mantle components was also proposed on the basis of the presence of dark microgranitoid enclaves as well as the similarity to the adjacent contemporary mantle derived magmatic rocks (Xu et al., 2010). According to the mineral assemblage, it is also proposed that the granodiorite of the Qingyang pluton is an I-type granitoid, and the monzogranite and alkali feldspar granite of the Jiuhua pluton are A-type rocks, or highly fractionated I-type granite (Wu et al., 2012).

9 Geobarometry using the total Al-content of magmatic amphibole

The emplacement mechanism of a pluton is strongly affected by the viscosity contrast between melts and their surrounding country rocks (Pitcher, 1979). If the viscosity contrast is low, the diapirism is the main mechanism, as exemplified by migmatitic domes all around the world (Charles et al., 2009). In the contrast, if the viscosity of country rocks is much higher than that of the melts, injection may become a likely mechanism (Talbot et al., 2005b). It is shown in many studies that the rheology of crustal rocks depends not only on temperature, but also on depth (e.g. Charles, 2010 and references therein). Therefore it is useful to estimate the

emplacement depth by calculating the pressure with the help of appropriate magmatic parageneses.

Furthermore, the knowledge of emplacement depth is an important factor, as it can influence the deformation style of the country rocks around a pluton. The pluton-related deformation is mostly brittle or ductile in the upper or lower, respectively. Since the shape of a pluton is affected by the pre-existing structure and lithological discontinuities (Pitcher 1979; Aranguren 2003), the depth estimation becomes essential for providing constraints on the interpretation of a gravity model.

Since the Qingyang and the Jinhua plutonic rocks contain green calcic amphiboles, it is possible to use the total aluminum content of amphibole rims as a barometer to estimate the intrusion depth, by assuming that the magmatic amphibole equilibration continues until wet solidus conditions are reached, and that it ceases in the subsolidus domain because the fluid escapes rapidly after solidification of the pluton (Hammarstrom and Zen, 1986; Hollister et al., 1987; Schmidt, 1992). However, the Al-in amphibole barometer is sensitive to oxygen fugacity and to temperature (Anderson and Smith, 1995). Therefore, if the amphibole-bearing granitoids are emplaced at conditions inconsistent with experimental calibrations, the derived pressures using these calibrations may differ by a factor two or more from the real pressures. Since magnetite is present in the magmatic parageneses of the Qingyang and Jinhua plutons, the oxygen fugacity during the crystallization can be considered high enough to prevent a misuse of the barometer.

9.1 Methodology

Element analyses of minerals were performed using a fully automated CAMECA CAMEBAX electron microprobe, jointly managed by BRGM, CNRS and the University of Orléans. The accelerating voltage was 15 kV, and the beam current was 10nA. The beam size was set to 10 μm. Counting time was 10 s on peak and 10 s on background for all elements. Natural and synthetic silicates and oxides were used as standards. The collected data were corrected with the ZAF procedure by use of the PAP software provided by CAMECA.

Three samples (QY18, QY24, QY33 with locations shown in Fig. 4-17) were chosen in order

to estimate the emplacement depth using amphibole compositions. The mineral assemblage in both granodiorite (QY18 and QY33) and monzogranite (QY24) consists of green calcic amphibole, biotite, plagioclase, alkali feldspar, titanite, magnetite and quartz (Fig. 4-18). The granodiorite shows a granular texture (Figs. 4-18a, b, c and d), whereas the monzogranite is porphyritic with phenocrysts of biotite, plagioclase, alkali feldspar, titanite, magnetite, quartz, and rare amphibole surrounded by a fine-grained groundmass of quartz and feldspar (Figs. 4-18e, f, h and i). In both types of rocks, plagioclase shows an optical zonation and alkali feldspar is perthitic (Figs. 4-18c and e). Amphibole and titanite grains contain magnetite exsolutions (Figs. 4-18c, e and f). In granular granodiorite, quartz infills the space between other euhedral to subeuhedral minerals (Figs. 4-18a and b).

We analyzed both cores and rims of plagioclase and amphibole grains in order to show possible heterogeneities. Attention was also focused on keeping away from the magnetite exsolution in amphibole, which can change the total Al content of amphibole in the adjacent area (Hammarstrom and Zen, 1986).

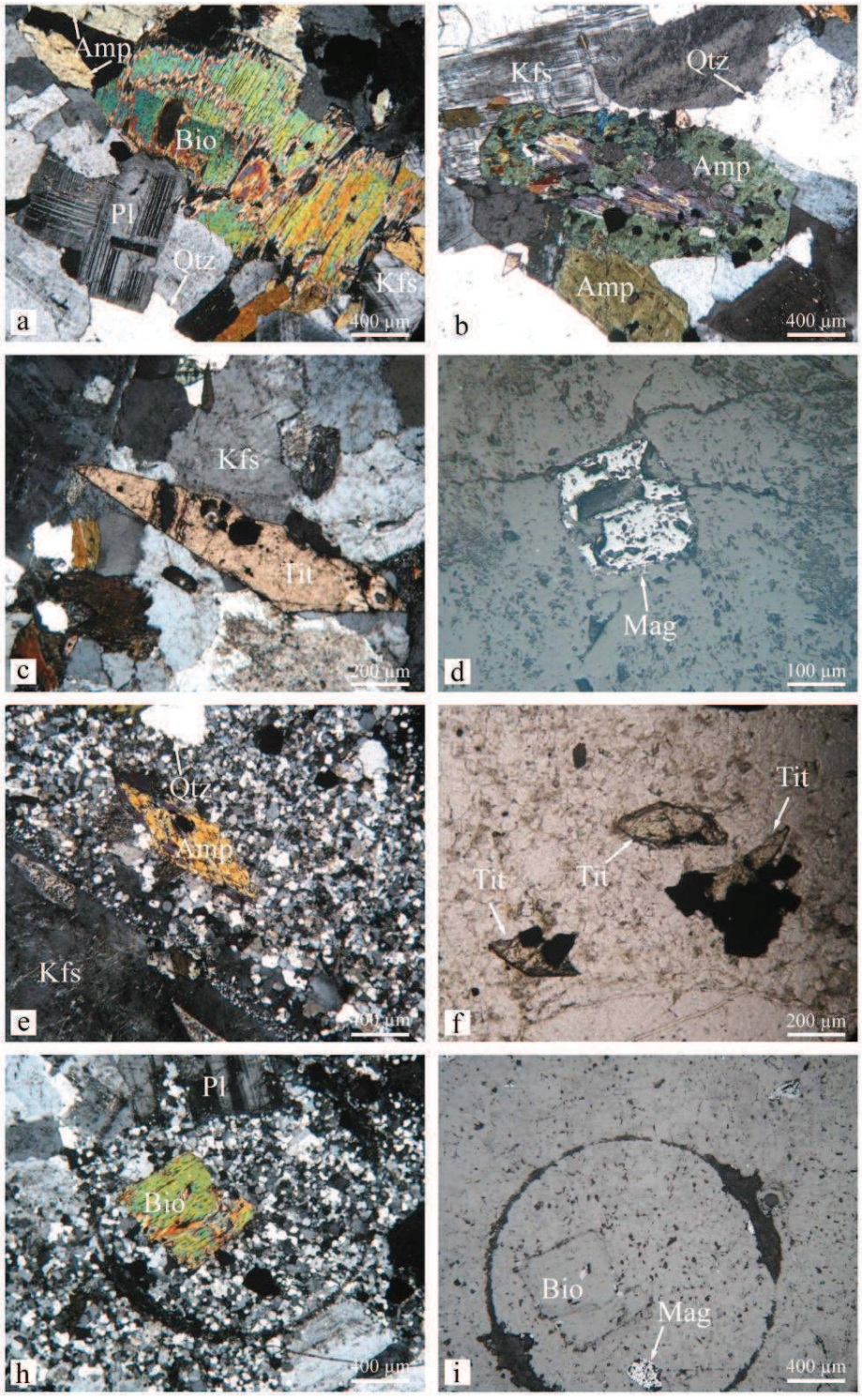

Figure 4 18: Mineral assemblage of the Qingyang-Jiuhua massif.

Amp: amphibole, Bio: biotite, Pl: plagioclase, Kfs: alkaline feldspar Qtz: quartz, Tit: titanite and Mag: magnetite. a, b, c and d are from the granodiorite of the Qingyang pluton. e, f, h and i are from the monzogranite of the Jiuhua pluton.

9.2 Results

The typical compositions of plagioclase and amphibole rims are shown in Table 4-3. Amphibole formula are calculated according to the procedure recommended by the International Mineralogical Association (Leake et al., 2004), with the assumption that there is no Fe^{3+} in the amphibole lattice. The results show that most of the amphibole rims have compositions of a magnesiohornblende, while a few rim compositions correspond to edenite (Fig. 4-19).

Table 4 3 Representative chemical compositions of amphibole and plagioclase

Sample	QY33-1	QY18-3	QY24-2	QY33-1	QY18-2	QY24-5
Mineral	Amp	Amp	Amp	Pl	Pl	Pl
SiO_2	47.355	49.715	48.241	58.942	58.893	61.190
TiO_2	1.161	0.646	0.729	0.048	0.025	0.000
Al_2O_3	6.912	5.011	5.615	25.109	24.927	24.156
FeO tot	14.066	12.797	14.551	0.068	0.166	0.032
MgO	13.404	15.127	13.391	0.012	0.074	0.000
MnO	0.613	0.842	1.444	0.000	0.010	0.000
CaO	11.620	11.585	11.654	7.197	7.095	5.345
Na_2O	1.157	0.913	1.019	7.531	7.415	8.399
K_2O	0.734	0.348	0.532	0.105	0.199	0.222
Total	97.022	96.984	97.176	99.012	98.804	99.344
Si^{4+}	7.03	7.30	7.17	2.66	2.66	2.73
Ti^{4+}	0.13	0.07	0.08	0.00	0.00	0.00
Al^{3+tot}	1.21	0.87	0.98	1.33	1.33	1.27
Fe^{2+}	1.75	1.57	1.81	0.00	0.01	0.00
Mg^{2+}	2.97	3.31	2.97	0.00	0.00	0.00
Mn^{2+}	0.08	0.11	0.18	0.00	0.00	0.00
Ca^{2+}	1.85	1.82	1.86	0.35	0.34	0.26
Na^{+}	0.33	0.26	0.29	0.66	0.65	0.73
K^{+}	0.14	0.07	0.10	0.01	0.01	0.01
Total	15.47	15.38	15.44	5.01	5.00	5.00
P (Kbar)	2.75	1.13	1.65	-	-	-
An (%mol)	-	-	-	35	34	26
Mg/(Mg+Fe)	0.63	0.68	0.62	-	-	-

Amp: amphibole, Pl: plagioclase, cations' values are calculated on the basis of 23 O and 2 OH for amphibole.

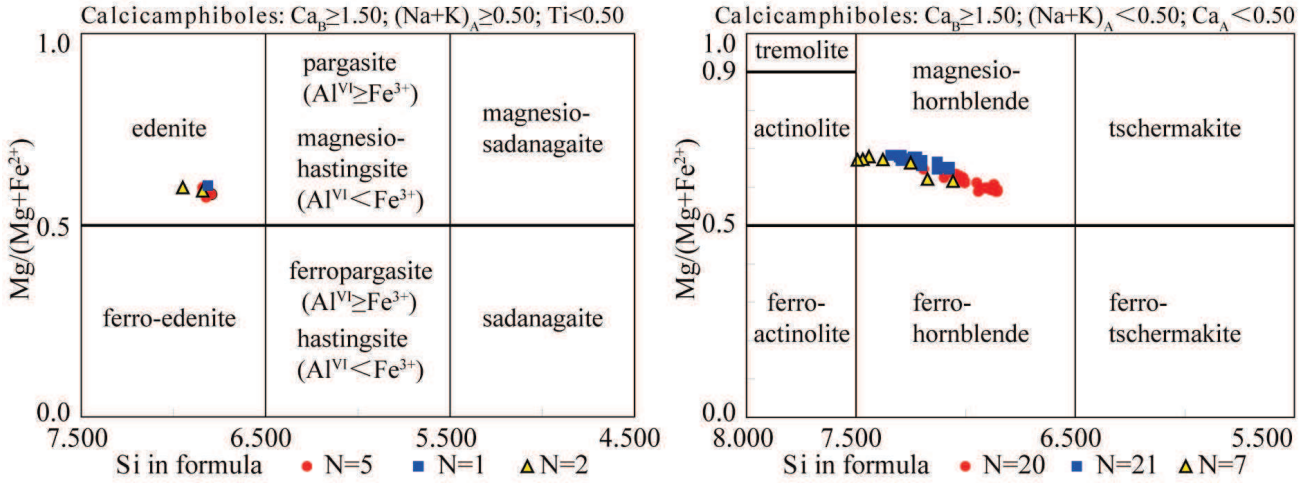

Figure 4 19: Chemical composition of calcic amphiboles analyzed in three samples coming from the Qingyang-Jiuhua massif.

Location of samples shown in Figure 4-17: QY18 (open square), QY24 (solid triangle) and QY33 (open circle). The formula is calculated on the basis of 23 O with 2 OH.

Chemical zonation is noticed in amphiboles (Fig. 4-20). The anorthite content is always within 25 to 35 mol % in the rims of plagioclase (Table 4-3), thus providing a compositional constraint allowing the calculation of pressure using the total Al content of amphibole (Hollister et al., 1987). The amphibole cores are richer in aluminum than the rims (Fig. 4-20). This may be due to the effect of unsaturation silicon in melts during the early stage of crystallization, which can enhance the Al^{total} content in the amphibole lattice (Hammarstrom and Zen, 1986). Therefore in order to get rid of the inexactness caused by this effect, we only used the rim compositions of amphibole to calculate the equilibration pressure at the solidus (Hollister et al., 1987).

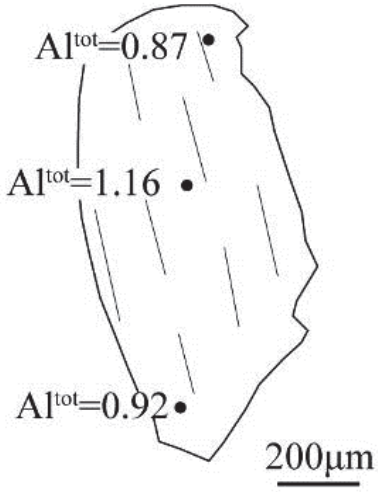

Figure 4 20: The total Al content of Amphibole in rim and core of granodiorite of the Qingyang pluton (calculated on the basis of 23 O and 2 OH).

The composition of amphibole rims shown in the plot of Al^{tot} pfu versus Al^{IV} pfu (Fig. 4-21) fits well with the linear regression on the data obtained for low-pressure rocks studied by Hammarstrom and Hollister (1986). This result can be clearly stated by using the Al-in amphibole geobarometer calibrated by Schmidt (1992). Equilibration of the assemblage composed of amphibole, biotite, plagioclase, orthoclase, quartz, titanite, Fe-Ti-oxide, melt and vapor from a natural tonalite, 15-20°C above its wet solidus, was fit by the equation:

$$P\ (\pm 0.6\ \text{kbar}) = -3.01 + 4.76\ Al^{tot},$$

where Al^{tot} is the total Al content of amphibole in cations per formula unit (calculated to 23 O and 2 OH). For QY33, the total Al content of amphibole is comprised between 1.03 and 1.43 cations pfu, which gives, after Schmidt (1992), a pressure between 1.3 and 3.3 kbar. For QY24, the Al^{total} values are in the range between 0.63 and 1.12 cations pfu, and the pressure is therefore lower than 1.6 kbar. For QY18, the Al^{total} value varies from 0.83 to 1.13, which leads to a pressure lower than 1.8 kbar.

As a result, all pressure values obtained using the total aluminum contents of amphibole rims are clearly lower than 4 kbar. If the assumption that no equilibration between amphibole and other phases took place in the subsolidus conditions is correct, this low pressure indicates that the emplacement of the Qingyang and the Jiuhua plutons occurred at shallow depth (5 to 12 km). This estimate is in accordance with the presence of andalusite in hornfels in the metamorphic

aureole of the massif.

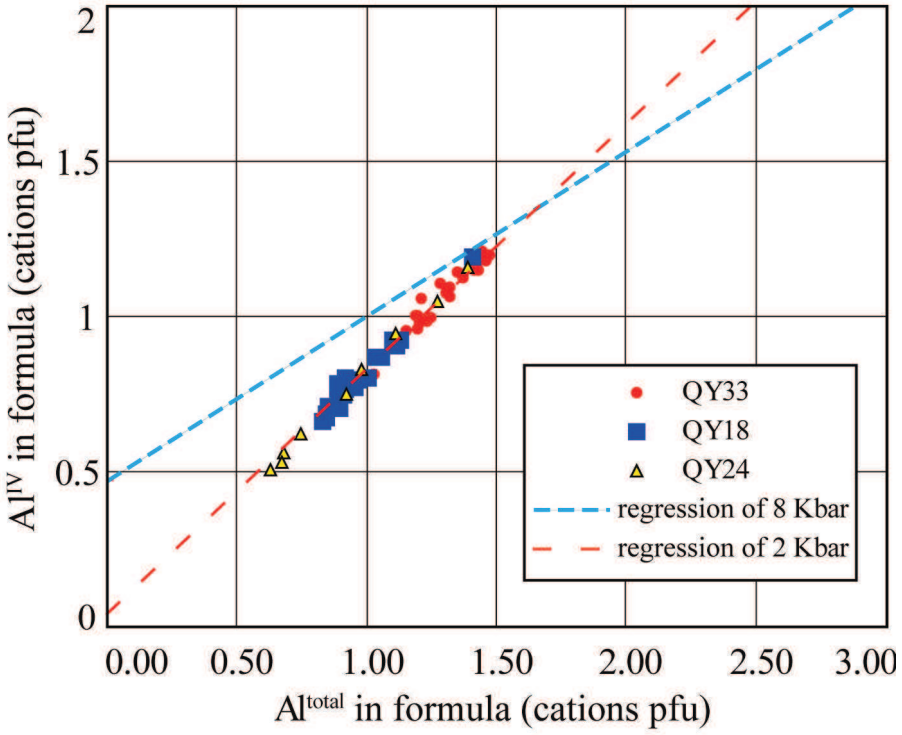

Figure 4 21: Al^{IV} and Al^{total} bivariate diagram of the Qingyang-Jiuhua massif.

Al^{IV} and Al^{total} values are calculated on the basis of 23 O and 2 OH (see Fig. 4-17 for location of samples). All values are from the rims of the amphibole grains.

10 Gravity method

Since gravity modeling has long been successfully used to address the geometry of plutons at depth (e.g. Aranguren 2003; Talbot et al., 2005a; Joly et al., 2009; Turrillot et al., 2011), we applied this method to constrain the shape of the Qinyang-Jiuhua massif. The Bouguer anomaly map we used is acquired from the Chinese 1:200000 Bouguer anomaly database. We modeled four NW-SE profiles and two NE-SW ones, covering the entire massif and crosscutting with each other (Fig. 4-22).

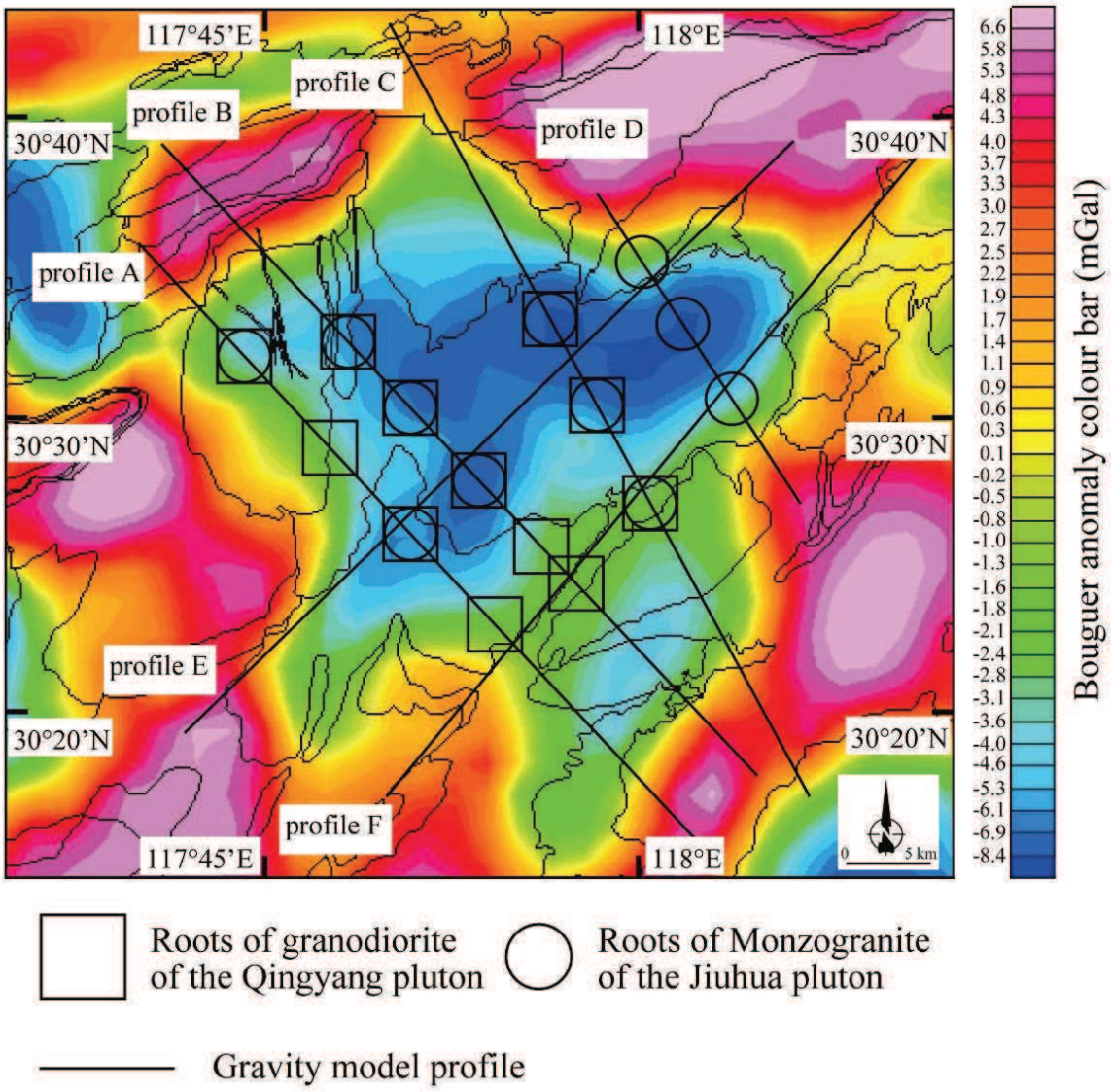

Figure 4 22: Residual Bouguer anomaly map of the Qingyang-Jiuhua massif and its surrounding area with modeled gravity profiles (shown in Fig. 4-23).

10.1 Bouguer regional and residual anomaly

The Bouguer map around the Qinyang-Jiuhua massif displays a clear long wavelength regional component, which blurs the local signature of the massif. Since our study focuses on anomalies related to density contrasts caused by lithologies in the first kilometers of the crust, we firstly removed the effect of deep density contrasts from the Bouguer map. This can be achieved by several techniques, which are aimed at removing the long wavelengths from the Bouguer anomaly. After several attempts, we used a low-pass Butterworth filter with a cutoff wavelength

of 70 km, which provided a regional anomaly map approximating well the original Bouguer map. Then we subtracted this regional anomaly from the original Bouguer anomaly to obtain a residual (or local) Bouguer map (Fig. 4-22).

In the original Bouguer anomaly map, one can observe that there is a clear regional trend from NW to SE, and that the anomaly contours cross-cut the pluton boundaries. In the residual Bouguer anomaly map, the negative and positive anomalies fit well with the granite and country rocks, respectively (Fig. 4-22). The contours of the residual Bouguer anomaly map are parallel to the boundary of plutons (Fig. 4-22). Within the country rocks, the NE-SW elongated pattern is apparent due to the fold trend. The highest intensity anomalies correspond to the Cambrian and Ordovician formations, which have the highest density in the studied area (Table 4-4). Based on the above observations, we consider that the residual Bouguer anomaly map properly accounts for the shallow depth of crust and can be used to model the geometry of the plutons and country rocks.

Table 4 4 Rock densities used in gravity modeling

Rocks	Average of measured density (g/cm^3)	Number of measured samples	Standard Derivation (g/cm^3)	Density used in modeling (g/cm^3)
Granodiorite	2.7116	2	0.0013	2.712
Monzogranite	2.6157	7	0.0168	2.616
Alkali granite	2.6043	1	-	2.604
Triassic	2.6983	1	-	2.698
Devonian	2.7225	1	-	2.722
Silurian	2.7324	4	0.0568	2.732
Ordovician	2.8435	2	0.0028	2.838
Cambrian	2.8283	1	-	2.838
Sinian	2.6668	1	-	2.667

Because of the small volume of samples for alkali granite and acidic dykes and the similarity of their density with mozogranite, we use density of monzogranite for these three lithologies in gravity modeling. For the thin Carboniferous and Permian strata, we did not measure the density, but use that of Devonian strata. As the densities of the Ordovician and the Cambrian strata are similar, we use the average density of them in the gravity modeling.

More specifically, the residual Bouguer anomaly features essential geological patterns. To the north, the boundary between the granitic massif and country rocks coincides with a strong anomaly gradient, which suggests a sharp contact between these two geological bodies. To the northeast and the east, the negative anomaly exceeds the geological boundary, which indicates an extension of the massif beneath the country rocks. To the southwest, a positive anomaly exists on the massif side, which suggests thinning of the pluton. The lowest negative anomaly is in the center of the massif and is slightly NE-SW trended, coincident with the outcrop of the monzogranite, which has the smallest density. Around the monzogranite, the contours of the lowest negative anomalies are convex along the granodioritic border, which indicates that the monzogranite might continue beneath the granodiorite.

In order to quantify these observations in shape and depth, we have performed modeling along 6 cross-sections cross-cutting the massif.

10.2 Gravity modeling

The gravity modeling undergoes several procedures, and shows remarkable features as follows. The boundaries of geological bodies, as well as the structure of country rocks of our model, are derived from the 1:200000 Chinese geological map. The thickness of the sedimentary layers is derived from the geological map guidebook. The densities of the main lithologies encountered in the study area were measured with the double weighting method. The density of each rock type is presented in Table 4-4. In order to take into account the effect of geological bodies around our target massif, we extended our profiles at both ends in the country rocks for several tens of kilometers.

We constructed four profiles in the NW-SE direction (Profiles A to D in Fig. 4-23), which are perpendicular to the elongation of the negative anomaly zone inside the massif, as well as to the elongation of fold belts in the country rocks. In this direction, variations of thickness of the massif and the shapes of country rock folds can be well constrained. Also, we constructed two profiles, (Profiles E and F in Fig. 4-23), in the NE-SW direction (Fig. 4-22), perpendicular to profiles A to D. These two crossing profiles are expected to strengthen the extent and geometry

of geological bodies at depth, where they cross.

One outstanding characteristic of our model is that all the four NE-SW profiles display significant thickness variations of the granitic pluton. Several "sinks" of granite reaching a thickness of about 4 km are identified in each profile. Between these "sinks", the thickness of the granite is 1 to 2 km in average (Fig. 4-23). So viewed in the scale of all gravity profiles, the proposed model has a laccolith-shaped upper part, and a lower part containing several “sinks”.

When transferring these "sinks" onto the gravity map (Fig. 4-22), it can be noticed that they align in the NE-SW direction, along the negative anomalies. Indeed, the overall shape of the massif appears to be controlled by a series of NE-SW elongated “sink zones” parallel to Profiles E and F. In these two profiles, the thickness variation of the massif is quite low.

Whether or not unique, the overall model agrees with available geological and geophysical information. It can be discussed as follows. Firstly, the residual Bouguer gravity anomaly is well reproduced by the calculated effect of the model. Secondly, the thickness of the geological bodies in all profiles is consistent at the crossings of profiles. Thirdly, the structure of country rocks provided by the geological map is consistently reproduced by the folded geometries in the model. More specifically, our model displays some variations of thickness within these folds; it is reasonable to assume that the thickness of strata can locally vary as a result of shortening during the Triassic thrusting and folding event (Schmid et al., 1999). Also, given that the density used in the modeling is an average value, the slight spatial variations of rock density may well be another reason for deviations in strata thickness in our model.

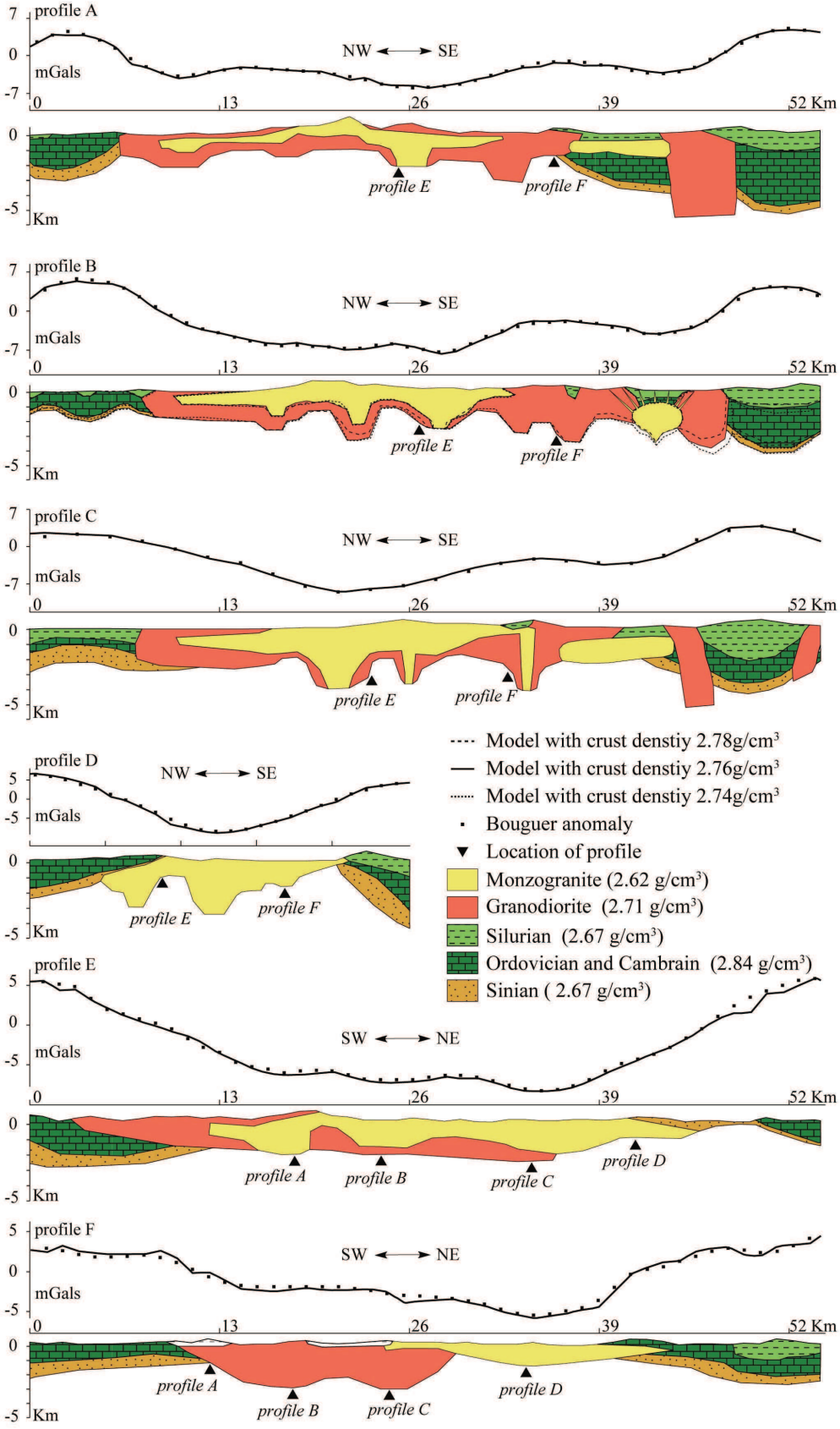

Figure 4 23. Forward gravity modeling conducted along 6 profiles across the Qingyang-Jiuhua massif (see Figs. 4-17 and 4-22 for profiles' locations).

Finally, the density of the undifferentiated upper crust beneath our model (2.76 g/cm^3) is an average value based on the Crust 2.0 model (Bassin et al., 2000). In order to evaluate the impact of errors on this density, we illustrate on Profile B in Figure 8 the effect on the model geometry with introducing ±0.02g/cm^3 density variations. The result shows that in some places, the granitic massif floor would vary about a maximum of 500m. But these variations do not significantly modify the overall shape of the model.

11 Discussion

In order to understand the mechanism and the tectonic context of the Qingyang-Jiuhua massif emplacement, the emplacement depth and the shape of the massif have been established by Al^{total} in amphibole geobarometry and 2D gravity modeling. For providing a clear view on the bearings of these methods, in this discussion we will firstly summarize the results, and then interpret them in terms of emplacement mechanism and the regional tectonic setting.

11.1 Summary of the results

The microscopic observation of the granodiorite and monzogranite thin sections indicates that the equilibrium has been reached. The An values in the plagioclase rims are within 25-35 mol %, and the magnesiohornblende and edenite nature of amphibole guarantee the validity of the geobarometric calculation. The estimated pressure does not exceed 4kbar (Fig. 4-21). The average pressure of QY18, QY24 and QY33 are 1.6±0.6 kbar, 1.4±1.3 kbar and 3.2±0.6 kbar, respectively. This result is consistent with the appearance of andalusite in the metamorphic aureole zone. The negative Bouguer residual anomaly follows the massif boundary (Fig. 4-22). A closer examination of each individual gravity profile reveals significant thickness variations along all the four NW-SE profiles, presenting several "sink" shapes in both the granodiorite of the Qingyang pluton and the monzogranite of the Jiuhua pluton, while the two NE-SW gravity profiles display gently undulating interfaces. The "sink" shapes of these two plutons overlap with each other in each individual NW-SE profile.

11.2 Implications on the emplacement mechanism of the massif

According to the deformation exerted by a granitic pluton on its country rock during its emplacement, the mechanism can be defined as forceful or permissive (Pitcher, 1979b). A permissive emplacement means that a space is created within the crust to allow the magma emplacement, and therefore the country rocks will not record a significant ductile deformation produced by the magma pressure, while the forceful one is just on the contrary. During its emplacement, the magma flow trajectory can be divided into vertical or lateral injection. For the former, one or several feeding roots exist beneath the pluton and the emplacement occurs via vertical conduits (Turrillot et al., 2011), while for the latter, single or multiple roots occur in one side of the pluton, and magma flows in other sides as shown in several examples (Aranguren et al., 2003; Talbot et al., 2004; Talbot et al., 2005a). The forceful or permissive emplacement mechanism, and the vertical or lateral magma intrusion will be discussed below for the studied massif.

11.2.1 Possible emplacement mechanism

According to our geobarometry result, both the Qingyang and the Jiuhua plutons intrude at a shallow crustal depth between 5-12 km. This is consistent with the absence of a regional ductile shear zone along the pluton boundary, and with the lack of significant ductile deformation in the country rocks (see Part I of these twin papers). Since the upper crust is relatively cold, a shallow depth magma intrusion will produce a sharp temperature contrast between the pluton and its country rocks, and thus will lead to a fast cooling of the pluton. The shallow depth calculated by Al^{total} in amphibole geobarometry is consistent with the fast cooling rate shown by amphibole and biotite ^{40}Ar-^{39}Ar dating (Chen et al., 1985). Usually at this depth, the deformation is dominated by brittle structures, which will provide fractures to be used as magma conduits, and create a space to accommodate the magma injection. This interpretation is supported by the general shape of the massif acquired by the gravity modeling, which shows high angle contacts between the two plutons and between the pluton and country rocks (Fig. 4-23). Plutons emplaced

into brittle domains at shallow depth are usually featured by a box-like shape, with a flat roof that rapidly turns-down into steep sides (Myers, 1975), having polygonal contacts with its country rock, and demonstrating detailed linear and angular edges controlled by preexisting or syn-emplacement fractures (Pitcher, 1979b). These features can be observed in the gravity model of the Qingyang-Jiuhua massif (Fig. 4-23).

The gravity modeling clearly reveals that the shape of the massif can be divided into two parts, namely, a laccolith-like upper part and the vertical “sinks” lower part (Figs. 4-23a, b, c and d). Comparing to other examples, these "sink" zones are interpreted as the root zones of the granitic massif (Talbot et al., 2005b; Turrillot et al., 2011; Yang et al., 2011). It should be noticed that the massif was emplaced into a brittle domain where fractures could be easily opened as tension gashes. These tension gashes can act as magma conduits allowing an upward magma injection during the pluton emplacement (Turrillot et al., 2011). The brittle fracturing of the upper crust will thus accommodate the space required by the magma intrusion. This dual feature in the pluton shapes can be interpreted in terms of a magma reservoir of a laccolitic upper part intruded by magma through the feeder conduits represented by the lower part roots. The overlap between the roots of the Jiuhua pluton and the roots of the Qingyang pluton indicates that the magma conduits used by the emplacement of the Qingyang pluton were still active during the emplacement of the younger Jiuhua pluton.

In this sense, a permissive emplacement mechanism seems to be the most plausible solution. This is consistent with the conclusion reached in Part I of these twin papers in which the macrostructural observations indicate that the previous fold structure of the Lower Yangtze fold belt was not modified, and almost no emplacement related deformation developed in the aureole. Moreover, the paleomagnetic study shows that the emplacement of the Jiuhua pluton did not rotate or push away its neighboring Qingyang pluton. These observations indicate that the emplacements of both plutons are permissive rather than forceful.

11.2.2 Injection trajectory

If there is a feeder root on one flank of the pluton from which the magma ascends to inject into the reservoir before flowing laterally, the maximum negative Bouguer anomaly zone will

appear in this flank of the pluton (Aranguren et al., 2003; Talbot et al., 2005a; Talbot et al., 2004). In this study, as shown in the residual Bouguer anomaly map (Fig. 4-22), the contours of the Bouguer anomaly are more or less parallel to the boundary of the massif, and the maximum negative Bouguer anomaly is located in the center of the massif rather than close to the flank of the massif. This suggests that the model of feeding on one flank before flowing laterally does not hold for the Qingyang-Jiuhua massif.

More details of the shape of the massif are shown in the gravity modeling profiles (Fig. 4-23). In each NW-directed profile, the top of the massif is flat or gently inclined, and on both sides, the walls are vertical or sub vertical. Several vertical roots are uniformly distributed with more or less the same spacing along the NW-directed profile. This means that the upwelling of the magma occurred vertically or sub-vertically throughout the conduits that were regularly distributed beneath the massif.

This argument is also supported by the AMS foliation pattern shown in Part I (Wei et al., 2013 this volume). The AMS foliation can be divided into two families. In the center of the massif, the majority of the AMS foliation is weakly inclined, while highly inclined ones dominate along the massif boundaries where they are oriented parallel to the boundaries (Fig. 4-11a in Part I of these twin papers). This AMS foliation pattern was assumed to be acquired due to the vertical and sub vertical injection and the stopping of the magma by the country rocks on the roof as well as asides. However, this assumption outlined by the AMS pattern requires very limited erosion of the massif and thus the AMS sites are very near to the massif roof. This condition is supported by the gravity modeling. There exists a NE-directed narrow stripe of country rocks in the southeast part of the Qingyang-Jiuhua massif, which is crossed by the gravity profile F (Fig. 4-17). Considering its narrow shape, the lithology, and U-Pb zircon age of the around igneous rocks on both sides (Wu et al., 2012), this stripe is interpreted as a septum in Part I of these twin paper. Our gravity modeling indicates that the thickness of this country rock stripe is just of a few hundred meters, and there exists a thick granodioritic “sink” that connects the outcroping granodiorite on both sides of the country rock stripe. Gravimetry modeling supports the view that this NE-SW striking narrow country rock stripe is really a septum within the same pluton, suggesting that erosion of the massif was very limited. Thus, the AMS sites are very close to the massif roof, which guarantees the validity of the interpretation of the AMS

pattern.

11.2.3 Overview of the emplacement process

Based on the discussion of the massif emplacement mechanism above, a three stage emplacement model is proposed. During the first stage, around 142Ma (Wu et al., 2012), the lower crust was partially melted, and a granodioritic magma was generated. At shallow depth, the crust of the Lower Yangtze fold belt was faulted to create tension gashes. Several conduits of magma connected the magma source area to the reservoir. The granodiorite magma was injected into the tension gashes before being crystallized to form the Qingyang pluton. During this process, the rising magma did not exerted any obvious pressure on the country rocks.

In the second stage, at about 130Ma (Wu et al., 2012), due to the regional tectonics, the formerly used magma conduits were reopened, and possibly new ones were formed in the upper brittle crust. At this time, the monzogranitic magmas were injected into the opening room, and crystallized to form the Jiuhua pluton.

During the third stage, the microgranite magma intruded the massif as evidenced by several parallel dykes found in the massif.

11.3 Pluton emplacement and regional tectonics

The pluton roots defined along the individual gravity profiles can be correlated one with each other, and thus reveal four nearly parallel, NE-SW striking, feeder zones (Figs. 4-22 and 24). Furthermore, along the two NE-SW directed profiles, the thickness of the massif is more constant than along the NW-SE directed profiles, indicating that the roots identified along the NW-SE directed profiles keep the same thickness along the NE-SW direction. The overlapping between the root zones related to the Qingyang and the Jiuhua plutons suggests that the NW-SE maximum stretching direction, lasted more than 10 Ma during the emplacement of the two plutons.

To the south of the Qingyang-Jiuhua massif, in the Jiangnan orogenic belt (Fig. 4-16), a Cretaceous NE-SW striking normal fault system, which is contemporary with the emplacement

of the Qingyang-Jiuhua massif developed (Yu et al., 2007). It is thus reasonable to interpret the NE-SW root zones of the Qingyang-Jiuhua massif as a result of the same tectonic pattern.

Accordingly, the NE-SW tension gashes of the Qingyang and the Jiuhua plutons may indicate that the Lower Yangtze area experienced a NW-SE extensional tectonic regime during the plutons emplacement. The map shape of the Qingyang-Jiuhua massif may also provide insights into this NW-SE extension. For instance, the monzogranite of the Jiuhua massif is rectangle-shaped with a NEE-SWW long side. Also, the NE-SW granodiorite "tail" in the southwestern part of the Qingyang pluton coincides with the location of a tension gash shown in our gravity modeling (Fig. 4-24). In this context, it is reasonable to interpret this part of the Qingyang pluton as a tension gash.

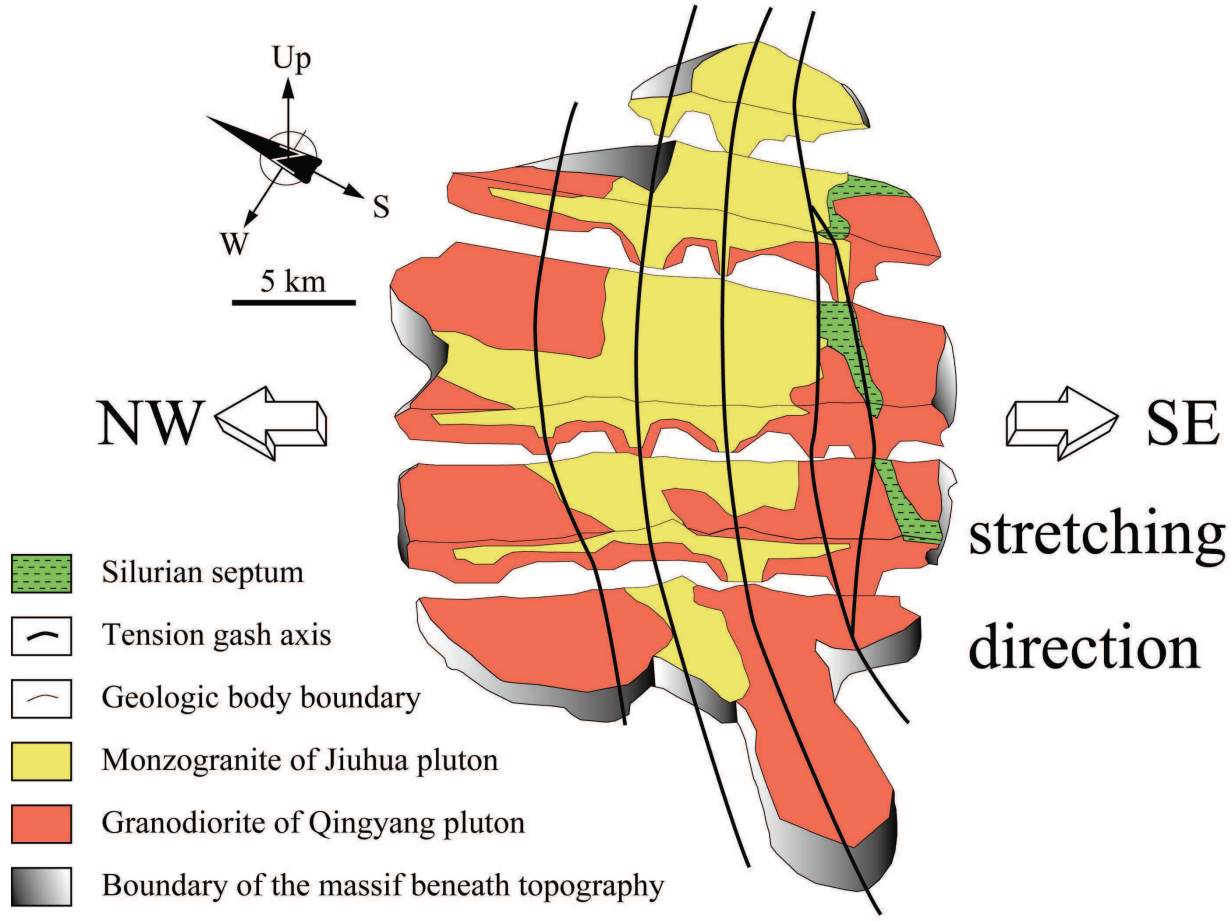

Figure 4 24: 3D Shape of the Qingyang-Jiuhua massif.

Conversely to the cases of metamorphic core complexes and syn-kinematic plutons bounded by low-angle ductile shear zones (i.e. detachment faults) that accommodate a large crustal

deformation, the amount of extension related to the emplacement of the Qingyang-Jiuhua massif was probably weak, because no significant emplacement-related deformation has been observed. Therefore, the quantity of the extension is probably just equal to the width of the tension gashes.

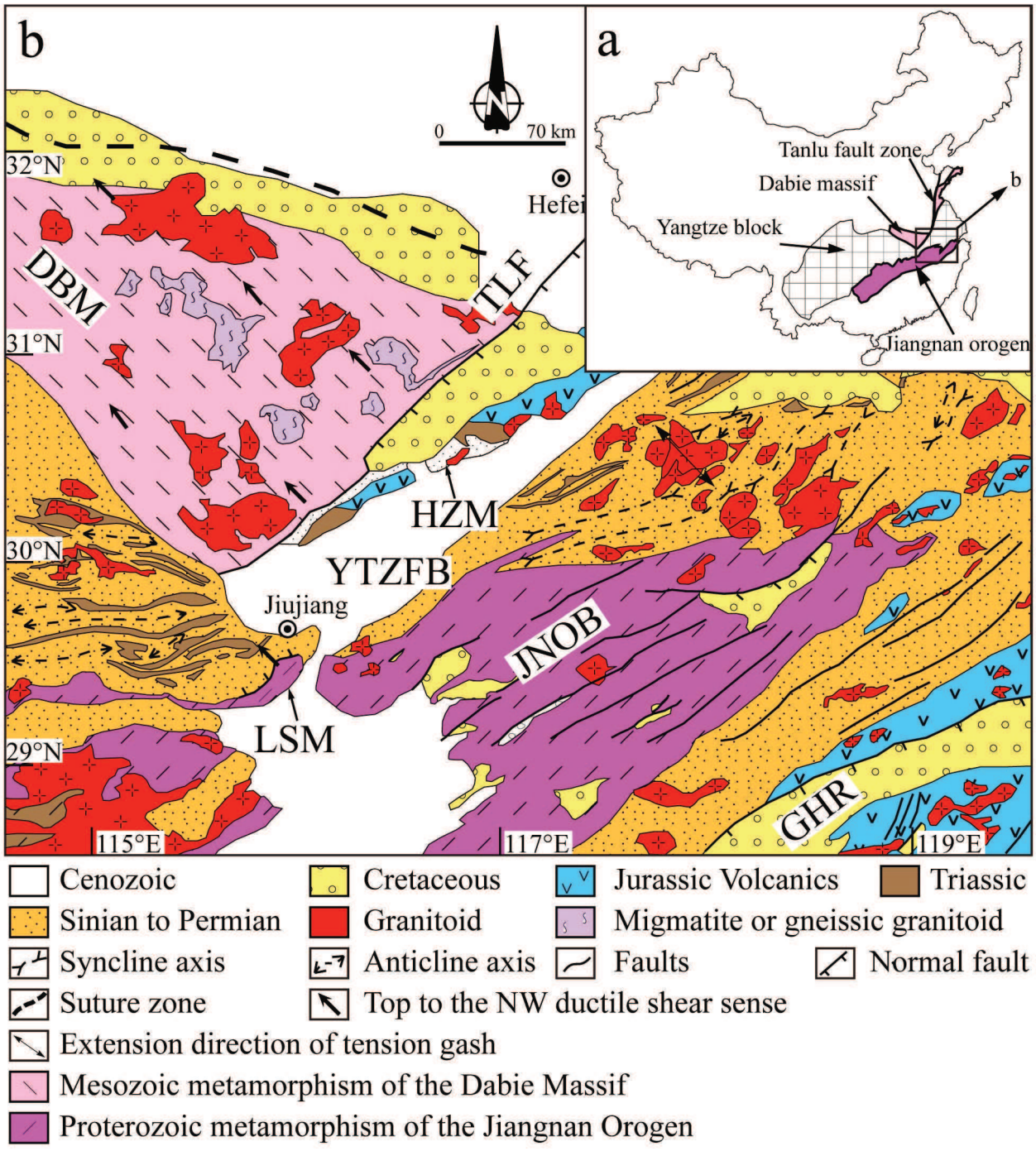

Figure 4 25. Cretaceous tectonic fabrics of adjacent areas of the Qingyang-Jiuhua massif.

TLF: the Tanlu fault, YTZFB: the Lower Yangtze fold belt, JNOB: the Jiangnan orogenic belt, GHR: the Ganhang rift basin, DBM: the Dabie massif, LSM: the Lushan massif, HZM: the Hongzhen massif.

Nevertheless, this NW-SE extension has been also recorded in the adjacent areas (Fig. 4-25). For example, in the Dabie massif, which is located to the northwest of the Qingyang-Jiuhua massif (Fig. 4-25), a pervasively distributed NW-SE lineation with a top- to-the-north shearing develops inside the North Dabie domain, the Central Dabie migmatite dome and the South Dabie domain (Fig. 4-25). These NW-SE lineations are interpreted to be formed in an extensional context during or soon after the exhumation of the Central Dabie migmatite dome (Faure et al., 2003). Recently, geochronological work has shown that the Central Dabie migmatite dome was formed in two episodes at ca. 137 Ma and ca. 124 Ma (Wu et al., 2007). The former age is coeval with the emplacement of the Qingyang-Jiuhua massif. Along the eastern boundary of the Dabie massif, the Tanlu Fault (Fig. 4-25) also acted as a normal fault with a NW-SE stretching direction at ca. 135-130Ma (Mercier et al., 2007). The Lushan massif, which is located to the southwest of the Qingyang-Jiuhua massif (Fig. 4-25), recorded four stages of deformation (Lin et al., 2000). Among these tectonic events, D1 which developed a NW-SE lineation with top-to-the-NW motion is interpreted to be a normal detachment ductile shear zone (Lin et al., 2000) and dated at about 140 Ma by ^{40}Ar-^{39}Ar dating on muscovite (Zhu et al., 2010c), coeval with the emplacement of the Qingyang-Jiuhua massif as well. A NW-SE regional extensional tectonic regime seems to characterize this part of the SCB during the Early Cretaceous.

12 Conclusions

The present study allows us to draw the following conclusions.

(1) According to the results of the Al^{total} in amphibole geobarometry, the box-like shape of the massif and the absence of the regional ductile deformation in country rocks, the Qingyang-Jiuhua massif was emplaced at shallow depth.

(2) The gravity modeling indicates that the massif has a laccolith-shaped upper part and a lower part that contains several vertical "sink" zones. The shape of these “sink” zones can be interpreted as the roots of the massif, which acted as feeder zones. During the magma injection, the upper crust was cracked (or normally faulted), causing the opening of NE-SW tension gashes

by the regional extension. These tension gashes provided magma conduits leading the magma to be injected upwards into the laccolith-shaped reservoir.

(3) The Qingyang-Jiuhua massif, which intruded the Lower Yangtze fold belt at ca. 142Ma and ca. 131Ma, was emplaced by a permissive mechanism with vertical to sub-vertical injection.

(4) The NE-SW striking tension gashes indicate that the Lower Yangtze area experienced a NW-SE extension, which accommodated the emplacement of the Qingyang-Jiuhua massif. This deformation was coeval with the Cretaceous extensional tectonics in the SCB. However, the NW-SE extensional stretching was rather weak, as ductile deformation in the plutons, and the country rock is rare. In spite of direct strain measurement, it can be assumed that the extension amount was equal to the width of tension gashes.

Acknowledgements

The first author benefited a scholarship from the Sino-Euro Joint Doctoral Promotion Program (DPP) of Chinese Academy of Sciences for his Ph.D. stay in ISTO (France). This study was funded by Chinese National 973 Project (2009CB825008), NSFC (41225009), the Innovative Project of the Chinese Academy of Sciences (Grant No. KZCX1-YW-15-1), the Major National Science and Technology Project (No. 2011ZX05008-001), and Ministry of Land and Resources (201211024-04).

Chapter 5 The emplacement of the Hengshan Granitic Massif and its tectonic bearings

The Hengshan granitic complex which is composed of a biotite pluton on the east and a two-mica pluton on the west, namely, the Nanyuan pluton and the Baishifeng pluton, respectively was ductile deformed by the Xiushui-Yongzhou long-distance fault on its west boundary. This chapter is aimed to present our systematic study which contains field structural observation, micro scope observation, magnetic fabric measurement and Monazite U-Th-Pb dating. In this chapter, we will discuss the emplacement mechanism of the Hengshan granitic complex, the contemporary regional tectonic regime and the relationship between emplacement of Baishifeng pluton and ductile fault on the west rim of the Hengshan granitic complex.

1 Introduction

The South China Block (SCB) in the Late Mesozoic is featured by opening of large amount of graben basins and semi-graben basins, the emplacement of huge volume of plutons, ore forming process, the eruption of bimodal volcanites, widly distributed dyke swarms and normal fault system (Gilder et al., 1991; Goodell et al., 1991; Zhou et al., 2006; Li et al., 2010; Mao et al., 2011). The emplacement of the plutons during this period showed a coastal ward migration polarity (Li and Li, 2007; Zhou and Li, 2000). Based on the results of different methodologies, scholars held different viewpoints on the tectonic regime of SCB in the Late Mesozoic period. Among them, some emphasized an extension regime as a major regime, well at the same time (Gilder et al., 1991; Faure et al., 1996; Faure et al., 2003; Zhou et al., 2006; Shu et al., 2009), the others emphasized a strike-slip regime as a major regime (Xu et al., 1987; Gilder et al., 1996; Li et al., 2001).

It is worthwhile to note that around 145 Ma, the magmatism in SCB was in quiescence (Li et al., 2010b). In this period, most plutons were emplaced in the Lower Yangtze River basin area. As our study in the Lower Yangtze River basin area indicates, within 140 Ma and 130 Ma, this area was under the control of NW-SE weak extension regime. Can this weak extension regime

represent a global tectonic regime of the whole SCB in this magmatism quiescence? In order to answer this question, it is better to investigate the tectonic features in other areas during this period and then compare or correlate them within these areas. The Baishifeng pluton which is the west part of the Hengshan granitic massif was emplaced at ca. 150. This emplacement age is also in the period of the magmatism quiescence, thus, it would be interesting to study the emplacement mechanism of the Baishifeng pluton with its tectonic regime (Fig. 5-1a). The previous studies mainly concentrated on the West Boundary Ductile Fault of the Hengshan granitic massif (WBDF). Based on the structural observations and chemical measurements, it was proposed that the Hengshan granitic massif was a metamorphic core complex or on situ re-melting migmatite. It was also considered that the emplacement of the Baishifeng pluton (west part of the Hengshan granitic massif) was under a regional extension regime. In recent years, as the precise U-Pb zircon dating indicates, the emplacement of the Baishifeng pluton was ca. 150 Ma which is earlier than the development of the WBDF (Li et al., 2013a) , thus the extensional WBDF can not account for the regional tectonic regime during the emplacement of the Baishifeng pluton. It is worthwhile to note the consideration of that developed a strike-slip fault system in the adjacent area of the Hengshan granitic massif (Li et al., 2001). This strike-slip fault system is regarded as a southwest counterpart of the Tancheng-Lujiang strike-slip fault system (Li et al., 2001).

In order to figure out the emplacement mechanism, the regional tectonic regime during the emplacement of the Baishifeng pluton and establish a correlation in larger areas, we have conducted multidisciplinary studies including field structural observations, microscopic observations, anisotropy magnetic susceptibility measurement, monazite U-Th-Pb microprobe dating. Our study is aimed to acquire the answers to several questions as follows:

(1) What is the emplacement mechanism of the Baishifeng pluton?

(2) What is the regional tectonic setting during the emplacement of the Baishifeng pluton?

(3) What is the relationship between the emplacement of the Baishifeng pluton and the development of the WBDF?

2 Geologic settings

2.1 The Hengshan granitic massif

The diamond-shaped Hengshan granitic massif is composed of the Nanyue biotite granitic pluton on the east and the Baishifeng two-mica granitic pluton on the west (Fig. 5-1b). There developed the gneissic granite and the augen gneissic granite in the west part of the Baishifeng pluton. The augen gneissic granite was used to be considered as a result of re-melting of crustal material in situ (Wang, 1990a; Wang, 1990b). The Baishifeng pluton was dated to be 149 Ma by means of U-Th-Pb chemical content in Monazite method (Zhang, 1994). In recent years, the Nanyue pluton and the Baishifeng pluton were dated by means of U-Pb isotropic content in zircon. The result shows that the Nanyue pluton was emplaced between 232-228Ma and the Baishifeng pluton was emplaced at ca. 150 Ma (Li et al., 2013a). Both of the Nanyue pluton and the Baishifeng pluton are rich in LREE and reduced in HREE (Wang, 1990b).

2.2 The West Boundary Ductile Fault of the Henghsan Granitic Massif

The west part of the Baishifeng pluton contacts the red sediment strata of the Zhajiang basin by a normal fault. This fault is a part of the Xiushui-Yongzhou crustal-scale deep fault (Zhang, 1994). In this study, this 500km long fault is called the West Boundary Ductile Fault of the Hengshan granitic massif (WBDF). Influenced by this fault, the west part of the Baishifeng pluton developed pervasive ductile deformation. Inside the deformed rocks, the strike of the foliation and are NNE-SSW and dip to WNW, the dip of the lineation are WNW, as indicated by several previous studies (Zhang and Zhu, 1989; Xu et al., 1998).The measurement of anisotropy of magnetic susceptibility (AMS) on oriented samples acquired in the deformed rocks indicates that the magnetic fabrics are parallel to the deformed fabrics (Zhang and Zhu, 1989). Based on several strain indicators in augen gneissic two-mica garnite such as boudinated quartz vein, the angle of the S-C fabrics and the axial ratio of the long porphyroid, the calculated strain quantity argues a 10 km displacement at least (Xu et al., 1998). Owing to the deformation of the WBDF is featured by dip-slip and the absence of the pressure effects of the emplacement of the Hengshan granitic massif on the country rocks, Zhang argued that the emplacement mechanism of the

Hengshan granitic massif was mainly passive (Zhang, 1992). In recent years, a system U-Pb isotropic dating on Zircons, ^{40}Ar-^{39}Ar isotropic dating on micas and c-axis statistics on Quartz have been conducted on the WBDF in order to get an overview of the development of the WBDF. The results show that the temperature of the deformation was between 400°-550°, the deformation was featured by quartz basal<a>，prism<a> axis glide, and the development of the WBDF was between 136-97 Ma (Li et al., 2013a).

2.3 The Zhajiang basin

The Zhajiang basin is a part of a lager basin called the Changsha-Hengyang basin (Wang, 1990a). This basin is filled with river and lacustrine face sediment from which many fossils have been discovered such as eggs and footprints of dinosaus, stonewort and sporopollen which indicate a Cretaceous age. The oldest sediment is the Lower Cretaceous Dongjing Formation which unconformably overlies on the underlain older sediment sequences.

3 Field observation and structural geometry

3.1 The Nanyue Biotite Granitic Pluton

In the field observation, the biotite granite of the Nanyue pluton is massive. The feldspar is grey, idiomorphic, gros and oriented. It can reach a length of 2-3 cm in long axis direction. When the magmatic foliation appears, the orientation of the feldspar can be seen along the NW-SE direction. For example, in the location 1 in Fig. 5-1b, the orientation of the feldspar is N145E. A large number of two-mica dykes with N85E strike are discovered in the same outcrop. Apparently the orientation of the feldspar in biotite granite and the two-mica dykes are perpendicular with each other (Fig. 5-2a).

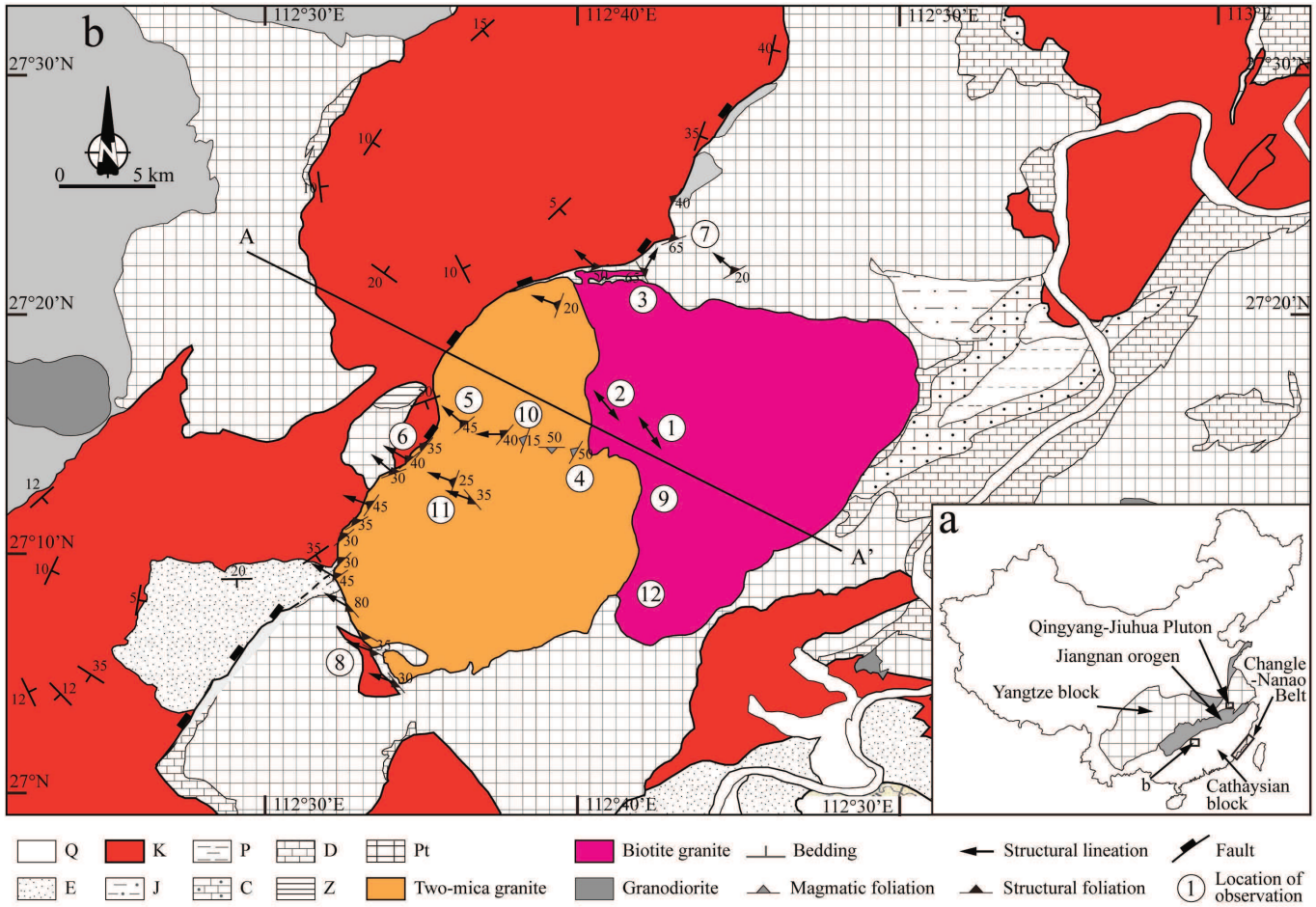

Figure 5 1: Geologic sketch map of Hengshan Massif and its adjacent area

a: Simplified tectonic map of SCB and the loacation of the Hengshan granitic massif, b: Simplified geologic map of the Hengshan granitic massif (The Nanyue Biotite Granitic Pluton and the Baishifeng Two-Mica Granitic Pluton）and its adjacent area.Q: Quaternary, E: Tertiary, K: Cretaceous， J: Jurassic，P: Permian，C: Caboniferous，D: Devonian, Z: Sinian, Pt: Proterozoic.

On the boundary between the Nanyue pluton and the Baishifeng pluton (Location 2 in Fig. 5-1b), biotite granite is featured by deformation of quartz and the orientation of feldspar which along the N140E direction. On the north boundary of the Nanyue pluton (Location 3 in Fig. 5-1b), bioitite granite was deformed to gneissic granite whose foliation is N150E, NE65. A lineation of N30E, NE25 developed on the foliation. The foliation is parallel to the strike of the boundary and the foliation is perpendicular to the strike of the boundary. Along the NE-SW section on this observation site of the boundary, a quartz dyke can be observed to deformed into "sigmoid" shape indicating a top-to-the-NE shear sense.

3.2 The Baishifeng two-mica granitic pluton

The east part of the Baishifeng two-mica granitic pluton is massive with euhedral feldspar and micas. A mount of micas are oriented to form magmatic foliation. In many outcrops, the biotite concentrates and is oriented to form schlieren. Both of the magmatic foliation and schlieren are striked NE-SW and dip to NW (Location 4 in Fig.5-1b and Fig. 5-2b). In the west part of the Baishifeng two-mica granitic pluton, the WBDF shows its influence and the granite was deformed to gneissic granite. The gneissic foliation is formed by stretched quartz, oriented feldspar and micas. The strike of the gneissic foliation is predominant by NE-SW, and dip to NW. A NW-SW stretched mineral lineation developed on the gneissic foliation. On the section which is parallel to the lineation and perpendicular to the foliation, the quartz is observed to be "sigmoid" shape with tails owing to the shearing. This indicates a top-to-the-NW shear sense (Location 5 in Fig. 5-1b and Fig. 5-2c). Inside the two-mica gneissic granite some micaschist xenoliths were discovered. The foliation of these xenoliths is striked NE-SW and dip to NW while the lineation dips to NW.

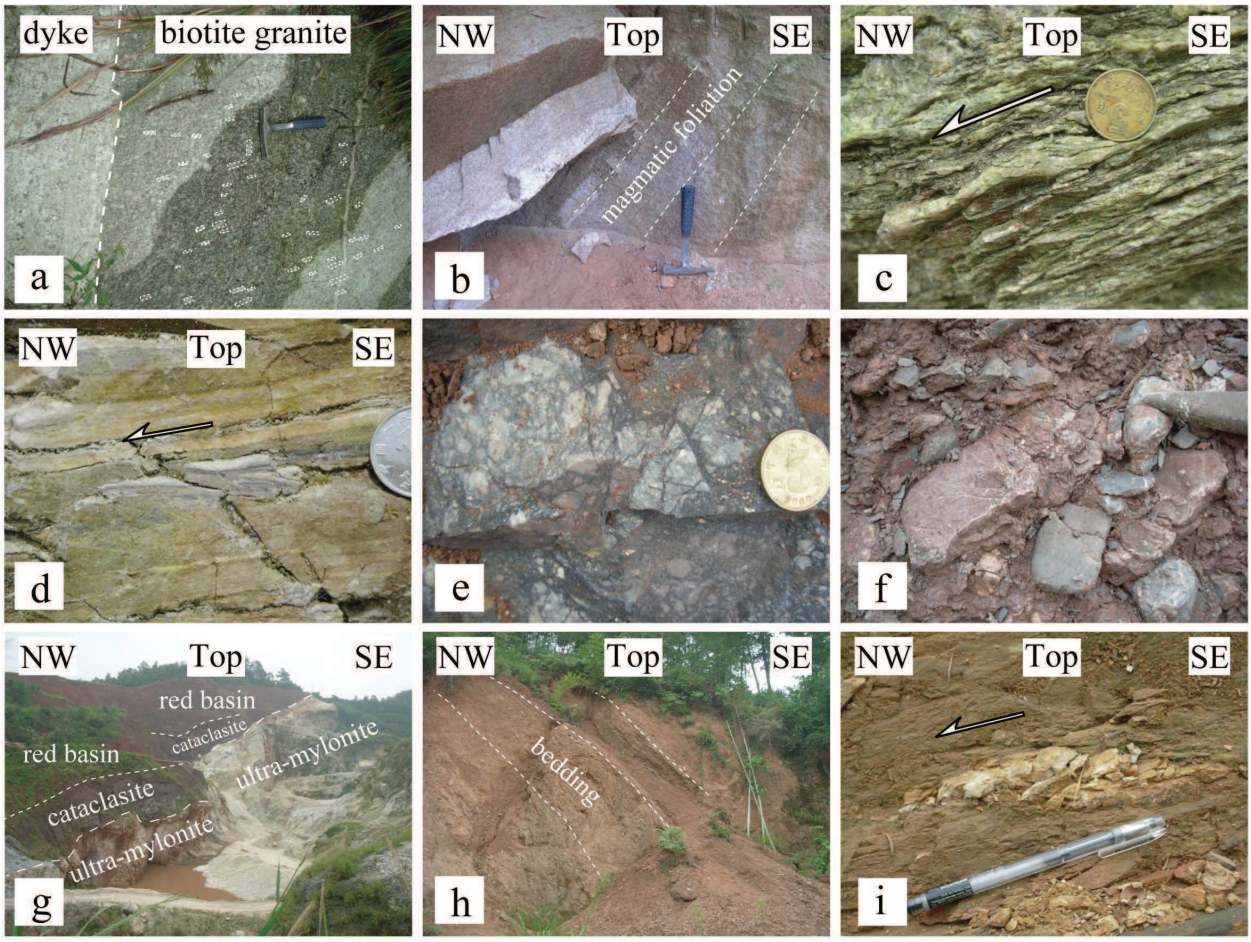

Figure 5 2: The macro structure of the Hengshan granitic massif (the Nanyue biotite granitic pluton and the Baishifeng two-mica granitic pluton) and its country rocks

a: The feldspar crystals of the Nanyue biotite granitic pluton are oriented (Location 1 in Fig. 5-1b), b: The east part of the Baishifeng two-mica granitic pluton is featured by well constrained magmatic foliation without deformation(Location 4 in Fig. 5-1b), (c) The west part of the Baishifeng two-mica granitic pluton was deformed to be gneissic granite, "sigmoid" shaped quartz indicates top-to-the-NW shear sense (Location 5 in Fig. 5-1b) , (d) The ultra-mylonite developed on the boundary between the Baishifeng two-mica granitic pluton and its country rocks, the over turned fold indicates a top-to-the-NW shear sense (Location 6 in Fig. 5-1b), (e) The ultra-mylonite of the west part of the Baishifeng two-mica granitic pluton was re-cracked into cataclasite (Location 6 in Fig. 5-1b), (f) The country rocks of the Baishifeng two-mica granitic pluton are red sediments, the pebbles of these red sediments were cracked where near the boundary of the Baishifeng two-mica granitic pluton (Location 6 in Fig. 5-1b), (g) On the boundary of the Baishifeng two-mica granitic pluton and its country rocks, there

developed untra-mylonite of gneissic two-mica granite, cataclasite, cracked red pebbles, from SE to NW, respectively (Location 6 in Fig. 5-1b), (h) The strata of the country rocks near the boundary of the Baishifeng two-mica granitic pluton dip to the SE， which indicates that the WBDF is a ductile normal fault, (i) The WBDF extends in to the Neoproterozoic and leads the quartz vein deformed to be a "sigmoid" shape indicating a top-to-the-NW shear sense (Location 7 in Fig. 5-1b).

3.3 The West Boundary Ductile Fault of the Hengshan Granitic Massif and the Zhanjiang Basin

Near the WBDF, both the Baishifeng two-mica granitic pluton and its country rock were influenced by the activity of the fault. On the pluton's side, there developed ultra-mylonite, cataclasite from the east to west. The mylonitic granite is featured by several feldspar relicts scattered in the matrix of diminish of the minerals. Quartz was stretched to be ribbon shape which forms mylonitic foliation whose strike is NE-SW and dip to NW (Location 6 in Fig. 5-1b and Fig. 5-2d). Owing to the continuing shearing, the mylonitic foliation was bended and formed oblique fold. The axis surface of this kind of fold dip to SE indicating top-to-the-NW shear sense (Location 6 in Fig. 5-1b and Fig. 5-2d). In the westward direction, the mylonitic foliation was cracked into breccia indicating a later brittle deformation imposed on the ductile deformation. The breccia is made up of cracked ultra-mylonite or white quartz veins. Usually the diameter of the breccia is ca. 3 cm (Location 6 in Fig5-1b and Fig. 5-2e). Specially, in some outcrops, the diameter of the breccia can attain several tens of centimeters. Above the cataclasite there overlay the red coarse clastic sediment of the Zhajiang basin, usually conglomerate. The breccia of the conglomerate which nears the fault usually cracks brittlely . The cracks are observed penetrates the breccia and the matrix (Fig. 5-2f). The juxtaposition of the ultra-mylonite, the cataclasite and the cracked conglomerate illustrates the activity of the WBDF vividly (Fig. 5-2g). In the Zhajiang basin, where the red strata is near to the WBDF, the strike is NE-SW and dip to SE (Fig.5-1b and Fig. 5-2h). This indicates that the opening of the Zhangjiang basin was strongly influenced by the activity of the WBDF. Considering that the shape of the Zhangjiang basin is NE-SW elongated rectangular along the WBDF, the WBDF is the major boundary fault of the

Zhajiang basin.

The WBDF is along but not limited to the boundary between the Baishifeng two-mica granitic pluton and the Zhanjiang basin. In the northwest corner of the Baishifeng two-mica granitic pluton, the WBDF extend northeast to the Neoproterozoic country rocks and cut two small plutons. The WBDF also separates the Neoproterozoic and the Cretaceous Zhanjiang basin by fault contact (Fig. 5-1b). On the outcrop scale, the WBDF made the Neoproterozoic sediment sequence to develop cleavage whose strike is NE-SW and dip to NW. Though no lineation has been discovered here, along the NW-SE section, quartz veins are observed "sigmoid" shape owing to the deformation, which indicates a top-to-the-NW shear sense (Location 7 in Fig. 5-1b and Fig. 5-2i). In the southwest corner of the Baishifeng two-mica granitic pluton, the WBDF was divided into two braches. One continues to extend southwest to the Neoproterozoic country rocks, the other diverted to southeast and along the boundary of the pluton (Fig. 5-1b). The former is vague due to the coverage of the Later Tertiary sediment. The latter shows a clear ductile deformation style with a NE-SW striking, dip to SW foliation and a NE-SW lineation. The foliation of this branch is parallel to the strike of the boundary of the pluton while the lineation is still parallel to the lineation elsewhere of the WBDF (Location 8 in Fig. 5-1b).

The shape of the Zhajiang basin is featured by narrow width and NE-SW elongation. In the east part of the basin which is near to the WBDF, the strike of the strata are NE-SW and dip to SE, the dip angle is between 30°and 50°. Inside the basin, the strikes and dips of the strata are variable, but the dip angles vary gently, usually within 20°. This phenomenon shows that the geometry of the basin was controlled by the WBDF. In the west part of the basin, the Cretaceous red strata overlies unconformably on the previous granite and sedimentary strata from the Neoproterozoic and the Jurassic. The strikes of the Cretaceous strata are NE-SW, the dip angle is very gentle, usually within 15°.

4 The magnetic fabrics of the Hengshan granitic massif

4.1 Sampling and measurements

In order to acquire the magnetic fabric information of the Hengshan garnitic massif and its

regional tectonic bearings during the emplacement, we used gasoline driller to conduct systematic sampling on the Nanyue biotite granitic pluton and the Baishifeng two-mica granitic pluton in 33 sampling sites (Table 5-1). In each pluton, the neighboring sites are at least 2 km away from each other. In individual site, 5 or 6 cores with 2.5 cm in diameter have been acquired. The cores are at least 2 m away from each other. Magnetic compass was used to measure the orientation of the cores. When the weather is qualified, sun compass was used to do the magnetic field correction. In the laboratory, each core is cut to be standard samples with 2.2 cm in height. In total, 282 standard samples are measured (Table 5-1).

In "Laboratoire de Magnétisme des Roches d'Orléans", KLY3 has been used to measured the anisotropy magnetic susceptibility and the bulk susceptibility. ANISOFT (offered by AGICO) has been used to conduct Jelinek statistics (Jelinek, 1981) and to calculate the orientation of the three axe (K_1 is the biggest magnetic axis and represents magnetic lineation, K_2 is middle magnetic axis, K_3 is the smallest magnetic axis and represents the pole of the magnetic foliation), shape parameter "T" and the anisotropy degree "P_J" of the AMS ellipsoid. More over, the hysterosis loops of the biotite granite and the two-mica granite have been measured in "the Paleomagnetic laboratory of Institut de Physique du Globe de Paris".

4.2 The magnetic carriers determination

As the result of the measurement shows, the biotite granite and the two-mica granite have low bulk susceptibilities. The value of the biotite granite is between 60 and 200×10^{-6} while that of the two-mica granite ranges from 10 to 80×10^{-6}, some samples'values can reach 160×10^{-6} (Fig. 5-3 and Table 1). Generally speaking, the bulk susceptibility of the biotite granite is higher than that of the two-mica granite.

Regardless of the lithology, the hysterosis loops of the biotite granite and the two-mica granite are both linear shaped. The magnetic motions are in proportion to the exerted magnetic field (Fig. 5-4). This phenomenon indicates that the main magnetism carrier mineral is predominant by paramagnetic minerals, for example, the biotite. The reason of the higher susceptibility of the biotite granite than that of the two-mica granite is that the biotite content is larger in the former than in the latter, as illustrated in the outcrop observation, the color of the biotite granite is darker than that of the two-mica granite.

Table 5 1 The result of AMS measurement of the Hengshan granitic massif in Hunan province

site	Coordinates		Lith	N	Km	P_J	T	K_1				K_3			
	Long (°E)	Lat (°N)			(10^{-6}SI)			Dec (º)	Inc (º)	a_{95max} (º)	a_{95min} (º)	Dec (º)	Inc (º)	a_{95max} (º)	a_{95min} (º)
HY01	27.25	112.72	BG	9	144.0	1.034	-0.161	317.2	14.5	16.6	3.7	216.5	35.6	37.7	3.4
HY02	27.24	112.71	BG	11	143.0	1.036	-0.294	314.7	11.9	13.0	8.4	77.3	68.7	61.6	10.3
HY03	27.25	112.69	TMG	7	48.9	1.037	-0.188	70.5	27.8	16.5	5.3	267.5	61.1	18.2	5.7
HY04	27.26	112.69	TMG	8	60.4	1.066	0.147	299.2	16.7	31.4	3.8	184.2	54.6	11.8	7.8
HY05	27.26	112.68	TMG	8	62.7	1.05	-0.049	53.9	31.8	7.1	4.7	298.2	35.0	15.2	3.5
HY06	27.26	112.65	TMG	11	45.3	1.082	0.456	95.8	33.8	15.5	5.6	264.5	55.7	15.4	5.2
HY07	27.27	112.63	TMG	4	47.4	3.745	0.232	-	-	-	-	-	-	-	-
HY08	27.27	112.61	TMG	7	178.0	1.304	0.198	263.7	33.7	17.3	4.3	73.1	55.8	16.0	10.7
HY09	27.28	112.60	TMG	8	34.9	1.137	0.489	264.8	7.7	31.4	6.8	167.2	44.3	18.3	6.3
HY10	27.32	112.75	BG	8	84.1	1.021	0.163	338.0	1.7	31.2	14.0	243.3	70.4	19.7	13.5
HY11	27.28	112.61	TMG	8	11.3	1.204	0.036	248.6	40.3	5.9	5.1	106.2	43.0	11.7	4.9
HY12	27.29	112.69	BG	9	119.0	1.09	0.395	138.1	9.9	8.1	2.5	272.6	76.0	8.1	4.0
HY13	27.28	112.70	BG	6	106.0	1.073	-0.009	137.0	17.7	8.6	1.3	282.9	69.0	10.6	2.1
HY14	27.27	112.72	BG	7	110.0	1.042	-0.156	133.6	6.6	6.6	0.9	265.4	80.1	12.8	3.9
HY15	27.26	112.72	BG	5	105.0	1.046	0.040	123.1	4.2	8.6	4.9	23.0	67.5	10.5	7.1
HY16	27.28	112.69	BG	6	149.0	1.088	0.077	137.1	24.8	3.7	2.7	277.2	58.9	5.9	3.6
HY17	27.27	112.68	BG	9	135.0	1.103	0.222	144.6	25.0	4.5	3.3	289.9	60.5	5.5	3.9
HY18	27.28	112.68	BG	6	190.0	1.13	0.491	137.8	17.2	7.4	2.3	275.6	67.4	7.1	2.9
HY19	27.26	112.68	TMG	9	63.0	1.072	0.375	300.7	33.9	8.5	4.6	182.0	35.5	10.5	2.5
HY20	27.25	112.67	TMG	9	71.2	1.11	0.638	7.4	44.4	40.9	8.2	157.8	41.6	20.1	7.9
HY21	27.24	112.66	TMG	10	43.8	1.103	0.900	149.3	11.9	70.0	3.3	352.9	77.1	5.7	3.9
HY22	27.24	112.64	TMG	8	54.0	1.212	0.852	140.0	7.3	14.7	1.8	31.9	67.7	3.8	2.0
HY23	27.24	112.63	TMG	10	32.1	1.104	0.573	24.3	45.0	13.3	6.0	230.3	41.9	9.8	6.5
HY24	27.24	112.63	TMG	9	43.2	1.096	-0.399	111.6	15.5	24.4	5.3	253.0	70.5	20.9	15.1
HY25	27.24	112.61	TMG	9	51.3	1.066	-0.118	259.4	23.4	15.8	9.3	35.7	59.0	19.2	10.5
HY26	27.26	112.66	TMG	9	61.6	1.088	0.413	289.0	45.8	6.1	2.9	146.2	37.8	20.6	2.9
HY27	27.27	112.64	TMG	14	66.1	1.055	-0.104	267.5	31.2	9.1	7.2	125.3	52.6	9.0	7.3
HY28	27.19	112.67	TMG	12	164.0	1.035	-0.355	153.8	39.4	9.8	6.3	18.3	41.0	23.2	6.2
HY29	27.19	112.70	BG	9	188.0	1.047	-0.004	175.8	42.7	7.5	2.4	314.6	39.3	7.6	3.6

HY30	27.19	112.70	BG	12	70.9	1.088	0.715	194.4	21.6	10.0	3.4	304.4	40.9	3.6	3.1
HY31	27.20	112.67	TMG	8	13.9	1.048	0.603	195.9	4.3	33.2	5.4	290.0	44.0	10.7	4.7
HY32	27.20	112.66	TMG	9	50.0	1.03	0.140	62.1	13.4	46.8	14.6	169.6	51.7	30.3	24.0
HY33	27.21	112.70	BG	8	178.0	1.033	-0.077	164.6	22.3	13.8	6.3	350	67.6	18.7	3.9

Site: sampling site, Lat: Latitude, long: Longitude, Lith: Lithology, Km: average susceptibility, P_J: Susceptibility anisotropy degree, T: The shape parameter of the AMS ellipsoid, K_1: Magnetic lineation, K_3:The pole of the magnetic foliation, Inc: Inclination, Dec: Declination, α_{95}max and α_{95}min: The long and short axis of the confidence ellipsoid at 95% level, BG: Biotite granite, TMG: Two-mica granite.

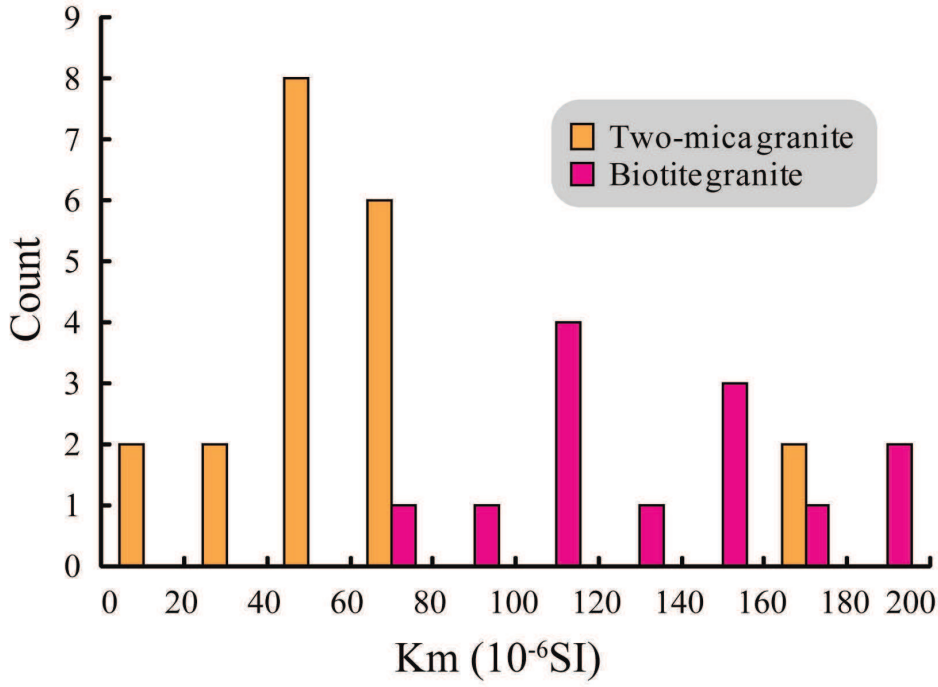

Figure 5 3: The susceptibilities distribution of the samples from the Nanyue biotite granitic pluton and the Baishifeng two-mica granitic pluton

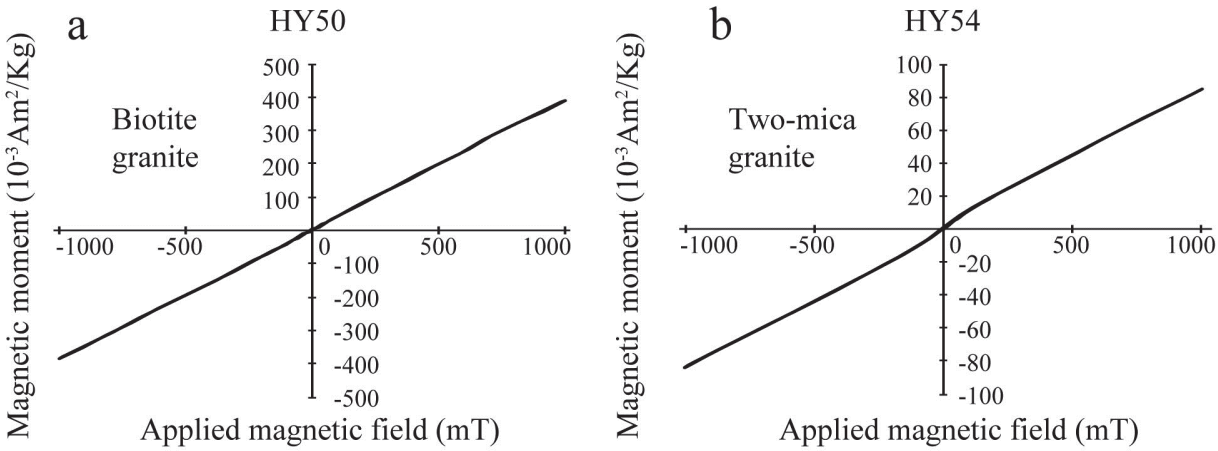

Figure 5 4: The hysterosis results of the samples of the Hengshan Granitic Massif

a: The Nanyue Biotite Granitic Pluton, b: The Baishifeng Two-Mica Granitic Pluton

4.3 The results of the AMS Measurements

4.3.1 The quality assessment on the AMS results

The AMS data of the Nanyue Biotite Granitic Pluton and the Baishifeng Two-Mica Granitic Pluton are presented in Table 1. As this table shows, theα_{95max} andα_{95min} of the most samples' K1 and K3 value are lower than 20°. So the AMS data of this study is well constrained. The quality is satisfactory to conduct a structural discussion.

4.3.2 The P_J and T value

The P_J value of the most samples of the biotite granite and the two-mica granite is lower than 1.2, except for three two-mica granite samples (Fig. 5-5a). These three samples are acquired from the west part of the Baishifeng Two-mica Granitic pluton which is influenced strongly by the WBDF and experienced ductile deformation (Location 5 in Fig. 5-1b). There is no obvious proportion relationship between PJ and Km (Fig. 5-5a). The T values of most samples are above 0 indicating the shape of AMS ellipsoid is predominantly oblate.

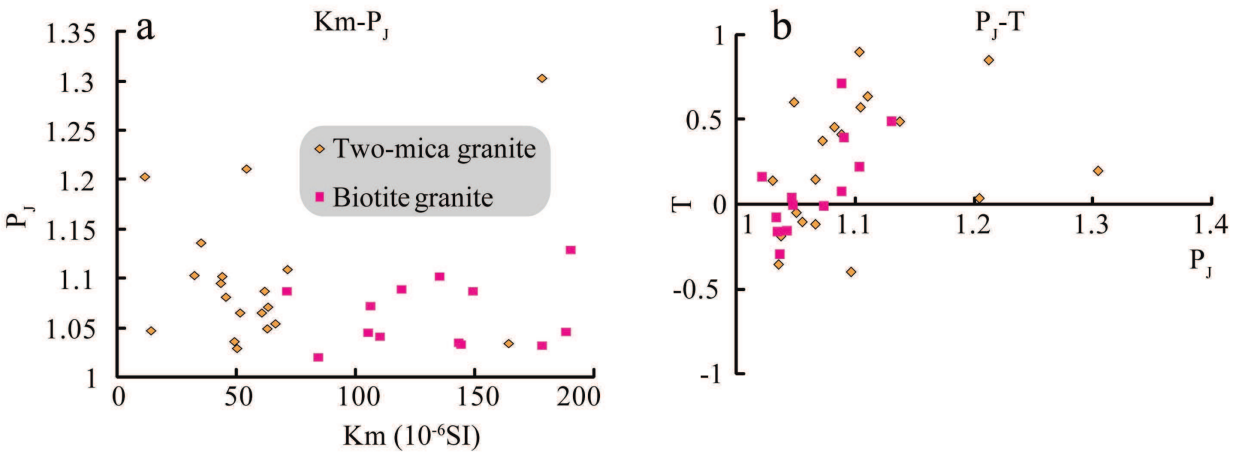

Figure 5 5: AMS parameter diagram of Hengshan Massif

a: T (Shape parameter) vs. P_J (anisotropy degree), b: P_J vs. Km (average susceptibility, 10^{-3} SI). The calculation of the T and P_J can be found in Jelinek (1981).

4.3.3 AMS mode

Sampling has been conducted in 13 sites of the Nanyue Biotite Granitic pluton and 20 sites of the Baishifeng Two-Mica granitic Pluton. Among them, just in one site of the Baishifeng Two-Mica Granitic Pluton the number of standard samples was made lower than 5, thus the average magnetic foliation and lineation can not be calculated (Table 5-1). Plotted the acquired results of magnetic fabrics in the Total Fabric Stereo Projection Diagram, as the results show, the pole of the magnetic foliation is arranged in cloud distribution (Fig. 5-6). The magnetic foliation of the Nanyue Biotite Granitic Pluton is concentrated and dips to SE with gentle angle while the magnetic foliation of the Baishifeng Two-Mica Granitic Pluton is variable. The magnetic lineation of both the Nanyue Biotite Granitic Pluton and the Baishifeng Two-Mica Granitic Pluton are concentrated to NW-SE direction.

Plotted all of the magnetic fabrics on the geologic map (Fig. 5-7), it is well observed that near the boundary between the Nanyue Biotite Granitic Pluton and the Baishifeng Two-Mica Granitic Pluton, in many sites of the Nanyue Biotite Granitic Pluton, the strikes of the magnetic foliations do not follow the contour of the boundary, in contrast, they usually perpendicular to the boundary. However, the magnetic foliations of the Baishifeng Two-Mica Granitic Pluton are parallel to the boundary. We interpret that the emplacement of the Nanyue Biotite Granitic Pluton

is older than the Baishifeng Two-Mica Granitic Pluton and the magnetic fabric formation time of the former is older than that of the latter. Apparently, the emplacement of the Baishifeng Two-Mica Granitic Pluton did not reform the magnetic fabric of the Nanyue Biotite Granitic Pluton, the magnetic foliation of the young pluton was constrained by the geometry of the boundary of the two plutons.

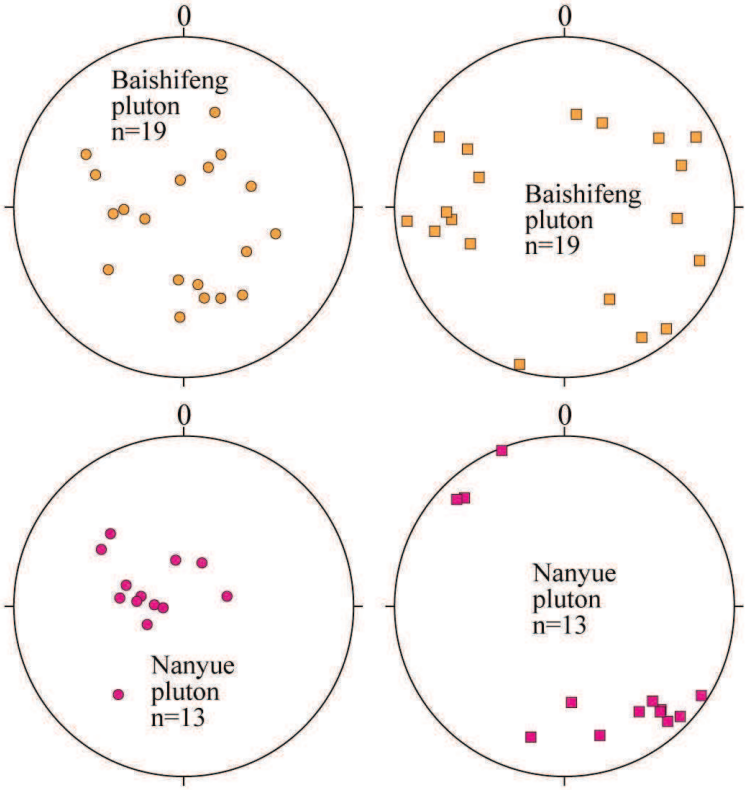

Figure 5 6: Total Magnetic Fabrics Stereo Projection of the Hengshan Granitic Massif

Equal area and lower hemisphere projection, solid circle and open rectangular represent the average direction of pole of magnetic foliation and average direction of magnetic lineation, respectively.

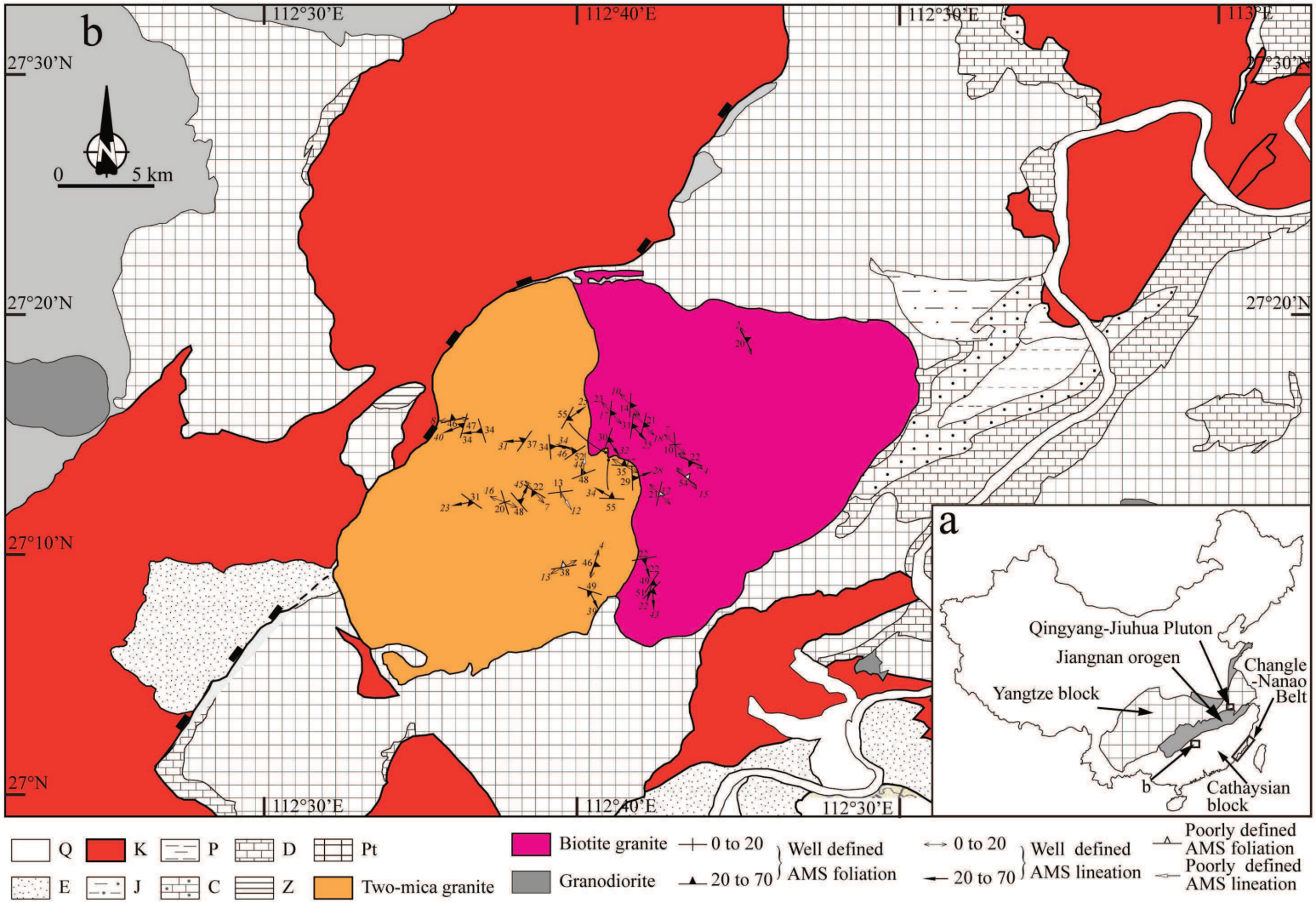

Figure 5 7 The structural geologic map with magnetic fabrics of the Hengshan Granitic Massif

Q: Quaternary, E: Tertiary, K: Cretaceous, J: Jurassic, P: Permian, C: Caboniferrous, D: Devonian, Z: Sinian, Pt: Neoproterozoic.

5 Microscopic observation and kinematics study

5.1 Thin section preparation

In order to observe the kinematics and the deformation styles of the WBDF and to determine whether the origin of the magnetic fabrics are original fabric during the emplacement or the secondary fabric during the later deformation, specimens from 7 sites of the Nanyue Biotite Granitic Pluton and 21 sites of the Baishifeng Two-Mica Granitic Pluton are selected to make oriented thin sections which are parallel to the magnetic lineation and perpendicular to the magnetic foliation. In the thin sections of the Baishifeng Two-Mica Granitic Pluton, 10 are along the WBDF, the rest are along an E-W section which are across the Baishifeng Two-Mica Granitic Pluton.

5.2 Deformation styles and kinematics

In the thin sections of the Nanyue Biotite Granitic Pluton, the feldspars are observed to be crashed. Along the cracks, an amount of feldspar fragments develop (Fig. 5-8a), a few feldspar grains are extinct wavily and even develop sub grains (Fig. 5-8b), while others develop mechanic twins (Fig. 5-8c); quartz grains are extinct wavily and develop sub grains (Fig. 5-8b and c); the cleavage of biotite are bended (Fig5-8b and c). In the course of making thin sections, when cut the standard AMS specimens along the direction which is parallel to the magnetic lineation and perpendicular to the magnetic foliation, quartz grains can be observed to be deformed to be “sigmoid” shaped with tails indicating a top-to-the-NW shear sense. Under the microscope, some feldspars can be observed to be cut to be “sigmoid” shaped, adjacent biotite grains form the tails of the “sigmoid”, this couple indicates a top-to-the-NW shear sense (Fig. 5-8b).

The thin sections from the east part of the Baishifeng Two-Mica Granitic Pluton are featured by the magmatic texture as shown by the undisturbed magmatic zonation and the carlsbad twins of Plagioclase as well as the tartan twin of microline; the biotite and the muscovite are idiomorphic, the cleavage plane is unbended (Fig. 5-8d); Quartz grains are extinct sharply or

wavily without developing sub grains (Fig. 5-8e). Turning westwards to which is influenced by the WBDF, the grains sizes of the feldspar and quartz are clearly diminished; quartz is stretched, oriented to form foliation; biotite and muscovite are deformed to be “sigmoid” shape (Fig. 5-8f) or to be “mica fish” (Fig. 5-8g), both indicate a top-to-the-NW shear sense; mica schist xenoliths develop shear bend indicating a top-to-the-NW shear sense as well.

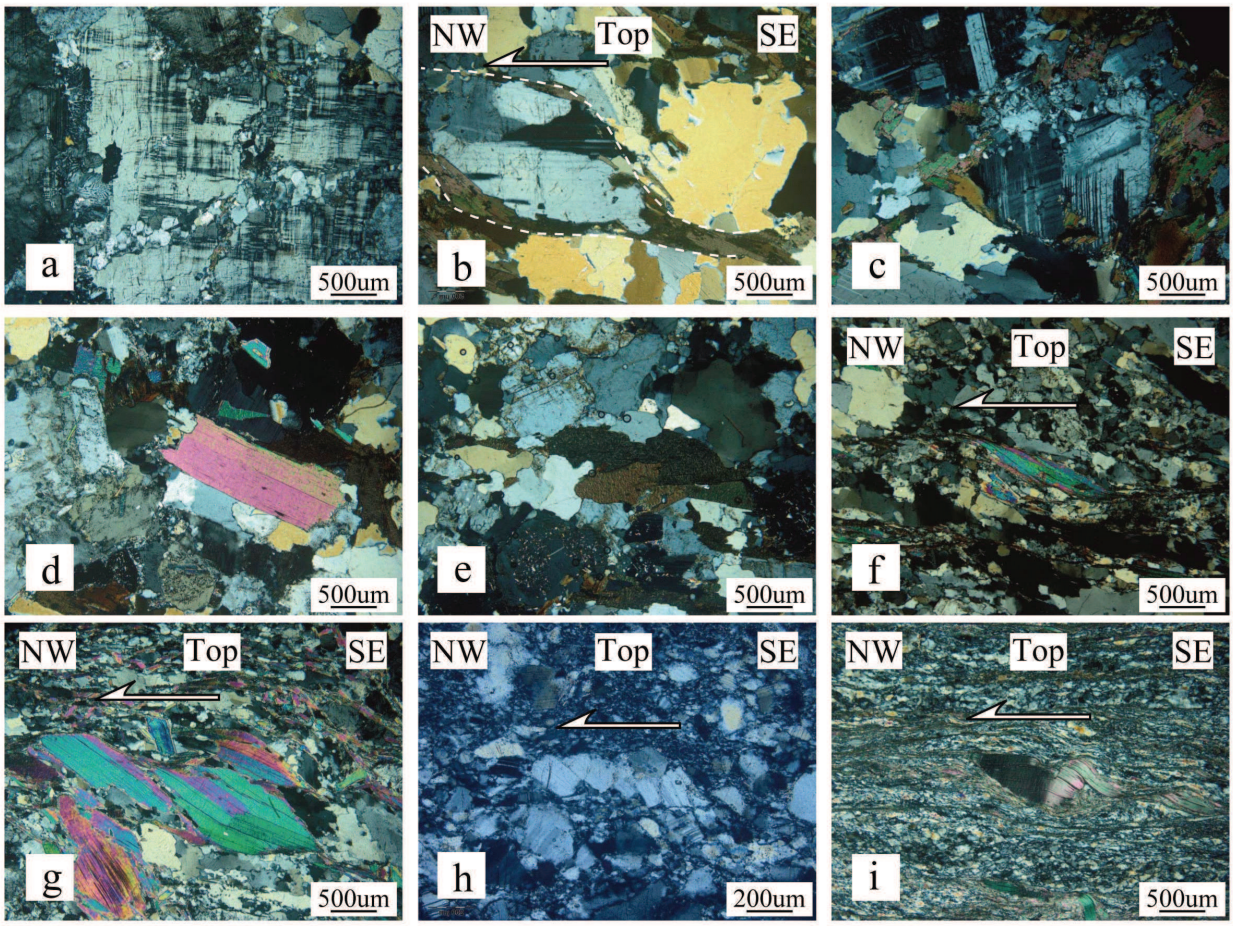

Figure 5 8 Micro structure of the rocks of the Hengshan Granitic Massif

a: feldspars in the Nanyue Biotite Granitic pluton were commonly crashed (Location 9 in Fig. 5-1b), b: in the Nanyue Biotite Granitic Pluton, biotites form tails of feldspar, indicating a top-to-the-NW shear sense (Location 2 in Fig. 5-1b), c: the feldspar in the Nanyue Biotite Granitic Pluton develops mechanic twins indicating a deformation after crystallization (Location 12 in Fig. 5-1b), d: the east Part of the Baishifeng Two-Mica Granitic Pluton (Location 4 in Fig. 5-1b), e: the middle part of the Baishifeng Two-Mica Granitic Pluton was slightly deformed，under microscope, quartz is wavy extinction and develops sub grains (Location 10 in Fig. 5-1b), f: in the west part of the Baishifeng Two-Mica Granitic Pluton, muscovite is ductile deformed

and developed tails to be "sigmoid" shape indicationg a top-to-the-NW shear sense (Location 5 in Fig. 5-1b), g: the mica fish in the west part of the Baishifeng Two-Mica Granitic Pluton indicates a top-to-the-NW shear sense (Location 11 in Fig. 5-1b), h: the dominal structure in the ultra-mylonite belt of the WBDF indicates a top-to-the-NW shear sense (Location 6 in Fig. 5-1b), i: muscovite of the ultra-mylonite belt along the southwest boundary of the Baishifeng Two-Mica Granitic Pluton was ductile deformed to be "sigmoid" shape with tails indicating a top-to-the-NW shear sense (Location 8 in Fig. 5-1b).

The deformation reaches a climax in the WBDF which is located on the west boundary of the Hengshan Granitic Massif. The Two-Mica granite experienced severe deformation and became ultra-mylonite belt. Under the microscope, feldspar was cracked and the fragments were rotated to form domino structure indicating a top-to-the-NW shear sense (Fig. 5-8h); quartz experienced dynamic re-crystalization to diminish its size (Fig. 5-8h) , or stretched to be "quartz ribbons"; micas were deformed to be "sigmoid" shape with tiny quartz tails, indicating a top-to-the-NW shear sense (Fig. 5-8i). On the southwest boundary of the Baishifeng Two-Mica Granitic Pluton, in the SE brench of the WBDF which is along the pluton's boundary, the strike of the foliation is NW-SE, and dip to SW. Microscopic study indicates a top-to-the-NW shear sense (Fig. 5-8i), illustrating a scenario of "the pluton moves to SE and the Neoproterozoic country rocks move to NW". Although this shear sense means a dextral strike-slip fault, it is logical to consider it is just a local kinematics of a normal fault system which represents the hanging wall of the fault moves to northwest and the footwall of the fault moves to southeast. This scenario is illustrated by each site in the WBDF no matter the location is on the northwest boundary of the pluton or on the southwest boundary of the pluton. This means the ductile deformation on the boundary of the pluton results from the regional ductile deformation rather than the relative movement between plutons and its country rocks during the emplacement.

6 The monazite U-Th-Pb dating

6.1 Sample's description

In order to determine the activity time of the WBDF, a gneissic granite sample "SC274" was acquired from the area influenced by the WBDF to make a thin section for a further monazite U-Th-Pb dating. In the outcrop where the "SC274" was acquired, feldspar and micas are well oriented; quartz is stretched or deformed to be "sigmoid" shape (Fig. 5-2c). Under the microscope, the rock making minerals of this sample are plagioclase, k-feldspar, biotite, muscovite and quartz. Feldspar is cracked, biotite is bended or deformed to be "mica fish" or "sigmoid" shape, quartz is stretched (Fig. 5-8f).

6.2 Experiments

After plating carbon, the thin section was observed by TEM to search monazite in Institut des Sciences de la Terre d'Orleans. In the sample SC274, totally 24 monazites have been found. Their sizes range from 5 um to 30 um in diameters. Under TEM, they are homogeneous without zonations. Their shapes are automorphic or with erosion harbor (Fig. 5-9a). All of the monazites found in SC274 are inclusions inside the igneous origin biotite, thus these monazite are products of crystallization in magma or hydrothermal liquid rather than metamorphic monazite.

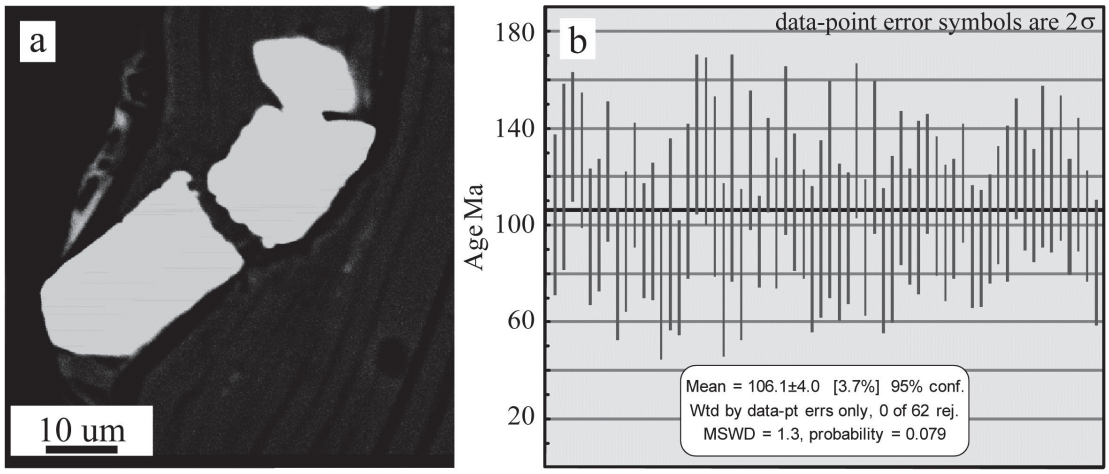

Figure 5 9: a: features of monazite found in SC274, b: dating result of the Monazite found in SC274

6.3 Experiment results

As the results shows, apparent ages of the monazites in SC274 are young. Owing to the low content of Pb and narrow variance of Th/U ratio, Th/Pb-U/Pb diagram can not be acquired (Cocherie and Albarede, 2001). However, the average age of the monazites in SC274 is 106.1±4.0Ma (Fig. 5-9b), it is well constrained with low error limits.

7 Discussion

In order to understand the regional tectonic regime during the emplacement of the Hengshan Granitic Massif, we have conducted a multi-disciplinary study including field structural observation, microscopic observation, magnetic fabric measurement and monazite U-Th-Pb microprobe dating. In what follows, we will first summarize our observations and experiment results briefly, and then we will interpret their relationship and bearings on the regional tectonic regime.

7.1 Observations and experiment results summarization

The Hengshan Granitic Massif consists of two parts, namely, the Nanyue Biotite Granitic Pluton on the east and the Baishifeng Two-Mica Granitic Pluton on the west, respectively. On the outcrop scale, the biotite granite is massive, it contains mega feldspar which is well oriented. Under the microscope, the feldspars of the biotite granite are crashed, the cracks penetrate the feldspar and its adjacent mineral. Along the cracks, an amount of tiny feldspar fragments develop. Some feldspars were deformed to be “sigmoid” shape, joint with their biotite tailes, they indicate a top-to-the-NW shear sense. Biotite was bended. Quartz is extinct wavily and develops sub grains. The east part of the Baishifeng Two-Mica Granitic Pluton is undeformed. On the outcrop scale, the mineral is randomly distributed or oriented. Magmatic foliation and schilieren develop. Under the microscope, feldspar, micas, quartz do not show deformation features. The deformation degree increases from east to west. On the outcrop scale, the west part of the Baishifeng Two-Mica Granitic Pluton is deformed to be gneissic granite. Feldspar, micas are oriented, quartz is deformed to be “sigmoid” shape indicating a top-to-the-NW shear sense.

Under the microscope, feldspar was cracked, the size of quartz shrinked, the micas were deformed to be “mica fish” or “sigmoid” shape indicating a top-to-the-NW shear sense. The deformation reaches its climax in the WBDF on the west boundary of the Baishifeng Two-Mica Granitic Pluton. Here develops ultra-mylonite. Under microscopic scale, feldspar was cracked to be tiny fragment to form domino structure, quartz was dynamic re-crystalization to be matrix, micas were deformed to be “sigmoid” shape, indicating a top-to-the-NW shear sense. The WBDF was imposed by later brittle deformation to form cataclasite. The WBDF is not limited to the west boundary of the Baishifeng Two-Mica Granitic Pluton, on the northwest and southwest corners of the pluton, the fault extend to the Neoproterozoic country rocks in which the shear sense is also top-to-the-NW. The WBDF is also the major boundary fault of the Zhajiang basin. In the east part of the Zhajiang basin, the strikes of the red strata are NE-SW and dip to SE, illustrating the influence of the WBDF. Accordingly, the red strata of the other flunk of the basin overlies unconformably on the previous basement. Generally speaking, the WBDF control the geometry shape of the Zhajiang basin.

The magnetic carriers of the Nanyue Biotite Granitic Pluton and the Baishifeng Two-Mica Granitic Pluton are both paramagnetic minerals. Interpreted together with the observations from the outcrop and microscopic scales, the main magnetic carrier is believed to be biotite. Thus, the magnetic fabrics are parallel to the mineral fabrics. This enables us to do direct structural analysis. The magnetic foliation of the Nanyue Biotite Granitic Pluton gently dip to southeast while its magnetic lineation is concentrated on NW-SE direction. The Magnetic foliation of the Baishifeng Two-Mica Granitic Pluton scatters, while the magnetic lineation of the pluton concentrates on the WNW-ESE direction. On the boundary between the Nanyue Biotite Granitic Pluton and the Baishifeng Two-Mica Granitic Pluton, the magnetic foliation of the Nanyue Biotite Granitic Pluton is not parallel with the contour of the boundary while the magnetic foliation of the Baishifeng Two-Mica Granitic Pluton is parallel with the boundary.

We have selected a sample from the gneissic two-mica granite influenced by the activity of the WBDF and made a thin section to conduct monazite U-Th-Pb microprobe dating. In this thin section, all the monazites are featured by crystallization from magma or hydrothermal liquid. The sizes of the monazites are between 5 um and 30 um in diameters. The average age of the monazites is 106.1±4.0Ma.

7.2 The origin of the magnetic fabric

The primary magnetic fabric which is due to magma crystallization reflects the magma flow direction or the regional tectonic regime during the emplacement (Archanjo and Bouchez, 1997; Callot et al., 2001; Neves et al., 2003; Talbot et al., 2005a, b;de Oliveira et al., 2010;), while the secondary magnetic fabric which is due to deformation reflects the regional tectonic regime after the fully crystallization of the pluton (Archanjo and Fetter, 2004; Charles et al., 2009). The primary and the secondary magnetic fabrics are the products of different tectonic events in different time. Thus in this study, in order to understand the tectonic regime and its time offered by magnetic fabric, we should discuss the origin of the magnetic fabric at first.

The anisotropy degree (P_J) provides a direct, fast way to determine the origin of the magnetic fabric. According to the statistics, when P_J >1.2, the magnetic fabric is due to deformation after magma crystallization while when P_J <1.2, it is original magnetic fabric during the magma crystallization (Tarling and Hrouda, 1993).

In this study, the P_J values of the samples from the east part of the Baishifeng Two-Mica Granitic Pluton are usually lower than 1.2 while the values of the samples from the west part of the pluton are usually higher than 1.2. In outcrop and microscopic observation, the samples from the east part are featured by magma texture while the samples from the west part are featured by gneissic texture due to the deformation exerted by the WBDF. Thus we can interpret that the magnetic fabric of the east part of the pluton is primary and the magnetic fabric of the west part of the pluton is secondary which reflect the influence of the WBDF. It should be noted that the magnetic fabric acquired in this study is consistent with the structural fabric observed in WBDF.

However, the situation of the Nanyue Biotite Granitic Pluton is much more complex. The P_J value of the Pluton is lower than 1.2. Theoretically, the magnetic fabric should be primary fabric. On the outcrop scale, feldspar and biotite orientation have been observed without obvious deformation. However, on the microscopic scale, it is easy to find the crashed feldspar and the deformation feature of quartz and biotite. Because the main magnetic carrier is biotite (Fig. 5-4a), the magnetic fabric of the Nanyue Biotite Granitic Pluton is probably altered due to the deformation and rotation of the biotite.

7.3 The emplacement mechanism of the Baishifeng Two-Mica Granitic Pluton

As previous studies show, the WBDF is featured by low angle detachment fault with at least 10 km displacement (Xu et al., 1998), and the west part of the Baishifeng Two-Mica Granitic Pluton crops augen gneiss which is believed to be augen migmatite, thus the emplacement mechanism of the Hengshan Granitic Massif could be correlated with basin and range province in western America (Xu et al., 1998). Some scholars name it as the Hengshan Metamorphic Core Complex (Zhang, 1994). However, the observations of this study and some previous studies show that the sediments of the Neoproterozoic in the footwall is devoid of metamorphism, and can not stand for lower crust materials (HNBGMR, 1987). Thus, the hypothesis that the WBDF has experienced large distance detachment and could be called Metamorphic Core Complex still needs further study. At least, the metamorphic degree could hardly verify this hypothesis.

The previous studies considered that the augen gneiss of the west part of the Baishifeng Two-Mica Granitic Pluton is “migmatite” (Wang, 1990b). After comparison between the two-mica granite of the pluton and the “migmatite”, the similarity of the REE distribution mode has been found (Wang, 1990b). This discovery was interpreted that the two-mica granite is the local re-melting products of the migmatite (Wang, 1990a). However, the deformation could solely lead to the formation of the augen gneiss. Given that the augen gneiss of the west part of the Baishifeng Two-Mica Pluton lacks mesosomes and leucosomes of the nebulitic structure of the migmatite (Vernon and Collins, 1988), it is more convenient to consider the augen gneiss as the deformation product of the two-mica granite when interpret the similarity of the REE distribution mode between the former and the latter.

As many previous studies put it, the primary magnetic fabric of a pluton could provide information on the emplacement mechanism of the studied pluton (Talbot et al., 2005b; Trubac et al., 2009; de Oliveira et al., 2010; Turrillot et al., 2011). This study is aimed to discuss this topic based on the newly acquired AMS data.

Except for the west part of the Baishifeng Two-Mica Granitic Pluton which was influenced by the WBDF, the magnetic fabrics in other sites of the pluton are primary fabric. These primary fabrics are used to discuss the emplacement mechanism of the Baishifeng Two-Mica Granitic

Pluton. The magnetic foliation of the Baishifeng Two-Mica Granitic Pluton scatters. Near the boundary of the pluton, the strike of the magnetic foliation is parallel to the contour of the boundary and dips to the outer side. This phenomenon indicates a magma vertical injection. Well on the other side of the boundary, the strike of the magnetic foliation of the Nanyue Biotite Granitic Pluton is usually perpendicular to the boundary without records any influences by the emplacement of the Baishifeng Two-Mica Granitic Pluton. It means that the emplacement of the Baishifeng Two-Mica Granitic Pluton is permissive rather than forceful (Pitcher, 1979b).

7.4 The regional tectonic regime during the emplacement of the Baishifeng Two-Mica Granitic Pluton

During the emplacement, a concentrated mode of the magnetic lineation usually indicates a regional extension regime. And the extensional direction is parallel to the magnetic lineation (Talbot et al., 2000; Talbot et al., 2005a; Joly et al., 2007; Joly et al., 2009; Turrillot et al., 2011). In this study, the primary magnetic lineation of the Baishifeng Two-Mica Granitic Pluton concentrates on WNW-ESE direction indicating that during 150 Ma, the region where the pluton intruded was under the control of a WNW-ESE extension regime.

It is the WBDF which makes the Baishifeng Two-Mica Granitic Pluton couple with the Zhajiang Basin. The Zhajiang Basin is a Cretaceous half graben basin whose geometry is controlled by the WBDF. The oldest sediment infilled in the Zhajiang Basin is the Early Cretaceous red sediment which is a little bit younger than the Baishifeng Two-Mica Granitic Pluton. The WBDF indicates a top-to-the-NW shear sense. The geometry of the Zhajiang Basin also indicates a NW-SE extension during Cretaceous. In one sentence, since the emplacement of the Baishifeng Two-Mica Granitic Pluton, the studied area has experienced a NW-SE extension during Late Jurassic and the whole Cretaceous.

7.5 Geodynamic background

The transitional period between the Jurassic and the Cretaceous was a magmatism quiescence (Li et al., 2010b). The pluton emplacement was inactive during this period. Only a few plutons emplaced in the Lower Yangtze Area (Li et al., 2010b). According to previous

studies, the paleo-pacific plate experienced break-off during this period and then rolled back and retreated coastal wards (Li and Li, 2007). The break-off of a subduction slab often leads to mantle swarms and regional extension. The NW-SE extension indicated by the Baishifeng Two-Mica Granitic Pluton and the Zhajiang Baisn is probably influenced by the slab break-off proposed by previous study.

7.6 The relationship between the WBDF and the the Baishifeng Two-Mica Granitic Pluton

When a ductile fault cuts the boundary of a pluton, the activity of the fault could be coeval to the emplacement of the pluton or later than the emplacement of the pluton. In the former situation, the activity of the fault plays an important role in the emplacement of the pluton. The pluton is considered as syn-tectonic pluton. The Guojialing pluton in Shandong belongs to this kind of situation (Charles et al., 2010). In the latter situation, the fault just cuts the pluton coincidently, there is no co-genic relationship between the fault and the pluton. The Yiwulushan Pluton in the south of Liaoning belongs to this kind (Lin et al., 2013a; Lin et al., 2013b). Because the U-Pb isotropic ages of the zircons from the Nanyue Biotite Granitic Pluton and the Baishifeng Two-Mica Granitic Pluton are 232-228 Ma and 150 Ma respectively. The activity period of the WBDF ranges from 136 Ma to 97 Ma. Thus the Hengshan Granitic Massif is not regarded as a syn-tectonic pluton (Li et al., 2013a). However, the meaning of the U-Pb isotropic age of zircon is the crystallization age of the measured zircon. During the activity of the fault, hydrothermal activity could lead to formation of new zircon grains. In previous studies, the age of the Baishifeng Two-Mica Granitic Pluton has once been acquired by Monazite U-Th-Pb microprobe dating. The result is 149 Ma which is very close to the zircon U-Pb isotropic age. In this study, monazite U-Th-Pb microprobe dating has been conducted on the gneissic two-mica granite near the WBDF. The result is 106 Ma which is more or less the same to the zircon U-Pb isotropic age of the WBDF. The microscopic observation indicatesthat the measured monazites are tiny crystallized monazite. Some are cracked. We interpret this kind of monazite as the products of the hydrothermal activity.

In this study, as the field and microscopic observation show, the deformation degree of the

Baishifeng Two-Mica Granitic Pluton increases from the east to the west, and reaches its climax in the WBDF on the boundary of the pluton and the Zhajiang Basin (Fig. 5-10). Besides the activity of the fault was coeval to the emplacement of the pluton, this phenomenon could be also aroused by a later activity of fault which deformed the pluton after the emplacement. However, in the east part where was not affected by the activity of the WBDF, the primary magnetic lineation concentrates on WNW-ESE direction indicating a WNW-ESE regional extensional regime. Together with the fabrics in the WBDF and the geometry of the Zhajiang Basin, it argues a consistent NW-SE extension regime since the Late Jurassic to the Late Cretaceous. Considering in the Jurassic and the Cretaceous, the South China Block was under the control of the Paleo-Pacific Plate retreating geodynamic background (Li and Li, 2007), we have to re-assess the temporal relationship between the emplacement of the pluton and the activity of the fault.

The origin of the magnetic fabric of the Nanyue Biotite Granitic Pluton is the key to understand this temporal relationship between the emplacement of the pluton and the activity of the fault. If the magnetic fabric of the Nanyue Biotite Granitic Pluton is primary, the regional tectonic regime is NW-SE extension during the emplacement. If the magnetic fabric is secondary, then the NW-SE magnetic lineation was probably caused by the activity of the WBDF. Considering the activity of the WBDF did not deform the Baishifeng Two-Mica Granitic Pluton pervasively, thus the WBDF was active before the emplacement of the Baishifeng Two-Mica Granitic Pluton and the pluton was a syn-tectonic pluton.

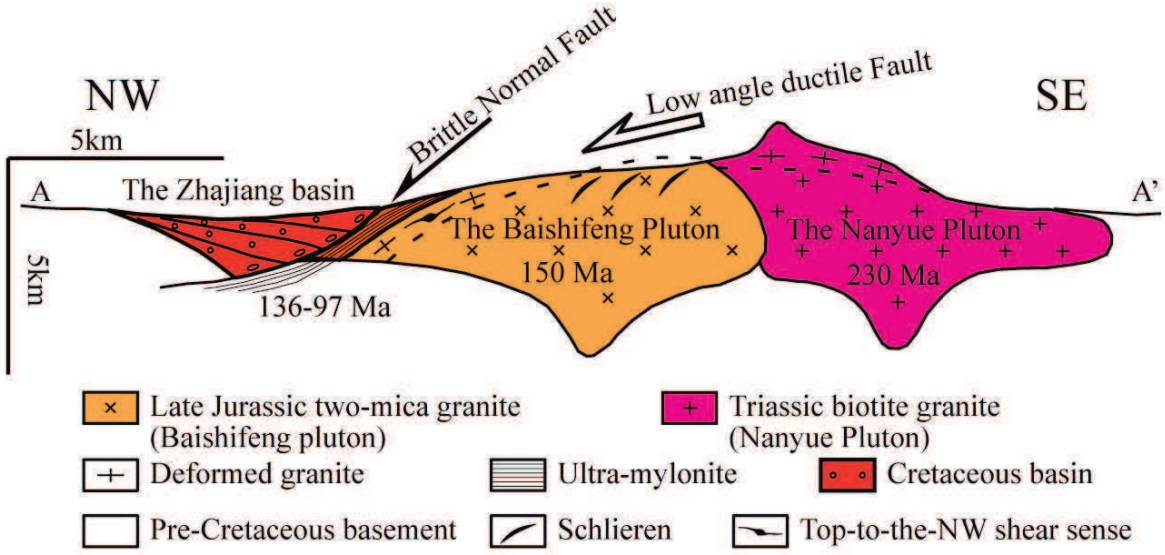

Figure 5 10: the Baishifeng Two-Mica Granitic Pluton and the WBDF

The basin and the pluton were coupled by the fault.

8 Conclusions and perspectives

The above observations and interpretations enable us to reach the conclusion as follows and put forward the suggestions for future studies.

8.1 Conclusions

1, The Nanyue Biotite Granitic Pluton experienced a limited deformation; the Baishifeng Two-Mica Granitic Pluton was strongly affected by the WBDF, from its east part to west part, the deformation degree increased.

2, The magnetic foliation of the Nanyue Biotite Granitic Pluton dips to southeast with gentle dip angle while the magnetic lineation of this pluton concentrates on NW-SE direction. The magnetic foliation of the Baishifeng Two-Mica Granitic Pluton scatters. On the east boundary of this pluton with Nanyue Biotite Granitic Pluton, the magnetic foliation of this pluton is parallel to the boundary and dips to the outer side. On the west part of this pluton, the magnetic foliation is strongly affected by the WBDF, the strike is NE-SW and dips to NW. The magnetic lineation of this pluton concentrates on WNW-ESE direction.

3, The emplacement of the Baishifeng Two-Mica Granitic Pluton did not alter the magnetic fabric of the Nanyue Biotite Granitic Pluton. The emplacement mechanism is most probably a permissive one.

4, In 150 Ma, during the emplacement of the Baishifeng Two-Mica Granitic Pluton, the studied area was under the control of WNW-ESE extension regime.

8.2 Perspectives

Whether the Baishifeng Two-Mica Granitic Pluton is a syn-tectonic pluton or not, the relationship between the NW-SE magnetic lineation of the Nanyue Biotite Grantic Pluton and the activity of the WBDF is a key to answer this question. The quartz C-axis statistics by U-stage could provide information on the deformation degree of the Nanyue Biotite Granitic pluton. The geometry of the pluton could also provide information on the emplacement course and the later deformation of the pluton, thus the study on the geometry of the pluton by gravity modeling will be another good method to solve this problem.

9 The brief outlines of this chapter

The Hengshan Granitic Massif consists of two parts, namely, the Nanyue Biotite Granitic Pluton on the east, and the Baishifeng Two-Mica Granitic Pluton on the west, respectively. In order to understand the emplacement mechanism and regional tectonic regime of the Hengshan Granitic Massif, we have conducted multi-disciplinary studies on the two parts of the Hengshan Granitic Massif including field structural observation, microscopic observation, magnetic fabric measurement, monazite U-Th-Pb microprobe dating. After analysis of the data, we consider that the emplacement of the Baishifeng Two-Mica Granitic Pluton was permissive; the studied area was under the control of WNW-ESE regional extension regime during the emplacement of the Baishifeng Two-Mica Granitic Pluton; the Baishifeng Two-Mica Granitic Pluton was strongly affected by WBDF, the deformation degree of the pluton increases from the east to the west. We have also proposed a project for further study .

Chapter 6 The Late Mesozoic Tectonic Evolution in the South China and the Discussions on its Geodynamic Background

The intensity of Late Mesozoic magmatic activities in the South China Block is rare from the perspective of either spatial distribution or temporal duration. The discussion on its tectonic evolution and dynamic background not only facilitates the understanding of the lithosphere evolution in South China, but also provides interpretations of the formation mechanisms of large deposits. Even though previous researchers have done abundant and fruitful geological mappings and scientific studies, some fundamental problems still remain unsolved or controversial, such as the magma formation mechanism, the general tectonic background and geodynamic features of magmatic activities, and other related problems. Therefore, this paper selects intrusive rocks and their related tectonic zones for field and lab multi-disciplinary study. Three regions are chosen in view of their distances to the Pacific subduction zone and the similar ages of their granite rocks and deformation. Based on the previous discussions, this chapter focuses on the Late Mesozoic tectonic evolution of South China Block and the corresponding geodynamic background. It begins with a brief account of new tectonic findings, and then analyzes the tectonic evolution of South China Block by incorporating the findings into the regional tectonic regime in the Late Mesozoic. Finally, a feasible geodynamic model is established to explain the late Mesozoic tectonic evolution of South China Block.

1 New Tectonic Findings

1.1 The Changle-Nanao Belt

A comprehensive study of deformed volcanic unit, gneiss unit, syn-tectonic granites and isotropic granites indicates that the major tectonic events of this tectonic zone can be divided into two phases: the compression event (D_1) with a top-to-the-NW shear sense between 130-110Ma, and a subsequent NW-SE regional extensional event between 105-90Ma (D_2). D_1 caused a 25 Ma

long volcanites eruption quiescence period between the Nanyuan Formation volcanites (K_1n) in the Early Cretaceous and the Shimaoshan Formation volcanites (K_2sh) in the Late Cretaceous. Accordingly, the pluton emplacement was less frequent during this period (Fig. 3-3). D_1 led to the metamorphism and deformation of pre-existing granites and sedimentary rocks to form the Gneiss Units, and developed penetrative foliations. Of the Deformed Volcanic Units, Duling Formation with the Late Jurassic age and the Nanyuan Formation with the Early Cretaceous age were involved in the deformation, developing a number of NE-SW extended ductile shear zones. On the foliation of these two units shows a NW-SE lineation with an overall top-to-the-NW shear sense. At the end of D_1 event, continuous NW compression caused the foliations to be folded, with the axial plane of folds going NE-SW. In some places, asymmetric folds indicate a top-to-the-NW shear sense. The syn-tectonic pluton which emplaced during D_1 developed steeply dipping magnetic foliations in the NE-SW trend. The NW-SE compression and contraction are indicated by the myrmikite texture growing along the magnetic foliations and the feldspar fracture growing perpendicularly to the magnetic foliations. The compression in the Changle-Nan'ao Belt may be related with the collision between the West Philippine micro-continental block and the South China block. Changle-Nan'ao Belt and the West Philippine Ophiolite Suture Zone constitute a thrust-back thrust faults couple growing on the margin of Andean-type active continent of South China in the Late Mesozoic. After 105Ma, this region came under a weak extensional tectonic regime in the NW-SE trend（D_2）, standing for the end of the orogeny caused by collision and the start of the post-orogenic extensional tectonic phase. In this stage, the opening of crust cracks formed surging channels upwards, resulting in the massive emplacement of isotropic granite plutons and mafic dykes as well as the enormous eruption of volcanic rocks from Late Cretaceous Shimaoshan Formation which contained the bimodal volcanite sequence. In this event, the NW-SE extensional direction is indicated by the slightly dipping magnetic foliation of intrusive granites, the NW-SE magnetic lineation, and the NW-SE aligned dyke swarms.

Certainly, the sign of strike-slip structure is also observed in this tectonic zone, but these signs are local and discontinuous spatially. The 200km strike-slip movement proposed by previous studies has not been confirmed by the field structure observation in this tectonic belt.

1.2 The Lower Yangtze Area

Located in the Lower Yangtze Area, the Qingyang pluton and the Jiuhua pluton emplaced at the Lower Yangtze Fold and Thrust Belt in about 142Ma and 131Ma respectively. The comprehensive study on southern Anhui Qingyang-Jiuhua Massif reveals: (a) regional ductile deformation is missing in surrounding country rocks. The main body of the massif is isotropic, and ductile deformation exists only in the narrow boundary between the pluton and country rocks. The pluton emplacement did not change the structure of pre-existing rock folds. (b) The magnetic foliation at the core of pluton declines slightly, while that near the border dips steeply and parallels to the contact surface with country rocks, the magnetic lineation running gently and dispersedly. (c) New paleomagnetic results confirm that no significant relative motion has been found inside the plutons, plutons relative to their country rocks or the lower Yangtze Area to the entire South China. (d) According to the measurement of Al-total content in Amphibole geobarometry, the emplacement pressure was smaller than 4 kbar, which is compatible to the presence of andalusite in the contact metamorphic belt; gravity modeling demonstrates that the pluton is in the shape of a box, flat top, steep walls, consisting of a laccolith-shaped upper part and a lower part with several vertical "roots". The Qingyang pluton's "roots" and Jiuhua pluton's "roots" coincided to overlap with each other and form several NE-SW root belts. The above facts show that emplacements occurred within the brittle shallow crust. The magnetic fabric of plutons was presented as the magmatic fabric formed by upwelling magma. The "roots" were ruptures or faults of crust, providing conduits for upwelling of magma. The pluton emplacement mechanism might have been a permissive one with vertical magma injection. The NE-SW trending of "roots" suggests a NE-SW extension of crust. According to the reference with geological records of other contemporary regions in the Lower Yangtze Area, the NW-SE extension is spread across the Lower Yangtze Area， such as the Dabie migmatite dome, semi-graben basins in Jiangnan orogenic belt, Lushan western boundary ductile shear zone and other geological bodies. Therefore, the Qingyang-Jiuhua massif reveals that this is an important extensional event. The intensity of this event, however, is weak in the Yangtze fold and thrust belt, the amount of stretch probably being equal to the width of Qingyang-Jiuhua pluton "roots".

1.3 The Hengshan Granitic Massif

Hengshan Granitic Massif includes the Nanyue Biotite Granitic Pluton in the east and the Baishifeng Two-Mica Granitic Pluton in the west. The former emplaced between 232-228Ma, while the latter in 150Ma. The deformation of biotite granites resulted in the fragmentation of feldspar, the bending of biotite as well as the wavy extinction and development of sub-grains of quartz. The magnetic foliation of all the sampling sites dips consistently southeastwards. The magnetic lineation runs NW-SE as well. A top-to-the-NW shear sense has also been observed in the oriented thin sections which is parallel to the magnetic lineation and perpendicular to the magnetic foliation. Although the anisotropy degree P_J is less than 1.2 in Nanyue plutons, this foliation and lineation configuration may be a secondary fabric caused by deformation. Field observation and laboratory microscopic observation have found that the degree of deformation of two-mica granites gradually increases from east to west. The east developed a magmatic texture, while the west grew gneissic structure under the influence of strong deformation. The magnetic fabric of two-mica granite was presented as a primary fabric formed at the time of magmatic crystallization in the east but a secondary magnetic fabric affected by posterior deformation in the west. Overall, the two-mica granite dips gently. Its magnetic foliation goes parallel to the faults on the western Hengshan edge and the border at the eastern boundary with biotite granite. Two-mica granite emplacement did not transform the magnetic fabric of older biotite granite at the boundary. Furthermore, the inclination of the primary magnetic foliation of the east part of the two-mica granite is not large. Thus, the way the granite emplaces is mainly permissive with magma vertical upward injection. The magnetic lineation mostly runs in the WNW-ESE direction, indicating that the emplacement of this region in 150 Ma was under the control of WNW-ESE extensional regime. In addition, 135-97Ma is the time when the West Boundary Ductile Fault of the Hengshan Granitic Massif cut the two-mica granite and took control of the Zhajiang bansin's geometry. In view of these observations, the kinematics indicates a top-to-the-NW shear sense, and the control of WNW-ESE extensional regime from the Late Jurassic to Early Cretaceous.

2 The Regional Tectonic Background of South China in the Late Mesozoic

2.1 The Early Cretaceous

In the Early Cretaceous, the most prominent event in south and southeast coastal areas was the wide eruptions of volcanites, distributed all the way from Zhejiang in the north to Fujian in the south, and Guangdong was also covered. The lithology of these volcanites includes rhyolite, trachyte and andesite. The geochemical investigation on them and the other contemporary intrusive granites demonstrates the enrichment of LREE and LILE and the lack of Nb and Ta. This shows that this set of volcanite-intrusive rocks are typical island arc magmatic rocks (Lapierre et al., 1997; Guo et al., 2012; Liu et al., 2012). Zhejiang-Fujian-Guangdong coastal areas are generally parallel to the paleo-Pacific subduction zone, which is in the tectonic location of the volcanic arcs caused by the paleo-Pacific subduction.

The vast areas of the South China Bolock on the northwest side of Zhejiang-Fujian-Guangdong volcanic arcs are the back-arc regions resulted from Paleo-Pacific subduction. Massive volcanic eruptions occurred between 140 Ma – 125 Ma in the Luzong area of southern Anhui. The lithology mainly includes shoshonite and trachyte in which there are rich LREE and LILE but poor Nb, displaying arc affinity. The same arc affinity is also shown in intrusive rocks from the contemporary Luzong area and the entire southern Anhui area in the Early Cretaceous (Xu et al., 2010; Yang et al., 2006). According to the Pb isotope study of mafic plutons from southern Anhui, their parent magma contains metasomatic mantle components (Yan et al., 2003).

During the period between 143 Ma – 139 Ma and 105 Ma – 98 Ma, a large amount of basalts were erupted along the Ganhang belt. These basalts are rich in LREE but poor in HREE, Nb and Ta, suggesting their connections with subduction (Yu et al., 2006b). In 137 Ma – 122 Ma, there were also emplacements of A-type granites which are also rich in LREE but poor in HREE, Nb and Ta (Yang et al., 2012). Furthermore, in southern Jiangxi, many mafic dykes that developed in 147-79Ma display the same traits (Xie et al., 2006)。

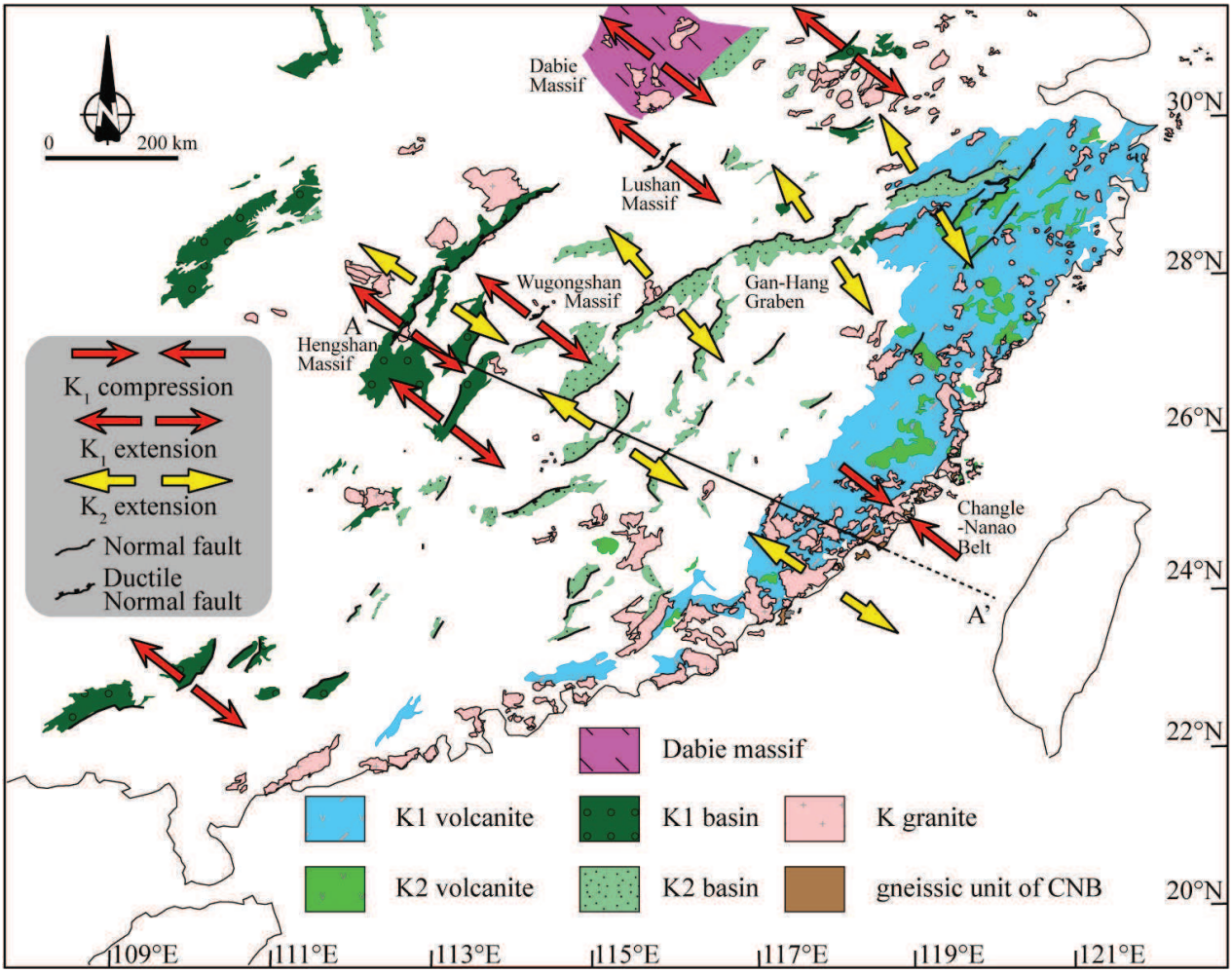

Figure 6 1: Geological Tectonic Map of South China Block in the Cretaceous

2.2 The Late Cretaceous

Along the Zhejiang-Fujian-Guangdong coastal areas, a new cycle of volcanic activities began after Early Cretaceous volcanic eruptions quiescence caused by the NW compression in 130-110Ma. Volcanites of Shimaoshan Formation during this period also shows the geochemical properties of rich in LREE and poor in HREE, Nb and Ta. In accordance with the diagrams of $E_{Nd}(t)$-$(^{87}Sr/^{86}Sr)_I$ and the trace element tectonic diagram, volcanites of this eruption cycle are mostly found in IAB area, implying their possible links with island arc activities (Lapierre et al., 1997; Chen et al., 2005b; Chen et al., 2008; Guo et al., 2012). In the areas west of Wuyi Mountain, namely the back-arc region in the Early Cretaceous, such as Changsha basin in Hunan, Hengyang basin, Lilin-Youxian basin, Ji'an-Taihe basin in Jiangxi, Ganzhou basin and Nanxiong basin, basalt dissections show rich LREE and poor HREE, but there is no lack of Nb and Ta. In

the diagrams of $E_{Nd}(t)$-$(^{87}Sr/^{86}Sr)_I$ and the trace element tectonic diagram, volcanites from these areas are presented in OIB, and distant from IAB (Chen et al., 2005b). This suggests that in the Late Cretaceous, east of Wuyi Mountain, namely Zhejiang-Fujian-Guangdong coastal areas, still remained in the subduction zone, whereas the west of Wuyi Mountain was no longer affected by subduction. Therefore, the area influenced by the Paleo-Pacific subduction, compared with the Early Cretaceous, had retreated to the southeast.

3 Tectonic Evolution of South China

The Cretaceous pluton is located on the southeast of the Jurassic pluton, and the migration of magmatic activities display a coast ward direction since the Jurassic to the Cretaceous (Zhou and Li, 2000； Li and Li, 2007). Previous research thought that the migration was caused by gradual deepening of paleo-Pacific subduction angle and the subsequent SE retreat of volcanic arc (Zhou and Li, 2000). However, based on more elaborate data of age structures, it is now believed that two blocks broke off in the transition period between the Jurassic and the Cretaceous, and the subducting slab rolled back, resulting in the SE migration of magmatic activities（Li and Li, 2007）.

The distribution pattern of plutons of different ages provides macro background information for geodynamic model in the Late Mesozoic. Several tectonic regimes, however, existed in the individual tectonic location relative with the subduciton zone simultaneously. The migration of subduction zone also led to the conversion of regional tectonic regimes. Thus more detailed tectonic constraints are needed in the investigation of Late Mesozoic geodynamic background of South China.

The study has found that during the period of 130 Ma – 110 Ma in the early Cretaceous, due to the NW subduction of Paleo-Pacific, the Philippine micro-continent continued to converge with the South China Block and eventually collided, leading to the NW compression tectonic regime of Changle-Nan'ao belt on the southeastern margin of South China Block. But at the same time, Hubei, northern Jiangxi, Hunan and Guangxi were under the control of NW-SE back-arc extensional regime. For example, the Jiangnan Orogenic Belt developed a NE-SW

normal fault system (Yu et al., 2007). Under the control of this fault system, the Jiangnan Orogenic Belt developed many half-graben basins with long axis of NE-SW direction. Contemporary NE-SW semi-graben basins formed in the Lower Yangtze Fold and Thrust Zone (AHBGMR, 1987). Due to the influence of NW-SE extensional regime on the Qingyang-Jiuhua Massif, the crust was cracked, developed tension gashes and the magma upwelled passively to emplace. In the Triassic, Dabie Orogen also responded actively to the Cretaceous extension, developing migmatites in 135 Ma and 125 Ma. The migmatites and the syn-tectonic granites that emplaced into it both grew NW-SE mineral stretching lineation, indicating a top-to-the-NW shear sense (Hacker et al., 1998a; Faure et al., 2003; Wang et al., 2011). The detachment fault of western Lushan Boundary took a NE-SW strike, and detached towards NW in a normal-fault manner (Lin et al., 2000; Zhu et al., 2010c). Hunan developed NE-SW semi-graben basins, such as Changsha basin, Zhajiang basin in Hengyang and Liling-Youxian basin. Zhajiang basin, with its marginal normal faulting developing in 136 Ma – 97 Ma, cut through the western edge of Hengshan Granitic Massif, which resulted in massive ductile deformation, indicating a top-to-the-NW shear sense (Zhang, 1992; Zhang, 1994; Xu et al., 1998; Li et al., 2013a).

In the early Late Cretaceous, a large amount of plutons, including the A-type granites, emplaced in the Changle–Nan'ao belt. The magnetic foliations of these granites were weakly inclined, and their magnetic lineations generally concentrated in NW-SE direction. Meanwhile, there were many intrusive NE-SW dyke swarms, probably suggesting the end of the collision between the Philippines micro-continent and the South China Block, and the beginning of NE-SW extensional regime's control over this region. Accordingly, a large number of dyke swarms, showing a preferred NE-SW direction, existed in the other southeastern coastal areas, proving the NE-SW extensional regime's control over the entire southeastern coastal areas (Dong et al., 2010; Tang et al., 2010; Chen et al., 2013). The extensional regime covered not only the land but also the East China Sea continental shelf. Man-made earthquakes studies, too, have revealed the development of NE-SW of semi-graben basins in the Late Cretaceous (Cukur et al., 2011).

In the west of Wuyi Mountain, a series of NE-SW semi-graben basins developed along the Neoproterozoic suture zone in Zhejiang and Jiangxi areas. The basins were filled with red sedimentary layers coupled with bimodal volcanites from the Late Cretaceous. Thus they are

called “Ganhang rift” (Gilder et al., 1991a; Goodell et al., 1991). In the meantime, the faulted basins developed in the Early Cretaceous continued their movement toward NW, forming the red layers in the Late Cretaceous (Shu et al., 2009b). These areas, therefore, was still controlled by the NW-SE tectonic regime.

4 A Feasible Geodynamic Model

This study proposes a feasible geodynamic evolution model of South China in the Cretaceous based on the new findings on granite emplacements and tectonic observations as well as chronological and geochemical analyses in the previous studies.

The first stage was 145-130Ma. In this period, the Paleo-Pacific subducted towards NW beneath the South China lithosphere along Japan, Taiwan and the Philippines, bringing the Philippine micro-continent gradually closer to the South China Block and evoking many continental arc volcanic activities in coastal areas of Zhejiang, Guangdong and Fujian. The southeast coast, at this time, was a Andean-type active continental margin (Li et al., 2012). In this region, magmatic rocks, typically the Nanyuan Formation volcanites and contemporary granitoid intrusive rocks, demonstrate island arc affinity (Lapierre et al., 1997; Guo et al., 2012), with enriched LREE and LILE and lack of HREE, HFSE, Nb and Ta. Farther away from subduction zone, Anhui-Hubei-Jiangxi-Hunan areas started to develop subduction-related volcanites and intrusive rocks of the same geochemical characteristics with magmatic rocks in the southeast coastal areas. At the same time, some semi-graben basins also began to grow. These changes represent a back-arc extensional regime which may be associated with the rollback at the front of subduction zone (Li and Li, 2007).

The second stage started in 130 Ma and lasted until 110 Ma. The Philippine micro-continent collided with the South China Block and brought the NW compressional tectonic regime to the southeast coast where volcanic eruptions stopped and activities of intrusive rocks also weakened correspondingly. Due to the proximity to the collision, Fujian coastal areas experienced the greatest impact, and thus developed the Changle-Nan’ao belt where the preexisting intrusive rocks was involved in pervasive compressional deformation and the Late Jurassic Duling formation volcanites and the Early Cretaceous Nanyuan Formation volcanites grew a number of

ductile shear zones in NE-SW strike. The minerals on the edge of plutons emplaced in this stage were mostly oriented. Most magnetic foliations took on NE-SW strike and steep dips. Microstructure observation also shows a NW-SE compression. The intrusive plutons then showed the geochemical property of arc affinity (Liu et al., 2012). However, due to the drag of its front, the continent - continent collision and its low density, the Philippine micro-continent discontinued the subduction and thus caused a break off of the subducting slab so that the asthenosphere underneath upwelled into the parent magma chamber of island arc（Figure 6-2b）. Therefore, the zircon EHf (t) isotopes of intrusive rocks in this stage were mostly positive, indicating the effects of depleted mantle (Li et al., 2013b). Meanwhile, at this stage, a new subduction zone probably began to form in the southeast of Philippine micro-continent and continued to subduct northwestwards. But its influence had not reached the Changle-Nanao belt. Southern China's inland areas were then controlled by the NW-SE extensional regime. Not affected by the new subduction and collision events, semi-graben basins were still growing and taking in the red layer depositions from the Early Cretaceous（Figure 6-2b）。

The third stage was 105Ma-90Ma. The collision between the Philippine Plate and the South China Block ended in the eruption of Late Cretaceous Shimaoshan Formation volcanites along the southeast coastal areas. In this period, there were many pluton and dyke emplacements. The NE-SW extension was indicated by horizontal magnetic foliation, NW-SE magnetic lineation and NE-SW dykes. The intrusive plutons then still showed the geochemical property of arc affinity. However, the rupture of the subducting slab in the last stage probably led to its break off and the massive upwelling of asthenosphere magma (Li et al., 2013b). Although the specific time of asthenosphere upwelling still remains uncertain, its height could be up to 50 km below the surface (Li et al., 2013b). The decrease of zircon E_{Hf} (t) in intrusive rocks suggest that the upwelling asthenospheric materials and the asthenospheric mantle were separated by some sort of geological process (Li et al., 2013b). Also, attention should be given to the arc affinity of Shimaoshan volcanites erupted in this stage (Lapierre et al., 1997; Guo et al., 2012), which means the newly developed subduction zone on the southeast of Philippine micro-continent had probably subducted to the Changle-Nanao tectonic belt, and separated the upwelling asthenospheric materials and the asthenosphere (Figure 6-2c). The subduction retreated from the southeast side of South China Block and the northwest side of Philippine micro-continent to the

southeast side of Philippine micro-continent, resulting in the southeastward movement of back-arc extensional center and the new semi-graben basins (Figure 6-1). Although the vast areas of northwest Wuyi Mountain were then under the control of extensional regime, they had not been affected by the new subduction and magmatic activities, thus showing no arc affinity in the newly developed basalts there (Chen et al., 2005b).

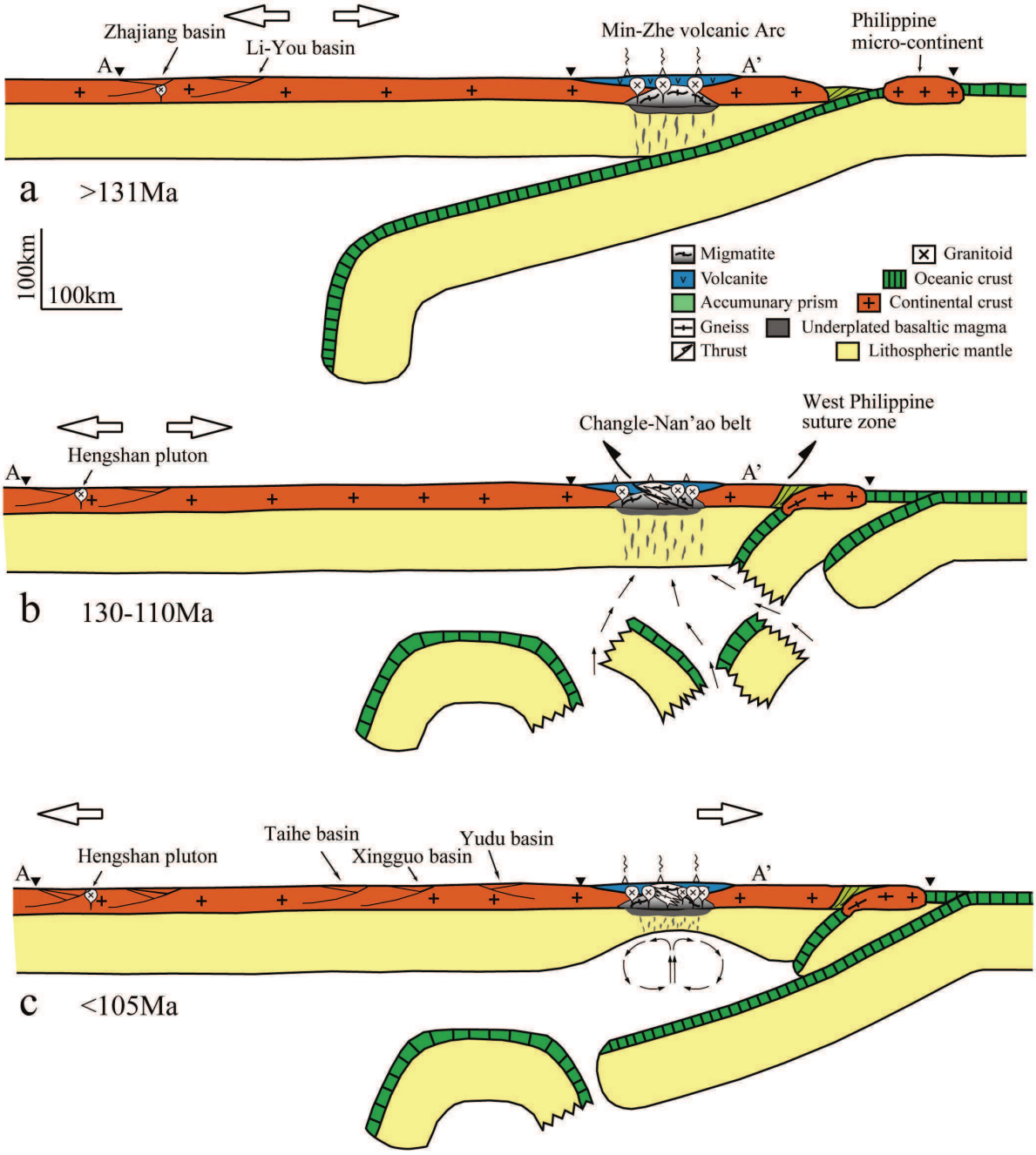

Figure 6 2: The Evolution Model of Geodynamic Background of South China in the Cretaceous

5 Summary

Based on previous studies and the comprehensive investigation on the Changle-Nan'ao belt, the Qingyang-Jiuhua Massif in southern Anhui and the Hengshan Granitic Massif in Hunan, this chapter discusses the South China tectonic evolution in the Late Mesozoic and its geodynamic bearing and then proposes a three-stage geodynamic model. (1) During the 145 Ma – 130 Ma period, the northwestward subduction of Paleo-Pacific and the Philippine micro-continent's approach to the South China Block evoked massive arc volcanic activities and developed subduction-related volcanic and intrusive rocks, forming a back-arc extensional regime; (2) in the 130 Ma – 110 Ma period, the Philippine micro-continent collided with the South China Block and brought the NW compressional tectonic regime to the southeast coastal areas, leading to the development of Changle-Nan'ao tectonic belt and a great number of deformations and ductile shear zones together; but the inland areas still remained under the control of NW-SE extensional regime; (3) during the period of 105 Ma – 90 Ma, the southeast side of Philippine micro-continent developed a new subduction zone whose subduction slab dived to the Changle-Nan'ao tectonic belt. Therefore, considering the possible previous break off of subduction slab, the asthenosphere upwelled in a large scale, causing the massive emplacements of plutons and dykes. The entire South China Block was subjected to the extensional regime at this stage.

Chapter 7 Conclusions and Perspectives

This chapter concludes the study and presents some preliminary ideas for further research. It begins with a review of the present research purpose and corresponding strategy and methods. And then major results and findings are stated in brief, which is followed by the author's understandings of the Late Mesozoic geodynamic background in the South China as well as broad propositions for future research.

1 Research Purpose and Strategy

The Late Mesozoic South China has undergone extensive crustal deformation, accompanied by a large number of granitoid pluton emplacements, formations of half-graben basins and eruptions of volcanic rocks. This paper attempts to describe tectonic deformation and evolution characteristics of some typical regions in the South China Block, seeking to understand the relationship between deformation and tectonic regime and trying to build its possible geodynamic model as well. The specific research questions include: (1) What are the emplacement mechanisms of Late Mesozoic plutons in the South China? (2) What are the regional tectonic regimes at the time of pluton emplacements? (3) What are the differences and connections of deformations and tectonic regimes between various regions in the South China? (4) How did the tectonic regimes develop in these regions all through the Late Mesozoic period? (5) Is it possible to establish a geodynamic model to explain the South China tectonic deformation and evolution in the Late Mesozoic?

Previous studies indicate that the Late Mesozoic tectonic evolution of South China is probably subjected to the Paleo-Pacific plate subduction toward Eurasia, and that the location of the Paleo-Pacific subduction trench and the suture formed by subsequent closure are in Japan-Taiwan Island-Philippines areas. Others argue that, in the Late Mesozoic, the Paleo-Pacific was divided into two large plates which subducted NNW and WSW respectively. The Mid-Ocean Ridge between them subducted westwards to the Yangtze River of South China. But these ideas still need further supporting tectonic research evidence, in particular

multi-disciplinary evidence, so as to better the understanding of South China tectonic features and evolution processes in the Late Mesozoic.

In response to these questions, the present study selected three key areas of South China, based on the subduction system proposed by the previous research, to implement multi-disciplinary investigations. The three key regions are: (1) the Fujian coastal areas which developed the Changle-Nan'ao belt and, as the closest region to the presumable Paleo-Pacific subduction zone, experienced the greatest impact; (2) the Lower Yangtze Area beneath where the Mid-Ocean Ridge is presumed to have subducted westwards; (3) the Hunan which was selected to explore the corresponding inland structure under the subduction system due to its distance to the subduction zone.

As the major research objects, one or more plutons and their country rocks were chosen in each of the three regions. A number of research methods were employed, such as field structural observation, microscopic observation in laboratory, magnetic fabric measurement, paleomagnetism, gravity modeling, Al-total content in Amphibole geobarometry calculation and monazite U-Th-Pb microprobe dating. According to the tectonic characteristics of each region, the study has conducted systematic research on the deformation features of the plutons and their country rocks, the emplacement mechanisms of the plutons as well as the regional tectonic regimes, and established a feasible geodynamic model in combination of geology, geochemistry, geophysics and chronology.

2 Major Results and Findings

The findings of field structural observation and other multi-disciplinary research are listed as follows:

(1)In the Changle-Nan’ao belt, the foliations of the Deformed Volcanite Unit, the gneissosities of the Gneiss Unit and the folds of these foliations were formed in a NW compressional event in about 130 Ma – 110 Ma. The Gneissic Unit which is of higher degree of metamorphism, therefore, thrusted over the Deformed Volcanite Unit, completing the process of exhumation from depth to shallow tectonic level. Because of the compression, volcanic eruptions subsided for about 25 My, and the pluton emplacement was also lessened. The magnetic

foliations of the syn-tectonic pluton, therefore, ran perpendicular to the compression direction. The microstructure of plutons also left many evidences for this compression.

(2) After 105Ma, the NW-SE weak regional tectonic regime started to influence the Changle–Nan'ao belt; owing to the opening of surface crust cracks and the formation of magma injection conduits, there were enormous emplacements of isotropic granite plutons and eruptions of undeformed Shimaoshan Formation volcanites in the Late Cretaceous. The magnetic foliations of the intrusive plutons in this period stayed at a horizontal level and the lineations were concentrated in a nearly horizontal NW-SE direction, pointing to the trend of extension.

(3) The collision between the West Philippine micro-continent and the South China Block was responsible for the NW thrust of Changle-Nan'ao belt which combined with the West Philippine Ophiolite Suture Zone to form a thrust-back thrust fault couple located on the Andean-type continent margin of the South China Block.

(4) Comprehensive multidisciplinary research shows that in the southern Anhui, the Qingyang-Jiuhua Massif emplaced in a permissive method. Magma injected vertically into brittle deformation domain in shallow crust which was formed by weak regional tectonic extension.

(5) The magma supply roots of Qingyang-Jiuhua plutons are arranged in the NE-SW trend, suggesting that during the period of emplacement in about 140Ma-130Ma, this region was still subjected to the NE-SW extensional regime.

(6) The Paleomagnetism study of Qingyang-Jiuhua plutons indicates that no strong strike-slip movements occurred within this region and the South China Block in large.

(7) The Baishifeng Two-Mica granite of Hengshan Massif has gently dipping magnetic foliations. At its boundary with the Nanyue plutons, its magnetic foliations parallel to the boundary, inclining to the Nanyue plutons. The pre-existing magnetic fabrics of Nanyue plutons remained intact. The emplacement mechanism of Baishifeng plutons, therefore, emplaced in a permissive way with magma injecting vertically.

(8) The magnetic lineations of Baishifeng Two-Mica Granitic Pluton were concentrated in the WNW-ESE direction, indicating the control of WNW-ESE extensional regime over this region in 150 Ma.

3 Conclusions: the South China Tectonic Evolution and its Geodynamic Background

3.1 The Late Mesozoic Tectonic Evolution in the East of South China Block

Based on our investigation on them and previous research on basins, faults and geochronology, we have reconstructed the history of the Late Mesozoic tectonic evolution. To be specific, there is a fairly large tectonic regime difference between the Changle-Nan'ao Belt of Fujian coastal areas in the Southeast China and the inland Anhui and Hunan. During the period from about 130 Ma to 110 Ma, Changle-Nan'ao Belt developed under the control of the NW compressional tectonic regime, whereas the southern Anhui was subjected to the weak NW-SE extensional regime in the Early Cretaceous, and the Hengshan Granitic Massif in Hunan was controlled by the strong WNW-ESE extensional regime from the transition period between the Jurassic and the Cretaceous to the Early Cretaceous. Though the tectonic regimes are different, arc affinity is displayed in the Early Cretaceous volcanites erupted in both Fujian coastal areas and the southern Anhui.

In the Late Cretaceous, the Fujian coastal areas were characterized by Shimaoshan Formation volcanic eruptions, massive isotropic granite emplacements and NE-SW dyke emplacements, indicating the beginning of NE-SW extensional regime. In view of the arc affinity of the erupted volcanites along the Fujian coastal areas, the dominating extensional regime should have been related to the subduction of the Paleo-Pacific Plate. Southern Anhui and Hunan, however, developed on the basis of Early Cretaceous faulted basins, and then continued the growth in the Late Cretaceous, suggesting the continued dominance of NW-SE extensional tectonic regime over this region. Unlike those from the Early Cretaceous, the volcanites erupted then no longer had arc affinity, which is distinct with the extensional regime of this region from that in the Fujian coastal areas.

3.2 The Feasible Geodynamic Background

(1) From 145 Ma to 130 Ma, the Paleo-Pacific that carried the Philippine micro-continent subducted northwestwards and approached the South China Block, evoking massive arc volcanic

activities and developing subduction-related volcanites and intrusive rocks along the Zhejiang-Fujian-Guangdong areas. The South China Block, thus, formed Andean-type active continental margin, and the back-arc extensional tectonic regime, coupled with some NE-SW faulted basins, began to develop;

(2) In the 130 Ma – 110 Ma period, the collision between the Philippine micro-continent and the South China Block brought the NW compressional tectonic regime to the southeast coast, developing the Changle-Nan'ao belt and resulting in many deformations and ductile shear zones in the crust. Under the lithosphere of South China Block, the subduction slab continued to subduct, but the Philippine micro-continent could not deepen its subduction, leading to the breakoff of the subduction slab and the new subduction zone's development to the SE side of the Philippine micro-continent; at this time, the southern inland areas were still under the control of the NW-SE extensional regime；

(3) In the 105 Ma – 90 Ma period, with the end of the collision between the South China Block and the Philippine micro-continent, the new subduction slab that grew on the SE side of the Philippine micro-continent may have arrived beneath the lithosphere of the Fujian coast, and asthenospheric materials upwelled due to the subduction slab breakoff. The Fujian coastal areas, thus came under the control of NW-SE extensional tectonic regime, and prompted the eruptions of volcanites with arc affinity and the enormous emplacements of plutons and dykes. As the subduction zone retreated southeastwards, the new semi-graben basins in southern inland moved southeastwards as well. The new subduction slab never went beyond the Wuyi Mountain. Thus, its northwest side in the southern inland was still controlled by the NW-SE extensional regime, but the volcanites erupted then did not show any arc affinity.

4 Problems and Implications

Although this paper has made advancement in the research of deformation characteristics of the east of South China, regional tectonic regimes and their geodynamic model, some questions still need further exploration. For instance, as far as the geodynamics is concerned, the vast inland areas to the west of Wuyi Mountain was controlled by the same NW-SE extensional regime in the Late Cretaceous as the Fujian coastal areas whose regime had a close bearing on

the extension and subduction. However, the volcanites found in the inland South China show no arc affinity. Then, what was the reason for its extension? Since the effects of subduction were confined to the east of Wuyi Mountain, why was the entire South China subjected to the extensional regime of a unified NW-SE strike? In addition, southern Anhui and Hunan were both affected by the arc extension, but why in different degrees? These questions need to be further investigated by means of rheological and geophysical study on the lithospheric scale. In terms of methodology in this study, it has proved to be effective to explore the regional tectonic regime based on pluton emplacement. However, by comparing the ways that plutons emplaced in the three regions, it is found that the magnetic fabrics of Fujian coastal plutons and Hunan Baishifeng Two-Mica Plutons are good reflections of the tectonic regimes at the time of their emplacements, but the Qingyang-Jiuhua Massif from southern Anhui are an exception. Their magnetic fabrics only reveal information on magma upwelling. Moreover, since the Southern Mountain plutons were partly affected by post-tectonic deformation, their limited deformation degrees make it difficult to distinguish whether the detected magnetic fabrics were the primary fabrics at the time of emplacement or the secondary fabrics resulted from later deformation. Therefore, as an effective method to discover the regional tectonic regime, the formation and transformation of pluton magnetic fabric is a promising research direction that needs further study.

5 Summary

In order to identify the regional tectonic regimes and establish a feasible geodynamic model of the eastern South China Block in the Late Mesozoic, this study collected a number of pluton samples from three regions of different tectonic positions—Fujian coastal areas, Lower Yangtze Area, and Hunan. The regional geological observation and emplacement mechanism study reveal new understandings on tectonic regimes in the Early Cretaceous and Late Cretaceous periods. It has been found that the subduction of Paleo-Pacific Plate has greatly impacted the tectonic evolution of South China in the Late Mesozoic, and questions remain on the existence of large-displacement NE-SW strike-slip events along the Fujian coastal areas in the Cretaceous. Also, this study has established a geodynamic model in combination of structural geology,

geochemistry, geophysics and geochronological data.

References

AHBGMR, 1987, Regional geology of Anhui Province: Beijing, China, geological plublishing house, 721 p.

Almasco, J., Rodolfo, K., Fuller, M., and Frost, G., 2000, Paleomagnetism of Palawan, Philippines: Journal of Asian Earth Sciences, v. 18, p. 369-389.

Aranguren, A., Cuevas, J., Tubia, J.M., Roman-Berdiel, T., Casas-Sainz, A., and Casas-Ponsati, A., 2003, Granite laccolith emplacement in the Iberian arc: AMS and gravity study of the La Tojiza pluton (NW Spain): Journal of the Geological Society, v. 160, p. 435-445.

Bassin, C., Laske, G., and Masters, G., 2000, The Current Limits of Resolution for Surface Wave Tomography in North America: EOS Trans AGU, v. 81, p.??

Borradaile, G.J., and Henry, B., 1997, Tectonic applications of magnetic susceptibility and its anisotropy: Earth-Science Reviews, v. 42, p. 49-93.

Bouchez, J.L., and Gleizes, G., 1995, 2-stage deformation of the Mont-Louis-Andorra granite pluton (Variscan Pyrenees) inferred from magnetic-susceptibility anisotropy: Journal of the Geological Society, v. 152, p. 669-679.

Charles, N., Chen, Y., Augier, R., Gumiaux, C., Lin, W., Faure, M., Monie, P., Choulet, F., Wu, F.Y., Zhu, R.X., and Wang, Q.C., 2011, Palaeomagnetic constraints from granodioritic plutons (Jiaodong Peninsula): New insights on Late Mesozoic continental extension in Eastern Asia: Physics of the Earth and Planetary Interiors, v. 187, p. 276-291.

Charles, N., Faure, M., and Chen, Y., 2009, The Montagne Noire migmatitic dome emplacement (French Massif Central): new insights from petrofabric and AMS studies: Journal of Structural Geology, v. 31, p. 1423-1440.

Charles, N., Gumiaux, C., Augier, R., Chen, Y., Zhu, R., and Lin, W., 2010, Metamorphic Core Complexes vs. synkinematic plutons in continental extension setting: Insights from key structures (Shandong Province, eastern China): Journal of Asian Earth Sciences.

Charvet, J., Faure, M., Xu, J.W., Zhu, G., Tong, W.X., and Lin, S.F., 1990, The Changle-Nanao tectonic zone, south east china: Comptes Rendus De L Academie Des Sciences Serie Ii, v.

310, p. 1271-1278.

Charvet, J., Shu, L., Faure, M., Choulet, F., Wang, B., Lu, H., and Le Breton, N., 2010, Structural development of the Lower Paleozoic belt of South China: Genesis of an intracontinental orogen: Journal of Asian Earth Sciences, v. 39, p. 309-330.

Charvet, J., Shu, L.S., Shi, Y.S., Guo, L.Z., and Faure, M., 1996, The building of south China: Collision of Yangzi and Cathaysia blocks, problems and tentative answers: Journal of Southeast Asian Earth Sciences, v. 13, p. 223-235.

Chen, B., 1997, Petrographic Evidences and Tectonic Significance for Two Phases of Metamorphism in Sillimanite- and Garnet- Bearing Mica Schists of Pintan-Dongshan Metamorphic Zone of Eastern Fuj ian, China: Acta Petrologica Sinica, v. 13.

Chen, C.H., Lee, C.Y., and Shinjo, R.I., 2008, Was there Jurassic paleo-Pacific subduction in South China?: Constraints from Ar-40/Ar-39 dating, elemental and Sr-Nd-Pb isotopic geochemistry of the Mesozoic basalts: Lithos, v. 106, p. 83-92.

Chen, J.F., Yu, G., Yang, G., and Yang, S.H., 2005a, A Geochronological framework of Late Mesozoic magmatism and metallogenesis in the Lower Yangtze valley, Anhui Province: Anhui Geology, v. 15, p. 161-169.

Chen, J.F., Zhou, T.X., and Foland, K.A., 1985, 40Ar/39Ar and Rb-Sr geochronology of the Qingyang batholith, Anhui Province, China: Geochemistry, v. 4, p. 220-235.

Chen, J.F., Zhou, T.X., Li, X.M., Foland, K.A., Huang, C.Y., and Lu, W., 1993, Sr and Nd isotopic constraints on source regions of the intermediate and acid intrusions from southern Anhui Province: Geochimica, v. 1993, p. 261-268.

Chen, N.-h., Dong, J.-j., Chen, J.-y., Dong, C.-w., and Shen, Z.-y., 2013, Geometry and Emplacement of the Late Cretaceous Mafic Dyke Swarms on the Islands in Zhejiang Province, Southeast China: Insights from High-Resolution Satellite Images: Journal of Asian Earth Sciences.

Chen, P., Kong, X., Wang, Y., Ni, Q., Zhang, B., and Ling, H., 1999, Rb-Sr isotopic dating and significance of early Yanshanian bimodal volcanic-intrusive complex from south Jiangxi Province: Geological journal of China universities, v. 5, p. 378-383.

Chen, W.F., Chen, P.R., Xu, X.S., and Zhang, M., 2005b, Geochemical characteristics of Cretaceous basaltic rocks in South China and constraints on Pacific plate subduction:

Science in China Series D-Earth Sciences, v. 48, p. 2104-2117.

Chen, W.S., Yang, H.C., Wang, X., and Huang, H., 2002, Tectonic setting and exhumation history of the Pingtan-Dongshan Metamorphic Belt along the coastal area, Fujian Province, Southeast China: Journal of Asian Earth Sciences, v. 20, p. 829-840.

Cocherie, A., and Albarede, F., 2001, An improved U-Th-Pb age calculation for electron microprobe dating of monazite: Geochimica et Cosmochimica Acta, v. 65, p. 4509-4522.

Cocherie, A., Legendre, O., Peucat, J., and Kouamelan, A., 1998, Geochronology of polygenetic monazites constrained by in situ electron microprobe Th-U-total lead determination: implications for lead behaviour in monazite: Geochimica et Cosmochimica Acta, v. 62, p. 2475-2497.

Cogné, J.P., 2003, PaleoMac: a Macintosh™ application for treating paleomagnetic data and making plate reconstructions: Geochemistry Geophysics Geosystems, v. 4, p. 1007-1014.

Cong, B.L., and Wang, Q.C., 1999, The New advantage in ultrahigh pressure metamorphic region in Dabie-Sulu Mountains: Chinese Science Bulletin, v. 44, p. 1127-1141.

Cui, J.J., Zhang, Y.Q., Dong, S.W., Jahn, B.M., Xu, X.B., and Ma, L.C., 2013, Zircon U-Pb geochronology of the Mesozoic metamorphic rocks and granitoids in the coastal tectonic zone of SE China: Constraints on the timing of Late Mesozoic orogeny: Journal of Asian Earth Sciences, v. 62, p. 237-252.

Cukur, D., Horozal, S., Kim, D.C., and Han, H.C., 2011, Seismic stratigraphy and structural analysis of the northern East China Sea Shelf Basin interpreted from multi-channel seismic reflection data and cross-section restoration: Marine and Petroleum Geology, v. 28, p. 1003-1022.

Deng, P., Shu, L., Yang, M., Guo, Y., and Yu, X., 2003, Geological features and dynamic evolution of the Ganjiang fault in Jiangxi Province: Geological review, v. 49, p. 113-122.

Dong, C.W., Li, W.X., Chen, X.M., Xu, X.S., and Zhou, X.M., 1998, Late Mesozoic magma mixing in SE-Fujian - Petrologic evidence from the Pingtan igneous complex: Progress in Natural Science, v. 8, p. 196-201.

Dong, C.W., Yan, Q., Zhang, D.R., Du, Z.Y., and Zhu, G.Q., 2010, Late Mesozoic extension in the coastal area of Zhejiang and Fujian provinces: A petrologic indicator from the Dongji Island mafic dike swarms: Acta Petrologica Sinica, v. 26, p. 1195-1203.

Dong, C.W., Zhang, D.R., Xu, X.S., Yan, Q., and Zhu, G.Q., 2006, SHRIMP U-Pb Dating and lithogeochemistry of basic-intermediate dike swarms from Jinjiang, Fujian Province: Acta Petrologica Sinica, v. 22, p. 1696-1702.

Fan, C., and Chen, P., 2000, Geochemical characteristics and tectonic implication of Beitou A-type granitic intrusive in South Jiangxi Province: Geochimica, v. 29, p. 358-366.

Faure, M., Lin, W., Monie, P., and Meffre, S., 2008, Palaeozoic collision between the North and South China blocks, Triassic intracontinental tectonics, and the problem of the ultrahigh-pressure metamorphism: Comptes Rendus Geoscience, v. 340, p. 139-150.

Faure, M., Lin, W., Scharer, U., Shu, L.S., Sun, Y., and Arnaud, N., 2003, Continental subduction and exhumation of UHP rocks. Structural and geochronological insights from the Dabieshan (East China): Lithos, v. 70, p. 213-241.

Faure, M., Lin, W., Shu, L.S., Sun, Y., and Scharer, U., 1999, Tectonics of the Dabieshan (eastern China) and possible exhumation mechanism of ultra high-pressure rocks: Terra Nova, v. 11, p. 251-258.

Faure, M., Lin, W., and Sun, Y., 1998, Doming in the southern foreland of the Dabieshan (Yangtse block, China): Terra Nova, v. 10, p. 307-311.

Faure, M., and Pons, J., 1991, Crustal thinning recorded by the shape of the Namurian-Westphalian leucogranite in the variscan belt of the northwest massif-central, France: Geology, v. 19, p. 730-733.

Faure, M., Shu, L.S., Wang, B., Charvet, J., Choulet, F., and Monie, P., 2009, Intracontinental subduction: a possible mechanism for the Early Palaeozoic Orogen of SE China: Terra Nova, v. 21, p. 360-368.

Faure, M., Sun, Y., Shu, L., Monie, P., and Charvet, J., 1996, Extensional tectonics within a subduction-type orogen. The case study of the Wugongshan dome (Jiangxi Province, southeastern China): Tectonophysics, v. 263, p. 77-106.

Fisher, R., 1953, Dispersion on a sphere: Proceedings of the Royal Society of London Series a-Mathematical and Physical Sciences, v. 217, p. 295-305.

FJBGMR, 1985, Regional geology of Fujian Province: Beijing, geological plublishing house.

Fu, Y., Ren, J., Chen, T., and Liu, Z., 1989, 40Ar/39Ar isotopic dating of migmatic granite and granulitite from the jinjiang area, fujian: Geological Review, v. 35, p. 552-557.

Gilder, S.A., Gill, J., Coe, R.S., Zhao, X.X., Liu, Z.W., Wang, G.X., Yuan, K.R., Liu, W.L., Kuang, G.D., and Wu, H.R., 1996, Isotopic and paleomagnetic constraints on the Mesozoic tectonic evolution of south China: Journal of Geophysical Research-Solid Earth, v. 101, p. 16137-16154.

Gilder, S.A., Keller, G.R., Luo, M., and Goodell, P., 1991a, Eastern Asia and the western Pacific timing and spatial distribution of rifting in China: Tectonophysics, v. 197, p. 225-243.

Gilder, S.A., Keller, G.R., Luo, M., and Goodell, P.C., 1991b, Timing and spatial distribution of rifting in China: Tectonophysics, v. 197, p. 225-243.

Goodell, P.C., Gilder, S., and Fang, X., 1991, A preliminary description of the Gan-Hang failed rift, southeastern China: Tectonophysics, v. 197, p. 245-255.

GDBGMR, 1988, Regional geology of Guangdong Province: Beijing, China, Geological Plublishing House.

GXBGMR, 1984, Regional geology of Guangxi Province: Beijing, China, Geological Plublishing House.

Guo, F., Fan, W.M., Li, C.W., Zhao, L., Li, H.X., and Yang, J.H., 2012, Multi-stage crust-mantle interaction in SE China: Temporal, thermal and compositional constraints from the Mesozoic felsic volcanic rocks in eastern Guangdong-Fujian provinces: Lithos, v. 150, p. 62-84.

Guo, L., Lu, H., Shi, Y., Ma, R., Sun, Y., Shu, L., Jia, D., Zhang, Q., Charvet, J., and Faure, M., 1996, On the Meso-Neoproterozoic Jiangnan island arc: its kinematics and dynamics: Geological Jour. of Universities, v. 2, p. 1-13.

Hacker, B.R., Ratschbacher, L., Webb, L., Ireland, T., Walker, D., and Shuwen, D., 1998a, U/Pb zircon ages constrain the architecture of the ultrahigh-pressure Qinling-Dabie Orogen, China: Earth and Planetary Science Letters, v. 161, p. 215-230.

Hacker, B.R., Ratschbacher, L., Webb, L., Ireland, T., Walker, D., and Shuwen, D., 1998b, U/Pb zircon ages constrain the architecture of the ultrahigh-pressure Qinling–Dabie Orogen, China: Earth and Planetary Science Letters, v. 161, p. 215-230.

Hammarstrom, J.M., and Zen, E.A., 1986, ALUMINUM IN HORNBLENDE - AN EMPIRICAL IGNEOUS GEOBAROMETER: American Mineralogist, v. 71, p. 1297-1313.

Harrowfield, M.J., and Wilson, C.J.L., 2005, Indosinian deformation of the Songpan Garze Fold

Belt, northeast Tibetan Plateau: Journal of Structural Geology, v. 27, p. 101-117.

HNBGMR, 1987, Regional geology of Anhui Province: Beijing, China, Geological Plublishing House.

Hollister, L.S., Grissom, G.C., Peters, E.K., Stowell, H.H., and Sisson, V.B., 1987, CONFIRMATION OF THE EMPIRICAL CORRELATION OF AL IN HORNBLENDE WITH PRESSURE OF SOLIDIFICATION OF CALC-ALKALINE PLUTONS: American Mineralogist, v. 72, p. 231-239.

Hsu, K.J., Sun, S., and Li, J.L., 1988, HUANAN ALPS, NOT SOUTH CHINA PLATFORM: Scientia Sinica Series B-Chemical Biological Agricultural Medical & Earth Sciences, v. 31, p. 109-119.

Hu, X., 1994, Geochronology of Lower Proterozoic Badu Group, southwestern Zhejiang province: Geochimica, v. 23, p. 18-24.

Huchon, P., Nguyen, T.N.H., and Chamotrooke, N., 1998, Finite extension across the South Vietnam basins from 3D gravimetric modelling: relation to South China Sea kinematics: Marine and Petroleum Geology, v. 15, p. 619-634.

Hutchison, C.S., 2004, Marginal basin evolution: the southern South China Sea: Marine and Petroleum Geology, v. 21, p. 1129-1148.

Jahn, B.M., 1974, Mesozoic Thermal Events in Southeast China: Nature, v. 248, p. 480-483.

Jelinek, V., 1981, Characterization of the magnetic fabric of rocks: Tectonophysics, v. 79, p. T63-T67.

Joly, A., Chen, Y., Faure, M., and Martelet, G., 2007, A multidisciplinary study of a syntectonic pluton close to a major lithospheric-scale fault - Relationships between the Montmarault granitic massif and the Sillon Houiller Fault in the Variscan French Massif Central: 1. Geochronology, mineral fabrics, and tectonic implications: Journal of Geophysical Research-Solid Earth, v. 112.

Joly, A., Faure, M., Martelet, G., and Chen, Y., 2009, Gravity inversion, AMS and geochronological investigations of syntectonic granitic plutons in the southern part of the Variscan French Massif Central: Journal of Structural Geology, v. 31, p. 421-443.

JXBGMR, 1984, Regional geology of Jiangxi Province: Beijing, China, Geological Plublishing House.

Kirschvink, J.L., 1980, The least squares line and the analysis of palaeomagnetic data: Geophysical Journal of the Royal Astronomical Society, v. 62, p. 699-718.

Lapierre, H., Jahn, B.M., Charvet, J., and Yu, Y.W., 1997, Mesozoic felsic arc magmatism and continental olivine tholeiites in Zhejiang province and their relationship with the tectonic activity in southeastern China: Tectonophysics, v. 274, p. 321-338.

Leake, B.E., Woolley, A.R., Birch, W.D., Burke, E.A.J., Ferraris, G., Grice, J.D., Hawthorne, F.C., Kisch, H.J., Krivovichev, V.G., Schumacher, J.C., Stephenson, N.C.N., and Whittaker, E.J.W., 2004, Nomenclature of amphiboles: additions and revisions to the International Mineralogical Association's amphibole nomenclature: European Journal of Mineralogy, v. 16, p. 191-196.

Lepvrier, C., Maluski, H., Van Tich, V., Leyreloup, A., Thi, P.T., and Van Vuong, N., 2004, The Early Triassic Indosinian orogeny in Vietnam (Truong Son Belt and Kontum Massif); implications for the geodynamic evolution of Indochina: Tectonophysics, v. 393, p. 87-118.

Li, J.-W., Zhao, X.-F., Zhou, M.-F., Ma, C.-Q., De Souza, Z.S., and Vasconcelos, P., 2009a, Late Mesozoic magmatism from the Daye region, eastern China: U–Pb ages, petrogenesis, and geodynamic implications: Contributions to Mineralogy and Petrology, v. 157, p. 383-409.

Li, J.H., Zhang, Y.Q., Dong, S.W., Su, J.b., Li, Y., Cui, J.J., and Shi, W., 2013a, The Hengshan low-angle normal fault zone: structural and geochronological constraints on the Late Mesozoic crustal extension in South China: Tectonophysics, v. 606, p. 97-115.

Li, J.W., Zhou, M.F., Li, X.F., Fu, Z.R., and Li, Z.J., 2001, The Hunan-Jiangxi strike-slip fault system in southern China: southern termination of the Tan-Lu fault: Journal of Geodynamics, v. 32, p. 333-354.

Li, S., Zhao, G., Zhang, G., Liu, X., Dong, S., Wang, Y., Liu, X., Suo, Y., Dai, L., and Jin, C., 2010a, Not all folds and thrusts in the Yangtze foreland thrust belt are related to the Dabie Orogen: Insights from Mesozoic deformation south of the Yangtze River: Geological Journal, v. 45, p. 650-663.

Li, W., Zhou, X., and Li, X., 2003a, U-Pb and 40Ar/39Ar dating of deformed igneous rocks from the Changle-Nan'ao fault: Chinese Journal of Geology, v. 38, p. 22-30.

Li, X., Zhou, G., Zhao, J., Fanning, C., and Compston, W., 1994, SHRIMP ion microprobe zircon U-Pb age and Sm-Nd isotopic characteristics of the NE Jiangxi ophiolite and its

tectonic implications: Chinese Journal of Geochemistry, v. 13, p. 317-325.

Li, X.H., 1999, U-Pb zircon ages of granites from the southern margin of the Yangtze Block: timing of Neoproterozoic Jinning: Orogeny in SE China and implications for Rodinia Assembly: Precambrian Research, v. 97, p. 43-57.

Li, X. H., 2000, Cretaceous magmatism and lithospheric extension in Southeast China: Journal of Asian Earth Sciences, v. 18, p. 293-305.

Li, X.H., Chen, Z., Liu, D.Y., and Li, W.X., 2003b, Jurassic gabbro-granite-syenite suites from Southern Jiangxi province, SE China: Age, origin, and tectonic significance: International Geology Review, v. 45, p. 898-921.

Li, X.H., Li, W.X., Li, Z.X., Lo, C.H., Wang, J., Ye, M.F., and Yang, Y.H., 2009b, Amalgamation between the Yangtze and Cathaysia Blocks in South China: Constraints from SHRIMP U-Pb zircon ages, geochemistry and Nd-Hf isotopes of the Shuangxiwu volcanic rocks: Precambrian Research, v. 174, p. 117-128.

Li, X.H., Li, W.X., Wang, X.C., Li, Q.L., Liu, Y., Tang, G.Q., Gao, Y.Y., and Wu, F.Y., 2010b, SIMS U-Pb zircon geochronology of porphyry Cu-Au-(Mo) deposits in the Yangtze River Metallogenic Belt, eastern China: Magmatic response to early Cretaceous lithospheric extension: Lithos, v. 119, p. 427-438.

Li, X.H., Li, Z.X., Li, W.X., Liu, Y., Yuan, C., Wei, G.J., and Qi, C.S., 2007, U-Pb zircon, geochemical and Sr-Nd-Hf isotopic constraints on age and origin of Jurassic I- and A-type granites from central Guangdong, SE China: A major igneous event in response to foundering of a subducted flat-slab?: Lithos, v. 96, p. 186-204.

Li, Z.-X., Li, X.-H., Wartho, J.-A., Clark, C., Li, W.-X., Zhang, C.-L., and Bao, C., 2010c, Magmatic and metamorphic events during the early Paleozoic Wuyi-Yunkai orogeny, southeastern South China: New age constraints and pressure-temperature conditions: Geological Society of America Bulletin, v. 122, p. 772-793.

Li, Z., Qiu, J.S., and Yang, X.M., 2013b, A review of the geochronology and geochemistry of late Yanshanian (Cretaceous) plutons along the Fujian coastal area of southeastern China: Implications for magma evolution related to slab break-off and rollback in the Cretaceous: Earth-Science Reviews, v. in press.

Li, Z.X., and Li, X.H., 2007, Formation of the 1300-km-wide intracontinental orogen and

postorogenic magmatic province in Mesozoic South China: A flat-slab subduction model: Geology, v. 35, p. 179-182.

Li, Z.X., Li, X.H., Chung, S.L., Lo, C.H., Xu, X.S., and Li, W.X., 2012, Magmatic switch-on and switch-off along the South China continental margin since the Permian: Transition from an Andean-type to a Western Pacific-type plate boundary: Tectonophysics, v. 532, p. 271-290.

Lin, W., Charles, N., Chen, Y., Chen, K., Faure, M., Wu, L., Wang, F., Li, Q., Wang, J., and Wang, Q., 2013a, Late Mesozoic compressional to extensional tectonics in the Yiwulüshan massif, NE China and their bearing on the Yinshan–Yanshan orogenic belt Part II: Anisotropy of magnetic susceptibility and gravity modeling: Gondwana Research, v. 2013, p. 78-94.

Lin, W., Faure, M., Chen, Y., Wenbin Ji a, Wang, F., Wu, L., Charles, N., Wang, J., and Wang, Q., 2013b, Late Mesozoic compressional to extensional tectonics in the Yiwulüshan massif, NE China and its bearing on the evolution of the Yinshan–Yanshan orogenic belt Part I: Structural analyses and geochronological constraints: Gondwana Research, v. 2013, p. 54-77.

Lin, W., Faure, M., Lepvrier, C., Chen, Z., Chu, Y., Wang, Q., N'guyen Van Vuong, and Van Tich Vu, 2011, The Early Mesozoic thrust and folds sheet structure along the southern margin of South China Block and its geodynamic: Chinese Journal of Geology, v. 46, p. 134-145.

Lin, W., Faure, M., Monie, P., Scharer, U., Zhang, L.S., and Sun, Y., 2000, Tectonics of SE China: New insights from the Lushan massif (Jiangxi Province): Tectonics, v. 19, p. 852-871.

Lin, W., Faure, M., Sun, Y., Shu, L.S., and Wang, Q.C., 2001, Compression to extension switch during the Middle Triassic orogeny of Eastern China: the case study of the Jiulingshan massif in the southern foreland of the Dabieshan: Journal of Asian Earth Sciences, v. 20, p. 31-43.

Lin, W., Wang, Q.C., and Chen, K., 2008, Phanerozoic tectonics of south China block: New insights from the polyphase deformation in the Yunkai massif: Tectonics, v. 27.

Ling, M.X., Wang, F.Y., Ding, X., Hu, Y.H., Zhou, J.B., Zartman, R.E., Yang, X.Y., and Sun, W.D., 2009, Cretaceous ridge subduction along the Lower Yangtze river belt, Eastern China: Economic Geology, v. 104, p. 303-321.

Liu, B.J., 1994, Atlas of Lithofacies and Paleogeography of China: Beijing, China, Science Press.

Liu, Q., Yu, J.H., Wang, Q., Su, B., Zhou, M.F., Xu, H., and Cui, X., 2012, Ages and geochemistry of granites in the Pingtan-Dongshan Metamorphic Belt, Coastal South China: New constraints on Late Mesozoic magmatic evolution: Lithos, v. 150, p. 268-286.

Mao, J., Xie, G., Duan, C., Pirajno, F., Ishiyama, D., and Chen, Y., 2011, A tectono-genetic model for porphyry-skarn-stratabound Cu-Au-Mo-Fe and magnetite-apatite deposits along the Middle-Lower Yangtze River Valley, Eastern China: Ore Geology Reviews, v. 43, p. 294-314.

Mattauer, M., Matte, P., Malavieille, J., Tapponnier, P., Maluski, H., Qin, X.Z., Lun, L.Y., and Qin, T.Y., 1985a, Tectonics of the Qinling belt: Build-up and evolution of eastern Asia: Nature, v. 317, p. 496-500.

Mattauer, M., Matte, P., Malavieille, J., Tapponnier, P., Maluski, H., Xu, Z.Q., Lu, Y.L., and Tang, Y.Q., 1985b, Tectonics of the Qinling belt - buildup and evolution of eastern Asia: Nature, v. 317, p. 496-500.

Mercier, J.L., Hou, M.J., Vergely, P., and Wang, Y.M., 2007, Structural and stratigraphical constraints on the kinematics history of the southern Tan-Lu fault zone during the mesozoic Anhui Province, China: Tectonophysics, v. 439, p. 33-66.

Mingram, J., Schettler, G., Nowaczyk, N., Luo, X.J., Lu, H.Y., Liu, J.Q., and Negendank, J.F.W., 2004, The Huguang maar lake - a high-resolution record of palaeoenvironmental and palaeoclimatic changes over the last 78,000 years from South China: Quaternary International, v. 122, p. 85-107.

Myers, J.S., 1975, Cauldron subsidence and fluidization: mechanisms of intrusion of coastal batholith of Peru into its own volcanic ejecta: Geological Society of America Bulletin, v. 86, p. 1209-1220.

Parrish, R.R., 1990, U-Pb dating of monazite and its application to geological problems: Canadian Journal of Earth Sciences, v. 27, p. 1431-1450.

Paterson, S.R., Pignotta, G.S., and Vernon, R.H., 2004, The significance of microgranitoid enclave shapes and orientations: Journal of Structural Geology, v. 26, p. 1465-1481.

Paterson, S.R., Vernon, R.H., and Tobisch, O.T., 1989, a review of criteria for the indentification of magmatic and tectonic foliations in granitoids: Journal of Structural Geology, v. 11, p. 349-363.

Pitcher, W.S., 1979, NATURE, ASCENT AND EMPLACEMENT OF GRANITIC MAGMAS: Journal of the Geological Society, v. 136, p. 627-662.

Qiu, J., Xiao, E., Hu, J., Xu, X., Jiang, S., and Li, Z., 2008, petrogenisis of highly fractionated I-type granites in the coastal area of northeastern fujian province: Constraints from zircon U-Pb geochronology, geochemistry and Nd-Hf isotopes: Acta Petrologica Sinica, v. 24, p. 2468-2484.

Qiu, J.i.S., Wang, D.Z., Satoshi, K., and Innes, B.I.A.M., 2000, Geochemistry and petrogenesis of aluminous A-type granites in the coastal area of Fuj ian Province: Geochimica, v. 29, p. 313-321.

Qiu, J.S., Wang, D.Z., and Zhou, J.C., 1999, Geochemistry and petrogenesis of the Late Mesozoic Bimodal volcanic rocks at Yunshan Caldera, Yongtai County, Fujian Province: Acta Petrologica et Mineralogica, v. 18, p. 97-107.

Roger, F., Malavieille, J., Leloup, P.H., Calassou, S., and Xu, Z., 2004, Timing of granite emplacement and cooling in the Songpan-Garze Fold Belt (eastern Tibetan Plateau) with tectonic implications: Journal of Asian Earth Sciences, v. 22, p. 465-481.

Schmid, J.C., Ratschbacher, L., Hacker, B.R., Gaitzsch, I., and Dong, S.W., 1999, How did the foreland react? Yangtze foreland fold-and-thrust belt deformation related to exhumation of the Dabie Shan ultrahigh-pressure continental crust (eastern China): Terra Nova, v. 11, p. 266-272.

Schmid, R., Ryberg, T., Ratschbacher, L., Schulze, A., Franz, L., Oberhänsli, R., and Dong, S., 2001, Crustal structure of the eastern Dabie Shan interpreted from deep reflection and shallow tomographic data: Tectonophysics, v. 333, p. 347-359.

Shi, J.J., 2010, Study on the tectonic deformation characteristics and Geo-dynamics of Changle-Nan'ao Metamorphic Zone [Doctoral Thesis thesis]: Beijing, China Univeresity of Geosciences (Beijing).

Shu, L.-S., Faure, M., Yu, J.-H., and Jahn, B.-M., 2011, Geochronological and geochemical features of the Cathaysia block (South China): New evidence for the Neoproterozoic breakup of Rodinia: Precambrian Research, v. 187, p. 263-276.

Shu, L., Faure, M., Wang, B., Zhou, X.-L., and Song, B., 2008a, Late Palaeozoic-Early Mesozoic geological features of South China: Response to the Indosinian collision events in Southeast

Asia: Comptes Rendus Geoscience, v. 340, p. 151-165.

Shu, L., Yu, J., Jia, D., Wang, B., Shen, W., and Zhang, Y., 2008b, Early Paleozoic orogenic belt in the eastern segment of South China: Geological Bulletin of China, v. 27, p. 1581-1593.

Shu, L.S., Deng, P., Wang, B., Tan, Z.Z., Yu, X.Q., and Sun, Y., 2004, Lithology, kinematics and geochronology related to Late Mesozoic basin-mountain evolution in the Nanxiong-Zhuguang area, South China: Science in China Series D-Earth Sciences, v. 47, p. 673-688.

Shu, L.S., Faure, M., Jiang, S.Y., Yang, Q., and Wang, Y.J., 2006, SHRIMP zircon U-Pb age, litho- and biostratigraphic analyses of the Huaiyu Domain in South China - Evidence for a Neoproterozoic orogen, not Late Paleozoic-Early Mesozoic collision: Episodes, v. 29, p. 244-252.

Shu, L.S., Faure, M., Wang, B., Zhou, X.L., and Song, B., 2008c, Late Palaeozoic-Early Mesozoic geological features of South China: Response to the Indosinian collision events in Southeast Asia: Comptes Rendus Geoscience, v. 340, p. 151-165.

Shu, L.S., Wang, Y., Sha, J.G., Jiang, S.Y., Yu, J.H., and Wang, Y.B., 2009a, Jurassic sedimentary features and tectonic settings of southeastern China: Science in China Series D-Earth Sciences, v. 52, p. 1969-1978.

Shu, L.S., Yu, J.H., and Wang, D.Z., 2000, Late Mesozoic granitic magmatism and its relation to metamorphism-ductile deformation in the Changle-Nan'ao Fault Zone, Fujian province: Geological Journal of China Universities, v. 6, p. 368-378.

Shu, L.S., Zhou, W.Q., Shi, Y.s., and Yin, J., 1993, Study of the high-pressure metamorphic blueschist and its Late Proterozoic age in the Eastern Jiangnan Belt: Chinese Science Bulletin, v. 38, p. 1879-1882.

Shu, L.S., Zhou, X.M., Deng, P., Wang, B., Jiang, S.Y., Yu, J.H., and Zhao, X.X., 2009b, Mesozoic tectonic evolution of the Southeast China Block: New insights from basin analysis: Journal of Asian Earth Sciences, v. 34, p. 376-391.

Shu, L.S., Zhou, X.M., Deng, P., and Zhu, W.B., 2007, Mesozoic-Cenozoic Basin features and evolution of Southeast China: Acta Geologica Sinica-English Edition, v. 81, p. 573-586.

Sun, T., and Zhou, X., 2002, Late Mesozoic extension in Southeast China: petrologic symbols: JOURNAL-NANJING UNIVERSITY NATURAL SCIENCES EDITION, v. 38, p.

737-746.

Sun, W.D., Ding, X., Hu, Y.H., and Li, X.H., 2007, The golden transformation of the Cretaceous plate subduction in the west Pacific: Earth and Planetary Science Letters, v. 262, p. 533-542.

Talbot, J.Y., Chen, Y., and Faure, M., 2005a, A magnetic fabric study of the Aigoual-Saint Guiral-Liron granite pluton (French Massif Central) and relationships with its associated dikes: Journal of Geophysical Research-Solid Earth, v. 110.

Talbot, J.Y., Faure, M., Chen, Y., and Martelet, G., 2005b, Pull-apart emplacement of the Margeride granitic complex (French Massif Central). Implications for the late evolution of the Variscan orogen: Journal of Structural Geology, v. 27, p. 1610-1629.

Talbot, J.Y., Martelet, G., Courrioux, G., Chen, Y., and Faure, M., 2004, Emplacement in an extensional setting of the Mont Lozere-Borne granitic complex (SE France) inferred from comprehensive AMS, structural and gravity studies: Journal of Structural Geology, v. 26, p. 11-28.

Tang, L., Chen, H., Dong, C., Shen, Z., Cheng, X., and Fu, L., 2010, Late Mesozoic tectonic extension in se China: Evidence from the basic dike swarms in Hainan Island: Acta Petrologica Sinica, v. 26, p. 1204-1216.

Tarling, D.H., and Hrouda, F., 1993, The magnetic anisotropy of rocks: London, Chapman & Hall, 1-217 p.

Tong, W.X., and Tobisch, O.T., 1996, Deformation of granitoid plutons in the Dongshan area, southeast China: Constraints on the physical conditions and timing of movement along the Changle-Nanao shear zone: Tectonophysics, v. 267, p. 303-316.

Turrillot, P., Faure, M., Martelet, G., Chen, Y., and Augier, R., 2011, Pluton-dyke relationships in a Variscan granitic complex from AMS and gravity modelling. Inception of the extensional tectonics in the South Armorican Domain (France): Journal of Structural Geology, v. 33, p. 1681-1698.

Vernon, R.H., and Collins, W.J., 1988, Igneous microstructures in migmatites: geology, v. 16, p. 1126-1129.

Wang, J., 1990a, Disscussion on some problems about Jiepai migmatite belt in the western margin of Hengshan mountain: Hunan Geology, v. 9, p. 39-50.

Wang, J., and Li, Z.X., 2003, History of Neoproterozoic rift basins in South China: implications for Rodinia break-up: Precambrian Research, v. 122, p. 141-158.

Wang, J.B., 1990b, Diwa-type granite of Hengshan: origin by fractural melting: Geotectonica et Metallogenia, v. 3, p. 007.

Wang, Q., Wyman, D.A., Xu, J.F., Zhao, Z.H., Jian, P., Xiong, X.L., Bao, Z.W., Li, C.F., and Bai, Z.H., 2006, Petrogenesis of Cretaceous adakitic and shoshonitic igneous rocks in the Luzong area, Anhui Province (eastern China): Implications for geodynamics and Cu-Au mineralization: Lithos, v. 89, p. 424-446.

Wang, Q.C., and Cong, B.L., 1999, Exhumation of UHP terranes: A case study from the Dabie Mountains, eastern China: International Geology Review, v. 41, p. 994-1004.

Wang, X.-L., Shu, L.-S., Xing, G.-F., Zhou, J.-C., Tang, M., Shu, X.-J., Qi, L., and Hu, Y.-H., 2012, Post-orogenic extension in the eastern part of the Jiangnan orogen: Evidence from ca 800-760 Ma volcanic rocks: Precambrian Research, v. 222, p. 404-423.

Wang, Y.S., Xiang, B.W., Zhu, G.A., and Jiang, D.Z., 2011, Structural and geochronological evidence for Early Cretaceous orogen-parallel extension of the ductile lithosphere in the northern Dabie orogenic belt, East China: Journal of Structural Geology, v. 33, p. 362-380.

Wang, Z.H., and Lu, H.F., 1997a, Ar-40/Ar-39 geochronology and exhumation of mylonitized metamorphic complex in Changle-Nanao ductile shear zone: Science in China Series D-Earth Sciences, v. 40, p. 641-647.

Wang, Z. H. and H. F. Lu, 1997b, Evidence and dynamics for the change of strike-slip direction of the Changle-Nanao ductile shear zone, southeastern China: Journal of Asian Earth Sciences, v. 15, p. 507-515.

Wang, Z. H. and H. F. Lu, 2000, Ductile deformation and Ar-40/Ar-39 dating of the Changle-Nanao ductile shear zone, southeastern China: Journal of Structural Geology, v. 22, p. 561-570.

Wei, w., Chen, Y., Faure, M., Shi, Y.H., Martelet, G., Hou, Q.L., Lin, w., Le Breton, N., and Wang, Q.C., 2013, A multidisciplinary study on the emplacement mechanism of the Qingyang-Jiuhua Massif in Southeast China and its tectonic bearings. Part I: structural geology, AMS and Paleomagnetism: Journal of Asian Earth Sciences.

Wu, F.Y., Ji, W.Q., Sun, D.H., Yang, Y.H., and Li, X.H., 2012, Zircon U-Pb geochronology and

Hf isotopic compositions of the Mesozoic granites in southern Anhui Province, China: Lithos, v. 150, p. 6-25.

Wu, R.X., Zheng, Y.F., and Wu, Y.B., 2005, Zircon U-Pb Dating and Element and Oxygen Isotope Geochemistry of Gabbro from Ophiolites in South Anhui: Acta Geoscientica Sinica, v. 26, p. 70-73.

Wu, Y.B., Tang, J., Zhang, S.B., and Zhao, Z.F., 2007, SHRIMP zircon U-Pb dating for two episodes of migmatization in the Dabie orogen: Chinese Science Bulletin, v. 52, p. 1836-1842.

Xiang, L., and Shu, L., 2010, Pre-Devonian tectonic evolution of the eastern South China Block: Geochronological evidence from detrital zircons: Science China Earth Sciences, v. 53, p. 1427-1444.

Xie, G.Q., Hu, R.Z., Mao, J.W., Pirajno, F., Li, R.L., Cao, J.J., Jiang, G.H., and Zhao, J.H., 2006, K-Ar dating, geochemical, and Sr-Nd-Pb isotopic systematics of late Mesozoic mafic dikes, southern Jiangxi Province, Southeast China: Petrogenesis and tectonic implications: International Geology Review, v. 48, p. 1023-1051.

Xie, X., Xu, X., Zou, H., Jiang, S., Ming, Z., and Qiu, J., 2005, Early J2 basalts in SE China: Incipience of large-scale late Mesozoic magmatism: Science in China Series D: Earth Sciences, v. 49, p. 796-815.

Xing, G.F., Lu, Q.D., Jiang, Y., Nie, T.C., Chen, R., Feng, Y.F., Chen, Z.H., Yu, M.G., Li, C.H., Huang, J.L., and Ke, X., 2010, Identification and significance of "gneissic" magma-mixed complex in the Changle — Nan'ao fault zone, southeastern Fujian, China.: Geological Bulletin of China, v. 29, p. 31-43.

Xu, H., Fu, W., and Xu, J., 1998, The deformation feature and strain analysis of the Jiepai Dip-slip ductile shear zone in Hengshan mountain: Hunan Geology, v. 17, p. 85-90.

Xu, J., Zhu, G., Tong, W., Cui, K., and Liu, Q., 1987a, Formation and evolution of the Tancheng-Lujiang wrench fault system: a major shear system to the northwest of the Pacific Ocean: Tectonophysics, v. 134, p. 273-310.

Xu, J.W., Zhu, G., Gao, D.L., Ling, S.F., and Ma, G.F., 1990, the Changle-Nanao large-scale shear zone and its tectonic significance, southeast China, symposium for evolution and dynamics of lithospheric plate, Volume 1: Beijing, Geological Publishing House, p.

145-153.

Xu, J.W., Zhu, G., Tong, W.X., Cui, K.R., and Liu, Q., 1987b, Formation and evolution of the Tancheng-Lujiang wrench fault system - a major shear system to the northwest of the pacific ocean: Tectonophysics, v. 134, p. 273-310.

Xu, M., 1992, Early Jurassic Bimodal Volcanic Rocks and Their Structure Environment in Yongding County, Fujian Province [J]: Geology of Fujian, v. 2, p. 005.

Xu, X., Dong, C., Li, W., and Zhou, X., 1999, Late Mesozoic intrusive complexes in the coastal area of Fujian, SE China: the significance of the gabbro-diorite–granite association: Lithos, v. 46, p. 299-315.

Xu, X.S., Suzuki, K., Liu, L., and Wang, D.Z., 2010, Petrogenesis and tectonic implications of Late Mesozoic granites in the NE Yangtze Block, China: further insights from the Jiuhuashan-Qingyang complex: Geological Magazine, v. 147, p. 219-232.

Yan, J., Chen, J.F., Yu, G., Qian, H., and Zhou, T.X., 2003, Pb isotopic characteristics of Late Mesozoic mafic rocks from the Lower Yangtze Region: evidence for enriched mantle: Geological journal of China universities, v. 9, p. 195-206.

Yang, Q.G., Qiang，Cheng, W., Bo，Zhu, Q., and Guang，Li, X., 2011, A discussion on two times southward thrusting of Xiangfan—Guangji Fault in South Dabie Orogen, Central China: Geological review, v. 57, p. 480-494.

Yang, S.-Y., Jiang, S.-Y., Zhao, K.-D., Jiang, Y.-H., Ling, H.-F., and Luo, L., 2012, Geochronology, geochemistry and tectonic significance of two Early Cretaceous A-type granites in the Gan-Hang Belt, Southeast China: Lithos, v. 150, p. 155-170.

Yang, X.Y., Yan, X.M., Jiang, L.L., Wang, K.R., and Sun, L.G., 2006, Geochemical study of Shaxi porphyry copper-gold deposit in southern part of Tan-Lu fault belt, East China: Journal of the Geological Society of India, v. 67, p. 475-494.

Yao, J., Shu, L., and Santosh, M., 2011, Detrital zircon U-Pb geochronology, Hf-isotopes and geochemistry-New clues for the Precambrian crustal evolution of Cathaysia Block, South China: Gondwana Research, v. 20, p. 553-567.

Yu, J.-H., Wei, Z.-Y., Wang, L.-J., Shu, L.-S., and Sun, T., 2006a, Cathaysia block: A young continent composed of ancient materials: Geological journal of China universities, v. 12, p. 440-447.

Yu, J.H., Zhou, X.M., Zhao, L., Jiang, S.Y., Wang, L.J., and Ling, H.F., 2005, Mantle-crust interaction generating the Wuping granites: evidenced from Sr-Nd-Hf-U-Pb isotopes: Acta Petrologica Sinica, v. 21, p. 651-664.

Yu, X., Wu, G., Zhang, D., Yan, T., Di, Y., and Wang, L., 2006b, Cretaceous extension of the Ganhang Tectonic Belt, southeastern China: constraints from geochemistry of volcanic rocks: Cretaceous Research, v. 27, p. 663-672.

Yu, X.Q., Jiang, L.L., Xue, W., Qiu, R.L., Du, J.G., and Dai, S.Q., 2007, Identification and basic characteristics of the Anhui-Zhejiang-Jiangxi fault zone: Earth Science Frontiers, v. 14, p. 102-113.

YNBGMR, 1984, Regional geology of Yunnan Province: Beijing, China, Geological Plublishing House.Zhang, J., 1994, Tectonic feature of the western edge in the metamorphic nucleus complex of Hengshan: Journal of East China Geological Institute, v. 17, p. 18-22.

Zhang, Q., Wang, Y.l., Jin, W.j., and Li, C.D., 2008, Eastern China Plateau during the Late Mesozoic: evidence, problems and implication: Geologcal Bulletin of China, v. 27, p. 1404-1430.

Zhang, Z., 1992, Characterristics, genesis and emplacement mechanism of the ductile shear zone along western margin of Hengshan granite: Hunan Geology, v. 11, p. 198-202.

Zhang, Z., and Zhu, Z., 1989, Comparing Study of the Magnetic Fabric with the Deformation Fabric of the Western Margin Ductile Shear Zone of Hengshan Composite Granite: Journal of Shijiazhuang University of Economics, v. 12, p. 313-324.

Zhao, J.H., Hu, R.Z., and Liu, S., 2004, Geochemistry, petrogenesis, and tectonic significance of Mesozoic mafic dikes, Fujian Province, Southeastern China: International Geology Review, v. 46, p. 542-557.

Zhao, J.L., Qiu, J.S., Li, Z., Liu, L., and Li, Y.L., 2012, Petrogenesis of the Taiwushan granite pluton in Fujian Province: Constraints from zircon U-Pb ages and Hf isotopes: Acta Petrologica Sinica, v. 28, p. 3938-3950.

Zheng, Y.-F., Zhang, S.-B., Zhao, Z.-F., Wu, Y.-B., Li, X., Li, Z., and Wu, F.-Y., 2007, Contrasting zircon Hf and O isotopes in the two episodes of Neoproterozoic granitoids in South China: Implications for growth and reworking of continental crust: Lithos, v. 96, p. 127-150.

Zhou, D., Ru, K., and Chen, H.-z., 1995, Kinematics of Cenozoic extension on the South China Sea continental margin and its implications for the tectonic evolution of the region: Tectonophysics, v. 251, p. 161-177.

Zhou, X.M., and Li, W.X., 2000, Origin of Late Mesozoic igneous rocks in Southeastern China: implications for lithosphere subduction and underplating of mafic magmas: Tectonophysics, v. 326, p. 269-287.

Zhou, X.M., Sun, T., Shen, W.Z., Shu, L.S., and Niu, Y.L., 2006, Petrogenesis of Mesozoic granitoids and volcanic rocks in South China: A response to tectonic evolution: Episodes, v. 29, p. 26-33.

Zhu, G., Niu, M.L., Xie, C.L., and Wang, Y.S., 2010a, Sinistral to Normal Faulting along the Tan-Lu Fault Zone: Evidence for Geodynamic Switching of the East China Continental Margin: Journal of Geology, v. 118, p. 277-293.

Zhu, G., Xie, C.L., Chen, W., Xiang, B.W., and Hu, Z.Q., 2010b, Evolution of the Hongzhen metamorphic core complex: Evidence for Early Cretaceous extension in the eastern Yangtze craton, eastern China: Geological Society of America Bulletin, v. 122, p. 506-516.

Zhu, G., Xu, J.W., Gao, D.L., Lin, S.F., and Ma, G.F., 1993, structural characteristics and deformation of the changle-nanao mega shear zone along the southeast China coast, The Tancheng-Lujiang Wrench Fault System: Chichester, Wiley, p. 201-209.

Zhu, Q.b., Yang, K.G., and Wang, Y., 2010c, Extensional Detachment and Magmatism of the Lushan Metamorphic Core Complex： Constraints From 40Ar / 39Ar and U-Pb Geochronology: Geotectonica et Metallogenia, v. 34, p. 391-401.

Zhu, W.-G., Zhong, H., Li, X.-H., He, D.-F., Song, X.-Y., Ren, T., Chen, Z.-Q., Sun, H.-S., and Liao, J.-Q., 2010d, The early Jurassic mafic–ultramafic intrusion and A-type granite from northeastern Guangdong, SE China: age, origin, and tectonic significance: Lithos, v. 119, p. 313-329.

Zijderveld, J.D.A., 1967, AC demagnetisation of rocks: analysis of results, Elsevier, 245-286 p.

ZJBGMR, 1989, Regional geology of Zhejiang Province: Beijing, China, Geological Plublishing House.

Zou, H.B., 1995, A mafic-ultramafic rock belt in the Fujian coastal area, southeastern China: A geochemical study: Journal of Southeast Asian Earth Sciences, v. 12, p. 121-127.

Appendix: paper in press

WEI W, CHEN Y, FAURE M, et al. 2014a. A multidisciplinary study on the emplacement mechanism of the Qingyang-Jiuhua Massif in Southeast China and its tectonic bearings. Part I: structural geology, AMS and paleomagnetism. Journal of Asian Earth Sciences 86:76-93.

WEI W, MARTELET G, LE BRETON N, et al. 2014b. A multidisciplinary study of the emplacement mechanism of the Qingyang–Jiuhua massif in Southeast China and its tectonic bearings. Part II: Amphibole geobarometry and gravity modeling Journal of Asian Earth Sciences 86: 94-105.

Wei WEI

Characteristics of the Late Mesozoic tectonic evolution of the South China Block and geodynamic implications

-multi-approach study on Qingyang-Jiuhua, Hengshan and Fujian coastal granitic massifs.

The vast distribution and long duration of the Late Mesozoic magmatism in the eastern part of South China presents a unique case in the world. This offers a natural laboratory to study the process of magma genesis, the magma emplacement mode, the relationship between magmatism and tectonics, the geodynamic role on the magma emplacement and lithospheric evolution. Since 50's, particularly 90's of the last century, geoscientists have made important efforts in geological cartography and carried out numerous studies with remarkable scientific achievements, building a solid background to understand the tectonic evolution of the South China Block (SCB). However, certain fundamental questions mentioned above remain unsolved and/or are in hot debate. In order to make progress in these scientific issues, we have carried out in a multi-disciplinary study in the Late Mesozoic Qingyang-Jiuhua massif, Hengshan massif and Fujian coastal zone according to their distance with respect to the paleo subduction zone of the Paleo-Pacific plate, the ages of granitic massifs and related tectonics, including field observation on the structure geology, micro-observation on thin section, U-Pb dating on monazite, AMS, paleomagnetism, gravity modeling and P condition concern the granite emplacement. In the view of deformation in these granitic massifs and their country rocks, mode and influence of regional tectonics on the emplacement, though each studied zone reveals its distinguished characteristics, they show some intrinsic and common relationships between them. With our new results and integrating previous data, in this thesis, we discuss the tectonic context of emplacement of these Late Mesozoic magmatic massifs and the geodynamic evolution of the SCB., We propose a 3-step geodynamic model: (1) during 145-130 Ma period, the Paleo-Pacific plate subducted northwestwardly, the West Philippines micro-continent, approaching to SCB, important subduction-related arc volcanism was produced in the coastal areas of Southeast China coast (Zhejiang-Fujian-Guangdong), forming a back-arc extension tectonic system in SCB; (2) during 130-110 Ma period, due to the collision between the West Philippines micro-continent and SCB, the compressional tectonic structures were developed in the Changle-Na'ao coastal zone, producing ductile deformation zones. However, the inland of the eastern part of SCB was under a NW-SE extensional tectonic regime; (3) during 105-90 Ma period, a new subduction zone was developed in the SE flank of the West Philippines micro-continent, the subducting slab reached the Changle Nan'ao tectonic belt, with the possible break-off of slab, the asthenospheric ascent was responsible for the important emplacement of plutonic massifs and dykes. The tectonics of the eastern part of SCB was characterized by a general extensional system in this period. This tectonic pattern has been significantly disturbed by the Oligocene-Eocene opening of the South China sea,and the Miocene shortening of the SCB margin in Taiwan. Of course, this model should be improved by more geological, geophysical and geochemical investigations.

Mots-clés : South China Block lithospheric tectonic evolution, Late Mesozoic, Magma emplacement mechanism, Structural observation, Anisotropy of Magnetic Susceptibility, Paleomagnetism, Gravity modeling, Amphibole AlTotal geobarometry.

Caractéristiques de l'évolution de la partie orientale du Bloc de Chine du Sud au Mésozoïque supérieur et implications géodynamiques

-Etude pluridisciplinaire de la mise en place des massifs granitiques de Qingyang-Jiuhua, Hengshan et de la côte du Fujian et des structures tectoniques associées

La vaste distribution géographique et la longue durée du magmatisme au Mésozoïque supérieur (Jurassique et Crétacé) en Chine du Sud présente le cas unique dans le monde. Ceci présente un laboratoire naturel très favorable a l'étude des processus de magmatogénèse, et des modes de mise place des plutons granitiques. Il permet également d'aborder l'analyse des relations magmatisme-tectonique et les contextes géodynamiques de la mise en place de magma dans leur cadre lithosphérique. Depuis les années 50, et surtout les années 90, des scientifiques ont mis un effort important sur la cartographie géologique, mené des études pétrologiques et géochronologiques et ainsi obtenu une base solide pour la compréhension de l'évolution tectonique du Bloc de Chine du Sud (SCB). Cependant, des questions fondamentales restent encore sans réponses ou vivement débattues. Dans le but de progresser sur ces sujets fondamentaux, nous avons mené des études pluridisciplinaires sur les massifs d'âge Mésozoïque supérieur de Qingyang-Jiuhua (Province d'Anhui), Hengshan (Province de Hunan) et certains plutons affleurant dans la zone côtière du Fujian. Le choix des massifs est fonde sur leur distance variable par rapport à la paléozone de subduction, les âges comparables de ces massifs et les déformations associées. Les méthodes d'étude comprennent l'observation de terrain, l'analyse microscopique de lames minces, la datation par U-Pb de monazite, l'ASM, le paléomagnétisme, la modélisation gravimétrique et la barométrie a partir de Al-total dans l'amphibole magmatique. Bien que chaque massif présente des caractéristiques distinctes, ils partagent des points communs du point de vue de leur orientation préférentielle, de la déformation de leurs encaissants et de l'influence de la tectonique régionale sur leur mise en place, D'après nos nouveaux résultats et en intégrant les données précédentes, nous discutons dans cette thèse les contextes tectoniques de mise en place de ces massifs granitiques et l'évolution géodynamique de SCB, et proposons un scénario géodynamique en 3 étapes. (1) Pendant la période 145-130 Ma, la subduction vers le NW de la plaque Paléo-Pacifique sous le continent asiatique fait rapprocher le micro-continent de l'Ouest-Philippines avec le continent de Chine du Sud, produisant l'important magmatisme d'arc et formant un regime tectonique en extension en SCB ? Dans l'arrière-arc; (2) Pendant la période 130-110 Ma, dûe à la collision entre le micro-continent de l'Ouest Philippines et SCB, une structure compressive vers le NW a été développée dans la zone de Changle Nan'ao, produisant des déformations ductiles. Cependant, l'intérieur de la partie orientale du SCB était encore en régime tectonique extensif de direction NW-SE; (3) Pendant la période 105-90Ma, une nouvelle zone de subduction a été développée au SE du micro-continent de l'Ouest Philippines, le panneau subductant atteint la zone de Changle-Nan'ao, avec probablement des morceaux de panneau cassé, provocant l'ascension de l'asthénosphère, responsable de la mise en place d'importants massifs granitiques et de filons. La tectonique de SCB pendant cette période est caractérisée par un système tectonique d'extension générale. Ce dispositif a ete significativement perturbe par l'ouverture oligo-miocène de la mer de Chine du Sud et par la compression miocène de la marge à Taiwan. Ce modèle géodynamique reste à être amélioré par de futures investigations géologiques, géophysiques et géochimiques.

Mots-clés : Bloc de Chine du Sud, zone tectonique de Changle-Nan'ao, Crétacé Mésozoïque supérieur, extension lithosphérique, mise en place passive de magma granitique, massif de Qingyang-Jiuhua, massif de Hengshan, etude pluridisciplinaire, analyse multi-échelle, micro-continent Ouest Philippines, magmatisme insulaire-arc, extension d'arrière-arc, Anisotropie de la Susceptibilité magnétique (AMS), paléomagnétisme, modélisation gravimétrique, barométrie d'Al-total dans l'amphibole.

Institut des Sciences de la Terre d'Orléans
Campus Géosciences
1A rue de la Férolerie
45071 ORLEANS Cedex 2